THE DESIGN OF UNSURFACED ROADS USING GEOSYNTHETICS

by

Peter H Little B.Eng

Thesis submitted to the University of Nottingham
for the degree of Doctor of Philosophy, May 1992.

ACKNOWLEDGEMENTS

The author wishes to acknowledge the following people, companies and institutions:

Professor S F Brown for making available the facilities of the Department of Civil Engineering at Nottingham University; the Science and Engineering Research Council for funding the project and for making the Bothkennar Soft Clay Site available; Netlon Limited, du Pont de Nemours Int. S.A, Rhône-Poulenc Fibres and Polyfelt Ges. m.b.h and their representatives for their industrial sponsorship and technical support; Denny Construction for their careful construction of the full-scale trials; and to Professor Alan McGown for making available the facilities of the Department of Civil Engineering at Strathclyde University.

During the course of the last three years I have been greatly aided by many friends and colleagues. Particular thanks are due to Mr A R Dawson, my supervisor, and Professor S F Brown for their advice, suggestions and guidance. I would further like to thank Mr M Langford and Mr D Belcher for their cheerful and enthusiastic assistance that made the long hours spent on-site so enjoyable.

On a more personal note, I would like to thank my wife, Alison, for her constant encouragement and support.

Finally, I wish to thank Glenis Fisher for her patient and efficient typing of this thesis.

If water passes through a road and fill up the native soil, the road whatever may be its thickness, loses support and goes to pieces. The erroneous opinion that by placing a large quantity of stone under roads, a remedy will be found for the sinking into wet clay or other soft soils ...(and) that a road may be made artificially strong to carry heavy carriages ... has produced most of the defects of the roads of Great Britain.

John L McAdam 1820

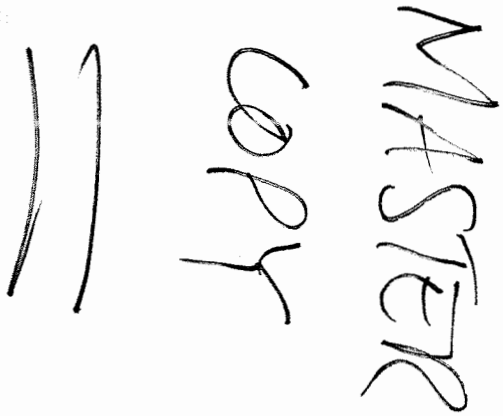

TABLE OF CONTENTS

ABSTRACT

Some of the current methods for the design of unpaved roads, with and without geosynthetics, were used for sixteen full-scale test sections which were constructed at the Bothkennar Soft Clay Site, Airth, Scotland. The full-scale trials consisted of twelve pavements including geosynthetics and four control pavements incorporating two types of aggregate and two design life expectancies.

The test pavements were instrumented to monitor the transient stress and strain distribution, permanent strain distribution, geosynthetic temperature and ground water level during the trafficking operation. Traffic loading was provided in two stages by a standard road-going vehicle. The vehicle used for Phase One applied an 80kN axle load and in Phase Two a 126kN axle load. Failure of the pavements was defined as a rut depth of 150mm. The passage of 2115 axles resulted in failure of three sections and significant deformations in many others.

Back-calculation to compare predicted and measured performance was performed and hence the existing design methods were critically assessed. Where possible the measurements obtained from field trials were used to examine the assumptions made within the design methods.

Previous methods were found to be essentially static in approach and did not model strain development adequately. A new approach ensuring strain compatibility between the elements of the system is proposed. This enhances the ability of the engineer to assess the value of differing products used in this application.

CHAPTER ONE

INTRODUCTION

1.1 BACKGROUND

In designing low volume roads, that is roads whose life expectancy is measured in hundreds or thousands of axle passes, it is often the most economical solution to construct a pavement that consists entirely of unbound materials. Such roads might be forestry, or farm, access tracks or haul roads in large muck-shifting or quarrying activities. The use of unbound materials in these applications reduces rutting, which would quickly develop should the traffic travel directly on the subgrade, and so the way remains traffickable and the plant using it can do so efficiently and maintenance costs are minimal.

It has been long understood that when roads cross soft ground even large quantities of aggregate are unable to prevent premature pavement collapse. The Romans used to place brushwood on the surface of soft ground before constructing their roads in order to prevent the stones being lost into the soft foundation. Today man-made materials are used in place of the brushwood and the general name for such materials used in geotechnical engineering is geosynthetics from the Greek, geo, meaning the Earth and synthetic, meaning artificially produced. The use of geosynthetics in unpaved roads over soft ground was one of the first application for these products. The geosynthetic market in Western Europe is growing at 12 to 15 per cent annually and currently stands at 300 million square metres per annum. Separation and stabilization account for 40% of the market with the remainder accounted for by amongst others, drainage, land-fill lining systems and asphalt overlay (Jagielski (1991)).

The economical benefits to be obtained from including geosynthetics in unpaved road design is determined by the reduction in the quantity of aggregate required to meet the serviceability criteria of the road. It is widely accepted that the saving of aggregate that is possible using geosynthetics is dependent mainly upon the shear strength or the Californian Bearing Ratio (CBR) of the subgrade and by some measure of the geosynthetic stiffness.

1.2 THE NEED FOR RESEARCH

A wide variety of geosynthetics are used in the context of unpaved roads varying from the very stiff to the very extensible. These materials vary substantially in their physical properties and no single, unified design method existed to predict the performance of any chosen material. The application has been very much driven by the producers of geosynthetics who have demonstrated that their individual products can be of benefit and each geosynthetic manufacturer has a design method which highlights the performance of their products. Different assumptions and factors of safety within each of the various methods make it difficult for the consumer to make an engineering judgement as to the suitability of any one product to any one situation or to compare products A & B directly.

The concepts behind each of the design methods currently available are as diverse as the products for which they are intended. Such diversity implies that, generally, there is a fundamental lack of understanding of the mechanisms involved in this type of problem. One of the aims of the research, therefore, was to examine, by the use of instrumented full-scale trials, the behaviour of unpaved roads including geosynthetics and compare it to those not including them. As a result of the trials it was hoped that the existing design methods could be validated and calibrated by predicting expected and measured performance. It was further hoped that a clearer understanding of the problem would result, leading to an improved method suitable for all types of geosynthetic.

1.3 THE RESEARCH

The full-scale trials involved in the research was based at a site on the banks of the Forth Estuary which had been purchased by the Science and Engineering Research Council (SERC) as a test site for research into the interaction of soft clay with a variety of Civil Engineering and building operations. An access road would plainly have to be constructed to enable access to various parts of the site and a proposal was made by SERC that this was an opportunity to research the performance of unpaved roads using geosynthetics.

The research was sponsored by SERC and by the following manufacturers of geosynthetics: Netlon Limited, Du Pont de Nemours Int. S.A., Rhône-Poulenc Fibres and Polyfelt Ges. m.b.h. These manufacturers, between them, produce most generic

types of geosynthetics. Involved in the trial were a geogrid, a heat-bonded fabric and two needle-punched felts - one made from polyester and one from polypropylene.

The industrial sponsorship consisted of a small financial contribution to the cost of the research, a quantity of each geosynthetic, a design based on their current design methods and technical advice and support. None of the sponsors of the project manufactured any woven geosynthetics and, hence, a woven geosynthetic was anonymously purchased and installed in the full-scale trials so that a full range of geosynthetics were represented.

The full-scale trials consisted of a loop road consisting of sixteen, twenty metre long sections, twelve of which contained geosynthetics and four of which were control sections. Two types of aggregate were utilised, a crushed rock and a sand and gravel mixture, six types of geosynthetic and two expected design lives (a thicker upper-bound solution and a thinner lower-bound one). Loading was provided by a standard road-going, two axled lorry which imposed upon the pavements 2115 load repetitions. This induced rupture in the geosynthetic in three sections and significant deformations in some of the remaining ones.

Measurements of stress/strain within the pavement were recorded as was the rut depth and a host of other parameters and these results are presented in Chapter 6 and in the appendices. The results are used to validate and calibrate the existing design methods and to identify within those methods the key mechanisms at work. Finally, a new method is proposed which advances the ability of the engineer to assess the value of differing products.

CHAPTER TWO

UNPAVED ROAD BEHAVIOUR AND DESIGN

2.1 GENERAL APPROACH

The use of unpaved, low-volume roads is usually restricted to access tracks and to haul roads. The application of repeated axle loadings to these pavements will cause permanent deformation or rutting to occur. The amount of this deformation that is permitted is dependent upon the serviceability requirements of the user but, commonly, is within the range 75 to 300mm. This serviceability requirement is likely to be controlled in a case such as a farm access, by vehicular axle clearance and, in the haul road case, by plant efficiency considerations.

In the case of haul roads and some access roads, the pavement is expected to remain serviceable during the application of a pre-determined number of axle passes. If it is constructed too thinly then larger rut depths will develop making the plant less efficient (and therefore incurring higher costs) and ultimately the pavement could become completely untraffickable necessitating remedial works to be made to the surface. If it is constructed too thickly then the pavement would have a longer life expectancy, but, it will cost more to install than is necessary. Thus, the correct design of unpaved roads should produce an efficient solution that uses neither too much aggregate nor too little.

One of the major problems with unpaved roads over soft ground is that very thick layers of aggregate are required to resist the deformations that occur as a result of trafficking. In these situations geosynthetics are often used in an attempt to reduce the quantity of aggregate required and hence the cost of construction. It is generally believed that geosynthetics are able to do this either by keeping the aggregate and the subgrade separate or by reinforcing the pavement in some way. Whether or not geosynthetics are incorporated is normally controlled by financial considerations, namely that the cost of the geosynthetic must be less than the cost incurred in providing and laying the additional aggregate that would be required in a pavement not including geosynthetics. Thus, numerous design methods have been proposed in order to demonstrate the value of geosynthetics in unpaved road design.

2.2 IMPORTANT MATERIAL PROPERTIES

2.2.1 Subgrade

The first and most important controlling parameter in the behaviour of unpaved roads is probably the shear strength of the subgrade. Especially when the shear strength is low, the thickness of the pavement required is very sensitive to even small changes in shear strength (as shown in Figure 2.3). The designer would be well advised to ascertain the exact value of shear strength that he should consider because rough estimates may lead to poor solutions.

2.2.2 Aggregate

Many design methods do not consider the properties of the aggregate. However the stiffness of the aggregate will determine the manner in which stresses are transmitted through the layer. The resilient modulus will determine the transient aggregate strain and the shear modulus will determine how the pavement flexes under the wheel load. The aggregate's resistance to permanent deformation is also important if permanent strain within the aggregate is not going to contribute significantly to the overall depth of rutting.

The required thickness of the aggregate layer, for any given pavement, will depend upon the magnitude and number of load repetitions that the pavement is expected to carry. The relationship between the required thickness and the above factors has been the subject of discussion and will be considered further in Chapter 2.3.2 and Chapter 7.1.3.

2.2.3 Geosynthetics

As this thesis is concerned with the design of unsurfaced roads using geosynthetics, an in depth discussion on the functions performed by these materials is warranted.

2.2.3.1 Separation

Separation is defined as the ability of the geosynthetic to prevent the loss of aggregate into the soft subgrade. In pavements without geosynthetics, the aggregate particles are pushed into the formation during the compaction and trafficking operations. Thus, in pavements including geosynthetics, the effective thickness of the aggregate layer is maintained and, as a consequence, its structural advantage to the pavement system remains constant.

Van Den Berg and Kenter (1984) suggested that the geosynthetic properties important in the separation function were puncture strength and tear strength. Puncture strength is the ability of the geosynthetic to resist rupture, caused by the compaction of aggregate on its surface and the subsequent trafficking of the pavement, and tear strength is the ability to resist tearing once the material had been damaged in any way. Obviously, unless the geosynthetic remains complete throughout the compaction and trafficking process, it is not going to act as a separator.

For safe design the geosynthetic should continue to act as a separator within a post-failure pavement. The Prandtl (1920) theory of failure wedges suggests that large local strains are likely to occur during the failure of the subgrade. It is possible, but not certain, that high strength geosynthetics might alter the failure mechanism of the subgrade but, even so, high and low stiffness geosynthetics may have to undergo large local strains if they are to avoid rupture. Therefore, geosynthetics which are designed to act as separators must either be extensible or, in failure, the geosynthetic must mobilize elongation by pulling material from the sides. However, it would appear that the option of mobilizing elongation in this manner is unlikely as the overburden stresses, coupled with aggregate/geosynthetic fictional interlock, will prevent the necessary slippage. Therefore it would appear that high-elongation-at-failure-geosynthetics are more likely to maintain the separation function in a post-failure pavement.

2.2.3.2 Filtration

Filtration is defined as the prevention of fines from the subgrade migrating up into the aggregate layer. This has the same net effect as separation, in that it maintains the effective aggregate thickness. Van den Berg and Kenter (1984) suggested that the

important properties involved in the filtration function of geosynthetics are the effective opening size (EOS) and the long-term permeability of the material. The EOS should be sufficiently small to retain the fine particles of the subgrade. Obviously some geosynthetics have an EOS that is much larger than the subgrade particle size, the grid materials for example, so the EOS of the geosynthetic can only be important to fabrics which rely on filtration as a major factor in determining the effectiveness of the soil-geosynthetic-aggregate system. The in-situ in-plane permeability of such materials should exceed the value attributed to the subgrade, otherwise pore water pressures are likely to build up beneath it.

Borrosson & Erikson (1986) undertook some tests on the long term properties of geosynthetics. They installed four heat-bonded and five needle-punched fabrics in a road in 1973 and then exhumed them in 1978 and 1983. The aggregate appeared not to contain any soil particles on ocular examination. Particle size analysis of the aggregate from samples recovered near to the fabrics and those near to the surface showed little difference, similarly there was little change in grading with time. This indicates that there has been little or no migration of fines from the subgrade into the aggregate. The geosynthetics recovered, however, did show some signs of ageing with reduction in tensile strength, elongation to failure and tear resistance, both after construction and with respect to time.

Dawson and Brown (1984) offered the following theory for a mechanism by which, in pavements not including geosynthetics, the aggregate is polluted by fines from the subgrade. As the traffic load is applied, the subgrade is stressed vertically at the points of aggregate/subgrade contact. Horizontal tensile strains develop at the interface with low vertical stresses between aggregate particles. The subgrade material, if soft enough, will tend to flow to these low stress points and as a result the aggregate sinks slightly. When the load is released the tensile strains are released too and the aggregate particles move together again. Subgrade material previously collected between them is forced up and down. When the next load cycle is applied the process is repeated and hence the contamination slowly ratchets upwards.

The inclusion of a fabric at the subgrade/aggregate interface may help to prevent pumping action by acting as a barrier against the upward movement of the subgrade material. Other possible solutions are that the geosynthetic reduces the point stress on the subgrade and hence the depression of the aggregate particles or that lateral restraint

prevents movement of the aggregate particles responsible for the mechanism described above.

2.2.3.3 Reinforcement

There has probably been more written on the reinforcement abilities of geosynthetics than on any of their other functions. Hausmann (1987) identified three mechanisms of geosynthetic reinforcement which can be referred to as the membrane effect, subgrade restraint and aggregate restraint.

The mechanisms by which geosynthetics reinforce soil-geosynthetic-aggregate systems have been considered by many authors. Earlier papers such as Nieuwenhuis (1977) and Giroud & Noiray (1981) suggested that a membrane effect predominated as the mechanism involved. The membrane effect theory suggests that the deformation of the geosynthetic provides an upward reaction under the wheel path and a downward pressure on the subgrade between the wheels, thus spreading the load to more of the formation and decreasing the high subgrade loads directly under the wheel path. This approach to reinforcement has been the subject of many papers. In order to generate a significant contribution to the performance of the pavement, a geosynthetic must have a high stiffness, generate large forces at low strains, and have a high ultimate strength if it is to work as a tensioned membrane.

Nieuwenhuis (1977) calculated the membrane effect reinforcement by assuming that the deformed profile of the geosynthetic assumed a circular disc shape under the wheel-path. Later theory by Giroud and Noiray (1981) suggested that the deformed profile was more accurately modelled by assuming a parabolic profile. In all cases the geosynthetic is assumed to transfer load from under the wheel path to the area out-side this location. Hence the load is distributed over a larger area. All of the analytical design methods consider a static analysis and then make allowances for the effects of trafficking or repeated loading. The assumption of membrane effect design methods is that eventually the soil-geosynthetic-aggregate system will reach some form of equilibrium when the net loading of the subgrade no longer exceeds the bearing capacity of the same, however that bearing capacity may be calculated. It appears obvious that the membrane effect can only play a noticeable role in the behaviour of reinforced pavements at large rut depths, or more correctly, large subgrade rut depths.

The geometry of forces at small deformations must either lead to the requirement of very stiff materials or to the break-down of the theory.

At low rut depths, the membrane effect plays a small rôle in the mechanism of the system. Thus more recent papers have concentrated on subgrade restraint, such as Milligan et al (1989a and b). They show that the bearing capacity of the subgrade decreases when normal and outward shear forces act together. Thus, the geosynthetic improves the bearing capacity of the formation by carrying the shear forces which would otherwise have been present on the surface of the layer. These shear stresses manifest themselves as tensile forces in the geosynthetic.

Design theory based on this concept was presented by Milligan et al (1989a and b) and will be discussed further in Chapter 2.6. The design philosophy is summarised in part of the abstract as follows: "The design is based on the concept that, as vertical loads are applied to a granular layer, horizontal stresses must also develop within that layer. These stresses are held in equilibrium by shear stresses at the surface of the subgrade and in unreinforced roads these shear stresses have a detrimental effect on the bearing capacity. The new method moves away from the emphasis on membrane action to explain the function of the reinforcement and is therefore able to account for observed improvements due to reinforcement at small surface deflections".

Aggregate restraint models, such as Sellmeijer (1990), consider that the strain compatibility between the aggregate of the geosynthetic is important to retain the integrity of the system. This is also known as the slab effect because, conceptually, the system behaves as a reinforced concrete slab.

In an aggregate restraint model, it is assumed that the aggregate stiffness predominates in resisting the deformation of the system under the wheel load. Sellmeijer asserts that the stiffness of the aggregate layer far exceeds that of even the stiffest geosynthetics, thus the inclusion does not control the deflection directly. However, the geosynthetic acts as a separator, preventing the loss of aggregate into the subgrade, and thus it is assumed that the full plastic bearing capacity of the subgrade can be mobilised in the reinforced case, offering additional resistance to the wheel-load.

As the system is loaded horizontal forces develop in the aggregate under the wheel load. This force is at a maximum under the wheel and reduces, as a result of frictional resistance at the aggregate/geosynthetic interface, to a residual value at some distance .

The frictional resistance is assumed to be provided by the geosynthetic which, given a stiffness, will generate a known strain. It is suggested that most efficient design therefore, occurs when the horizontal strain in the aggregate, caused by the wheel load, matches the strain induced in the geosynthetic, ie the pavement is fully reinforced at this point, and any difference in the geosynthetic stiffness leads to either under or over reinforcement.

Aggregate restraint is occasionally subtitled the slab effect because of the analogy that can be drawn with reinforced concrete. Like concrete, aggregate has a high compressive strength and a low tensile strength, and as with steel in reinforced concrete, the tensile forces in reinforced pavements are assumed to be taken by the geosynthetic. To continue the analogy, if one over-reinforces a slab, the deflections are low, but the collapse at failure is dramatic. Under-reinforcement yields high deformations leading to failure by serviceability criteria and not by the failure of the reinforcing elements.

2.2.3.4 Drainage

By keeping the aggregate clean the geosynthetic prevents a decrease in the permeability of the fill and hence maintains the pavement performance in wet and frosty conditions. The geosynthetic itself may improve the lateral permeability of the soil-geosynthetic-aggregate system by its own in-plane permeability or transmissivity. This reduces local pore water pressure differences in the subgrade and thereby improves the system's performance.

Improved drainage appears to be a secondary effect of separation and filtration and therefore will not be considered further.

2.2.3.5 Construction Platform

The geosynthetic increases the compacted density of the fill material by reflecting the shock waves emitted by the roller, thereby improving the properties of the aggregate that resist the deformation of the material by trafficking. Van Den Berg & Kenter (1984) suggested that the construction platform function was a mixture of lateral restraint and separation, but dismissed it as unimportant.

Field trials under taken by CIRIA and described in the Technical Note 126 (1986) showed no evidence of this. The measured compacted densities were all within experimental scatter no matter whether geosynthetic was included or not. This finding has also been noted during field trials at Bothkennar. The density and the stiffness of the aggregate in the unreinforced sections (Sections D and K) is not significantly different from the reinforced pavements as shown in Tables 3.5 and 3.8 and therefore little credence can be given to the existence of such an effect.

2.3 UNREINFORCED BEHAVIOUR

2.3.1 Introduction

The unreinforced sections at Bothkennar were designed with reference to the work of Giroud and Noiray (1981). In the analysis for unreinforced roads presented by Giroud and Noiray, reference is made to unreinforced unpaved road trials undertaken by Webster and Watkins (1977) and Webster and Alford (1978). New relationships based on their work were proposed by Giroud and Noiray which led to a simple analysis.

Time constraints at the start of the project, led to the unreinforced sections being designed on this basis. Subsequently a more in depth study of the earlier work on unreinforced pavement design has been carried out and is now discussed in detail.

2.3.2 Prediction of the number of passes of an axle to induce a 0.075m rut - a logarithmic analysis

Hammitt (1970) reported on extensive trials of unreinforced unpaved roads, where a variety of wheel loads, tyre pressures and subgrade stiffnesses were utilised. Failure of the pavements was defined as when the permanent deformation exceeded 0.075m, or the transient deformation exceeded 0.038m, when measured using a 3m straight edge.

An empirical model was developed by Ahlvin (1959) for use with flexible surfaced pavements, namely that:-

$$h = f\sqrt{\frac{P}{56CBR} - \frac{A}{\pi}} \qquad (2.1)$$

where h = thickness of the granular layer (m)

P = wheel load (kN)

f = traffic influence factor = 0.23 log N + 0.15

A = contact area (m^2)

N = The number of passes.

It should be noted that the thickness of the granular layer is a function of $\sqrt{\text{axle load}}$. A 4th power law for non-standard axle loads is not applied as is commonly assumed in pavement engineering (Giroud and Noiray (1981)). For a constant tyre pressure an increase in load will result in an increase in the contact area. Equation 2.1 therefore implies that as the axle load rises, the increase in thickness required is slightly offset by the increase in contact area.

Hammitt (1970) suggested that a similar relation for unsurfaced pavements existed and would be in the form as shown in Equation 2.2.

$$h = f' \sqrt{\frac{P}{56CBR} - \frac{A}{\pi}} \qquad (2.2)$$

where a different traffic influence factor, f ', would apply and it would be in the form log N + C. The transference of the general form of the equation, from the flexible surfaced road to the unsurfaced, should be viewed critically. The stress distribution characteristics of the two types of pavement are different, as are the modes of pavement failure. The assumption that the thickness of aggregate required is a function of the logarithm of the number of axle passes is common for surfaced pavements which tend to suffer from fatigue related failure. However, this assumption may be not valid in the case of low volume, unpaved roads.

An analysis of 59 test pavements was undertaken by Hammitt (1970). The study included data from a variety of trials where P, A, h, and N were all known. The traffic influence factor, f ', was plotted against log passes to failure and the results are shown in Figure 2.1. It should be noted that the data exhibits a large degree of scatter. Simple linear regression of the data led Hammitt to suggest that, for unreinforced roads, the thickness of the pavement required is determined by Equation 2.3.

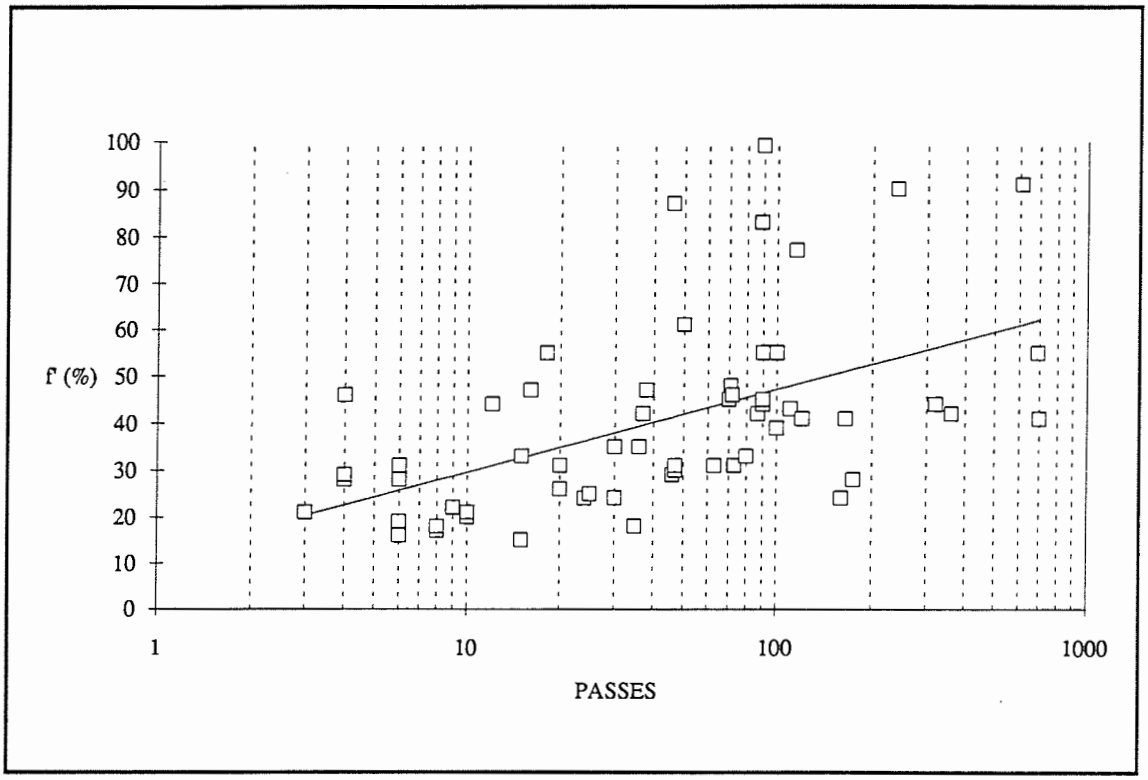

Figure 2.1 Traffic Influence Factor (f') After Hammitt (1970)

$$h = (0.176\log N_{75} + 0.12)\sqrt{\frac{P}{56CBR} - \frac{A}{\pi}} \qquad (2.3)$$

where N_{75} is the number of passes to generate a rut depth of 0.075m.

Based on this work, Giroud and Noiray (1981) suggested that an approximation for standard loading might be:-

$$h = \frac{0.19\log N_{75}}{CBR^{0.63}} \qquad (2.4)$$

Equation 2.4 is more simple and, as will be shown later, enables mixed traffic to be catered for. For a standard load it is a fair approximation to Equation 2.3, as can be seen from the examples shown in Figures 2.2 and 2.3.

2.3.3 Prediction of the design thickness for depths not equal to 0.075m - a logarithmic analysis

Experimental data on the development of rutting with application of load passes for any unreinforced unpaved road, especially for high rut depths, is sparse. Webster and Watkins (1977) examined six pavement structures to a rut depth of 275mm, only one of which was unreinforced. All of Webster and Alford's (1978) work related to reinforced pavements. However, accepting the contention that rut development is either linear with passes or the logarithm of passes of the axle, extrapolation to larger rut depths may be performed with some confidence, in the unreinforced case, because the rate of development of rut depth might be considered to be constant regardless of the rut depth. Extrapolation of reinforced pavements might, by comparison, prove to be more uncertain because there is a reliance on the geosynthetic and at large rut depths it might rupture leading to a more rapid deterioration in the pavement.

Giroud and Noiray (1981) suggested that from examination of Webster and Watkins' (1977) data Equation 2.4, could be modified by substituting Equation 2.5.

$$\log N_{75} = \log N - 2.34\,(r-0.075)\,. \qquad (2.5)$$

thus by substituting Equation 2.5 into Equation 2.4

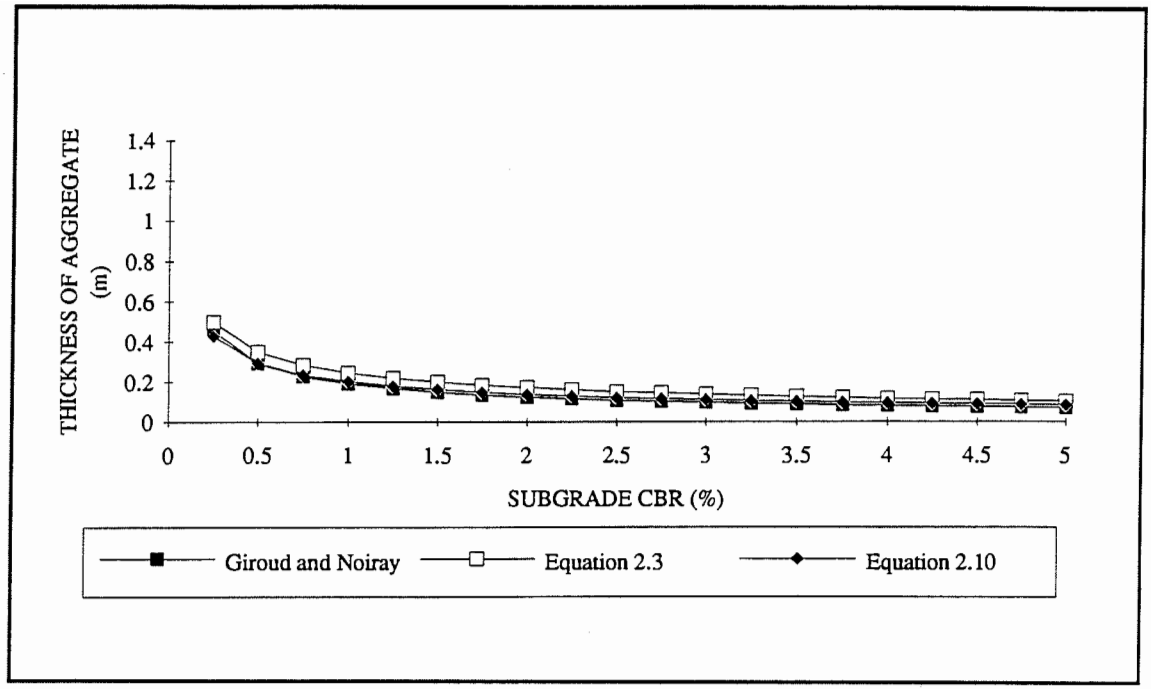

Figure 2.2 Thickness of Aggregrate Required for a 75mm Rut After 10 Passes of an 80kN Axle. After Hammitt (1970) and Giroud and Noiray (1981)

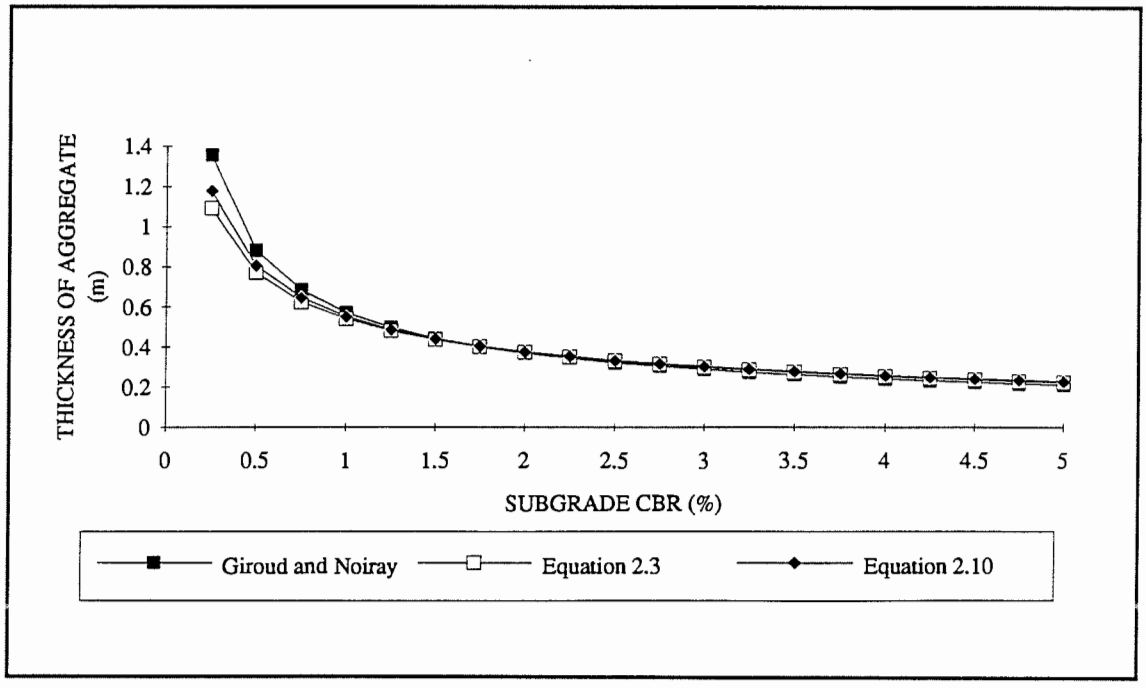

Figure 2.3 Thickness of Aggregrate Required for a 75mm Rut After 1000 Passes of an 80kN Axle. After Hammitt (1970) and Giroud and Noiray (1981)

$$h = \frac{0.19\ (\log N - 2.34\ (r-0.075))}{CBR^{0.63}} \qquad (2.6)$$

For any given CBR and N, it can be seen that h is proportional to r, as shown in Figure 2.4. Giroud and Noiray's approximation is plainly inadequate at r = 0, because no matter how large h, the passage of some axles (N), will produce some rut. Also it is possible for r to be negative such as when considering the case at Bothkennar.

example

if h = 0.4m N = 1,000 CBR = 3.5%

$$0.4 = 0.19\frac{(3 - 2.34\ (r - 0.075))}{3.5^{0.63}}$$

then

r = - 0.623m

It is possible to overcome this problem, and hence improve Giroud & Noiray's rut depth prediction at low rut depths, by replacing log N with log N_{75} as shown in Equation 2.7.

$$\log N_{75} = \frac{\log N}{\left(\frac{r}{0.075}\right)^{0.18}} \qquad (2.7)$$

Thus Equation 2.4 becomes Equation 2.8.

$$h = \frac{0.19 \log N}{CBR^{0.63}\left(\frac{r}{0.075}\right)^{0.18}} \qquad (2.8)$$

The power 0.18 has been obtained by adjusting an equation in the form of Equation 2.8 until a good fit was achieved with the data of Webster and Watkins (1977).

So, if r = 0.025m at 1000 passes of an axle then it is to be expected that a 0.075m rut will occur after N_{75} passes, defined as follows:-

$$\frac{\log 1000}{\left(\frac{0.025}{0.075}\right)^{0.18}} = \log 3.65 \text{ passes} = 4528 \text{ passes}$$

A comparison between Equations 2.6 and 2.8 is shown in Figure 2.4 based on the assumption that the CBR of the subgrade is 0.5%.

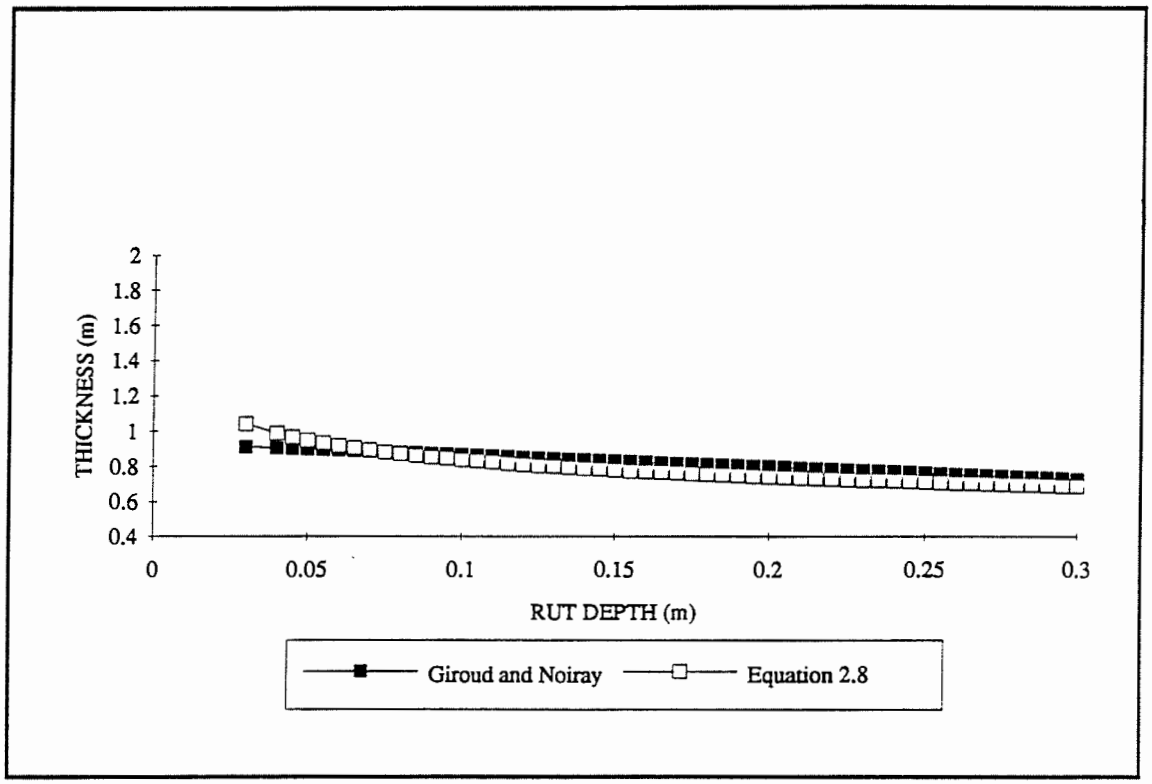

Figure 2.4 The Effect of Permissible Rut Depth on Pavement Thickness for 1000 passes of an 80kN Axle on a Subgrade CBR of 0.5% After Giroud and Noiray (1981) and Equation 2.8

The modification suggested above appears more sensible than the option proposed by Giroud and Noiray (1981) Equation 2.5 as the thickness required increases more rapidly as the permissible rut depth approaches zero. From Figure 2.4 it would appear that the modification for allowing different rut depths proposed by Giroud and Noiray (1981) is optimistic for low rut depths and pessimistic at higher rut depth. However, in the case of haul roads, serviceability criteria are unlikely to be require rut depth lower than 0.1m and therefore the change in thickness required is small, and in most cases would be lost in the inherent variability of any single trial. Thus, this new analysis predicts that some small saving in aggregate thickness could be justified in most practical cases.

2.3.4 Predicting rut depth development for a given pavement thickness - a logarithmic analysis

Giroud and Noiray (1981) suggest that the development of rutting for a given thickness of aggregate and subgrade shear strength will be governed by Equation 2.5, namely that:

$$\log N_{75} = \log N - 2.34\,(r-0.075)\,. \tag{2.5}$$

For any given pavement it can be seen from Equation 2.5 that the application of more passes will result in an increase in the rut depth, r. However, for the reasons given in 2.3.3 this formula appears unsatisfactory in some cases, and as has been previously suggested, Equation 2.5 can be improved upon by Equation 2.7.

$$\log N_{75} = \frac{\log N}{\left(\frac{r}{0.075}\right)^{0.18}} \tag{2.7}$$

From the field data of Webster and Watkins (1977), it is possible to determine Log N_{75}, which is a constant. Thus, it is possible to predict from Equations 2.5 and 2.7 the development of the rut depth and to compare it with that of the field trials, as is shown in Figure 2.5. It should be noted from Figure 2.5 that none of the plots shown suggest that a linear relationship exists between rut depth and the logarithm of passes.

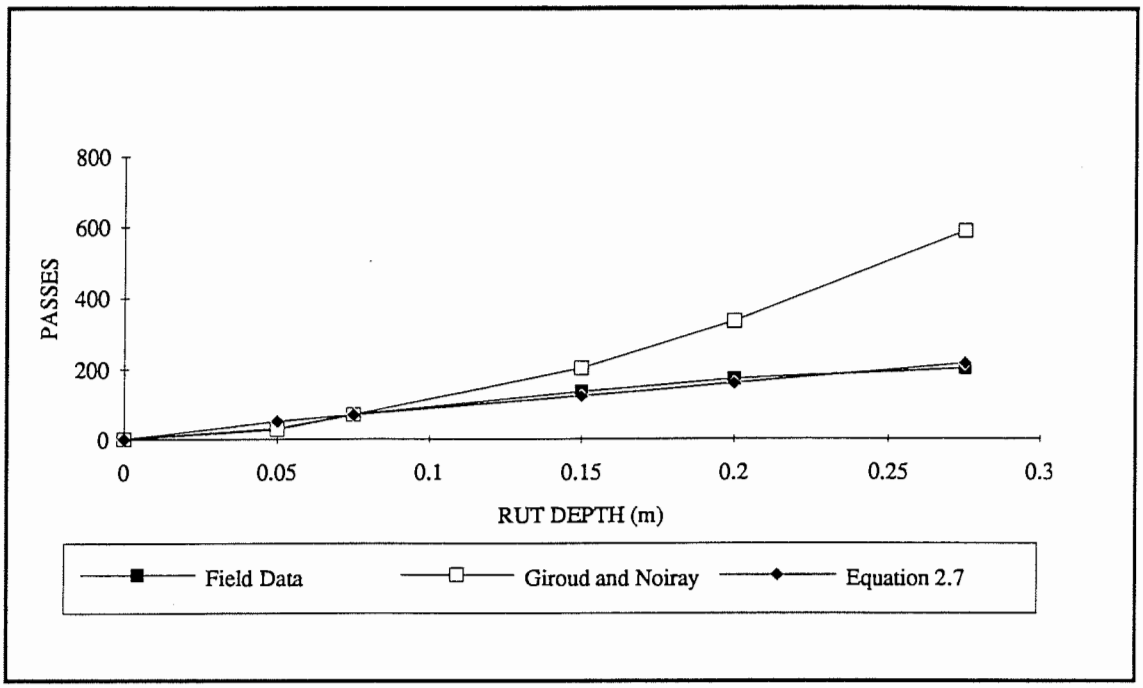

Figure 2.5 Predictions of Rut Depth Development After Field Data of Webster and Watkins (1977), Giroud and Noiray (1981) and Equation 2.11 Based on a Logarithm Passes Scale

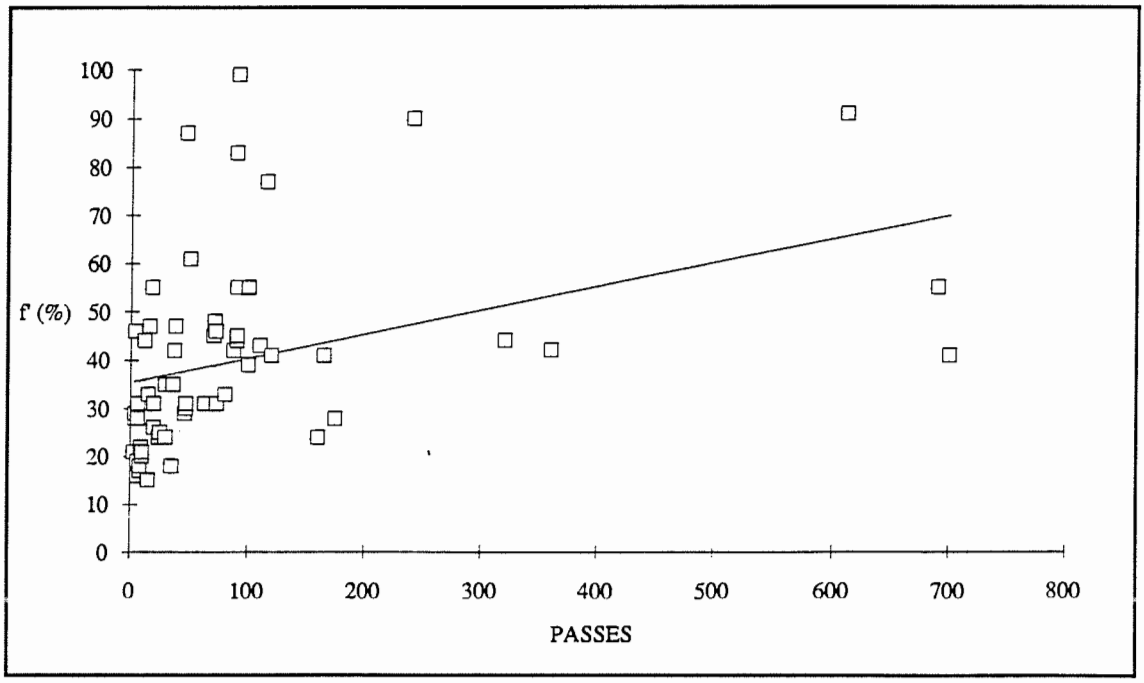

Figure 2.6 Traffic Influence Factor (f' = 0.000493N + 0.352) Plotted on a Linear Passes Scale After Hammitt (1970)

2.3.5 Prediction of the number of passes of an axle to induce a 0.075m rut - a linear analysis

There is some doubt about the validity of using an analysis based upon the logarithm of the number of passes. Hammitt's data can also be re-plotted on a natural axis, as shown in Figure 2.6, to give a relationship between rut depth and passes. On a natural passes scale it can be seen that the data is a little concentrated in the range of 0 to 200 passes. However, a linear relationship between permanent deformation and number of passes can be produced for the complete data set. Simple linear regression of Hammitt's (1970) data leads to the following relationship which appears to fit the data no less poorly than Hammitt's original proposal.

$$f' = (0.000493N + 0.352) \tag{2.9}$$

$$h = (0.000493N + 0.352)\sqrt{\frac{P}{56.1CBR} - \frac{A}{\pi}} \tag{2.10}$$

The thickness of aggregate required by Equation (2.10) is also shown in Figures 2.2 and 2.3 and as can be seen, is generates good agreement with Hammitt's original data and with the approximation of Giroud and Noiray (1981).

2.3.6 Prediction of the design thickness for depths not equal to 0.075m - a linear analysis

Equation 2.10 can be extended to examine the development of rut depths not equal to 0.075m. If it is assumed that the development of rut depth is linear with the number of passes, then N can be replaced by N_{75}

$$\text{where } N_{75} = \left(\frac{0.075}{r}\right)N \tag{2.11}$$

$$\text{then, } h = (0.000493N_{75} + 0.352)\sqrt{\frac{P}{56.1CBR} - \frac{A}{\pi}} \tag{2.12}$$

An examination of this data is shown in Figure 2.7 and it can be seen that Equation 2.12 generates a thickness requirement that is asymptotic as the permitted rut depth nears zero. It should be noted that Equation 2.12 suggests that the required

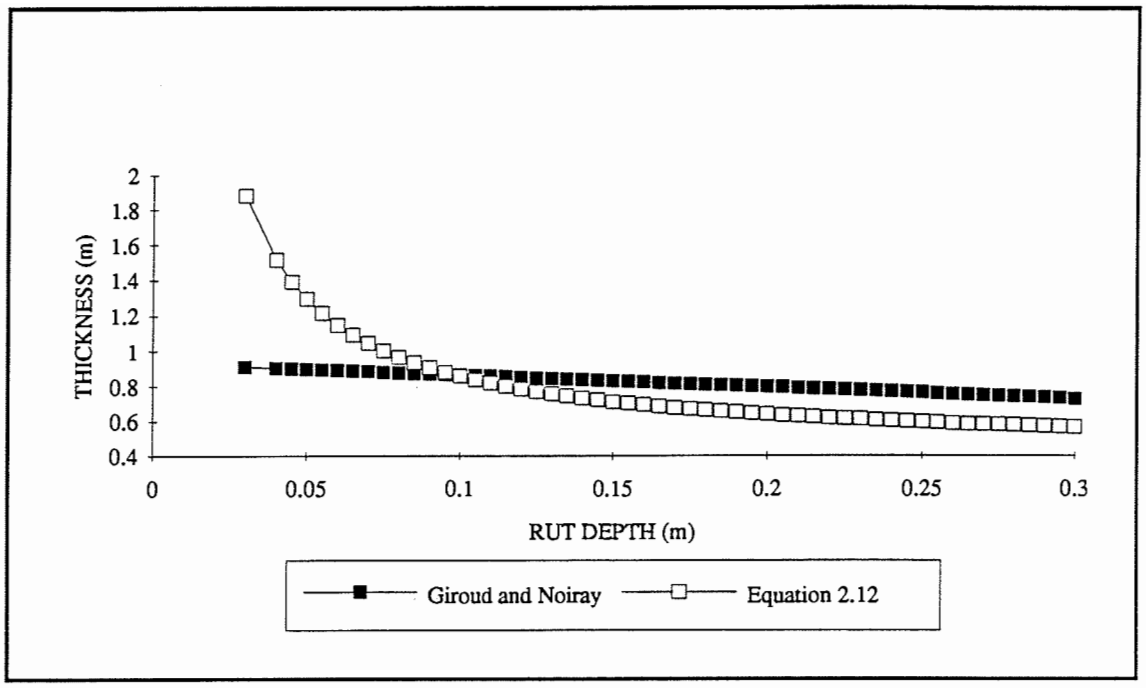

Figure 2.7 The Effect of Permissible Rut Depth on Pavement Thickness for 1000 passes of an 80kN Axle on a Subgrade CBR of 0.5% After Giroud and Noiray (1981) and Equation 2.12

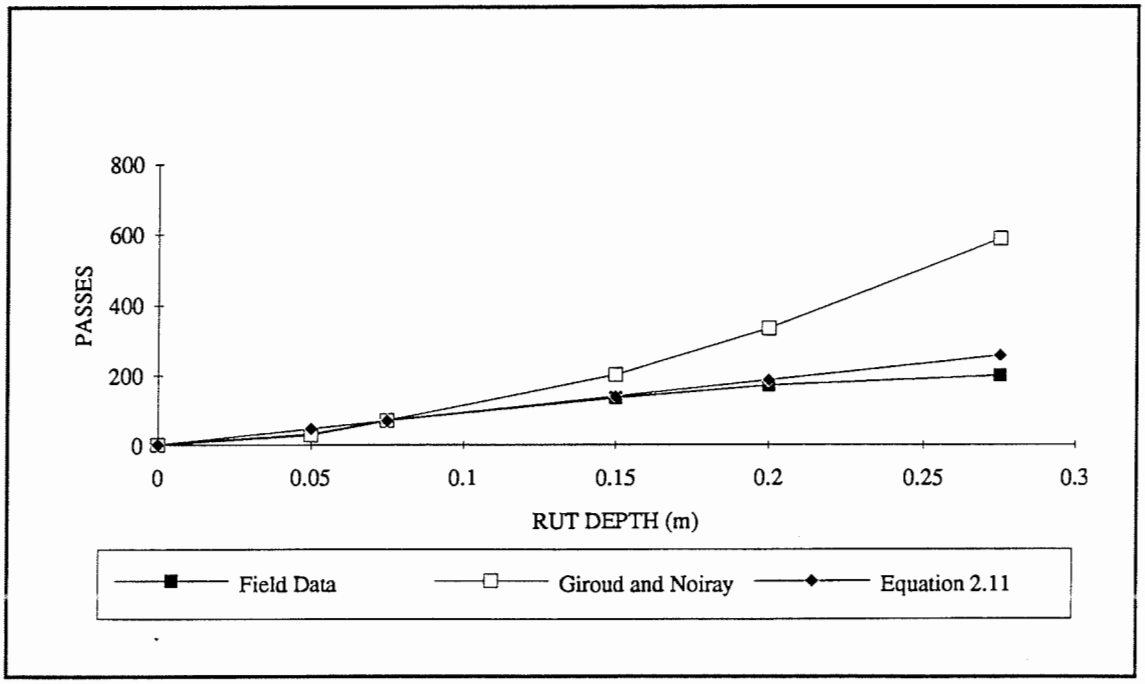

Figure 2.8 Predictions of Rut Depth Development After Field Data of Webster and Watkins (1977), Giroud and Noiray (1981) and Hammitt (1970) Based on a Natural Passes Scale

thickness rises more quickly at the low rut depth regions than suggested in Equation 2.8.

2.3.7 Predicting rut depth development for a given pavement thickness - a linear analysis

From the field data of Webster and Watkins (1977), it is possible to determine N_{75}, which is a constant. Thus, it is possible to predict from Equation 2.11 the development of the rut depth and to compare it with that of the field trials, as is shown in Figure 2.8. It should be noted, that knowing the number of passes to generate a 0.075m rut depth, Equation 2.11 accurately models the rut depth development. There is a large difference in the expected rut depth development depending on the choice of linear or logarithmic passes scale and this is shown by including in Figure 2.8 the logarithmic assumption of Giroud and Noiray (1981) (Equation 2.5) for comparison.

The concept of linear development of rut depths for unsurfaced pavements appears to hold for those pavements that include geosynthetics. Figures 2.9 and 2.10 examine data presented by Webster and Watkins (1977) for geosynthetic reinforced pavement sections. The calculated development of rut depth is based on Equation 2.11 utilising the observed deformation of the reinforced sections at a rut depth of 0.075m. The measured number of passes required to induce a 0.075m rut depth is taken as the basis of how each individual pavement will perform. As can be seen, the agreement for the woven section is excellent and is fair for the Bidim. The Giroud and Noiray (1981) prediction (Equation 2.5) is shown for comparison but, given that it was proposed assuming relationship between rutting and the logarithm of the number of passes, shows poor correlation with the observed results.

2.3.8 Comparison with model trials

Fannin (1986) performed repeated loading tests of layered systems which he presented against logarithm of cycles (Figure 2.11). However, the data can be re-plotted on a linear scale and it can be seen that with some scatter, and some initially large deformation in the first few cycles, the development of vertical permanent deformation is linear with passes (Figure 2.12).

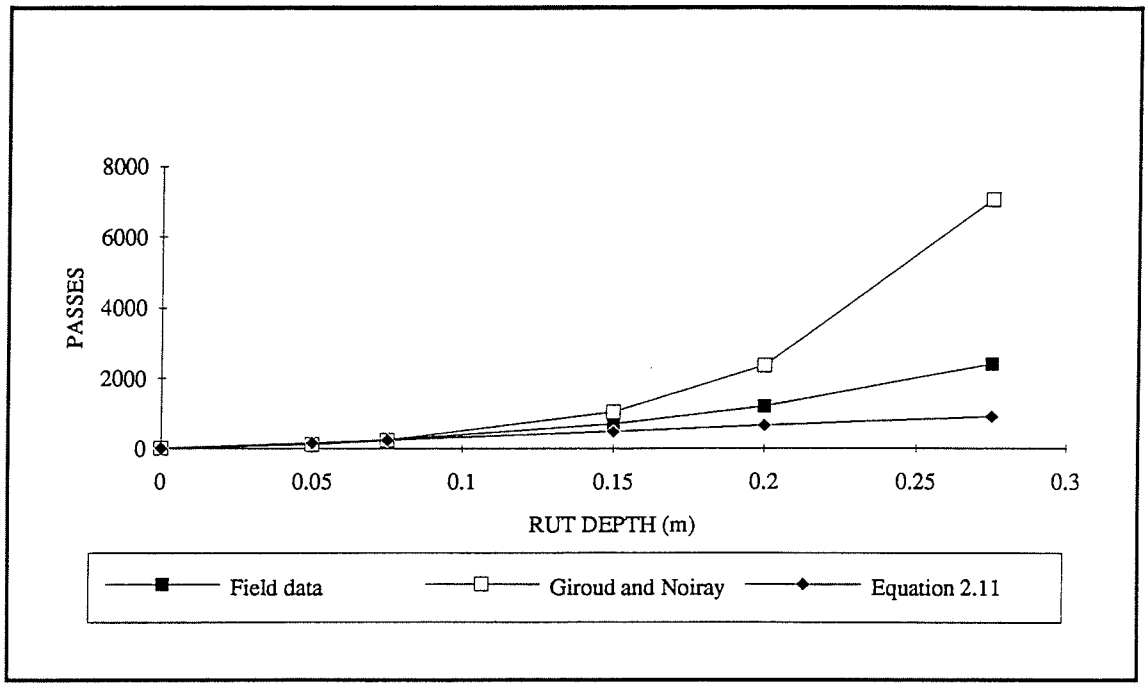

Figure 2.9 Prediction of Rut Depth Development After Giroud and Noiray (1981) and from Equation 2.11 Compared to Field Data Of Webster and Watkins (1977) - Bidim Section

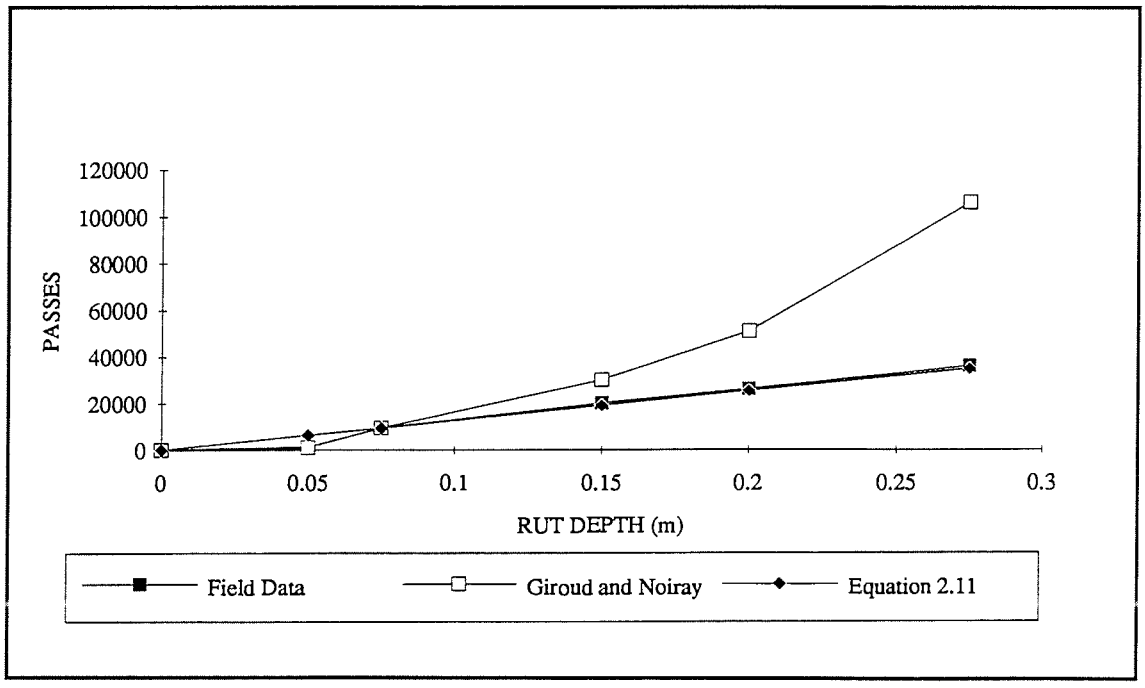

Figure 2.10 Prediction of Rut Depth Development After Giroud and Noiray (1981) and from Equation 2.11 Compared to Field Data Of Webster and Watkins (1977) - Woven Section

2.3.9 Conclusions

It would appear that rut depth development can be related to passes of an axle, not to log passes, for unpaved roads. Examination of the performance of the Webster and Watkins (1977) pavements (Figures 2.8, 2.9 and 2.10) demonstrate approximate linearity with passes as do the model tests of Fannin (1986) (Figures 2.11 and 2.12).

From the work done by Hammitt (1970) on pavements not including geosynthetics, it is possible to predict the thickness of aggregate such that a given number of passes will generate a 0.075m rut. This formula has been modified to a linear relationship which appears to fit the data more closely.

The variation of geosynthetic properties will prevent the empirical prediction of the number of passes required for a given rut depth for reinforced pavements, as utilised for the unreinforced case. However, it has been demonstrated from Webster and Watkins (1977) reinforced trials that the rut depth development, for reinforced pavements, is also linear with passes.

2.4 EMPIRICAL REINFORCED PAVEMENT DESIGN

2.4.1 Overview

The design of geosynthetic reinforced unpaved roads by empirical, or semi-empirical methods is common. All of the non-woven geosynthetic manufacturers represented at the Bothkennar trials, utilise these approaches to design. It would appear that this reliance on empirical data is a function of the fact that it is difficult to demonstrate, analytically, how observed improvements in performance occur. Resl & Werner (1986) explained these benefits in terms of the separation and filtration functions of these materials.

2.4.2 Purely empirical approach

The simplest method of empirical design is to examine case histories and choose a design based upon experience. The Comité Français des Geotextiles (1981) produced 88 variations of possible designs, based on traffic type, axle loads, permissible rut

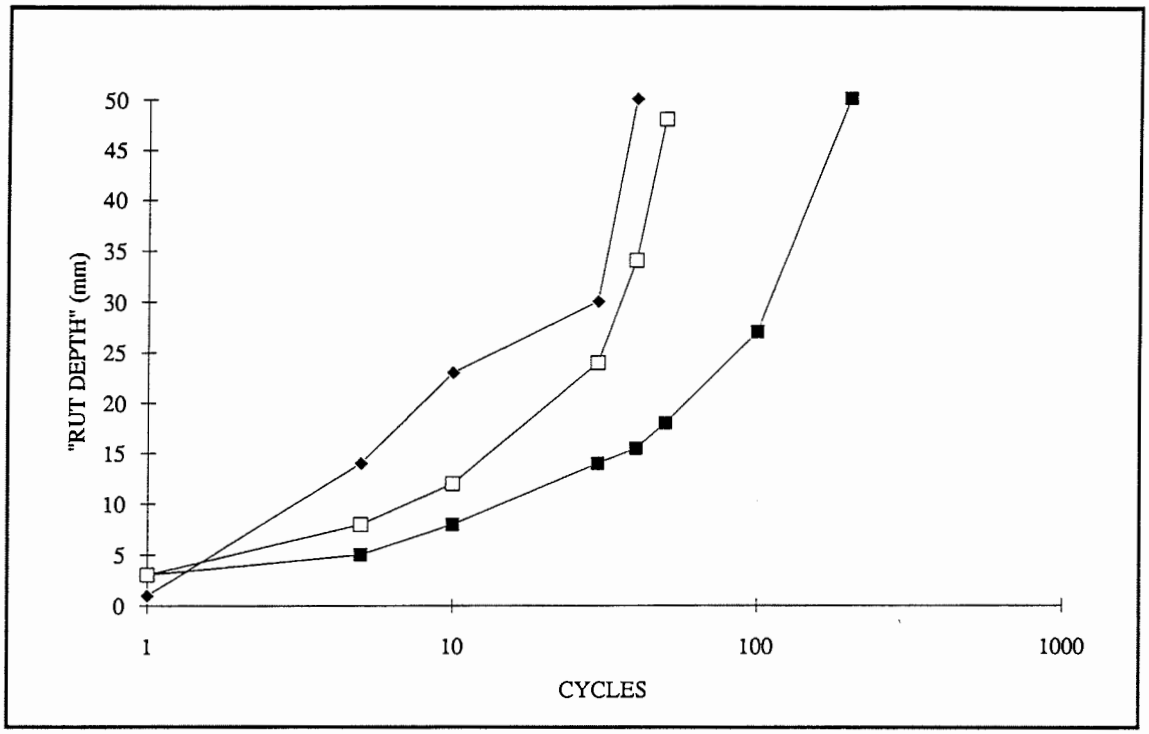

Figure 2.11 Model Data of Fannin (1986)
Unreinforced Tests Plotted against Logarithm Cycles

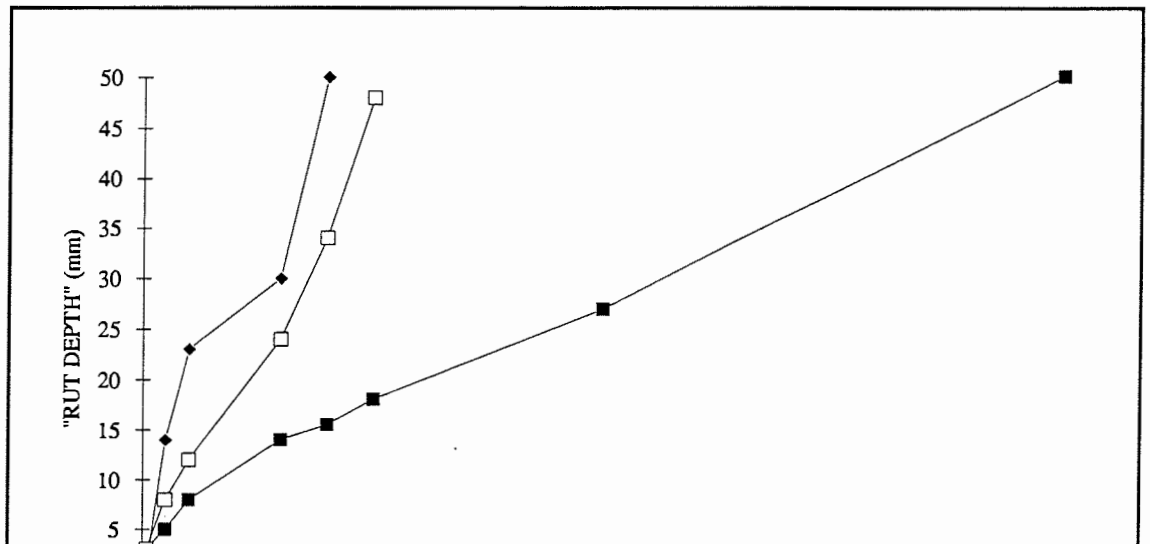

Figure 2.12 Model Data of Fannin (1986)
Unreinforced Tests Plotted against Cycles

depth, subgrade CBR, thickness of granular layer and fill type. On comparison of the specific design requirements with the example which most closely matches these case studies, the required physical characteristics of the geosynthetic are given.

This type of method has many draw backs in that it is restricted to the field of experience to date, is unable to predict the effects of changing the material properties of the system and is unable, analytically or empirically to demonstrate the advantage of including a geosynthetic. However, it does give a simple to use rough-and-ready approach to design and given that the design of haul roads is not an exact science this quick method may be as good as any.

2.4.3 Semi-empirical approach

Resl & Werner (1986) noticed that the inclusion of geosynthetics in the soil-geosynthetic-aggregate system improves the bearing capacity. Although they were unable to explain this improvement in any analytical terms, they recognised that the inclusion affected the failure mechanism of the system.

A series of plate bearing tests utilising a specific geosynthetic and comparisons with the control case yields design charts for the thickness of material required to withstand the application of one load cycle. This thickness is then modified to take account of the many repetitions of load, by reference to the Comité Français des Geotextiles (1981) or similar.

While this technique demonstrates the value of including a geosynthetic, the manner in which it does so must be questioned. The mechanisms of failure in the single plate loading test are likely to be different to those occurring under the repeated loading of in-field service conditions. Under normal contact stresses, the surface transient deformations are not altered by the inclusion or otherwise of the geosynthetic (Sellmeijer (1990)) and neither is the stiffness of the pavements (King (1990)).

Because it is believed that separation and filtration are significant factors in the design of unpaved roads using "low" stiffness geosynthetics, design methods for these products often carefully check the survivability of the geosynthetic during the construction and trafficking process and the hydraulic properties required by the geosynthetic. It is obvious that the inclusion must remain integral if it is to act as a

separator in the pavement and should not have an adverse effect on local pore water pressures that might develop during transient loading. However, if the value of low stiffness geosynthetics in unpaved roads is to demonstrated, some analytical or empirical method for determining the value of separation to the pavement needs to be developed.

2.5 GIROUD & NOIRAY (1981) DESIGN APPROACH

2.5.1 Overview

The design method of Giroud and Noiray (1981) is a static analysis of pavements with and without geosynthetic reinforcement. The stress applied to the aggregate surface by the wheel load is transferred to the subgrade via a load spreading angle (α) leading to a rectangular stress distribution on the surface of the subgrade.

In the unreinforced case the maximum stress permissible on the subgrade is the elastic bearing capacity,(πS_u) whereas in the reinforced case the plastic bearing capacity ($(\pi+2)S_u$) provides the limit. It is this change in bearing capacity which generates most of the benefit produced by including the geosynthetic, however, some of the benefit is attributed to "the membrane effect". "The membrane effect" suggests that the vertical stress imposed upon the subgrade is reduced by examining the vertical component of the stress in the geosynthetics shown in Figure 2.13 which, in turn, is generated as the geosynthetic is stretched as it is passed downwards - like a membrane.

A saving of aggregate for the reinforced over the unreinforced case is calculated and the benefit leads to a reduction in the thickness of aggregate normally required for unreinforced design on the basis of empirical data.

2.5.2 Calculation

The stress distribution is assumed to be of the form shown in Figure 2.14

It can be seen that the stress applied at the base of the aggregate layer is given by Equation 2.13.

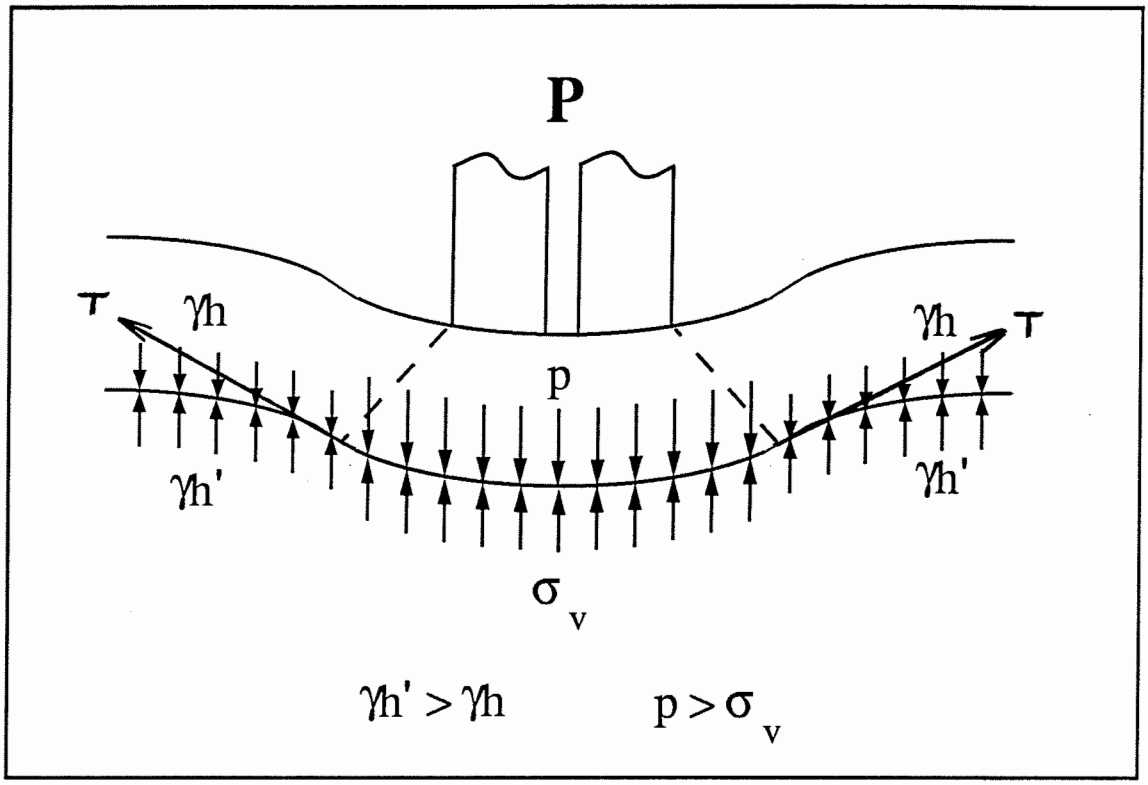

Figure 2.13 The Membrane Effect - After Giroud and Noiray (1981)

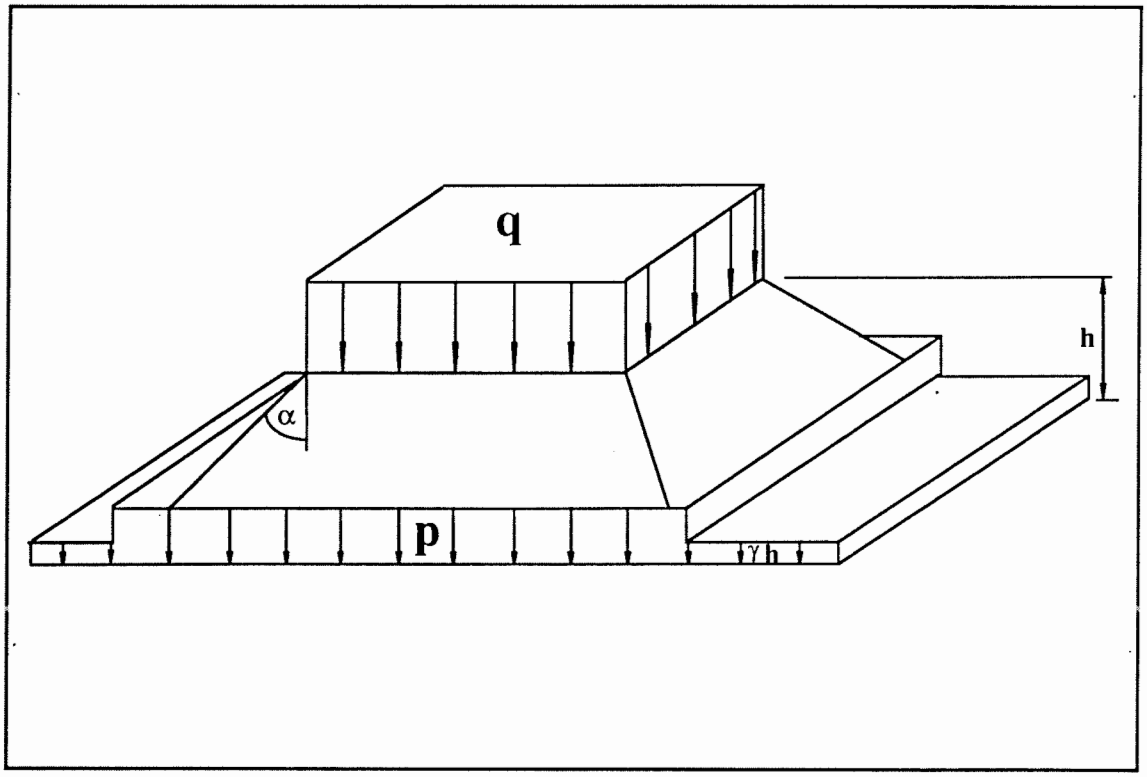

Figure 2.14 Stress Distribution - After Giroud and Noiray (1981)

$$\Delta\sigma_v = \frac{P}{(W+2h\tan\alpha)\,(L+2h\tan\alpha)} + \gamma h \qquad (2.13)$$

The thickness of the aggregate (h) varies in the reinforced and unreinforced cases. Given that the internal angle of friction for the aggregate is ϕ, a suggested value for α is given as $\pi/4 - \phi'2$, representing the inclination of the shear planes which would occur if the aggregate layer was failed by punching. A characteristic value of α is taken, such that $\tan\alpha = 0.6$, which implies ϕ' is approximately 30°. The load spread angle is deemed not to change from the unreinforced to the reinforced case.

2.5.2.1 Unreinforced analysis

If the deflections of the subgrade are to be small then the pressure exerted on it must be limited by the elastic bearing capacity, q_e, such that:

$$\Delta\sigma_v = q_e + \gamma h = \pi S_u + \gamma h \qquad (\gamma h = \text{the adjacent overburden stress})$$

and by combining this with Equation 2.13 above

$$\pi S_u = \frac{P}{(W+2h\tan\alpha)(L+2h\tan\alpha)} \qquad (2.13a)$$

Thus a solution to h can be found.

2.5.2.2 Reinforced Analysis

In the reinforced case the stress imposed upon the subgrade is permitted to rise to the ultimate, or plastic value of $(\pi+2)=S_u$. The change in the value of bearing capacity adopted is not properly justified, but it will be shown later that the inclusion of the geosynthetic alters the nature of the stresses applied to the subgrade and in the reinforced case a bearing capacity of $(\pi+2)S_u$ is a fair assumption.

Therefore, in the reinforced case the maximum stress that can be imposed upon the subgrade is $(\pi+2)S_u + \gamma h$, and it is this change in bearing capacity, from πS_u in the unreinforced case, which produces most of the benefit from including the geosynthetic.

However, at large rut depths, the membrane effect will start to affect the stress on the surface of the subgrade. Thus the maximum permissible stress at the base of the aggregate layer can exceed the maximum permissible on the surface of the subgrade such that:

$$\Delta\sigma'_v = \Delta\sigma_v + p_r \tag{2.14}$$

where p_r is the reduction in vertical subgrade stress attributable to the membrane effect.

Unlike some of the more analytical design methods, where the shape of the membrane is described mathematically, the membrane is assumed to deform to a parabolic shape. The strain, and therefore stress, induced in the geosynthetic is calculated by utilizing the properties of parabolas. The geosynthetic is assumed to take a concave parabolic shape under the wheel of length 2a and a convex shape between the wheels of length 2a', as shown in Figure 2.15.

Two possible outcomes now occur, either a'> a or a'< a:

If a' > a

then half the area displaced by the vertical movement equals half the area increased in the hog between the wheels. From the known properties of parabolas, the area displaced from under the wheel is such that

$A=\frac{2as}{3}$ and the area added to between the wheels, $A', =\frac{2a'(r-s)}{3}$ (2.15)

The vertical displacement (s) under the wheel is found by equating the two areas

$$s = \frac{ra'}{a+a'} \tag{2.16}$$

If a > a'

then less than half the area displaced by the vertical movement contributes to the hogging.

$$s = \frac{ra^2}{2a^2 + 3a\ a'\ a^2} \tag{2.17}$$

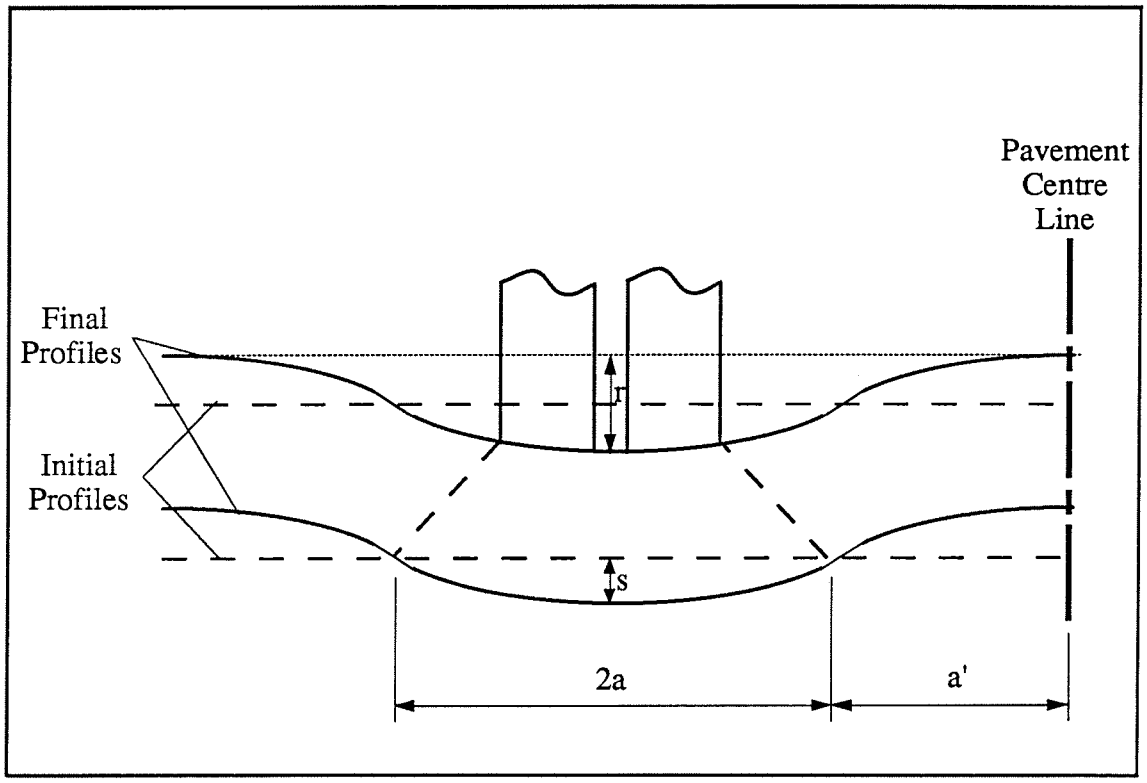

Figure 2.15 Geometry of the Deformed Profile
After Giroud and Noiray (1981)

If a' > a this leads to $\frac{s}{a'} > \frac{(r - s)}{a'}$ therefore the elongation and thus the tension under the wheels is greater than the tension between them. As a result the textile moves as the overburden masses are too small to generate enough friction to resist the horizontal forces. The authors then make the assumption that therefore the geosynthetic must be under constant tension and elongation.

$$\varepsilon = \frac{b + b'}{(a + a')} \tag{2.18}$$

b = final textile length of geosynthetic in the loaded are
b' = final textile length between the wheels.

Using parabolic relationships of arcs and cords of parabola the authors get strain terms of a, r and s for both under the wheel and in between them.

If a > a' then $\frac{(r - s)}{a'} > \frac{s}{a}$ and as a consequence, the tension between the wheels is greater than under them, but it is assumed that no slip occurs because the normal stresses under the wheel prevents slippage.

The reduction in the pressure on the subgrade can be calculated by examining the angle the geosynthetic makes to the vertical (β) at the edge of the loaded area.

$$ap = T\cos\beta \tag{2.19}$$

according to the theory of the parabolas: $\tan\beta = \frac{a}{4s}$ and as the tension $T = k\varepsilon$.

$$p_r = \frac{E\varepsilon}{a\sqrt{1 + \left(\frac{a}{2s}\right)^2}} \tag{2.20}$$

Thus the stress permitted at the top of the aggregate layer is controlled by Equation 2.21.

$$(\pi + 2)S_u = \frac{P}{(W + 2h\tan\alpha)\,(L + 2h\tan\alpha)} - \frac{E\varepsilon}{a\sqrt{1 + \left(\frac{a}{2s}\right)^2}} \tag{2.21}$$

This leads to a required thickness of aggregate, h. By comparison to Equation 2.13a a saving of aggregate by including a geosynthetic is calculated and this saving is applied to the design of unreinforced pavements as calculated by reference to the work of Hammitt (1970). It must be highlighted that the thickness of aggregate, h, is that thickness required to resist the single application of a wheel load. The actual thickness required in any given pavement will be increased to allow for the affects of trafficking.

2.5.3 Example calculation

2.5.3.1 Unreinforced Case

$$\pi S_u = \frac{P}{(W + 2h_o\tan\alpha)\,(L + 2h_o\tan\alpha_o)} + \gamma h_o$$

$$W = \sqrt{\frac{P}{Pc}} = \sqrt{\frac{80}{500}} = 0.4\text{m}$$

$$L = \frac{W}{\sqrt{2}} = 0.283\text{m}$$

say $\tan\alpha = 0.6$ & $\gamma = 20\text{kN/m}^3$

$$45\pi = \frac{80}{2(0.4 - 1.2h_o)\,(0.283 + 1.2h_o)} + 20h_o$$

therefore $h_o = 0.168\text{m}$

2.5.3.2 Reinforced Case

Say $r = 0.15\text{m}$ $\quad h = 0.25\text{m}$ $\quad \tan\alpha = 0.6$

$$a = \frac{W}{2} + h\tan\alpha = 0.35\text{m}$$

$$a' = \frac{e}{2} - a = 0.6\text{m as } e = 1.8\text{m as } a' > a$$

$$s = \frac{ra'}{a + a'} = 0.095\text{m}$$

CALCULATION OF GEOSYNTHETIC STRAIN

From the properties of parabolas it can be shown that under the loaded area:-

$$\frac{b}{a} - 1 = \frac{1}{2}\left[\sqrt{1 + \left(\frac{2s}{a}\right)^2} + \frac{a}{2s} \ln\left(\frac{2s}{a} + \sqrt{1 + \left(\frac{2s}{a}\right)^2}\right) - 2\right] \qquad (2.21a)$$

$$= \frac{1}{2}(1.137 + 0.956 - 2)$$

$$b = 0.383m$$

Similarly in the area between the wheel paths:-

$$\frac{b'}{a'} - 1 = \frac{1}{2}\left[\sqrt{1 + \left(\frac{2(r-s)}{a'}\right)^2} + \frac{a'}{2(r-s)} \ln\left(\frac{2(r-s)}{a'} + \sqrt{1 + \left(\frac{2(r-s)}{a'}\right)^2}\right) - 2\right]$$

$$= \frac{1}{2}(1.016 + 0.995 - 2)$$

$$b' = 0.607m$$

$$\varepsilon = \frac{b + b'}{a + a'} - 1$$

$$\varepsilon = \frac{0.607 + 0.383}{0.95} - 1 = 4.2\%$$

$$p_r = \frac{k\varepsilon}{a\sqrt{1 + \left(\frac{a}{2s}\right)^2}}$$

From Tensar SS2 specification ref 3/84, "Tensar test methods and physical properties of Tensar Geogrids" (undated)

$$k\varepsilon \text{ @ } 4\% = 21kN/m$$

$$p_r = \frac{21}{0.538} = 39kPa$$

$$(2 + \pi)Su = \frac{P}{(B + 2h\tan\alpha)(L + 2h\tan\alpha)} - p_r$$

$$(2 + \pi)\ 45 = \frac{80}{(0.4 + 1.2h)\ (0.283 + 1.2h)} - 39.0$$

$$(0.4 + 1.2h)\ (0.283 + 1.2h) = 2\ \frac{80}{((2 + \pi)\ 45 + 39.0)} = 0.148$$

$$-\ 0\ 0.35 + 0.48h + 0.340h + 1.440h^2 = 0$$

therefore, h = 0.040m

Thus, the saving of aggregate possible by including the geosynthetic, Δh, is given by:

$$\Delta h = h - h_o = 0.168 - 0.040 = 0.128m$$

2.5.3.3 Unreinforced Case (Giroud and Noiray (1981))

$$h'_o = \frac{119.24 \log N + 470.98 \log P - 279.0r - 2283.34}{S_u^{0.63}}$$

N = 1,000 P = 80,000N r = 0.15m S_u = 45kPa

therefore, h'_o = 0.400m

Thus, for SS2 Design thickness = $h'_o - \Delta h = 0.400 - 0.128 = 272m$

2.6 "OXFORD" METHOD After Milligan et al (1989a)

2.6.1 Overview

The majority of the improvement in performance predicted by the Giroud and Noiray (1981) design method, was caused by the arbitrary shift from a bearing capacity of πS_u in the unreinforced case to $(2 + \pi)S_u$ in the reinforced. Milligan et al (1989a) noted that when a vertical load is applied to the surface of a granular layer over a finite width, an increase in horizontal compressive force is caused at the base of the layer. They suggest that these horizontal forces are partly resisted by earth pressures and partly shear stresses on the aggregate/subgrade interface. Shear stresses on the surface of the

subgrade can reduce the bearing capacity by up to one half of the value that could be obtained for purely vertical loading. If the inclusion of a geosynthetic leads to the transferring of the shear stress which would otherwise have been carried by the subgrade to the geosynthetic, then purely vertical forces are transferred to the subgrade below. Thus, the full bearing capacity can be mobilized in the reinforced case.

2.6.2 Calculation

2.6.2.1 Bearing Capacity

If the shear stress at the aggregate/subgrade interface is τ and the vertical subgrade stress under the wheel load is σ_v, and away from the wheel load γh, then solution of the upper and lower bound theorems of plasticity theory gives the exact solution.

$$\frac{\sigma_v - \gamma h}{S_u} = N_{ca} = 1 + \frac{\pi}{2} + \cos^{-1}\psi + \sqrt{1 - \psi^2} \qquad (2.22)$$

where $\psi = \frac{\tau}{S_u}$

It should be noted that when the shear stress applied to the surface of the subgrade, τ, equals 0, $\psi = 0$ and so $N_{ca} = (2 + \pi)S_u$, and that when $\tau = S_u$, $\psi = 1$ and so

$$N_{ca} = \left(1 + \frac{\pi}{2}\right) S_u.$$

It can be seen that Giroud and Noiray's (1981) assumption that the bearing capacities of πS_u in the unreinforced case and $(2 + \pi)S_u$ in the reinforced, bear remarkable similarities to this more rigourous treatment of the subgrade properties.

However, a range of possible subgrade shear forces are possible depending upon the geometry and properties of the system and therefore a range of values of ψ, and thus bearing capacities, are permissible. These are shown in Figure 2.16.

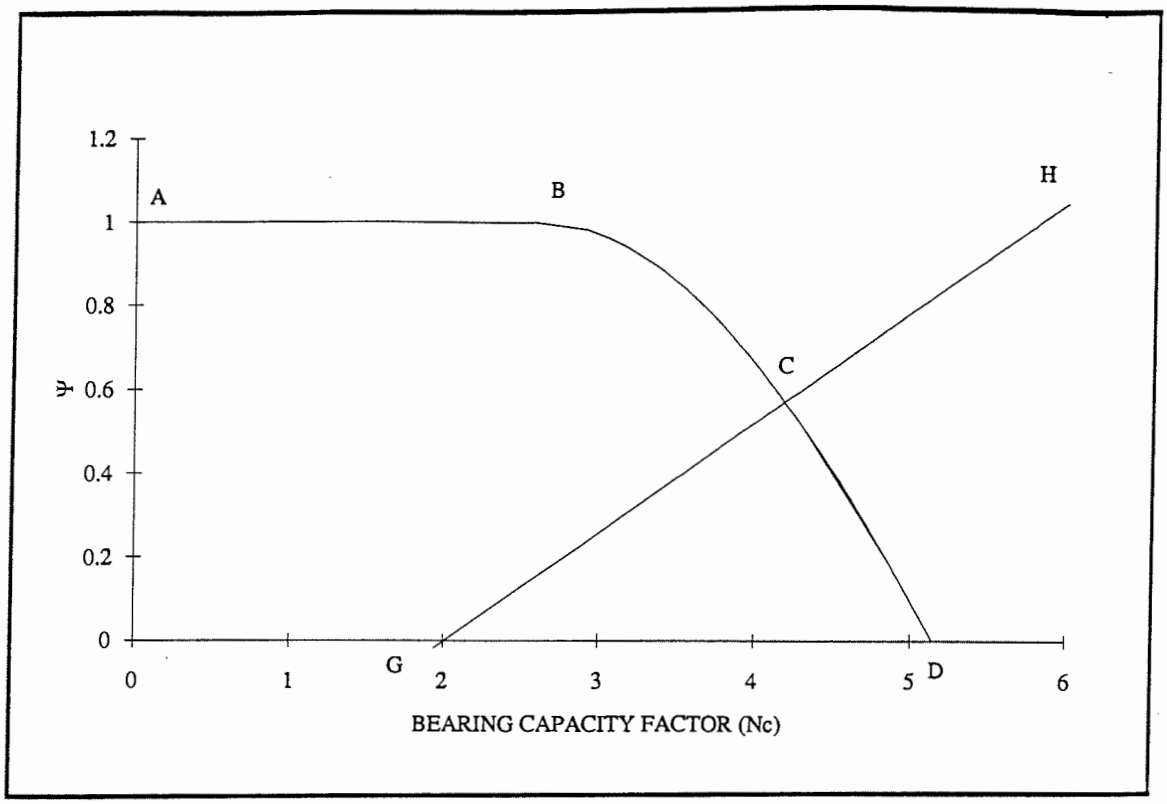

Figure 2.16 Interaction Diagram - After Milligan et al (1989a)

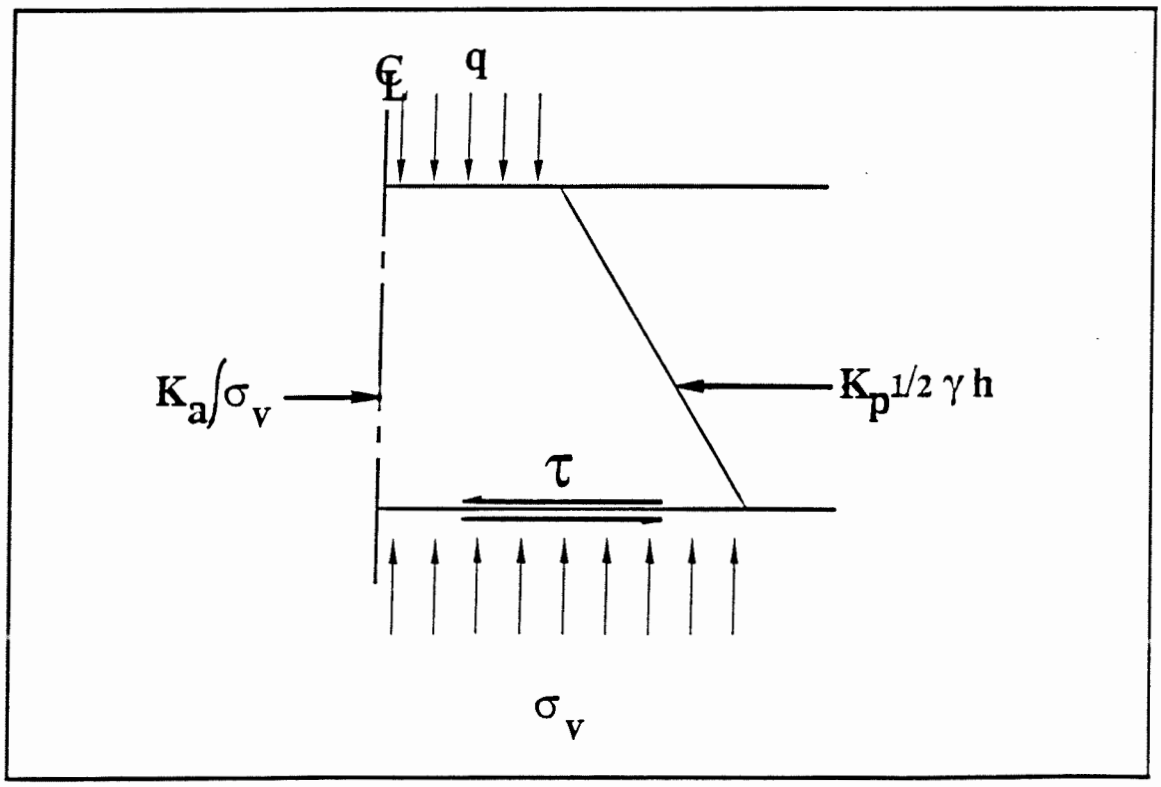

Figure 2.17 Stress Distribution - After Milligan et al (1989a)

2.6.2.2 Stress distribution through the granular layer.

Figure 2.17 shows the stress distribution through the aggregate layer. It should be noted that a load spread angle (α) is utilised which yields a stress imposed upon the subgrade (σ_v) of:-

$$\sigma_v = h + q\left(\frac{W/2}{W/2 + h\tan\alpha}\right) \qquad (2.22a)$$

where W = footing width
q = contact stress

As can be seen in Figure 2.17, active earth pressures are developed along the centre line as the driving force of the wheel load attempts to move the aggregate out of the wheel path.

If the active earth pressure co-efficient, K_a, is defined such that:

$$K_a = \frac{1 - \sin\phi}{1 + \sin\phi}$$

Then it can be seen that the force on the surface AD is given by Equation 2.23.

$$K_a \int \sigma_v \, dh \qquad (2.23)$$

By substituting Equation 2.22a into Equation 2.23 it can be seen that:

$$K_a \int_0^h \sigma_v dh = \tfrac{1}{2} K_a \gamma h^2 + \frac{K_a q W/2}{h\tan\alpha} \ln\left(\frac{W/2 + \tan\alpha}{W/2}\right) \qquad (2.24)$$

These active forces are resisted by both the passive resistance and the shear forces at the aggregate/subgrade interface. The passive resistance is a maximum at the base of the aggregate layer and is described as $\frac{1}{2}K_p \gamma h^2$ where the passive earth pressure coefficient, K_p, is defined such that:

$$K_p = \frac{1 + \sin\phi}{1 - \sin\phi}$$

So, as the shear stress at the aggregate/subgrade interface is the difference of the active and passive forces:

$$\tau(W/2 + h\tan\alpha) = \tfrac{1}{2}(K_a - K_p)\gamma h^2 + \frac{K_a q W/2}{\tan\alpha} \ln\left(\frac{W/2 + \tan\alpha}{W/2}\right) \qquad (2.25)$$

By taking the minimum value of active force and the maximum value of passive force, Equation 2.25 provides a means of obtaining represents the minimum value of τ generated. However, passive forces usually require large strains to mobilize maximum values so it would appear likely that the value of the shear stresses will be higher.

Equation 2.25 can be expressed in a non-dimensional form by the substitutions $\psi = \frac{\tau}{S_u}$.

$$\text{and } N_c = \frac{q W/2}{S_u (W/2 + h\tan\alpha)}$$

Thus, Equation 2.25 becomes:

$$\psi = \tfrac{1}{2}(K_a - K_p)\frac{\gamma h^2}{S_u (W/2 + h\tan\alpha)} + N_{cr}\left[\frac{K_a}{\tan\alpha} \ln\left(\frac{W/2 + h\tan\alpha}{W/2}\right)\right] \qquad (2.26)$$

which is the line GCH in Figure 2.16

For the unreinforced case, the appropriate design occurs at the largest available value of N_c, which occurs at the intersection point C. Having found the mobilized value for N_c the permissible surface stress, q, can be calculated as:-

$$q = N_c S_u \left(\frac{W/2 + h\tan\alpha}{W/2}\right) \qquad (2.27)$$

In the fully reinforced case the subgrade is subject to pure vertical loading and thus N_c takes a maximum value of $2 + \pi$ and q is determined by Equation 2.27 using $N_c = 2 + \pi$.

The tension in the reinforcement should be calculated at $T = \tau (W + h\tan\alpha)$.

2.6.3 Example calculation

Assuming $W/2 = 0.16$ $\quad h = 0.4$ $\quad \tan\alpha = 0.6$

then $W/2 + h\tan\alpha = 0.40$

further, assuming $\phi = 45°$ $\quad S_u = 45kPa$ $\quad \gamma = 21kN/m^3$

$$K_a = \frac{1 - \sin\phi}{1 + \sin\phi} = 0.17$$

$$K_p = \frac{1}{K_a} = 5.83$$

$$\psi = \frac{1}{2}(K_a - K_p)\frac{\gamma h^2}{S_u (W/2 + h\tan\alpha)} + N_c\left[\frac{K_a}{\tan\alpha} \ln\left(\frac{(W/2 + h\tan\alpha)}{W/2}\right)\right] \quad (2.26)$$

$$\psi = -0.53 + 0.26N_c$$

The line $\psi = -0.53 + 0.26N_c$ is plotted as the line GCH on Figure 2.16.

As can be seen, the intercept C occurs at $N_c = 4.19$, and substitution into Equation 2.27 yields q = 471kPa in the unreinforced case. In a fully reinforced pavement the bearing capacity factor is given at $2 + \pi = 5.14$ and so the permissible surface stress q = 570kPa for the reinforced case.

It should be noted that at N = 5.14, $\psi = 0.82$.

Tensile force (T) in the geosynthetic $= 0.82S_u (W/2 + h\tan\alpha)$,
$= 14.8kN/m.$

At Bothkennar the contact stress was 500kPa so the design values calculated above are not realistic they grossly underestimate the traffic which may be carried. So it can be seen from the above calculations that the assumption that unpaved road design can be equated to strip footing design is not valid. In the axisymmetric case (Milligan et al (1989b)), the three dimensional load spreading reduces vertical stresses more rapidly, the bearing capacities are somewhat higher and the passive pressures from the fill have greater influence. This may give a more viable result.

Without the aid of finite element packages, it would appear prudent to use this design method to calculate the savings of aggregate that are possible, through reinforcement, over the unreinforced case. These savings can be calculated as follows:

The required thickness of the unreinforced pavement should be calculated according to Hammitt (1970) and for the sake of this example it is assumed that the unreinforced design thickness is 0.400m. As can be seen from the above analysis, the maximum permissible contact stress in the unreinforced case is 471kPa. In order to calculate an aggregate saving, the reinforced pavement must also have a maximum permissible contact stress of 471kPa. Thus if N_c is 5.14 in the reinforced case it can be seen from Equation 2.27 that the require thickness of aggregate can be found.

$$q = 5.14S_u\left(\frac{W/2 + h\tan\alpha}{W/2}\right) \tag{2.27}$$

$$471 = 5.14 \times 45\left(\frac{0.16 + h \times 0.6}{0.16}\right)$$

and therefore h = 0.275m and thus an aggregate saving of 0.125m is possible.

2.7 SELLMEIJER (1990)

2.7.1 Overview

The Sellmeijer (1990) model presents a method of calculating the deflection under the wheel load, by examining the shear modulus of the aggregate layer and by solving the deflection equation. Sellmeijer argues that the stiffness of the aggregate layer far exceeds that of even the stiffest geosynthetics and therefore the inclusion does not directly improve the performance. However, there is a recognition that the inclusion improves the bearing capacity of the subgrade, but the failure stresses used are not defined.

The required properties of the geosynthetic are determined by considering the strain compatibility of the system. Under the vertical stresses imposed by the wheel load horizontal stresses are generated. This stress is at its maximum under the wheel and reduces to a residual value at some point away from the concentration of vertical load. This change of horizontal stress results from the frictional resistance at the

aggregate/geosynthetic interface generating forces, and hence strains, in the geosynthetic.

The change in horizontal stress also generates horizontal strains in the aggregate layer and, according to Sellmeijer, the most efficient design occurs when the strains in the geosynthetic and aggregate are matched, which yields a well defined stiffness requirement from the calculated stresses and strains in the geosynthetic.

2.7.2 Stress distribution and geometry

The stress distribution on an element is shown in Figure 2.18. It can be seen that the aggregate is assumed to deform, resisted by the shear modulus of the aggregate. Furthermore, there is assumed to be a friction component between the aggregate and the geosynthetic and cohesion and friction components between the subgrade and the geosynthetic.

The geometrical layout is shown in Figure 2.19. The length over which the vertical subgrade stress, σ_v, acts is determined by vertical equilibrium. The concept of a load spread angle is not utilised and indeed if the subgrade shear stress, S_u, is high enough the length b could be less than the width of the surface loaded area. The contact stress, q, is assumed, for the purposes of analysis, to act on the geosynthetic over the same length as at the surface.

The shape of the deformed pavement is controlled by the shear modulus of the aggregate and can be found by the solution of Equation 2.28, the derivation of which comes from an examination of Figure 2.18 and is shown in Appendix F.

$$Gh \frac{d^2y}{dx^2} = \Delta\sigma_v - q \qquad (2.28)$$

It can be seen from Equation 2.28 that the solution will generate a catenary type of curve. It should be noticed that the deformation is controlled by shear modulus of the aggregate, G, and that no properties of the geosynthetic are considered. However, the inclusion is assumed to give a higher permissible value of subgrade vertical stress, σ_v, as in pavements including geosynthetics, Sellmeijer (1990) argues, a plastic bearing capacity can be developed.

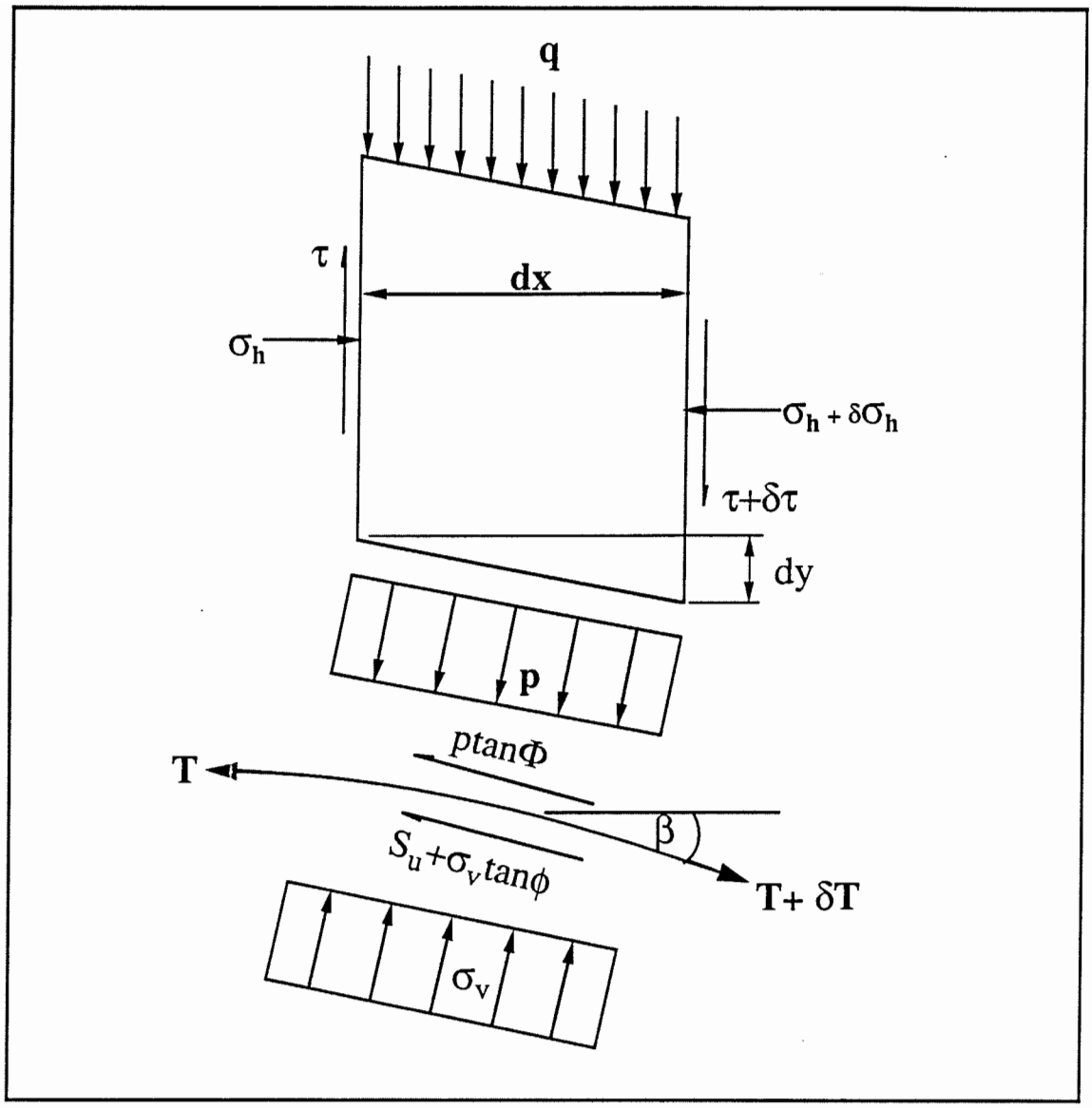

Figure 2.18 Forces Acting upon an Element - After Sellmeijer (1990)

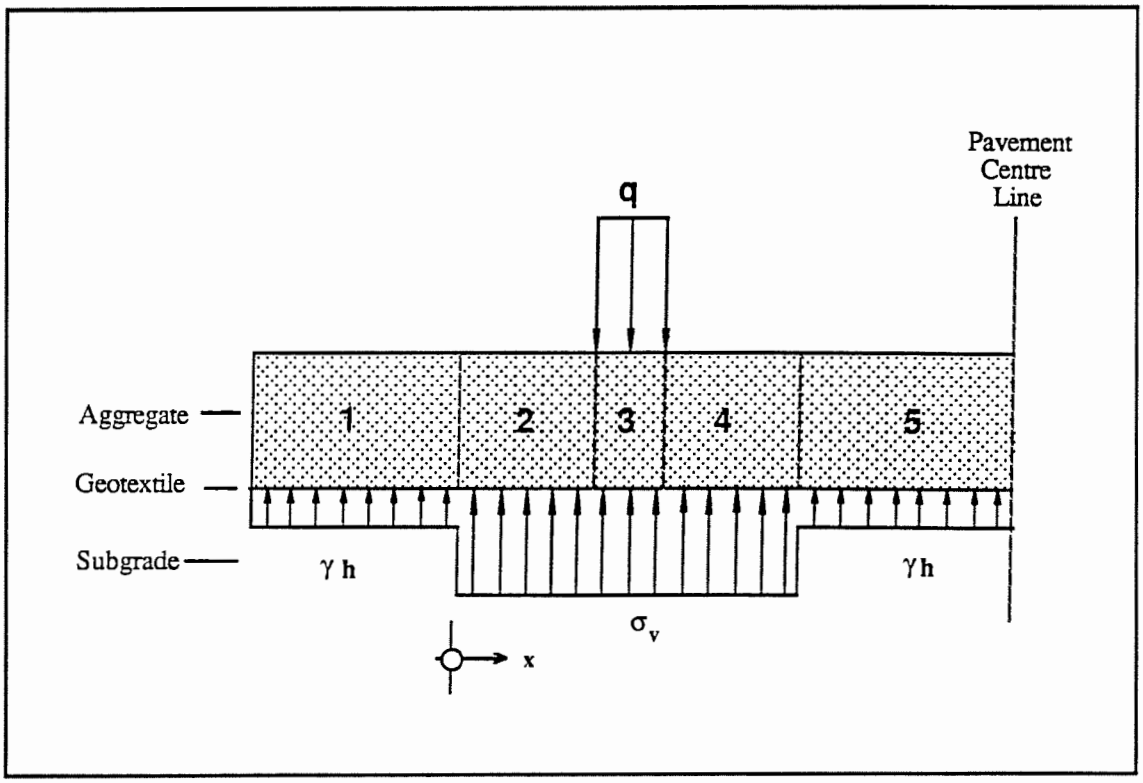

Figure 2.19 Geometrical Layout - After Sellmeijer (1990)

Examination of Equation 2.28 indicates that the geosynthetic will deform in a convex manner in sections 2 and 4 (ie $Gh\frac{d(\tan\beta)}{dx}$ is positive) as the vertical applied stress, q, is not deemed to be active in this region. Conversely the pavement will deform in a concave manner in section 3, where $Gh\frac{d(\tan\beta)}{dx}$ it is negative, as q is larger than σ_v. Therefore, the inclination of the geosynthetic, β, is at a maximum at the junctions of sections 2 and 3, and 3 and 4 and thus the shear forces within the aggregate are at a maximum. By examination of Figure 2.19, it can be seen that the maximum aggregate shear force will be as shown in Equation 2.29.

$$|\tau| = \frac{1}{2}(b - W)(\Delta\sigma_v) \tag{2.29}$$

Utilising the boundary conditions that in sections 1 and 5 no deflection occurs and that the geosynthetic must be continuous at the junctions of sections 2 and 3 and 3 and 4, Equation 2.28 can be integrated twice to obtain the solution for the deformation (Δw) under the wheel load.

$$\Delta w = (b - W)^2 \frac{q}{8Gh} \frac{\Delta\sigma_v}{q - \Delta\sigma_v} \tag{2.30}$$

2.7.3 Horizontal stress calculation

In order to prevent passive failure within the aggregate layer, the horizontal stresses generated by the imposition of the wheel load must be examined. The maximum horizontal stress that can occur at the junction of sections 2 and 3 will either be determined by the passive resistance of the aggregate at the junctions of sections 1 and 2 coupled with the frictional resistance of the aggregate along the length of section 2, or as a result of the stresses induced directly from the wheel load. The stresses at these two locations are described by the Mohr's circles shown in Figures 2.20 and 2.21.

From Figure 2.21 it can be seen that the horizontal stress generated by the wheel load is given by Equation 2.31 and an indication of its derivation is shown in Appendix F.

$$\sigma_{h\,max} = (\sec^2\phi - \tfrac{1}{2})(\sigma_v+q)h - \sec\phi\sqrt{\{(\sigma_v+q)h\}^2\tan^2\phi - (\Delta\sigma_v{}^2\text{-})\,(b\text{-}W)^2} \tag{2.31}$$

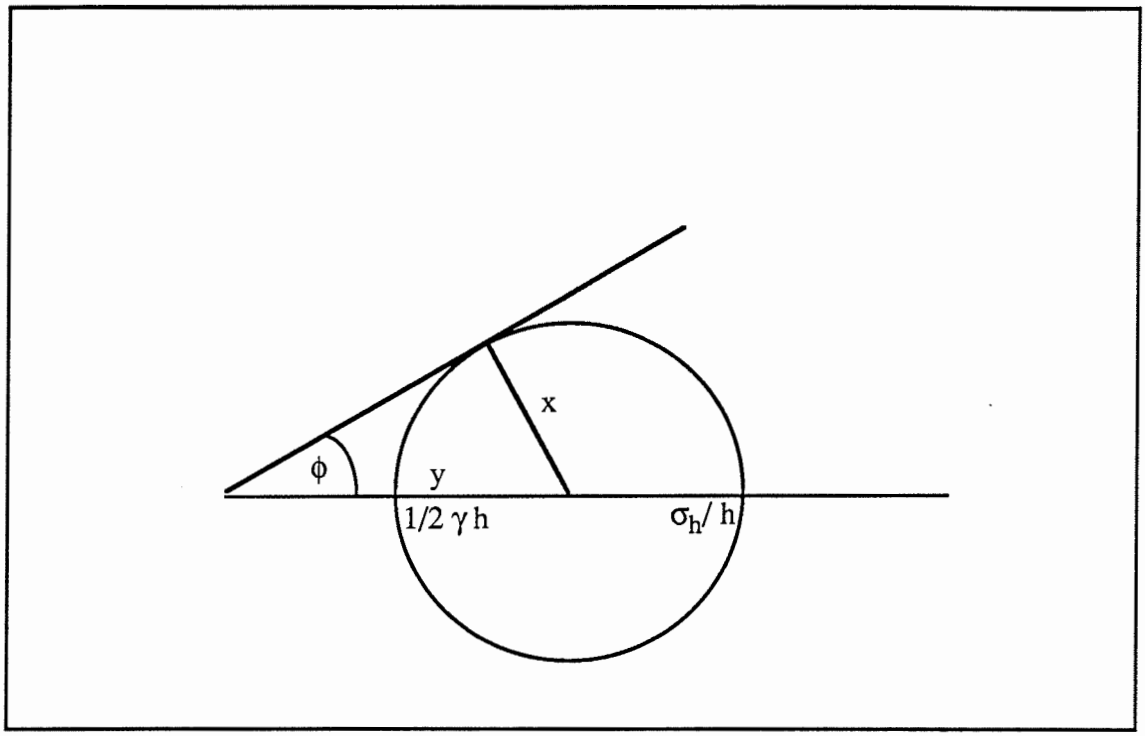

Figure 2.20 Mohr's Circle for Stresses at the Junction of Sections 1&2 After Sellmiejer (1990)

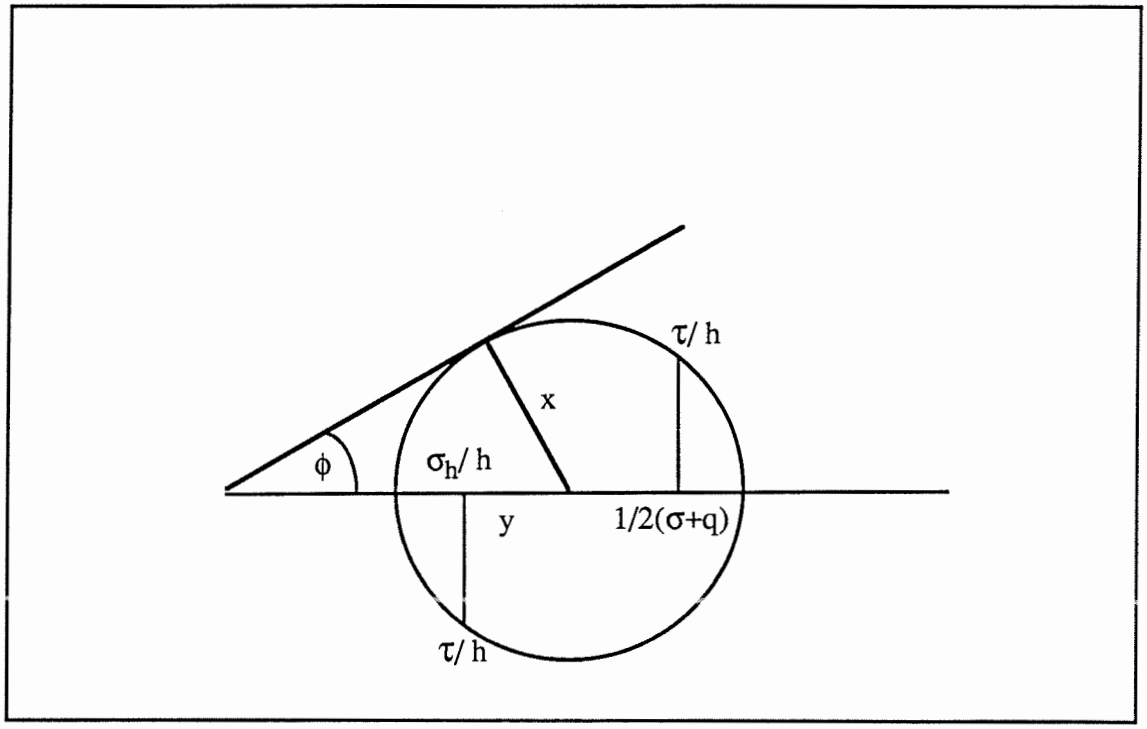

Figure 2.21 Mohr's Circle for Stresses at the Junction of Sections 2&3 After Sellmiejer (1990)

Sellmeijer (1990) argues that if the pavement is not to fail as a result of the aggregate then the horizontal stress determined in Equation 2.31 should not cause passive aggregate failure at the junctions of sections 1 and 2. Thus the maximum horizontal force is further limited by Equation 2.32 and the design calculations should check that this restraint is not exceeded.

$$\sigma_{h\,max} = \frac{1}{2}(b - W)\,\sigma_v \tan\Phi + \frac{1}{2}\gamma h^2 \frac{1+\sin\phi}{1-\sin\phi} \qquad (2.32)$$

2.7.4 Strain compatibility

Sellmeijer (1990) argues that for an efficient design, the strain induced in the aggregate layer should be matched to the strain induced by tension in the geosynthetic. This leads to specific stiffness requirements for the geosynthetic, too stiff and the resulting design is likely to be inefficient, not stiff enough and the surface deformations will increase. The equations for calculating the strain compatibility of the aggregate and geosynthetic are complex, but an indication of their derivation is given in Appendix F.

2.8 OTHER DESIGN METHODS

2.8.1 Nieuwenhuis (1977)

An early attempt to put a mathematical input into the design of soil-geosynthetic-aggregate systems was put forward by Nieuwenhuis (1977). While he appreciated the importance of the filtration and separation functions of the geosynthetic Nieuwenhuis put forward a basic mathematical model based on one of the assumed functions of the membrane, namely the reduction of vertical stress imposed on the subgrade. The deflected membrane is assumed to take a disc shape and the reduction in vertical stress imposed upon the subgrade as a result of the vertical component in the membrane stress reduces the deformation. In this sense it is a transient deflection model and the deflections in the reinforced and unreinforced are compared.

The flaws in this design method centre around the assumptions that the subgrade acts in a linear elastic manner and that the calculated transient deflections are unlikely to be

directly related to permanent deformations. There are also doubts that the membrane effect is a valid method of analysis, especially at low rut depths.

2.8.2 Sellmeijer et al (1982)

Sellmeijer et al (1982) produced a design method which again concentrated on the geosynthetic acting as a deflected membrane. The authors argued that, in the reinforced case, the subgrade was able to mobilise its ultimate bearing capacity, whereas in the unreinforced the bearing capacity was limited to the elastic limit. A vertical stress reduction, as a result of a catenary shaped membrane, is calculated but the originality of the model is in the appreciation that there must be strain compatibility as the interface which determines the force in the geosynthetic.

2.9 DISCUSSION OF DESIGN METHODS

2.9.1 Unreinforced design

The design of unsurfaced, unreinforced pavements relies on the empirical data of Hammitt (1970) and Webster and Watkins (1977). The data supporting the prediction of those conditions which would yield a 0.075m rut are reasonably wide, however the data to predict rut depths not equal to 0.075m is a little more sparse. There is a large degree of scatter in Hammitt's (1970) data and it also concentrates on pavements of relatively short life expectancies (generally less than 300 passes). However, at this time, models predicting the deformations that will occur within the aggregate and subgrade are likely to be less accurate than this data base.

There is an implicit assumption in most of the design methods that the reinforced pavement can provide aggregate savings over the unreinforced case and following on from this that a reinforced pavement can be expected to deform in a similar manner to a thicker unreinforced one. This is a reasonable assumption if one assumes that the inclusion itself does not affect the mechanism of the deformation. It is difficult to validate this assumption but in order to use the empirical data of Hammitt (1970) the assumption has to be made. Such data existing data as there is does not contradict the assumption. The appropriateness of the proposal in the light of the Bothkennar trials is unclear. However, as can be seen from the results presented in Chapter 6, the control

sections have not performed in a noticeably different manner than those sections including geosynthetics even though the pavements were of different thicknesses.

2.9.2 Bearing capacity

The bearing capacity of the subgrade may well be improved by the inclusion of a geosynthetic. Many of the design methods predict an improvement and a summary of the bearing capacities assumed by designers or as a result of empirical observations is shown in Table 2.1.

Author	Un-reinforced	Reinforced
Steward et al (1977)	2.8	5
Bender & Barenberg (1978)	3.3	6
Giroud & Noiray (1981)	3.14	5.14
De Groot et al (1986)	3	5

Table 2.1 Bearing capacities for use in design methods

Generally the design methods assume that the bearing capacity is limited to some elastic value in the unreinforced case and by some plastic value in the reinforced case. Milligan et al (1989a) suggest that a variety of bearing capacities exist in the unreinforced case, depending on the properties and geometry of the system, and that in the reinforced case it is taken to be the full upper bound plastic solution. This appears to be the most sensible and rigourous treatment of the subgrade's properties. However, the assumption that any geosynthetic is going to have a miraculous effect on the bearing capacity appears flawed. There must be a range of reinforced bearing capacities varying between the unreinforced value and $(2+\pi)S_u$ dependent upon the stiffness of the geosynthetic or, more particularly, its relative stiffness to the aggregate.

2.9.3 Strain compatibility

If it is assumed that no slippage occurs between the elements of the soil-geosynthetic-aggregate system then strain compatibility must exist within the system. Sellmeijer (1990) presents a method of calculating the strains that occur within the system and by equating them leads to a prediction of the stiffness of the geosynthetic required for an

efficient design. The term efficient is ill-defined, but can be taken to mean the limiting stiffness of the geosynthetic, beyond which no further improvement of the performance of the pavement is possible.

2.9.4 Aggregate properties

The role of the aggregate within the soil-geosynthetic-aggregate system is plainly important. The active and passive earth pressures generated within the aggregate are included within both the Milligan et al (1989a) and Sellmeijer (1990) models and the magnitude of these developed stresses are controlled by the quality of the aggregate. Sellmeijer (1990) further argues that the shear modulus of the aggregate will influence the magnitude of the transient pavement deflection. However, the transient response of unpaved roads is unlikely to be of as much interest as the permanent deformation characteristics. The permanent deformations resulting from repeated loading are unlikely to be directly related to the transient responses and therefore calculations of the transient deformations are not as valuable as they might first appear.

2.9.5 The membrane effect

Design methods which claim to be concerned with the contribution to the system of the membrane effect often make further assumptions about the bearing capacity of the subgrade. The reduction in vertical stress imposed upon the subgrade as a result of the tensioned membrane varies from nothing at low rut depths to little at even quite large deformations shown in the example calculation. The amount of deformation that occurs in an unpaved road is subject to a large degree of scatter and the small contribution that any membrane effect could make is almost certain to be significantly lower than this scatter.

2.9.6 Separation

Although the value of separation is highlighted in many of the design methods, especially those relating to less stiff geosynthetics, no analytical or empirical models exist for predicting the amount of aggregate that is lost to the subgrade in the unreinforced case. It is unfortunate that this is the case because separation is a function

that all proprietary geosynthetics perform and is probably the principal mechanism by which less stiff geosynthetics benefit the pavement and it probably represents a large proportion of the benefit obtained from including geosynthetics whose major role might otherwise be considered to be solely reinforcement.

CHAPTER THREE

BOTHKENNAR

It is intended in this Chapter to introduce the Bothkennar Soft Clay Site and to examine the roles and engineering properties of the materials used in the construction of the full-scale trials.

3.1 THE BOTHKENNAR SOFT CLAY SITE

3.1.1 Purpose (after Nash et al (1985))

A soft clay site was sought by the Science and Engineering Research Council to be a national research facility. It was envisaged that research on soft clays might include large scale testing, site investigation techniques and laboratory testing. It was hoped that by carefully documenting all of the work carried out on the site, a series of inter-relating case studies could be built up.

When the site was being searched for, it was envisaged that the site should be a green field site of approximately 5 hectares and with a low risk of vandalism. That it should consist of a minimum of 10m of soft clay with a shear strength of less than 40kPa and that the deposit should be uniform without significant peaty or sandy lenses.

Several general areas were considered for the site, notably the Severn and Forth Estuaries. Other areas were considered but were thought, for geological reasons, unlikely to produce a suitable site. Finally, the site at Bothkennar, on the banks of the Forth Estuary, was chosen as it fulfilled the criteria required of a soft clay research test bed.

3.1.2 Geology (after Gostelow & Browne (1986))

The geology of the area surrounding the Bothkennar Soft Clay Site consists of a synclinal carboniferous basin centred on Grangemouth. This is overlain by glacial

deposits consisting of stiff boulder clay, followed by post-glacial soft marine clays and loose silts.

Relative sea level rose in the post-glacial period when the marine and esturine clays were deposited on the site. Isostatic uplift of the area was continuing at a diminishing rate during this period, raising the deposits above sea level.

3.1.3 Engineering geology (Paul et al (1991))

It is possible to divide the sediment at Bothkennar into 4 categories, bedded, laminated, mottled and weathered. The sediment originated by tidal transport and the sedimentary structures are recorded by the bedded layers ranging in thickness from a few millimetres to 10 centimetres. Local, more energetic conditions lead to laminated layers while reduced rates of sedimentation allowed burrowing organisms to re-work the deposit, causing the mottled appearance. Weathering and desiccation occurred when the sediment was exposed to the surface elements and is restricted to the top 3m of the site.

The grain size is uniform with depth and the clay minerals are kaolinites and illites. The silt fraction contains quartz, feldspar and ferromagnesium materials. Clay represents between 35 and 45% of the deposit, the rest being mainly silts. The organic content is, on average, 2-3% of dry weight and is thought to be the residue of soft bodied organisms, mostly in the form of oils and fats. It is these residues which are thought to improve the plasticity of the material above that which could be expected from its silt content.

The clay is sensitive, with a re-moulded shear strength of around 5 to 10kPa compared to a minimum in-situ shear strength of around 20kPa as shown in Figure 3.1.

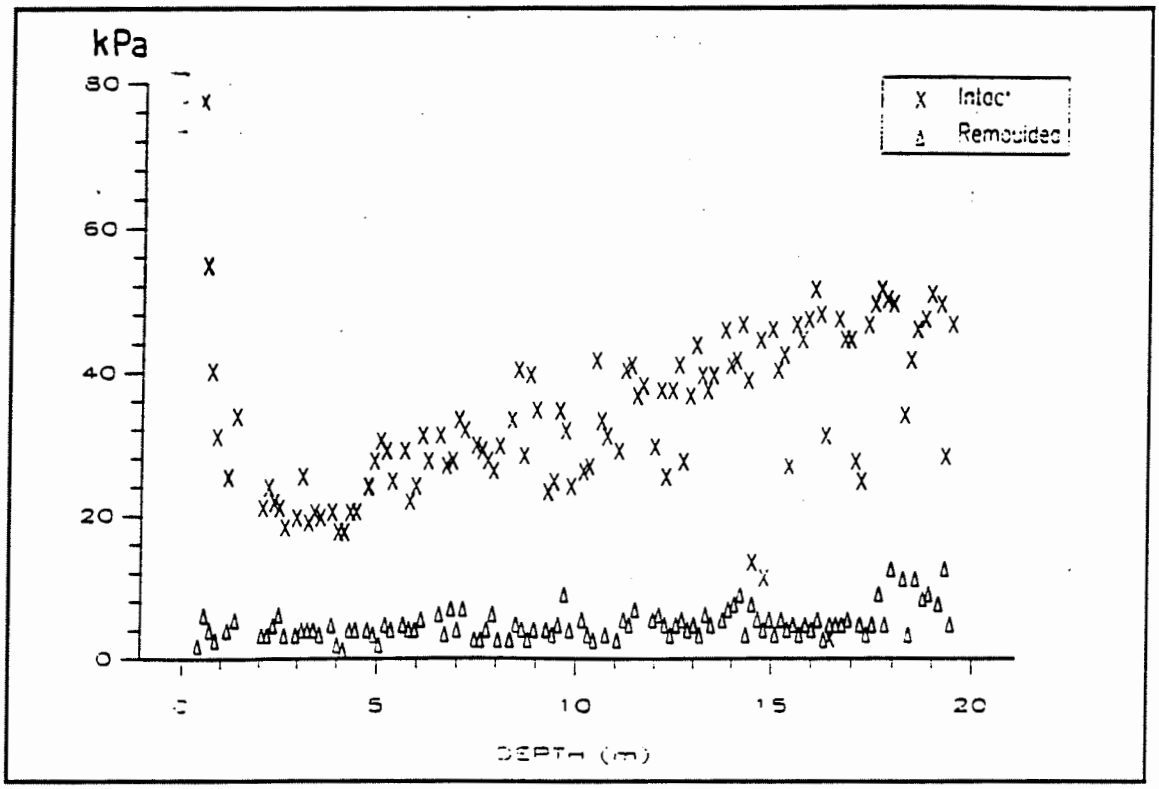

Figure 3.1 Undrained Shear Strength with Depth at Bothkennar After Paul et al (1991)

3.2 THE PROPERTIES OF THE BOTHKENNAR CLAY

3.2.1 Sampling

In order to determine the engineering properties of the clay at Bothkennar, a series of index and other tests were performed. Some of these were performed in the field, but for laboratory testing a range of samples were recovered, as detailed below.

3.2.1.1 Moisture content at construction

Samples of the subgrade at Bothkennar were recovered, at the time of construction, from each reading location (as described in Chapter 4.1) on each section from depths of 0mm, 200mm and 300mm below formation level. The moisture content of each sample was determined at the earliest opportunity in order that further moisture loss was minimized. The results of the moisture samples are shown in Appendix B and can be seen to vary between those pavements that were constructed at the start of the programme, when it was dry, and the end when it rained more.

3.2.1.2 Bulk samples

The bulk samples of subgrade soil were recovered from the side of the formation at each reading location. The samples were hand dug from a pit 200 x 300 x 350mm deep and were transported to the laboratory in heavy duty plastic bags sealed by a wire crimp. The samples did not dry out significantly between excavation and testing for Atterberg limits, particle size analysis and organic content.

3.2.1.3 38mm diameter triaxial samples

Three 38mm diameter samples were recovered from the formation level at each reading location at the time of construction; one each from the left hand side, centre line and right hand side of the formation. The sample tubes were sealed with wax, capped and stored in a high humidity room until required for quick undrained triaxial testing, as described in Chapter 3.2.2.5.

3.2.1.4 U100 samples

U100 samples were recovered at the time of construction by pushing the U100 tubes into the subgrade at formation level with the rear bucket of a JCB 3C excavator. The ends were sealed with wax and the tubes were stored in a high humidity room in the laboratory. Some of the samples were extruded to form 38mm diameter triaxial samples if the 38mm diameter samples discussed in Chapter 3.2.1.3 were found to be unsuitable. Others were used to familiarise the author with the 76mm diameter triaxial apparatus and finally all of the remaining samples were opened and split to examine the fabric of the material.

3.2.1.5 Post trafficking sampling

Further U100 samples were recovered, in a similar manner to that described above, from the lower-bound sections at the end of trafficking, during the exhumation of the geosynthetics. They were recovered from formation level in the wheel path and were sealed with wax on site to maintain the in-situ moisture content. They were stored in a high humidity room until they were used for resilient modulus and shear strength testing as described in Chapter 3.2.3.1.

3.2.2 Index testing

3.2.2.1 Atterberg limits

The Liquid and Plastic Limits were determined for samples drawn from the bulk samples recovered from each reading location. The Plasticity Index and Liquid Limit results are shown in Figures 3.2 and 3.3 and the samples are identified by the section letter code plus the reading location from which they were taken as identified in Chapter 4.1, (i.e. the sample from Section E, Reading Location 2 is shown as E2).

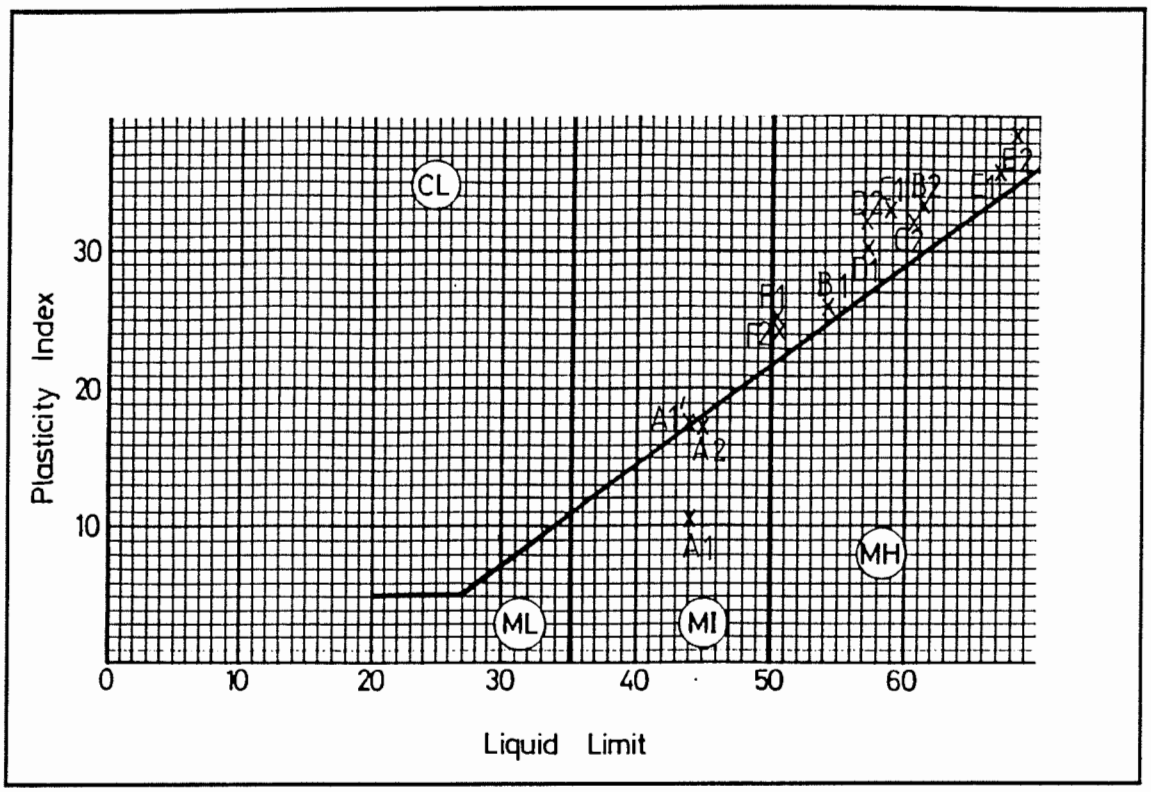

Figure 3.2 Plasticity of Upper-bound Samples

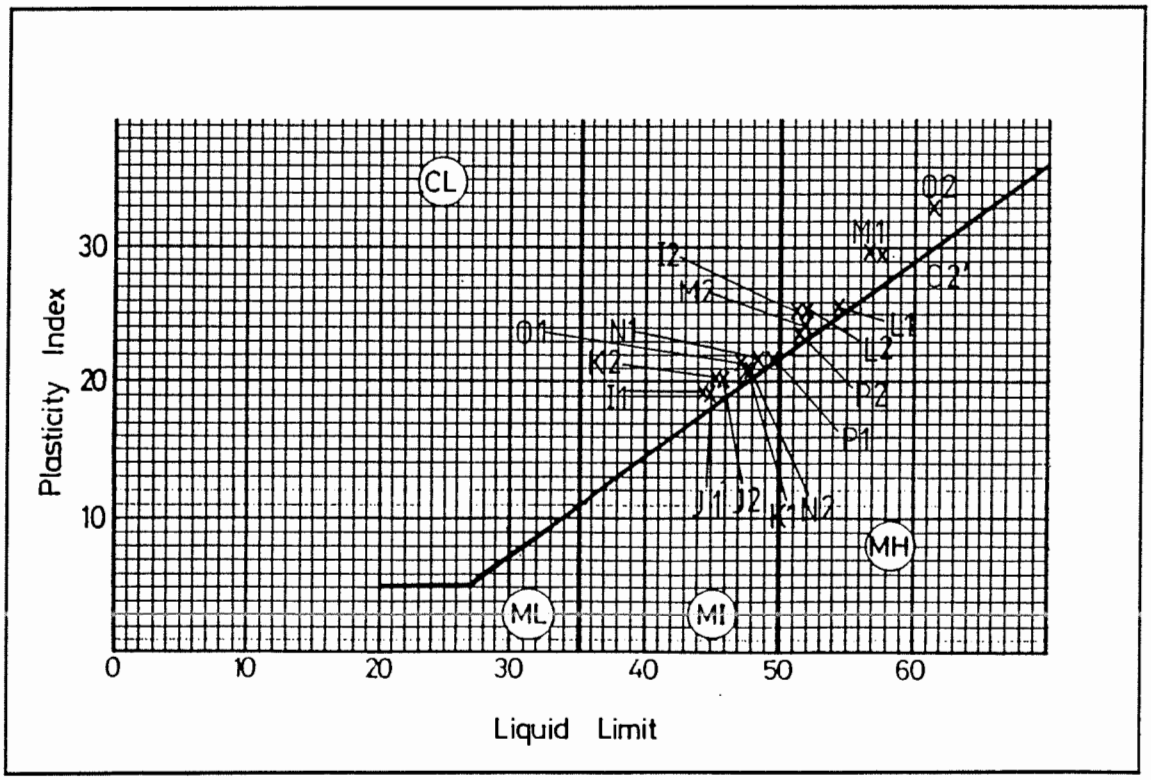

Figure 3.3 Plasticity of Lower-bound Samples

3.2.2.2 Choice of samples for further analysis

It would have been impractical to perform a wide range of soil tests on the full range of soil samples and therefore, based on the results of the Atterberg Limit tests, a selection of soils was chosen for further study.

From the results presented in Figures 3.2 and 3.3 it appears that four slightly differing soils can be identified. A group of results falls around the clays of intermediate plasticity, namely: I1, J1, J2, K1, K2, N1, N2 and O1. A group of clays of high plasticity, namely: B1, B2, C1, C2, D1, D2, E1, E2, L1, M1 and O2; a group for clays on the border of the two, namely: F1, F2, I2, M2, P1, P2 and L2. A1 and A2 appear to be in a class of their own, although similar to the group of intermediate plasticity. Some of the subsequent testing was extended to include Section A, but for some of the tests this soil group was not included, on the grounds of cost or time, and was then presumed to be included in the clays of intermediate plasticity. Because of the results on the samples A1 and 02 were so far removed from other results, the soil was re-tested yielding the results nominated A1' and O2'. Perhaps some sampling error had occurred because the subsequent results fitted the rest of the data more satisfactorily and hence were considered to fit the groups of samples indicated.

3.2.2.3 Subgrade particle size analysis

The method chosen from BS1377 (1975) to undertake particle size analysis was the sedimentation (pipette) method. This test was performed on four subgrade samples and the results are shown in Figure 3.4.

3.2.2.4 Organic content

The organic content of four samples has been determined in accordance with BS1377 (1975). The full results are shown in Table 3.1 and as can be seen are in good agreement with those found by Paul et al (1991)

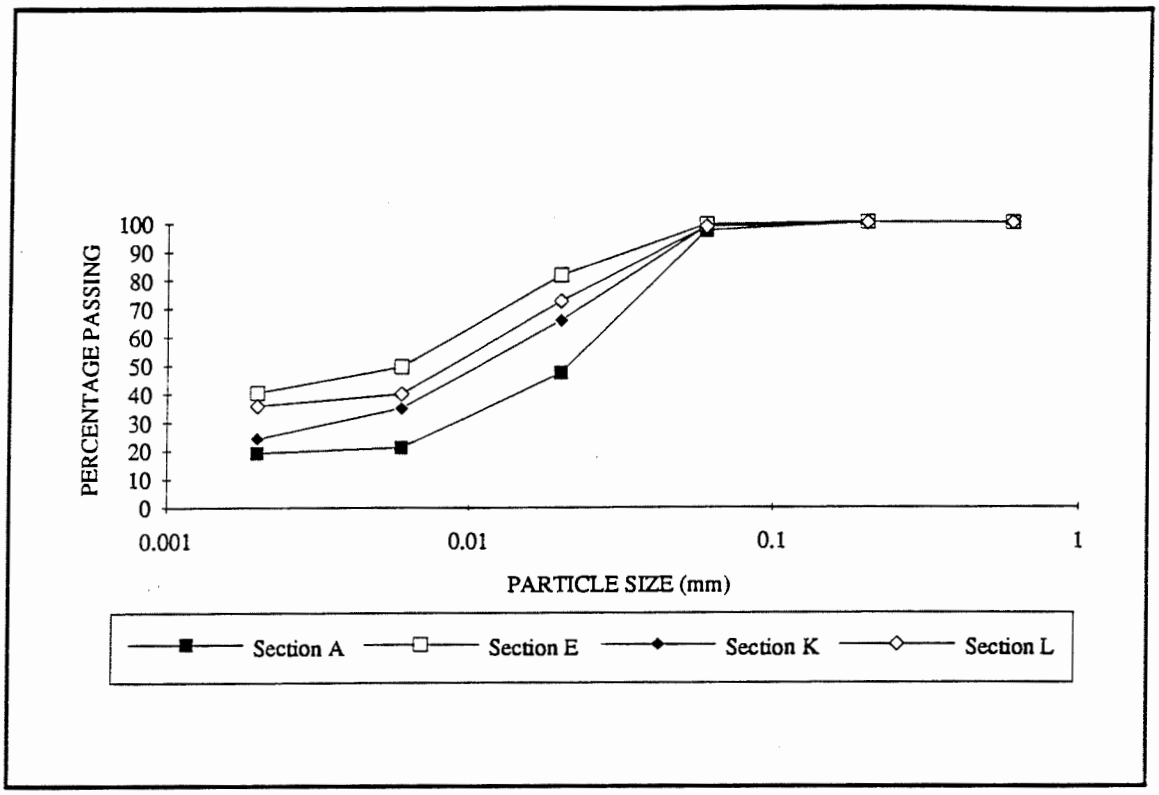

Figure 3.4 Subgrade Particle Size Analysis - After BS 1377 (1975)

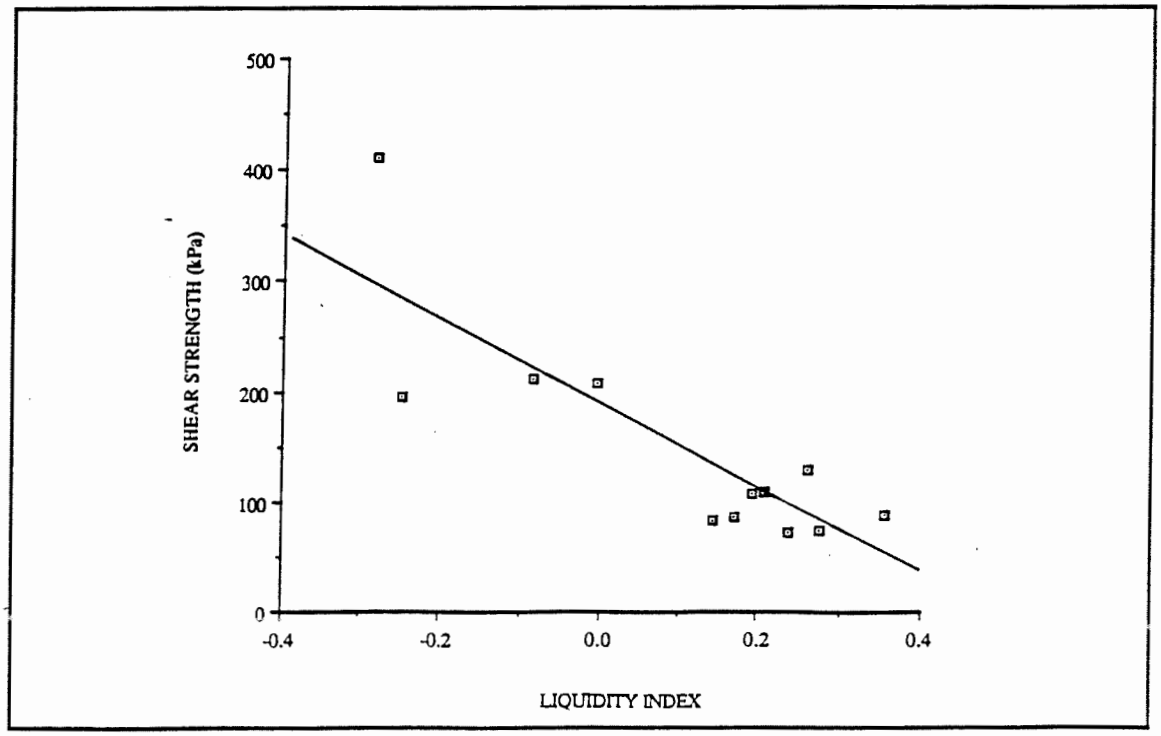

Figure 3.5 Undrained Shear Strength and Liquidity Index
38 mm Diameter Triaxial Results

Sample Plasticity	Section Code	Organic Content
Section A	A1	1.0%
Intermediate	K1	1.6%
Int/High Border	E2	2.3%
High	L2	2.0%

Table 3.1 Organic Contents of the Subgrade

3.2.2.5 38mm diameter triaxial results

Standard 38mm diameter quick undrained triaxial tests at confining stresses of 10, 20 and 40kPa were performed on 35 samples and the results show a great deal of scatter. The results are plotted as Liquidity Index (obtained from the determination of Atterberg Limit on adjacent samples) against undrained shear strength (Figure 3.5) in the expectation that there should be a relationship between the two. From this plot it was considered that an estimate of the on-site shear strength, by the determination of the moisture content of the subgrade, could be accomplished. However, the scatter of the results leads to an uncertainty as to whether or not this would be possible. Regression analysis of Liquidity Index v S_u showed that for all samples $R^2 = 0.57$ and that for the average values of each reading location $R^2 = 0.73$. The scatter could imply that the samples were disturbed on excavation and, indeed, 38mm diameter samples are prone to such disturbance. Thus, it was decided to use a hand held shear vane to determine the on-site shear strength of the subgrade.

3.2.2.6 Specific gravity of subgrade material

The specific gravity of the subgrade material was determined in accordance with BS1377 (1975). Four samples were tested and yielded a specific gravity of 2.67 ± 0.01.

3.2.3 Other laboratory tests

3.2.3.1 Resilient modulus determination

U100 samples were recovered from the wheel path of the post trafficked pavement and four lower-bound samples were chosen for testing in the 76mm diameter repeated loading triaxial apparatus at Nottingham University. The samples were chosen on the basis of being evenly spaced along the length of the lower-bound sections.

The samples were extruded in the laboratory and carefully pared down to a 76mm diameter. Each sample was then tested using an axial load cycling between 10 and 120kPa and a confining stress cycling between 15 and 66kPa. The frequency of the cyclic load was 1 Hertz and the number of cycles performed was approximately 2,000. The samples were not equipped with on-sample instrumentation and so only the confining stress, axial stress and axial strain were monitored: no measure of radial strain was recorded. Data was captured from the monitoring instruments, using an analog to digital device and a personal computer, in blocks of 25 cycles around 0 1,000 and 2,000 cycles. Figures 3.6 to 3.9 show the stress strain relationships that the four samples exhibited during testing and a summary is shown in Table 3.2

SAMPLE LOCATION	MOISTURE CONTENT %	BULK DENSITY kg/m^3	MEAN INITIAL RESILIENT MODULUS (MPa)
H	32	1933	16.2
J	33	1854	16.3
L	34	2004	11.6
P	33	1912	14.0

Table 3.2 Resilient Moduli (M_r) of lower-bound samples (MPa)

It should be noted that the resilient modulus of the samples appears not to degrade with the number of cycles and that the incremental plastic axial strain that occurs with each cycle gets progressively smaller as the test continues.

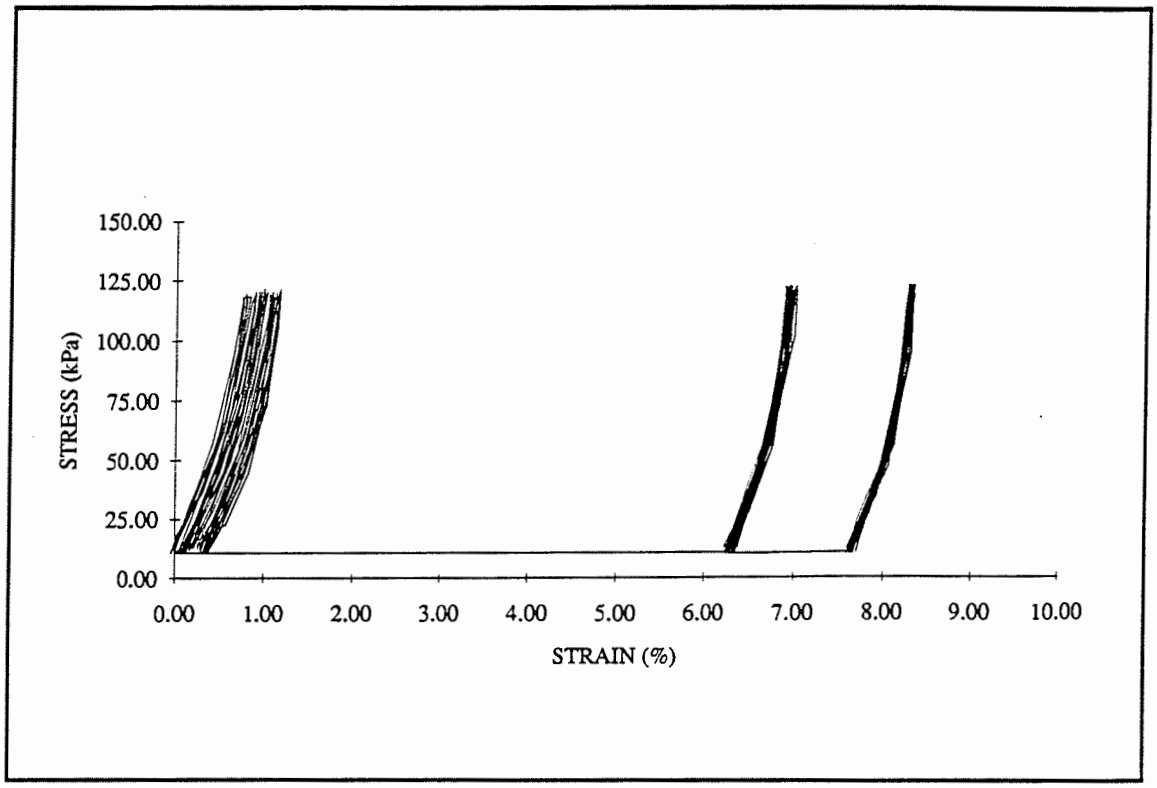

Figure 3.6 Repeated LoadTriaxial Test - Section H

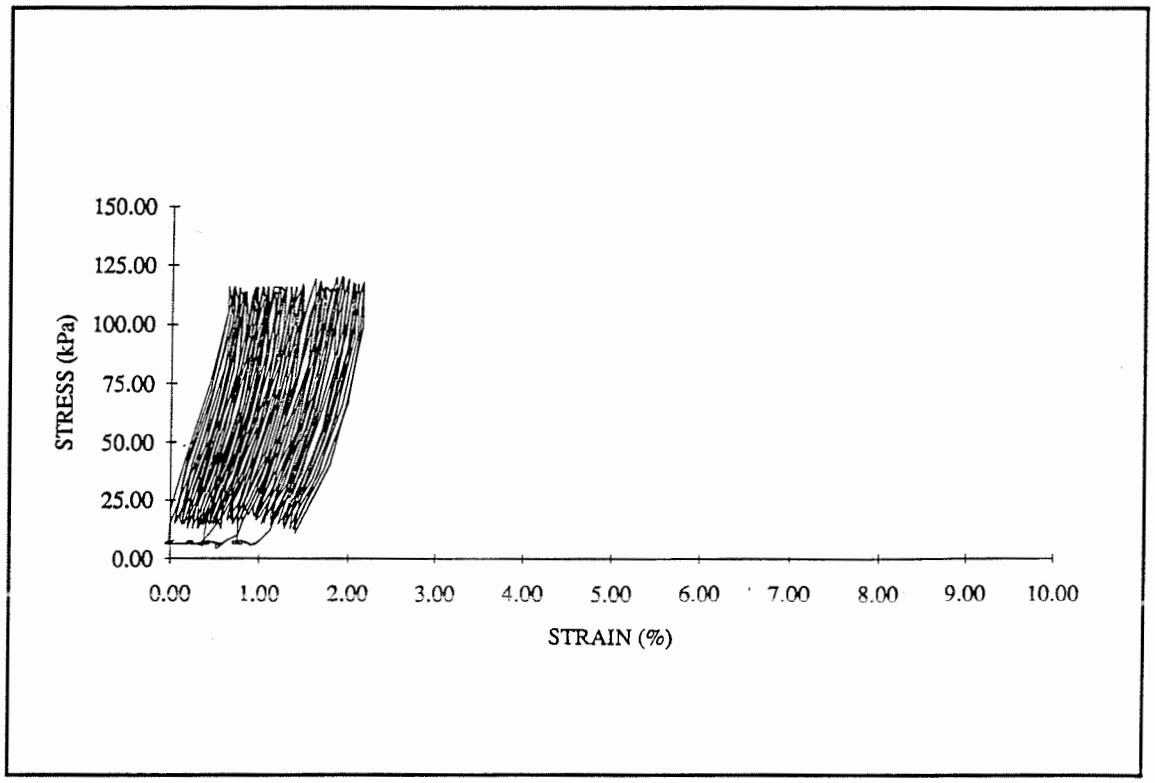

Figure 3.7 Repeated LoadTriaxial Test - Section J

3.2.3.2 Calibration of the hand held shear vane

Three of the 76mm diameter triaxial samples were subjected to a quick undrained triaxial test at the end of the cyclic testing programme. The fourth sample was destroyed during a surge in the power supply to the triaxial equipment. The results of the quick undrained test are compared to the mean values obtained from the hand held shear vane taken from around the sample before retrieval. As can be seen from Table 3.3 the two sets of results are in close agreement.

SAMPLE LOCATION	76mm DIAMETER TRIAXIAL (kPa)	HAND-HELD SHEAR VANE (kPa)
H	81	82
L	85	77
P	77	76

Table 3.3 Comparison of Quick Undrained Triaxial and Hand Held Shear Vane to Determine Subgrade Shear Strength

3.3 THE PROPERTIES OF THE AGGREGATE USED AT BOTHKENNAR

3.3.1 Sampling

Aggregate samples were not taken on a section by section basis, but were taken on a chronological basis. The aggregate could not be placed on each section individually without substantially effecting the contractor's work pattern. Aggregate was therefore placed on several adjoining sections simultaneously and thus it was more sensible to take aggregate samples on a time basis. Six Type1 samples were taken during the construction of the twelve Type1 sections, and two samples of the sand and gravel mixture were taken. The date when each sample was taken and the location which it is deemed to represent is shown in Table 3.4. Each sample was recovered from one lorry load of material before it was placed. Each sample was taken from more than one location around each pile of aggregate in an attempt to avoid any sampling errors which might have affected the results.

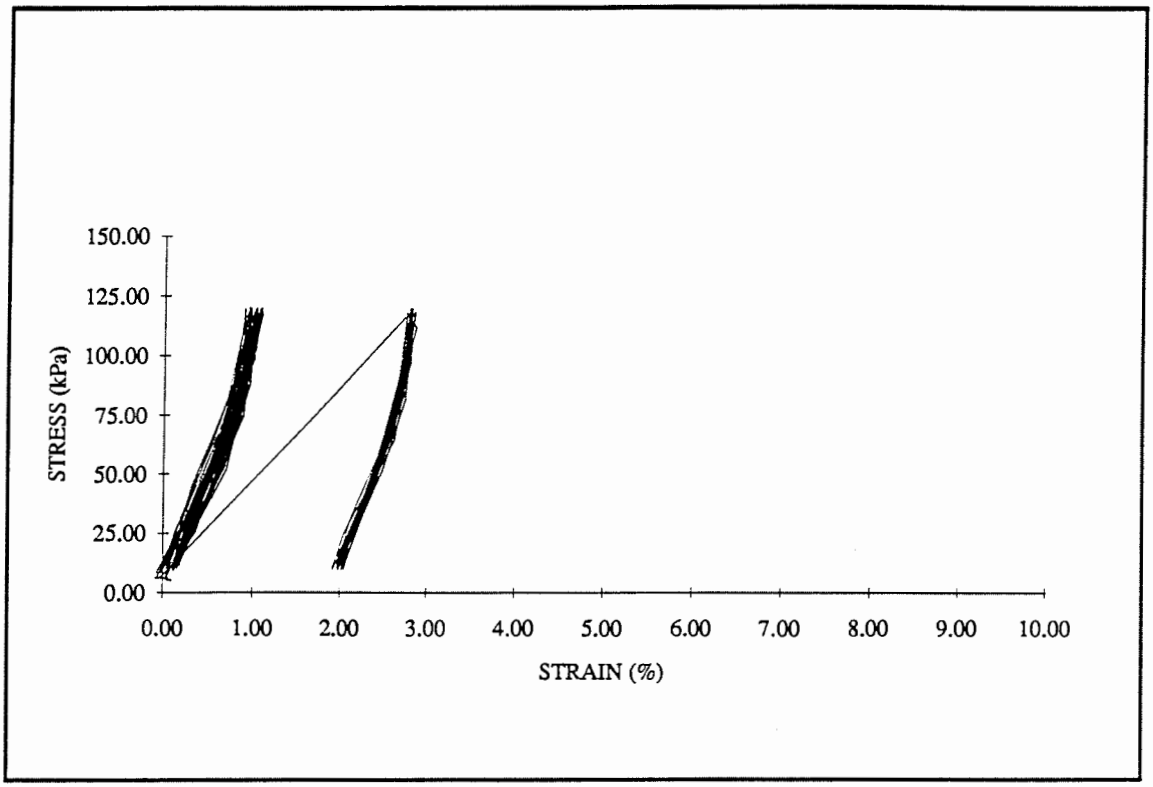

Figure 3.8 Repeated LoadTriaxial Test - Section L

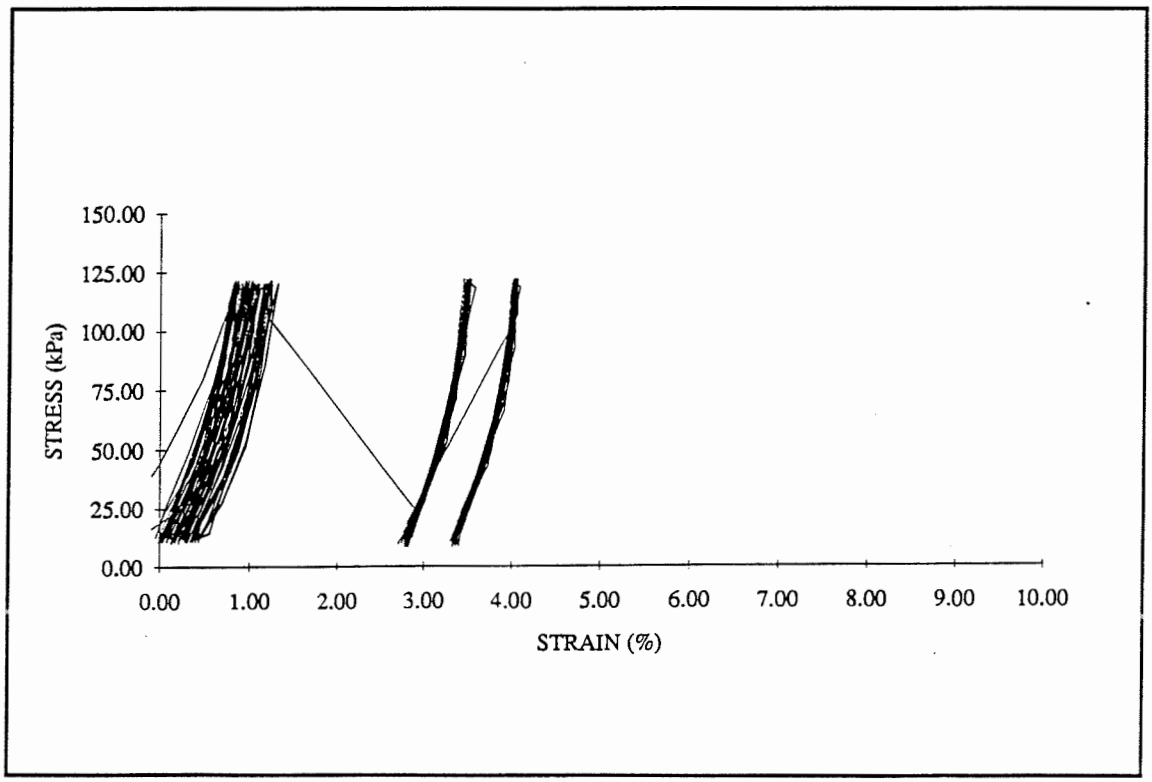

Figure 3.9 Repeated LoadTriaxial Test - Section P

Sample Number	Date retrieved	Section	
1	25/10/89	Polyfelt / Netlon	Lower bound
2	31/10/89	Bidim	Lower bound
3	12/07/89	Netlon / Typar	Upper bound
4	19/07/89	Netlon / Typar	Upper bound
5	12/09/89	Control / Woven	Upper bound
6	29/09/89	Control / Woven / Typar	Upper bound
7	11/09/89	Oxford Section / Control	Lower bound
8	14/09/89	Oxford Section / Control	Upper bound

Table 3.4 Aggregate Sample Locations

3.3.2 Index testing

3.2.2.1 Aggregate particle size analysis

The samples were riffled and sieved in accordance with BS 812 (1975) and particle size distributions are shown in Figures 3.10 to 3.13. As can be seen from the plots the sand and gravel mixture falls within the specified envelope very satisfactorily, being almost in the centre of the two allowable limits. This should have been expected because the material was blended to the project's specific requirements.

The gradings of the Type1 material generally fell within the envelope specified. However, samples 1 and 2 fell marginally outside the permitted envelope at a few sieve sizes. This material has been placed on the Polyfelt and Bidim lower-bound sections and on the second lift of the Tensar lower-bound section. It was felt that the material was not significantly out of specification. Furthermore, sampling errors could account for the discrepancies observed. As can be seen from the Nuclear Density Meter results in Table 3.6 specification grading has not affected the final compacted densities.

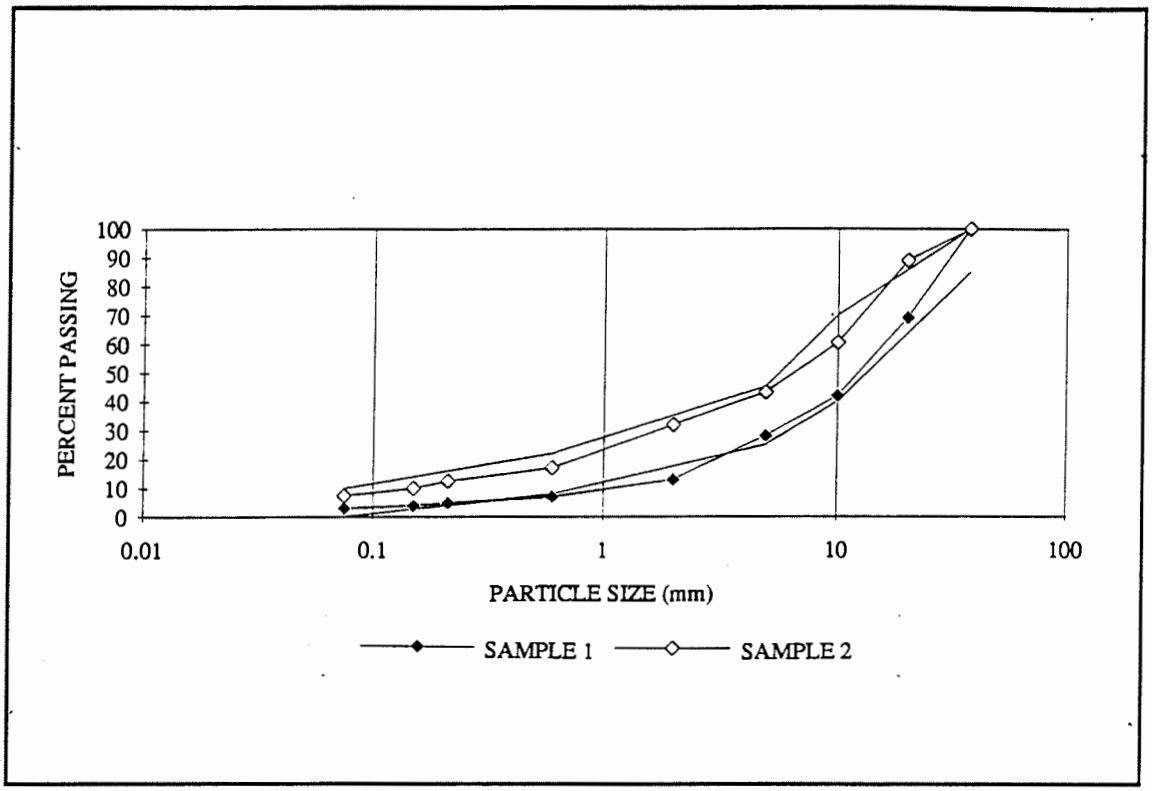

Figure 3.10 Aggregate Particle Size Analysis After BS 812(1975)

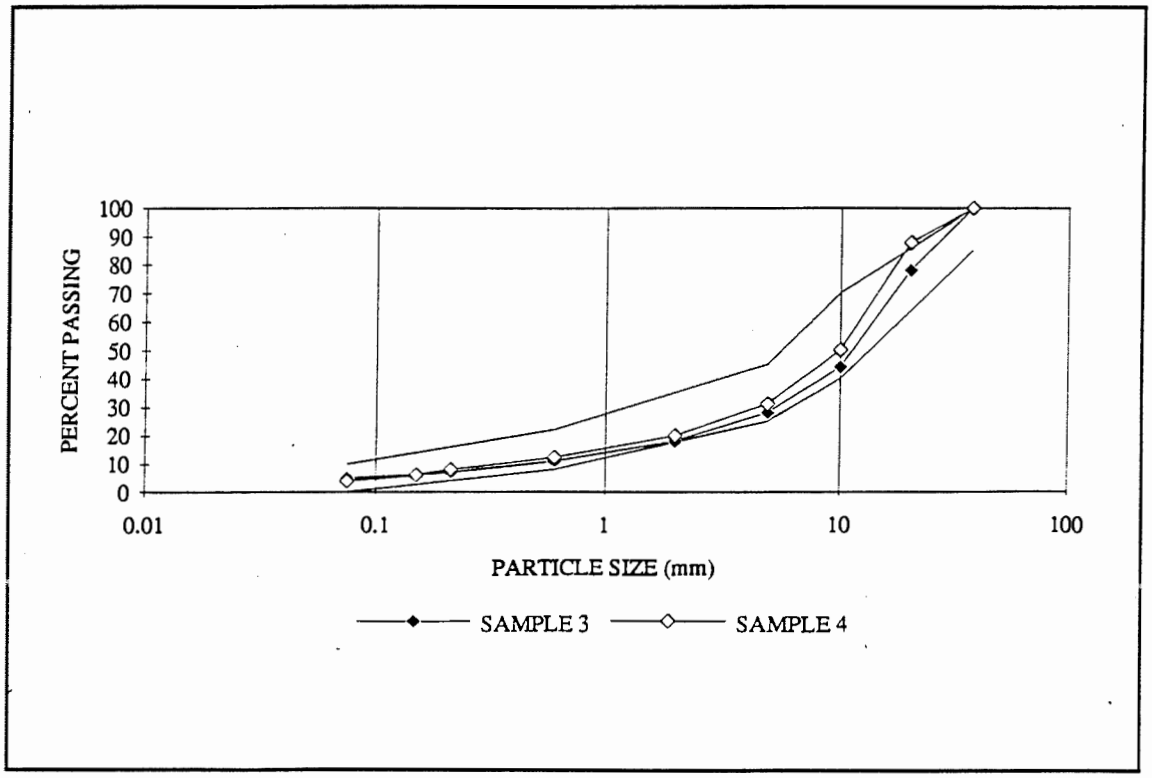

Figure 3.11 Aggregate Particle Size Analysis After BS 812(1975)

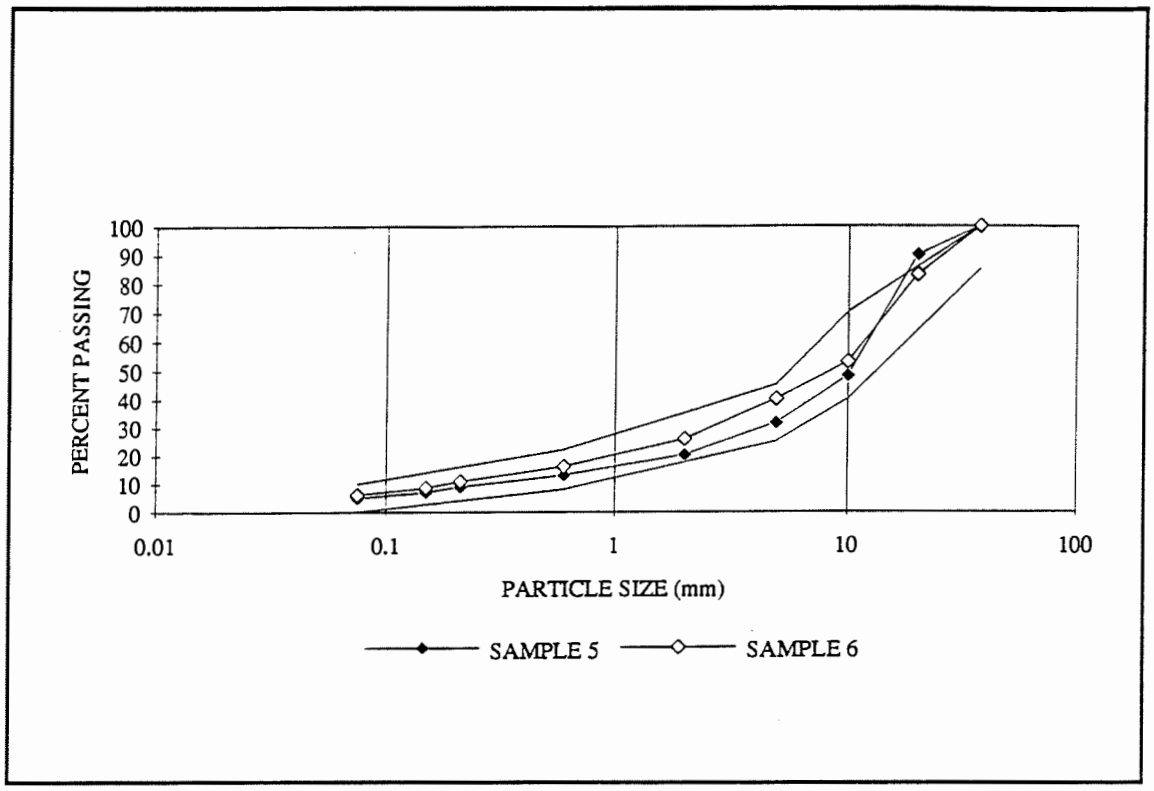

Figure 3.12 Aggregate Particle Size Analysis After BS 812(1975)

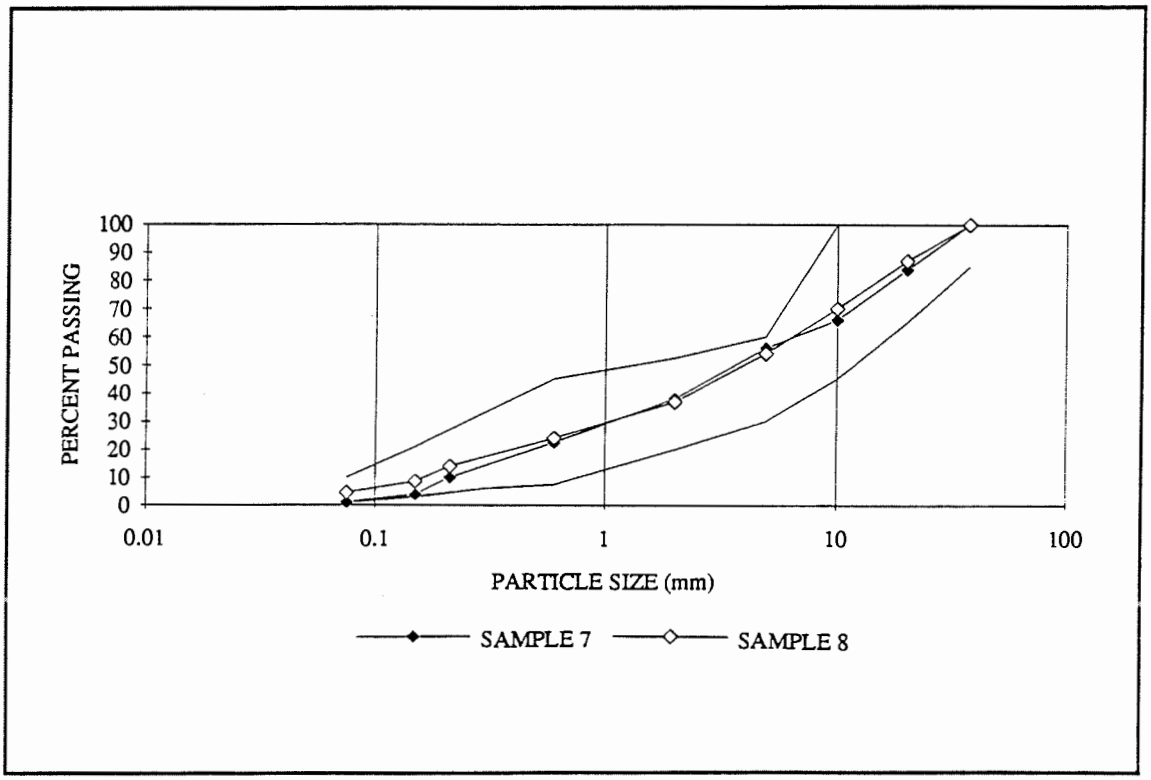

Figure 3.13 Aggregate Particle Size Analysis After BS 812(1975)

3.2.2.2 Specific gravity

The specific gravity of the aggregates was determined according to BS1377(1975) and the specific gravity of the Type1 was found to be 2.85 and that of the sand and gravel was 2.74.

3.3.3.Field testing

3.3.3.1 Density measurements

The density of the aggregate was determined in the instrumented wheel path of each section by using a nuclear density meter prior to trafficking, in March 1990. It was used in the direct transmission mode and the moisture content, bulk density and dry density of the top 200mm, 150mm, 100mm and 50mm of the aggregate layer was determined in two directions. The process was repeated at three locations on each section: at Reading Location 1 (5m into the section); Reading Location 2 (15m into the section); and at the mid-point of each section and the mean results at each place are shown in Table 3.5.

Section	Distance into Section (m)	Measured Bulk Density (kg/m^3)	Measured Dry Density (kg/m^3)	Measured m/c (%)
A	5	2247	2118	5.9
	10	2122	2002	5.9
	15	2225	2115	5.2
B	5	2176	2077	4.7
	10	2179	2072	5.1
	15	2175	2064	5.1
C	5	2286	2168	5.3
	10	2293	2172	5.5
	15	2378	2234	6.3
D	5	2337	2208	5.8
	10	2331	2190	6.3
	15	2322	2178	6.5
E	5	2313	2167	6.6
	10	2350	2210	6.3
	15	2292	2160	6.0
F	5	2300	2145	7.1
	10	2255	2091	8.0
	15	2285	2127	7.3
H	5	2298	2135	7.5
	10	2196	2047	7.2
	15	2208	2056	7.3
I	5	2312	2153	7.3
	10	2263	2104	7.4
	15	2263	2102	7.6
J	5	1958	1877	4.2
	10	2320	2171	6.7
	15	2304	2173	5.9
K	5	2292	2162	5.9
	10	2237	2105	6.2
	15	2270	2130	6.4
L	5	2292	2159	6.0
	10	2363	2212	6.7
	15	2321	2192	5.8
M	5	2329	2195	6.0
	10	2398	2263	5.9
	15	2186	2059	6.1
N	5	2344	2204	6.3
	10	2404	2261	6.2
	15	2327	2186	6.4
O	5	2237	2124	5.2
	10	2358	2212	6.5
	15	2356	2237	5.2
P	5	2230	2102	6.0
	10	2310	2179	5.9
	15	2367	2229	6.1

Table 3.5 Nuclear Density Meter Results for the Aggregate Layer

At a distance of 5m into Section J there is noticeably low density recorded. The aggregate, where the density was determined, exhibited a high degree of segregation and this low density may help to explain the poor performance of the haul road at this location.

The statistical analysis of the nuclear density meter results is shown in Table 3.6.

	Bulk Density (kg/m^3)		Dry Density (kg/m^3)		Moisture Content (%)	
Aggregate type	mean	Standard deviation	mean	Standard deviation	mean	Standard deviation
Type1	2284	87	2154	75	5.9	0.5
Sand & Gravel	2264	38	2109	34	7.4	0.3

Table 3.6 Statistical Analysis of Results from the Nuclear Density Meter

It should be noted that there is a discrepancy between the bulk density, dry density and moisture contents for the values quoted in Table 3.5. The density meter reads bulk density and corrects for moisture content and so, theoretically, the bulk density will be more accurate. The good agreement between these 3 parameters shown in Table 3.6 implies that little or no bias exists in the nuclear density meter's determination of moisture content.

3.3.3.1.1 Density meter calibration

Four sand replacement tests were performed in accordance with BS1377 (1975) and the results are shown in Table 3.7. The tests were undertaken in an attempt to calibrate the results of the nuclear density meter. The results show a tendency for the sand replacement test dry densities to be slightly higher than those obtained from the nuclear density meter. Also the moisture contents determined by the nuclear density meter were slightly higher than those obtained in the replacement test. However, this latter difference may be explained as the result of there being no on-site moisture content determination facilities at the time. Consequently there may have been a small amount of moisture loss between Bothkennar and Nottingham despite the fact that the aggregate was stored in sealed polythene bags. Unfortunately, when using the Nuclear Density Meter on this occasion, only dry densities were recorded but it can be seen from Table 3.7 that the bulk densities that could be obtained from the two methods would be more in agreement.

	Nuclear Density Meter		Sand Replacement Test	
Test Location	Dry Density kg/m^3	Moisture content (%)	Dry Density kg/m^3	Moisture content (%)
Type1 upper-bound	2156	5.7	2194	3.5
Type1 upper-bound	2150	7.5	2232	7.1
Sand & Gravel upper-bound	2011	8.3	2153	5.8
Sand & Gravel lower-bound	1971	10.5	2187	7.4

Table 3.8 Nuclear Density Meter Calibration using the Sand Replacement Test

The value of calibrating Nuclear Density Meters by comparison with the sand replacement test must be questioned. The latter is subject to great operator variability, which may exceed the range of error of the Nuclear Density Meter. The absolute values of the density of the aggregate at Bothkennar may not be as determined by the Nuclear Density Meter, however, it is not sensible to make a correction on the basis of so few sand replacement tests, especially as the difference between determinations resulting from the two methods is small. The benefit of the Nuclear Density Meter is the large number of non-destructive tests it is possible to perform in a short space of time. The absolute values of the densities may not be as shown in Table 3.5 but they do give a good guide to the consistency of the layer.

3.3.3.2 Falling weight deflectometer (FWD)

The Falling Weight Deflectometer (FWD) was used to assess the stiffness of the pavement layers prior to trafficking. On each section there were five readings taken in the instrumented wheel path, three on the centre-line and three in the un-instrumented wheel path. The mean results are shown in Table 3.8.

The FWD applies a measured stress to the surface of the aggregate by utilising a weight falling onto a platen. Seven remote geophones monitor the resulting deflection of the surface and the "deflection bowl" generated is recorded. The shape of the bowl is a function of the stiffness of the various layers within the pavement structure and the results are back-analysed in an iterative manner until a theoretical bowl, generated by a

computer program using estimated stiffness of the layers, matches that measured in the field.

There are several computer programs that can be used to back-analyse the FWD deflection bowls. The one used in this study is PADAL: (**PA**vement **D**eflection **A**na**L**ysis) (Tam 1987), which is a self-iterating program. PADAL seeks to predict the observed deformations by progressively better estimates of the stiffness of the layers. The results obtained from PADAL in this study are not ideal. There was often a poor match between the calculated and measured deflections at some geophones. For technical reasons this error, of up to 25%, does not imply that the final calculated stiffnesses are in error to the same degree. However, the program is principally designed to analyse pavement structures with bound layers and the high deflections, obtained from the Bothkennar pavements, are not typical. The nature of aggregate surfaces, being uneven, also causes problems as the geophones may not lie properly on the surface. This causes a distortion of the results, particularly at the remotest geophone's position, where the readings are smallest. There is a granular materials version of PADAL called PADALGR. However, the program requires the input of estimated layer stiffnesses from the operator for each iteration and is consequently time consuming to perform. Given that there were 165 FWD results to be analysed, PADALGR was not a useful option. One of the objectives of other work currently under way at Nottingham, is to improve the mathematical models that determine the response of the granular materials, in the hope of getting a better match of bowls for unbound pavements in the PADAL program.

The PADAL program assumes that the stiffness of the subgrade increases with depth. However, at Bothkennar there is a stiffer crust on the surface of the site (as shown in Figure 3.1) and therefore an artificial layer, 0.7m thick, was created in the input of the program in an attempt to model this effect.

Section	Aggregate Stiffness (MPa)	Crust Stiffness (MPa)	Subgrade Stiffness (MPa)
A	81	31	38
B	103	64	32
C	134	40	25
D	203	40	56
E	129	38	38
F	100	31	32
H	84	22	34
I	98	17	16
J	76	17	17
K	83	16	31
L	97	14	24
M	87	22	28
N	100	27	28
O	70	20	39
P	63	15	38

Table 3.8 Mean Wheel Path Stiffnesses Calculated from FWD Data using PADAL (after Tam 1987)

3.3.3.3 The ODIN device (Boyce et al (1989))

The ODIN Device (Boyce et al (1989)) is essentially a large drop hammer which has the ability to vary the contact stresses by the use of plates of differing sizes and using different drop heights. It is being developed by Geotechnics Ltd and Loughborough University and calculates the stiffness of the pavement by double integration of the deceleration (to get vertical displacement) and by measuring contact stress. The device was used to determine the apparent modulus on impact of a selection of sections. The mean results from ODIN are shown in Table 3.9 and a more complete record is shown in Appendix D.

Section	A.M.I. (MPa)
A	160
B	160
D	120
E	150
F	75
H	60
I	70
J	130
K	170
M	140
N	170
O	150

Table 3.10 Apparent Modulus on Impact as Determined by ODIN

3.3.4 280mm Diameter triaxial testing

Both aggregates were tested using the 280mm diameter triaxial apparatus developed at Nottingham University by Cheung and Dawson (1990) as shown in Plate 3.1. Each sample was 560mm long and is contained within a loose fitting PVC membrane. The confining stress to the sample was supplied by a vacuum line, which lowered the air pressure within the sample, and the axial stress was applied by using a hand jack.

Samples of the aggregates, retrieved from Bothkennar, were prepared in a suitably sized mould. The moisture contents of the aggregates had been previously adjusted to the values obtained from the mean site values shown in Table 3.6. The aggregates were compacted in the mould using a vibratory hammer in eight layers of 70mm to a density equal to the mean bulk density values shown in Table 3.6.

Two confining stresses of approximately 15kPa and 50kPa were applied to each sample and a deviator stress of approximately 100kPa was applied in a cyclic manner using the hand jack. 25 load/unload cycles were performed for each confining stress and sample. The resilient modulus was determined for each test, as was the poissons ratio of the material. Finally a multi-stage quick undrained triaxial test was performed to determine the angle of internal friction for each aggregate. The results are shown in Table 3.10.

	Type		Sand & Gravel	
Confining stress (kPa)	20	45	11	50
Poissons ratio	0.33		0.40	
Resilient modulus (MPa)	360	450	325	600
Angle of Internal Friction	.54		58°	

Table 3.11 Triaxial Testing of Aggregates - Summary of Results

3.4. GEOSYNTHETIC SAMPLING AND TESTING

The properties of the geosynthetics were considered likely to change during the course of their use. Therefore, it was decided to try and identify how their properties changed by performing a range of index tests on the geosynthetics at various stages during the trials. The index tests were performed on samples recovered as described below.

3.4.1 As delivered to site

It was necessary to identify the index values of the materials delivered to site so that the geosynthetics could be properly defined. Samples were cut from all of the geosynthetics delivered to site and were stored in a windowless container on the site. No sample was cut from any geogrid because after discarding the first and last 5m of the roll, there was none remaining for testing. This was rectified at the time of testing by the provision of more material of approximately the same index test standards. The container, when closed, was virtually light free. The geosynthetics remained on site until January 1991 when samples were taken and used to examine the effects of the construction processes on the properties of the materials. Post construction and site stored samples were then transferred to Strathclyde University, where they were stored in a dark room until required for testing.

3.4.2 Compaction damage

A series of tests were performed in order to estimate the amount and nature of damage sustained by the geosynthetics in the construction process. It was felt that the tests

performed at the TRRL by Watts & Brady (1990) were too severe on the geosynthetics, with the model of a steel plate for the subgrade. Thus, the compaction damage trials at Bothkennar tried to more accurately model the effects on the geosynthetics. A steel plate, of approximate dimensions 2.6 x 1.3m, was covered in 150mm of re-moulded subgrade material which was compacted with a 1000kg/m vibratory roller. The geosynthetics were then placed on top of the re-moulded subgrade material and attached to one end of the steel plate using a bar and clamps. Type1 material was then laid on top of the geosynthetics in layers of 150mm and compacted with 16 passes of a 1000kg/m vibratory roller. 300mm of aggregate was compacted over each geosynthetic and then the whole sample was lifted, by the steel plate, from one end (as shown in Plate 3.2). The aggregate then fell off the sample, or was easily removable without causing damage to the geosynthetic. The samples were then stored in dark conditions with constant temperature and humidity at Strathclyde University until required for testing.

3.4.3 Post trafficking

At the end of the trafficking of the haul road, samples of each type of geosynthetic were recovered. A full roll width of each material, by 3 or 4m along the length of the pavement, was recovered across each lower-bound pavement (except the Tensar SS1 which was recovered from the upper-bound section). The aggregate was excavated by machine until 70 to 100mm of material remained above the geosynthetics. The remaining amount was excavated by hand. Care was taken to minimise damage of the geosynthetics during exhumation that could have been caused either by the excavating tools or by placing undue stresses on the materials. Any areas where the operators believed that damage was attributable to the exhumation process, were marked with paint and were excluded from testing. These samples were then transferred to Strathclyde University for testing.

3.4.4 Interface friction angles

The friction angles developed at the interfaces in unpaved roads were examined by using a 300mm shear box. The method used was broadly that suggested in BS6906 Part 8 (1991) with the geosynthetic (where applicable) clamped to one end. Two variations were made to the British Standard Method. Firstly, the full Type1 grading

was used as opposed to the fraction passing 10mm. Secondly, the British Standard suggests that the lower half of the shear box is filled with a rigid substrate, in these tests however a model pavement was constructed using the subgrade, geosynthetic and aggregate materials from site. The clay samples were at a moisture content where the re-moulded shear strength was approximately 85kPa and the aggregate was compacted to a bulk density of 2280kg/m^3. The geosynthetic was placed at the junction of the two halves of the shear box.

A series of tests were performed where the aggregate was sheared over different geosynthetics. As can be seen from Table 3.11 the angles of friction determined by the tests, are very close to the angle of internal friction of the aggregate as determined in the 280mm diameter triaxial apparatus which is shown as 54^o in Table 3.10.

It was felt that the good interlock which probably occurs between the geogrids and aggregates would mean that the angle of peak shearing resistance would, in this case, be determined solely by the aggregate. After completing the tests shown in Table 3.12 it was felt that the mechanism controlling the peak angle of shearing resistance was not a function of the geosynthetics, but the angle of internal friction of the aggregate. Thus, the remaining geosynthetics were not tested.

Geosynthetic	Confining stress (kPa)	Peak angle of shear resistance
Needle-punched	100	51°
Heat-bonded	100	54°
	50	64°
	10	56°

Table 3.11 Aggregate/Geosynthetic Friction Angles

A few tests were performed where the subgrade material was sheared over the geosynthetic. It was found that the shear plane occurred within clay itself, and not along the interface (see Plate 3.3). It was thus assumed that the subgrade/geosynthetic shear resistance is controlled by the shear strength of the soil and not the friction angle between the soil and the aggregate.

3.4.5 Index tests

A full range of standard index tests were performed on the geosynthetics at Bothkennar and the full results are given in Appendix A. These principally included tensile strength (BS 6906 part 1 (1987)), Mass per unit area, the CBR plunger tests (BS 6906 part 4 (1989)) and the cone drop test (BS 7906 part 6 (1990)). It is interesting to note that the properties of the geosynthetics alter as progressively more damage is done to them.

The stress/strain response of geosynthetics is probably the most commonly required information for design methods. The findings of Watts and Brady (1990), that compaction damaged geosynthetics become stiffer, weaker and more brittle, has been confirmed by the testing programme. It has also been found that this change of properties continues further with compaction and traffic-damaged samples. The observation that the ultimate strain is much reduced in the post trafficking samples explains why geosynthetic rupture can occur at relatively low rut depths (which indicates geosynthetic strains far below the failure value of index tests on factory samples).

CHAPTER FOUR

THE INSTRUMENTATION AND CONSTRUCTION OF THE EXPERIMENTAL HAUL ROADS

4.1 INTRODUCTION

Construction started on site on 10 July 1989 and was completed on 8 November 1989. A total of sixteen sections were constructed (Figure 4.1) together with un-instrumented bends and three un-instrumented, ad hoc, bays. Each section had dimensions of 20m long by 4.5 to 5m wide. This width enabled the geosynthetics to be installed at the manufactured width, as shown in Figure 4.2, without recourse to longitudinal laps or, conversely, any action to reduce the width of the delivered material. No attempt was made to pre-tension or place end restraint on the geosynthetics.

Two types of aggregate were used in the construction of the haul road and these were both obtained locally. The Type1 material, known locally as 'Whinstone', was obtained from the nearby Wimpey Asphalt quarry. It was a crushed rock of igneous origin, probably a diorite and met the requirements of Type1 as specified by the Department of Transport (1986). The sand and gravel mixture was also obtained locally but had to be separately blended. The specification for the sand and gravel mixture was obtained from the Sand and Gravel Association Limited (undated). The use of sand and gravel as a sub-base material in this part of Scotland appears to be limited, hence, the mixture was more expensive than the Type1 material.

The instrumentation layout was designed to measure a number of "key" parameters of the soil-geosynthetic-aggregate system. It was intended to measure the transient and permanent horizontal strains of the geosynthetic directly under the wheel path and transversly across the pavement, which would give some indication of the strain distribution along the inclusion. Transient and permanent vertical strains at the top of the subgrade and at the base of the aggregate layer would give some indication of the vertical strain distribution and of the contribution to surface deformations generated at these levels. Transient stress measurements would determine the peak vertical stresses at the base of the aggregate layer and at the top of the subgrade and would give some indication of the stress distribution through the aggregate layer. The ambient temperature of the geosynthetic would be monitored during the trafficking trials and the

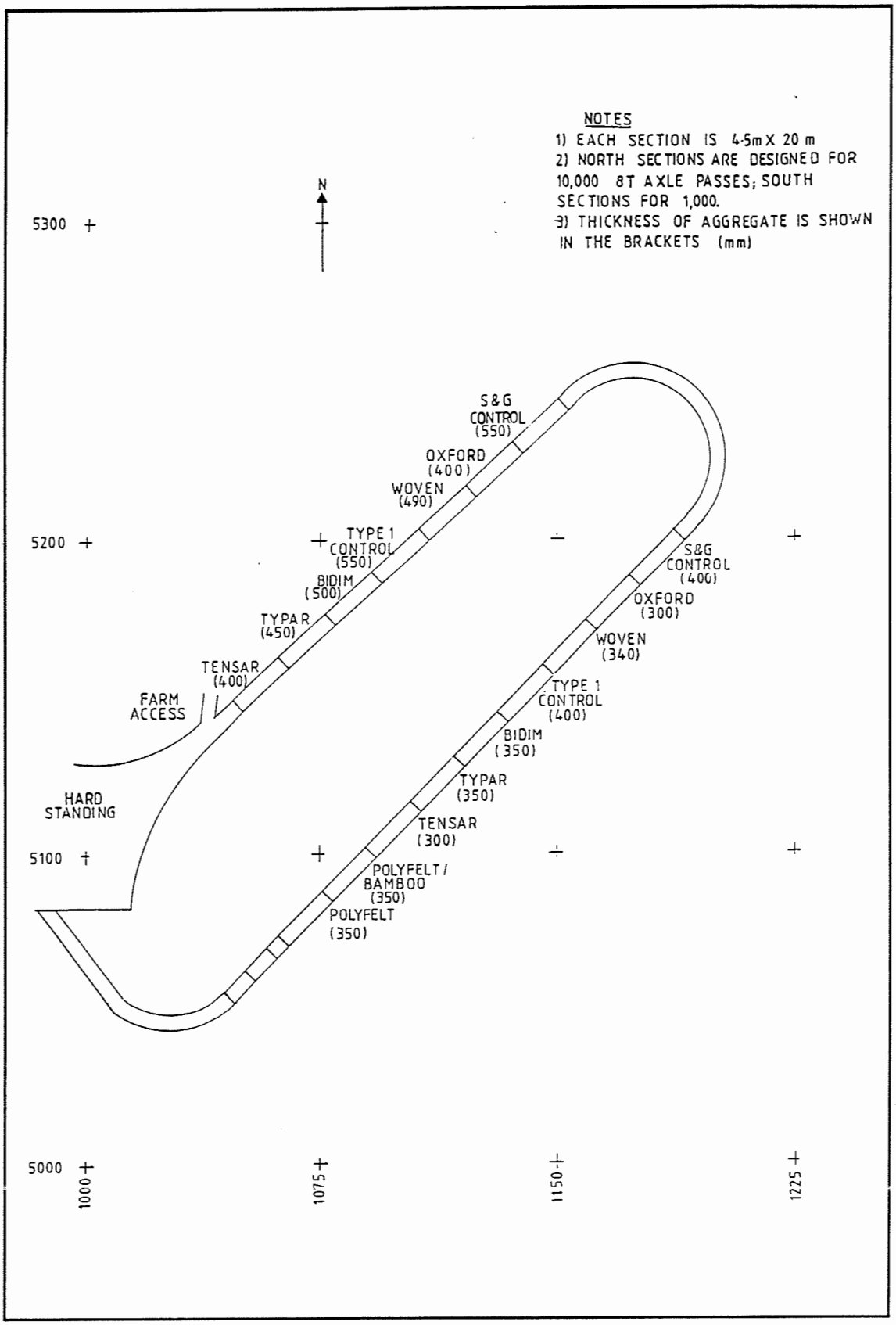

Figure 4.1 Site Layout

pore water pressure at the top of subgrade would be estimated. The instrumentation was concentrated in two areas within each section, 5m and 15m from the start, and these will be referred to as Reading Locations 1 and 2 respectively. The two reading locations broadly contained the same instrumentation some of which generated duplicate results. This duplication provided some insurance against loss of instruments during the construction and trafficking processes.

The lower-bound sections contained more instruments than the upper-bound. It was expected that the lower-bound sections were likely to provide more information about the mechanism of the system in a shorter period of time and hence, for reasons of economy of time and money, it was decided to concentrate the instrumentation into the lower-bound sections.

The layout of the instrumentation for the lower-bound sections is shown in Figure 4.2 and for the upper-bound sections in Figure 4.3.

4.2 INSTRUMENTATION MANUFACTURE AND CALIBRATION

The instrumentation for the project came from a variety of sources. With the exception of the piezometers, the instrumentation was manufactured by local firms in Nottingham or at the University. Pressure cells were fabricated by the University Engineering Faculty Workshop. They were then calibrated by exerting a range of known pressures on the surface of the cell and noting the resulting voltage shift, an example of which is shown in Appendix E.

Strain coil formers were fabricated by a local firm in Nottingham using "Carp" grade "Tuffnol", and the coil winding and attaching of cables was undertaken by another local company. The coils were then calibrated out of soil using the Bison equipment for transient and static conditions. Before using the coils on site, silicone rubber was used to seal the coil and the wire in order to exclude water and to increase the strength of the coil-wire joint.

The strain coils were calibrated using the Bison system. However, full calibrations were not necessary because Dawson (in print) has shown that, for any family of coils, the amplitude/spacing relation for any individual coil pair can be predicted from three known amplitude/spacing co-ordinates. Furthermore, Dawson found that the out of

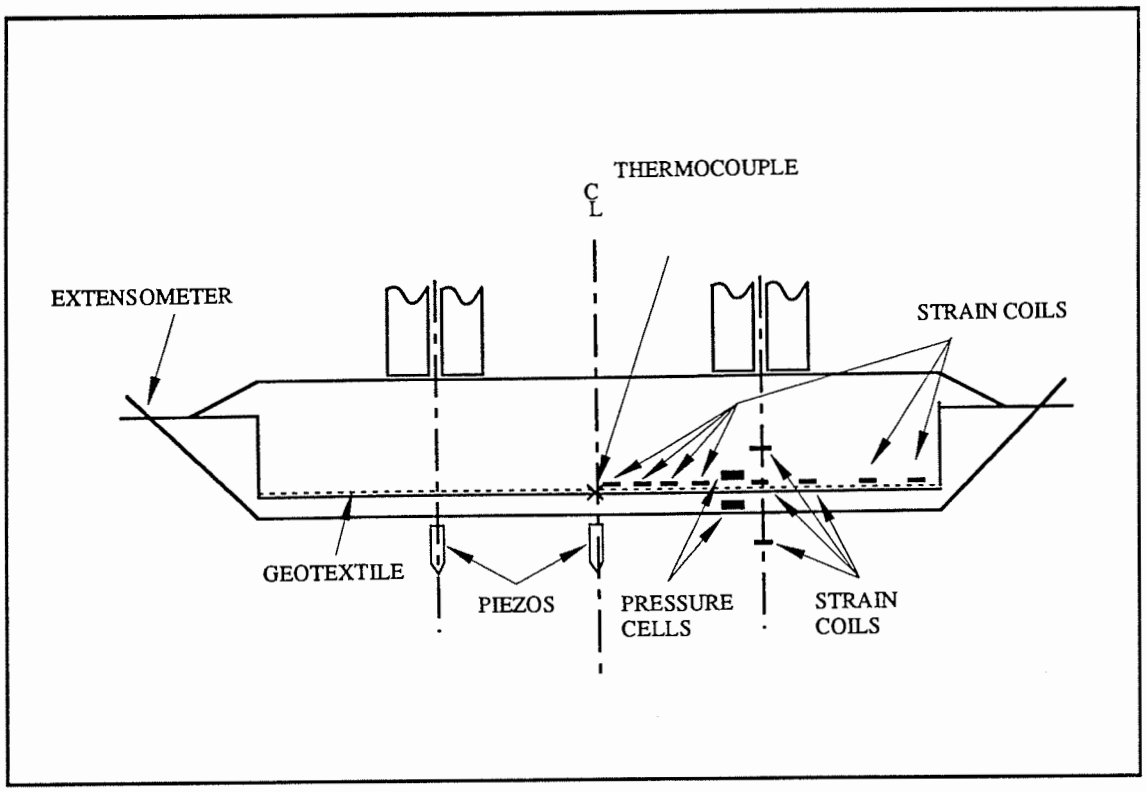

Figure 4.2 Instrumentation Layout - Lower-bound Pavements

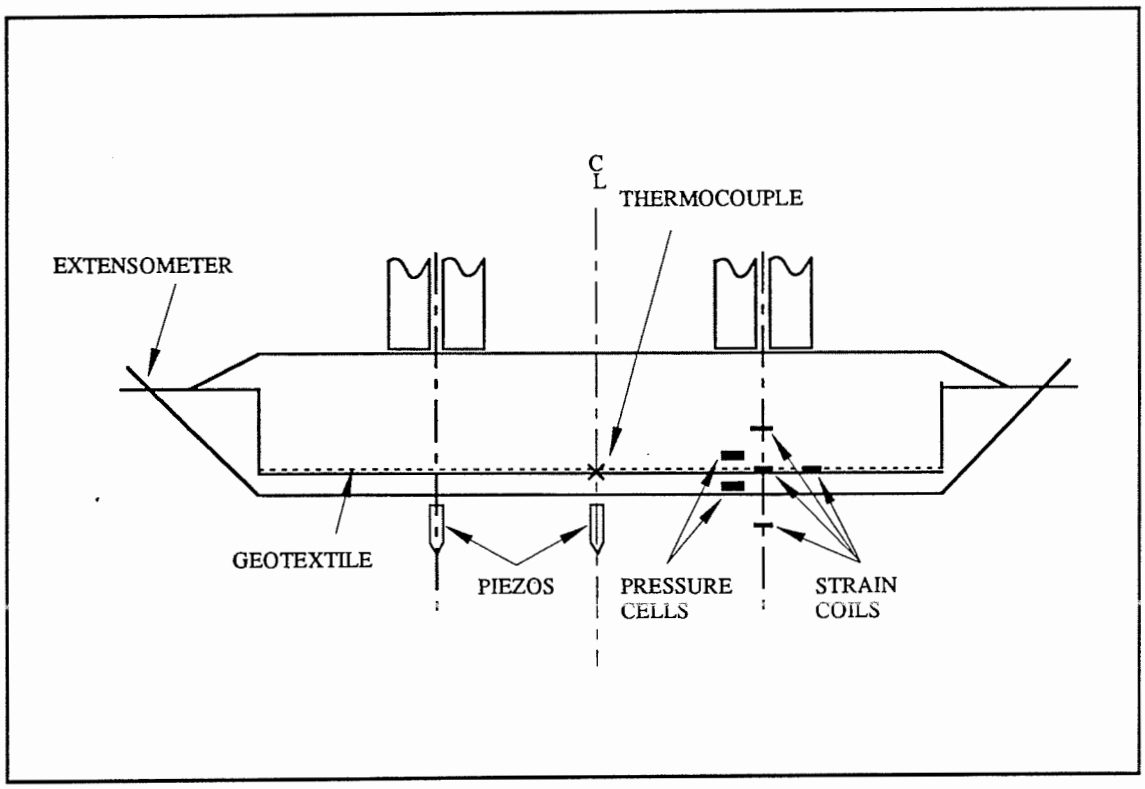

Figure 4.3 Instrumentation Layout - Upper-bound Pavements

balance voltage relating to movement of the coils is a function of the gradient of the amplitude/spacing curve at the spacing of interest. Thus complete calibrations were generated using 3 amplitude/spacing co-ordinates and 2 out of balance voltage/strain measurements. The coils were subsequently read using the Emu system (see Chapter 4.4) and so a cross-calibration between the two systems was performed using coils of the same family. Example calibrations and the cross calibration between the Bison and Emu systems are shown in Appendix E.

The holders for the magnets for the horizontal extensometer were manufactured by the University Engineering Faculty Workshop and the magnets were bought from a company in the West Midlands. The units were then fabricated on site. The vertical inspection tubes were made from "Heavy Duty Vaccuflex" supplied by a firm in Nottingham. Thermocouple wire was purchased from a propriety manufacturer and the junctions were welded at the University.

4.3 INSTRUMENT INSTALLATION

4.3.1 Subgrade

Two pressure cells were installed in the subgrade of each section 500mm in advance of each of the two reading locations. Previous trials (Brunton and Ackroyd (1990)) have shown that as vehicles approach, the subgrade pressure cell generates a rise in the out of balance reading, which can be used to prompt the data acquisition system to start recording. Thus, the subgrade pressure cell was installed 500mm in advance of the other instruments in order to be certain that all values were recorded. The cells were buried horizontally with the top of the diaphragm 20mm below the surface of the formation. This protected the instrument from being damaged by angular pieces of aggregate pressing onto the casing and aided reading accuracy.

A strain coil pair was installed in a vertical, axial orientation at the top of the subgrade directly beneath the wheel path at each reading location. The gauge length was set to approximately 100mm by burying the lower coil in the subgrade. This strain coil pair was installed to measure the transient and permanent subgrade strains immediately under the geosynthetic.

A horizontal extensometer was installed 3m past the first reading location, placed transversly across the pavement. The six extensometer plates carried the magnets and were spaced so that the first magnet was located on the centre-line of the pavement, the last on one edge, and the others equidistant in between. It was hoped that the extensometers would give some indication of the gross horizontal strains occurring in the subgrade across the full half-width of the pavement.

Two high air entry Bishop-type piezometers were installed, one under the wheel path and one on the centre-line, both at the second reading location. These were buried with the centre of the ceramic portion of the piezometer at a depth of approximately 200mm from the surface of the formation. This depth enabled all the fittings close to the instrument to be comfortably buried. All the piezometers were soaked in water overnight before being placed in the ground in order to saturate the ceramic portion prior to installation.

Thermocouples were not included in all sections as the temperature of the geosynthetics was unlikely to vary significantly between one section and the next. The upper-bound sections contain three thermocouples in total and the lower-bound contained four.

4.3.2 Geosynthetic

A strain coil pair was attached to the geosynthetic directly below, and in a transverse direction to the wheel path. In the lower-bound pavements a further three strain coils pairs were attached to the geosynthetic transversly across the pavement at each reading location. The offsets of these coils from the centre-line of the pavement were different for each reading location as can be seen from Figure 4.2 and Table 4.1. This was done so that a better estimate of the transient strain distribution could be made. As the geosynthetic was expected to strain in a tensile manner the gauge length of the strain coils was set to the lower spacing of their range (approximately 75mm).

Transverse Coil Pair	Reading Location 1	Reading Location 2
A	0.35	0.65
B	1.50	1.40
C	2.00	1.75

Table 4.1 Location of Remote Geosynthetic Strain Coils

It was considered preferable that the strain coils did not embed themselves in the subgrade, which could cause resistance to any slip that might naturally occur at the soil/geosynthetic interface. In an attempt to minimize any inaccuracies that this effect might generate, a patch of the same geosynthetic was placed between the strain coil and the subgrade, and a little sand was used to produce a smooth profile as shown in Figure 4.4.

The coils were attached to the non-woven heat-bonded geosynthetics by melting a 6mm diameter hole through the fabric with a soldering iron. The coil was then attached to the fabric by the use of a 0BA nylon nut and bolt which fitted tightly into the 6mm diameter hole in the centre of the strain coil. The coils were attached to the woven and non-woven needle-punched geosynthetics in a similar manner to the heat-bonded non-woven except that the fibres of the material were eased apart and the 0BA bolt was pushed through. Strain coils were attached to the grid using small plastic clamps and four nylon 4BA screws on each corner of a node. It was thought to be unnecessary to create a "patch" between the grid and the subgrade.

The section constructed in conjunction with Strathclyde University (McGown et al (1990)) using Polyfelt and bamboo consisted of 3.3m long, 65mm diameter poles placed at 150mm centres transversly to the direction of the traffic flow, immediately on top of the geosynthetic. It was not feasible to instrument the bamboo itself and so the geosynthetic was instrumented in exactly the same manner as the other lower-bound sections.

A small quantity of finer material, that part of the aggregate passing 1.18mm, was placed on the geosynthetic above the strain coils to protect them from damage during the compaction of the aggregate. Some aggregate was then placed carefully over the strain coils prior to the section being filled. This helped to prevent the coils moving

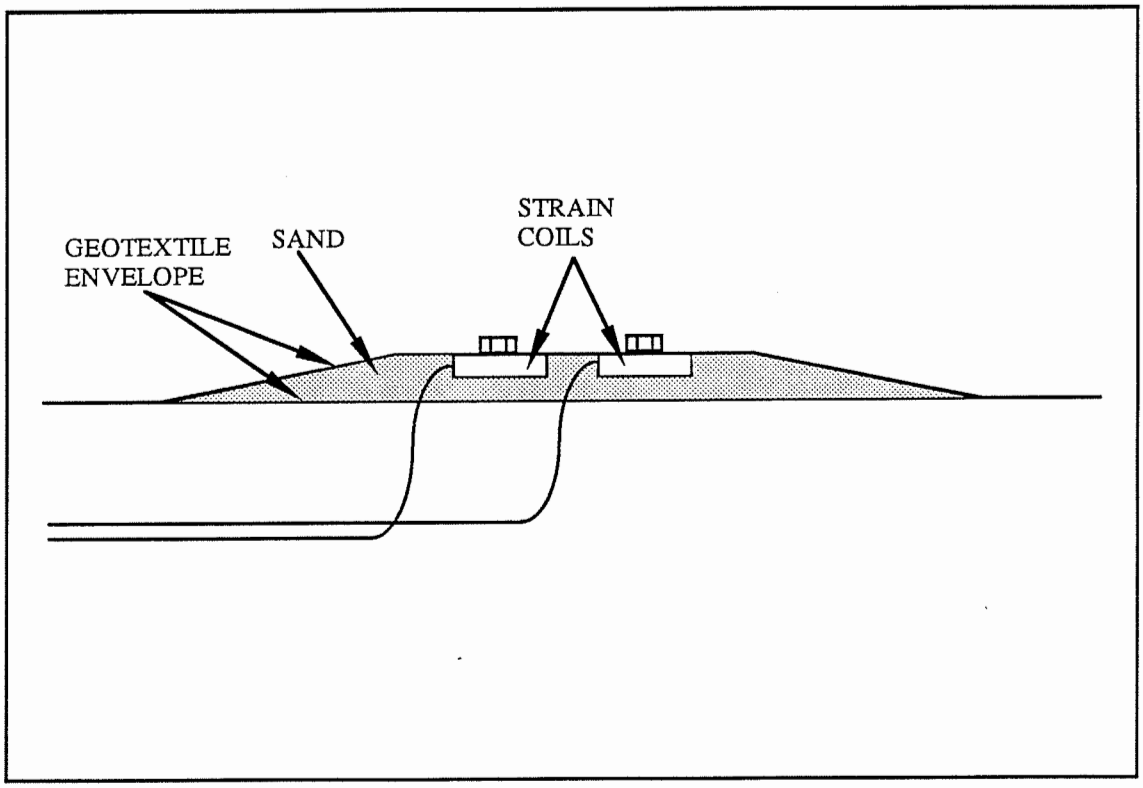

Figure 4.4 Strain Coil Attachment to Geotextiles

away from their position during the construction process and to minimize the danger of damage to the coils.

4.3.3 Aggregate

One strain coil pair was installed under the wheel path at each reading location in a vertical, axial orientation, with an initial gauge length of 100mm, at the base of the aggregate layer and with the lower coil being the one attached to the geosynthetic. The upper coil was surrounded with finer material passing 1.18mm sieved from the aggregate. This bedding of the instrument on fines enabled the coil to be installed horizontally which is important for this type of instrument as the calibration is sensitive to any tilt in the coils. The fines also prevented the coils from becoming damaged during the compaction or trafficking processes.

One pressure cell was installed under the wheel path 500 mm past each of the reading locations. The pressure cells were installed horizontally with the diaphragm 50mm above the geosynthetic and they were bedded on finer material, passing 1.18mm, sieved from the aggregate. Fines were also placed on top of the pressure cell diaphragm to protect it from damage and to improve the reading accuracy of the instrument. The instrument and fines were all installed within a thin walled plastic bag to ensure that the fines remained in place during construction and trafficking.

A set of six vertical inspection tubes were placed transversly over half of the pavement in equal distances from the centre line to the edge of the geosynthetic at each reading location. The function of these tubes was to provide direct access to the geosynthetic below. Direct profiles of the geosynthetic were to be obtained during the course of the trial by levelling the top of a 1m long bar lowered into the tube and placed on the geosynthetic.

4.3.4 Level control

The subgrade was levelled in a 0.5m grid so that it could be compared to the level of the finished aggregate surface. The level information was also used to determine the finished level of the aggregate. A "base formation level" was calculated on the basis that 85 percent of the formation level readings fell below it. The required thickness of

aggregate was added, by the contractor, using a laser level which was set so that the foresight reduced level was the base formation level plus the required thickness. Thus, it was hoped that 85 percent of the section would be covered by the appropriate design thickness of aggregate.

The final aggregate surface was levelled in a 0.5m grid before any trafficking commenced and the results were compared to the results obtained from the levelling of the subgrade. The exact thickness of material at each location on the 0.5m grid was then calculated.

4.4 DATA COLLECTION ARRANGEMENTS

All of the signal cables from the electrical instrumentation were terminated in an instrumentation pit by the side of each section. The strain coils and pressure cell cables were fitted with plug sockets to enable a sound and speedy connection to the instrumentation during data collection procedures.

The pressure cell signals were amplified using strain gauge amplifiers before they were recorded, through an analogue to digital converter, to a personal computer. The amplification applied was 4,000 which gave an approximate calibration of 1 V per 100 kPa for these pressure cells.

The signals from the strain coils were operated and received by the Emu device (Dawson (in print)). The Emu device generates a high frequency alternating current in the transmitting coil and by inductance, a voltage is generated in the receiving coil. This spacing voltage is unique for any given strain coil pair and thus, by previously calibrating the coils, this static spacing voltage generates a unique spacing of the coils. Changes in this value represents permanent strain. The static strain coil spacing voltage was recorded manually and the amplified dynamic output was recorded in the same manner as the pressure cells. The voltage generated by the dynamic output of the Emu device as a result of transient strain depends on the magnitude of the strain, the spacing of the coils, the amplification to the signal by the device and the individual coil pair. Therefore, no simple approximate calibration existed for these instruments.

The analogue to digital device was capable of recording twenty channels at the same time, although the maximum that was actually recorded at any one time was eight. The

data was recorded at 5 millisecond intervals which ensured that the sampling rate was much higher than the duration of the recorded event. The full-scale deflection of the analogue to digital machine was set to ± 5V. This scale was divided into ± 32,000 bytes and so the resolution of the output was below 1mV.

Due to restrictions on the number of read-out and recording devices available, it was possible to read only one instrument reading location in any one pass. Since the layout of the road was such that there were un-instrumented sections between the upper-bound and lower-bound sections, it was possible to record the transient effects of the pass of the lorry for one upper-bound and one lower-bound reading location per circuit. As Sections G and H had no instrumentation, it was possible to read all of the six upper-bound instrumentation reading locations within twelve passes, and the eight lower-bound sections in sixteen passes. Thus, in each complete circuit the data from each upper-bound reading location and its corresponding lower-bound partner was recorded.

4.5 CONSTRUCTION

4.5.1 Construction method

The contractor was originally requested in the specification for the works (Little (1990)) to use the existing constructed pavements as a platform from which to work. This was specified because, on the previous site visit in April 1989, the ground was so soft that it was considered unlikely that it would be able to withstand the construction traffic. However, the dry summer of 1989 resulted in a firmer crust developing on the site, which enabled the construction traffic to run directly on the surface. Thus, none of the sections were trafficked during the construction period, removing the uncertainty of estimating the amount of damage each section received as a result of construction traffic.

The dates when each section was constructed are given in Table 4.2. It should be noted that those sections which were constructed during July 1989 were built on much firmer ground conditions than those constructed in October of the same year. However the subgrade remained firm throughout the whole period and, even in October, if the weather remained fair, the shear strength of the soil could reach as high as 100 kPa .

	Upper-Bound Sections	Lower-Bound Sections
Tensar	11/7/89 - 14/7/89	4/10/89 - 5/10/89
Typar	17/7/89 - 19/7/89	28/9/89 - 29/9/89
Bidim	19/7/89 - 20/7/89	24/9/89 - 27/9/89
Type1 Control	21/7/89	2/10/89 - 3/10/89
Woven	5/9/89 - 6/9/89	11/9/89 - 12/9/89
Oxford	8/9/89 - 12/9/89	12/9/89 - 14/9/89
Sand & Gravel Control	11/9/89	12/9/89
Polyfelt/Bamboo		23/10/89 - 25/10/89
Polyfelt		26/10/89 - 28/10/89

Table 4.2 As built programme for the haul roads at Bothkennar

The amount of exposed formation at any one time was limited to 40m because, firstly, the exposed formation was vulnerable to changes caused by the weather (ie drying out or becoming too wet) and, secondly, because the method provided an efficient use of plant as it represented a day's work for the tracked excavator on site.

The removal of 40 linear metres of topsoil exposed more of the formation than could be instrumented at any one time. Therefore, the formation was covered with heavy duty polythene with the aim of protecting the formation in the event of rain. However, as it transpired, the major beneficial effect of the covering was to prevent moisture loss from the subgrade. Even so, some further drying of the formation did occur in the hot, dry weather experienced at the start of the project. The polythene could not keep out all weathers and at the end of the project the rain did manage to get under the polythene and had a significant effect on the condition of the subgrade. These effects are noticeable from the shear vane tests that were taken at the time. Some of the shear vane readings for the surface of the formation were regularly off the scale of the instrument in July (ie they were greater than 126 kPa) and became as low as 60 kPa later in the year.

The fill material was placed on the geosynthetics with as much care as could be expected from any contractor. The material was never tipped directly onto the geosynthetics, but placed using the back-actor of the machine. In this manner the construction damage should have been kept to a minimum.

4.5.2 Sampling and In-Situ Testing

Shear strength readings were obtained, at the time of construction, using a small hand-held shear vane of dimensions 19mm by 28mm. Readings were recorded at depths of 30, 200, 300, 400, 500 and 800mm at each reading location (see Appendix B).

Clegg Hammer readings of the subgrade were taken at three points on each reading location at the time of construction, as were six cone penetrometer readings. The results of these can be found in Appendix B.

Bulk samples of the subgrade material were retrieved from the edge of the pavement at formation level at each reading location. These samples were used to determine the Atterberg Limits, particle size analysis and specific gravity. 38mm diameter triaxial samples were taken from the subgrade at formation level underneath each wheel path and the centre-line. Quick undrained triaxial tests were performed at Nottingham University as discussed in Chapter 3.2.1.5

The moisture content of the subgrade was determined at the formation level and at 200mm below and 350mm below formation at the time of construction.

4.6 MISCELLANEOUS COMMENTS

An uncapped borehole from a previous site investigation was discovered in the lower-bound grid section (Section N). The borehole was located 5.5m past the start of the section on the centre-line of the pavement. Because of its location in the centre of the road, it was not possible to relocate the section. Also, because the borehole was on the centre-line, it was thought that it would have little effect on the performance of the section. However, as a precautionary measure, the first reading location was moved from 5m to 3m into the section. The depth of the hole was in excess of 4m. It was capped using a timber board at a depth of approximately 500mm and back-filled with suitable material prior to placing the geogrid.

The contractor had to undertake some remedial work on 12 September 1989 when he inadvertently buried the heavy duty polythene that was covering the sand and gravel control section. In the removal of the material, geosynthetic in the Oxford upper-bound section was damaged at 17.4m from its start. The damage was so severe that it was

decided to remove the remains of the damaged section and replace it with new geosynthetics. This was done using a lap length of 1m from 16.4m to 17.4m from the section's start point.

The Polyfelt/Bamboo section was designed by the team at Strathclyde University (McGown et al (1990)) and it consisted of Polyfelt TS500, 3.1m x 60/65mm diameter bamboo placed directly on top of the geosynthetic, with 350mm of Type1 aggregate. Thus the geosynthetic grade and the depth of Type1 material is the same for both the Polyfelt/Bamboo and the Polyfelt sections. No attempt was made to restrict the movement of the bamboo in relation to the geosynthetic by stitching or enclosing it in geosynthetic "envelopes". The bamboo itself was not instrumented so the section was instrumented in the same manner as the other lower-bound sections. The bamboo came from a supplier in Glasgow, Tropical Cane Limited, but its strain and country of origin is uncertain. This section is 5m wide, as opposed to the other sections which are 4.5m, in order to obtain the required overlap of the bamboo on the centre-line. The bamboo was laid at 300mm centres transversly to the direction of the traffic flow, with a lap length of 1.2m.

An accident caused damage to the upper-bound grid section during the installation of the vertical inspection tubes. The result of this damage was an "L shaped" tear that was 7 nodes long in the direction of trafficking and 13 nodes wide. This event was photographed and recorded but the section was not reconstructed. This accident was used to examine, at least qualitatively, the effects of construction damage on the life expectancy at that location. The damage occurred at one of the two reading locations on the un-instrumented half of the pavement. There is no evidence that instrument readings were affected. That part of the section was monitored closely but no premature rutting contributable to this construction damage was noted. The vertical inspection tubes (see Chapter 4.3.3) were moved to a different location from the damage.

4.7 ANCILLARY WORKS

During October the Oxford and the Woven fabric lower-bound sections were subject to flooding, with water standing on the aggregate surface. It was decided to install some shallow drainage to remove the surface water from the aggregate of the affected

sections. A rubble drain was installed along the side of all sections from the sand and gravel lower-bound control to the Bidim lower-bound sections inclusive.

The test sections themselves were fenced off with wooden posts and plain wire. This precautionary measure was undertaken to prevent people from thoughtlessly using the haul road as an access route to other parts of the site. While use of the upper-bound sections for this purpose was never ruled out, the existence of the fencing and the gated ends enabled some control to be exercised over access.

CHAPTER FIVE

TRAFFICKING AND INSTRUMENT PERFORMANCE

5.1 INTRODUCTION

Seasonal monitoring of the subgrade suggested that the crustal shear strength reached a minimum in late Spring. Therefore, the original intention was to traffic the haul roads in the Spring of 1990 to their design life span of 1,000 passes of an 80kN axle. However, at the time of trafficking the crust on the site was much firmer than it had originally been found to be and so after 1,000 passes of the 80kN axle little damage was noticeable and complete failure had not been generated in any of the sections. Therefore, it was decided to subject the pavements to at least a further 1000 passes of a 126kN axle in the Spring of 1991, in order to generate significant deformations and/or failure in most of the sections.

5.2 THE VEHICLE AND LOADING ARRANGEMENT

The lorry used to apply the loading was a road-going vehicle with a single rear axle and twin tyres as shown in Plate 5.1. The lorry was loaded, for the first 1000 passes, by the means of two, two tonne, steel blocks. The axles were individually weighed on a public weigh-bridge and the loads were found to be:-

Front - 8130kg $\pm$ 10kg
Rear - 3140kg $\pm$ 10kg.

The lorry was weighed at the start and at the end of the trials to ensure that the load remained constant throughout. The rear axle weight was 24kg below the 8154kg specified (80kN). An analysis of the stresses in the pavement was undertaken using a multi-layered linear elastic analysis (Peutz et al, (1968)). It showed that the spacing was such that the front axle exerted a negligible influence on the vertical stresses on the subgrade at the aggregate interface beneath the rear axle. The same type of analysis, of vertical stresses at the subgrade/aggregate interface directly under one of the wheels, implied that tandem axled vehicles imposed no higher vertical stresses than a single axle

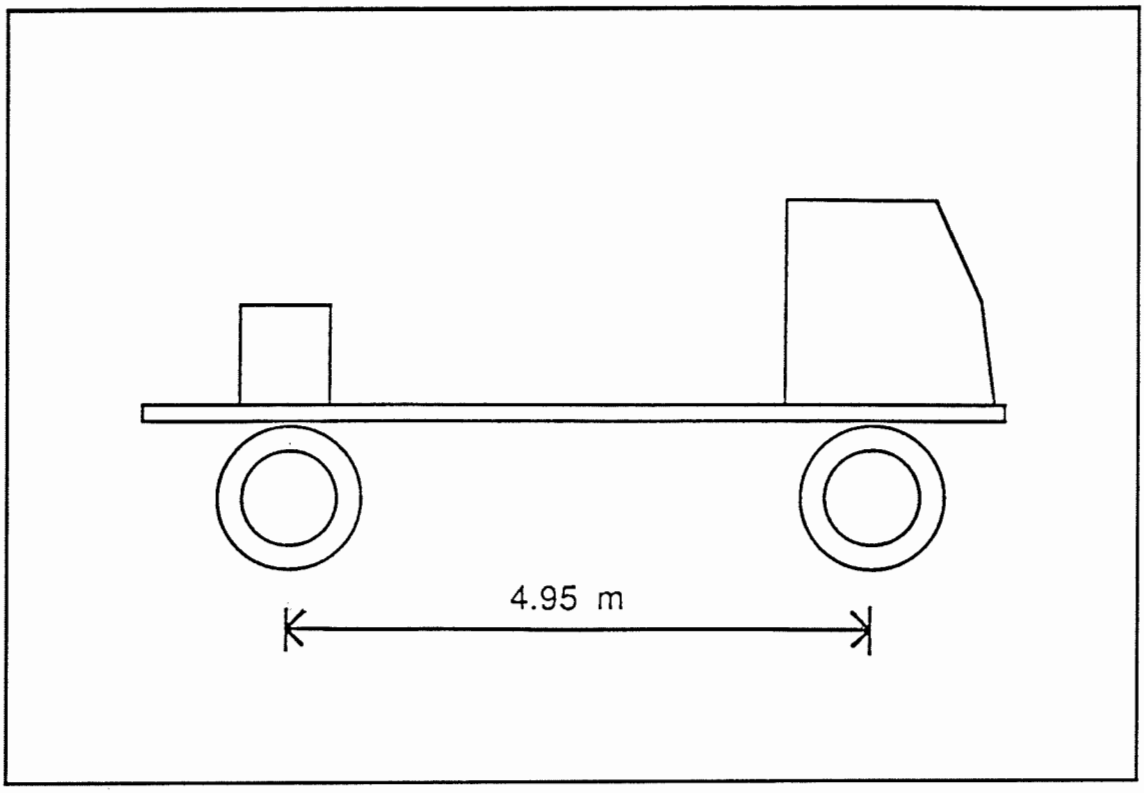

Figure 5.1 Vehicle Axle Spacing

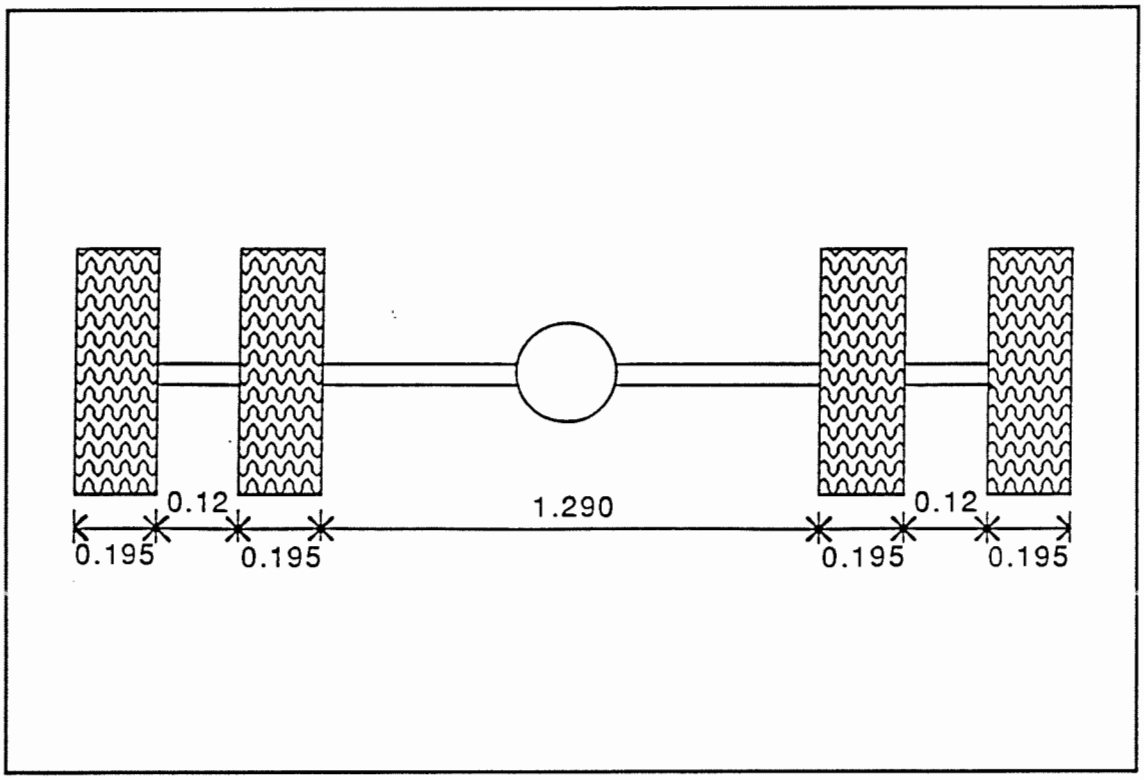

Figure 5.2 Rear Axle Tyre Configuration

and therefore, one assumes, would be no more damaging than the sum of the standard axles applied.

The vehicle used for the trafficking trials in 1991 was the same road-going lorry used in the 1990 phase of loading. Kentledge on this occasion was provided by concrete blocks placed over the rear axle. An initial 15 passes of an 80kN axle were applied in order to re-compact any looseness of the aggregate surface that might have resulted from frost heave or other movement over the intervening year. A further 100 passes were then applied to the pavement in the hope that a comparison between the damage done by 80kN and higher axle loads could be made. For the 115 passes of the axle at approximately 80kN, the axle weights were:-

Front - 5620$\pm$ 10kg

Rear - 8790 $\pm$ 10kg

The vehicle was then loaded to the maximum value that the operator judged to be safe and re-weighed. The axle loadings were:-

Front - 5100 $\pm$ 10kg

Rear - 12880$\pm$ 10kg

giving rear axle load of approximately 126kN.

The two rear wheels were weighed individually and were found to be:-

Nearside - 6700 $\pm$ 10kg

Offside - 6180$\pm$ 10kg

The haul road was loaded by a further 1000 passes at this axle load. Because of direction of trafficking the nearside wheel traversed the outer un-instrumented wheel path of the loop of the trial road.

The lorry proceeded at 3 m/s (6mph) for the first 50 passes in order to permit the pavements to "settle" after construction. After 50 passes the lorry speed was increased to about 10 m/s (20mph). This increase in the speed of application of load enabled a reasonable number of passes to be applied each day. It was observed that the speed of loading did not affect the rate of rut development in the Sandleheath trials (CIRIA (1986)). The speed was reduced to 3 m/s on each of the subsequent occasions when the transient responses of the instrumentation were measured.

In an attempt to increase the rate of deformation in the pavements, the lorry's tyre pressures were increased from 70psi to 90psi (490 to 630kPa) after 250 passes of the 126kN axle load. This was done in the belief that higher tyre pressures lead to a higher contact stress, hence to higher vertical stresses within the pavement and therefore to higher deformations. However, at the base of the aggregate layer little increase in vertical stress was recorded from the pressure cells as a result of the increase in the contact stress and also the rate of rut depth development did not noticeably increase.

5.3 FREQUENCY OF MEASUREMENTS

In planning the test programme for the Spring of 1990, it was assumed that damage to pavement structures was a function of the logarithm of the number of passes. Therefore, it was decided to monitor the pavements more frequently at the start of the trial. Readings of permanent deformation were taken after 0, 1, 3, 11, 50, 100, 250, 500 and 1000 passes. The readings of transient stress and strain took 16 passes to collect due to the limited number of monitoring units available and therefore transient values were taken as groups around 8, 50, 100, 250, 500 and 1000 passes.

A more pragmatic approach to the in-situ measurements was taken in 1991. For sections which performed well, the rate of sampling was reduced, until failure started to occur, when the sampling rate rose sharply. Generally, a full set of readings (static and transient) occurred at or around pass numbers:-

1000 (start of 1991 season)
1015 (to account for re-compaction due to frost effects etc)
1115 (end of 80kN applications)
1220
1365
1615 (lower bound cases only)
2115 (end of trafficking)

5.4 OBSERVATIONS ON PERFORMANCE

5.4.1 General

Generally the pavement sections performed well compared to the original design proposals of a 150mm rut after 1000 passes of an 80kN axle. However, this was to be expected given that the shear strength of the subgrade increased so markedly between design and trafficking. The progression of rutting with traffic was slow although it was possible to see the lorry's path after a few passes. A small amount of aggregate compaction occurred in the first few passes even though the surface of the aggregate was rolled with a dead 1000kg/m roller prior to the onset of the trials and the reasons for this are discussed in Chapter 7.1.

It was possible to see significant transient deflections at the pavement surface as the wheel of the lorry passed over. These deflections were more pronounced on the lower-bound sections. The flexing of the pavement structure to this extent probably caused the cracking which appeared in the surface of the aggregate. These cracks were similar in appearance to the fatigue cracks normally associated with asphaltic pavements. It is possible that these were tension cracks generated by the large deflections of the pavement surface under the wheel load. Suctions within the aggregate layer may have permitted them to stay open for a short while, during which time small particles may have been displaced into the cracks preventing closure when the suctions dissipated. This effect may have reduced the amount of compaction that could have occurred within the aggregate layer.

5.4.2 Failure

On those sections that performed well, the passage of 2115 axles of differing load magnitude has produced little damage. Examination of the trends imply that failure for some sections is not imminent. However, it was found that the failure was brittle in nature in that the rate of rut depth development increased dramatically in the post-failure pavements. Visual inspection of a section close to failure indicated that a large rise in the surface transient deflections occurred. This was coupled with transverse surface cracks appearing in the wheel path which were probably a result of the mechanisms discussed in 5.4.1.

In the majority of cases the ruts were reasonably uniform along the length of each section. Notable exceptions were Section J, and to a lesser extent Sections O and P, where larger, local rut depths occurred leading to localised failure. The rut depths for each section were measured in the offside (RHS) wheel path. Not surprisingly, given the slight discrepancy in the wheel loading in the 1991 trials, the nearside (LHS) wheel path suffered greater damage in some sections.

5.4.3 Localised phenomena

On some of the lower bound sections, localised rutting started to develop at the instrument reading locations. Section J, Reading Location 1, was noticeably poor from near the onset of the trials, as had been expected from the low density of the aggregate at this location as determined by the Nuclear Density Meter as shown in Table 3.6 However, other sections showed minor localised rutting at the reading locations where the instrumentation had been installed after the construction of the pavement sections, an example of which is Section P, Reading Location 1. This effect was probably caused by the excavation of the aggregate layer during the installation of aggregate pressure cells and strain coils, which disturbed the homogeneity of the layer. This experience highlights one of the difficulties when using instruments, namely that the inclusion itself can alter the structure of the material and, therefore, the properties being measured. In this case, the localised rutting is caused either as a result of aggregate segregation, resulting from the excavation process, or because the excavation disrupted the locked-in lateral stresses that are thought to exist in this type of material, or by poor compaction of the material replaced in the excavated hole. All three causes have probably played a part.

It was decided not to undertake any remedial work on the areas of localised rutting in question. The ruts were of a small size and never exceeded 100mm in depth. The fact that these were the areas where the instrumentation had been installed made them important to the trial. It was, therefore, considered better to permit the rut to develop and to be able to relate the surface deformations to the internal aggregate strains measured from the instrumentation, rather than to patch the holes with an unknown quantity of material and to loose that correlation.

5.4.4 The premature failure of the 'Oxford' lower-bound section

A localised failure was apparent in the 'Oxford' lower-bound section (Section I) almost from the on-set of the trials. This was on the un-instrumented wheel path near to the junction with Section J. The surface rut at this location rapidly exceeded the design value of 150mm and the geogrid ruptured. The failure caused large amounts of heave to occur on either side of the rut. As the rut developed the heave was so significant that the subgrade was shaved by the front axle of the lorry on every pass, as can be seen in plate 5.2.

At the end of the trafficking period in 1990 the area in question was excavated to investigate the cause of such localised failure. The subgrade was extensively tested with a hand held shear vane and the results from the wheel path yielded a typical value of about 40kPa. Because the subgrade material at Bothkennar is sensitive and that during failure some re-moulding of the subgrade occurs, the measured shear strength of the subgrade after failure, at 40kPa, might be expected. While 40kPa was the design strength, it is difficult to determine whether a soft-spot existed in the subgrade or not.

It is possible that the geogrid was damaged at this location on installation, however, no record of such damage had been noted in the records taken at the time and the site staff have no recollection of any event which may have caused such damage. The installation of the drain next to the 'Oxford' section may have affected the performance. The drain was installed in an attempt to remove excessive free water standing on the surface of the section and was installed with the invert at formation level. If there had been a low spot in the formation at this point, then it is possible that water could have entered the formation from the drain. However, the next section, Section J, should also have suffered as the level of the formation was lower than that of Section I.

The geosynthetic in this section was a light-weight geogrid and index testing on samples recovered after trafficking indicated that the ultimate strain was on average only 3.1%. If it is assumed that the subgrade rut depth equals the surface rut depth and that the deformed geosynthetic profile is parabolic, then it can be shown that 3.1% geosynthetic strain is equivalent to a surface rut depth of 124 mm. Although failure occurred before a 124 mm rut depth was obtained, the 3.1% ultimate strain is an average figure and so at this location geogrid rupture could have occurred at lower strains and therefore lower surface rut depths.

The rupture of the geosynthetic was examined carefully and was followed back to the edge of the rupture. The grid was apparently failing along a line of nodes, with the bars of the grid splitting in half lengthways. The grid was failing on a line parallel to the direction of trafficking. The area of geogrid next to the point of propagation was plainly in compression as the surface of the geogrid was buckled along an axis perpendicular to the line of trafficking.

Before further loading was undertaken, the Oxford section was repaired. The aggregate was removed, the subgrade depression was levelled and, where necessary, refilled with material won from a nearby borrow pit. The subgrade was compacted using a 1000kg/m vibrating roller, a patch of another geosynthetic was used to replace the damaged geogrid and the aggregate layer was re-installed with an appropriate quantity of aggregate. On further trafficking this part of the section started to show signs of distress but, given the nature of the re-moulded subgrade, this was expected. The rut that developed was filled at an early stage, and the pavement remained traffickable, with occasional repair work, until the end of the trials.

5.5 INSTRUMENT PERFORMANCE

5.5.1 General

Some of the instrumentation intended to monitor the pavement performance had been installed ten months before the trafficking commenced. During this time a certain amount of deterioration was expected. Table 5.1 shows the status of the instrumentation in the Spring of 1990. The effect of long-term exposure to moisture was to render some of the instruments useless, some required remedial work and some were unaffected. The survival rate for the strain coil pairs was encouraging with approximately 80% functioning satisfactorily. It was thought that fewer of them would survive the construction process and long term moisture effects.

Section	Pressure Cell Aggregate	Pressure Cell Subgrade	Wheel path geosynthetic Coil pair	Wheel path aggregate Coil pair	Wheel path subgrade Coil pair	Coil pair A	Coil Pair B	Coil Pair C
A1	×	×	✓	✓	✓	N/A	N/A	N/A
A2	×	×	✓	×	✓	N/A	N/A	N/A
B1	×	×	×	✓	×	N/A	N/A	N/A
B2	×	✓	×	✓	✓	N/A	N/A	N/A
C1	×	×	✓	✓	✓	N/A	N/A	N/A
C2	×	✓	×	✓	✓	N/A	N/A	N/A
D1	✓	×	×	✓	✓	N/A	N/A	N/A
D2	✓	✓	×	✓	✓	N/A	N/A	N/A
E1	✓	✓	✓	✓	✓	N/A	N/A	N/A
E2	✓	✓	✓	×	✓	N/A	N/A	N/A
F1	✓	×	✓	✓	✓	×	✓	✓
F2	✓	✓	✓	✓	✓	×	✓	✓
I1	I	I	✓	✓	✓	×	✓	×
I2	✓	I	✓	✓	✓	✓	✓	×
J1	✓	✓	✓	✓	✓	✓	✓	×
J2	✓	I	×	×	✓	✓	×	✓
K1	✓	×	✓	✓	✓	N/A	N/A	N/A
K2	✓	×	✓	✓	✓	N/A	N/A	N/A
L1	✓	✓	✓	✓	✓	✓	✓	✓
L2	✓	✓	×	×	×	✓	✓	✓
M1	✓	✓	✓	✓	✓	✓	✓	✓
M2	✓	×	×	×	×	✓	✓	
N1	✓	×	✓	✓	×	✓	✓	✓
N2	✓	×	✓	✓	✓	✓	✓	✓
O1	✓	×	✓	✓	✓	✓	✓	✓
02	✓	I	✓	✓	✓	✓	✓	✓
P1	✓	✓	✓	✓	✓	✓	✓	✓
P2	✓	✓	✓	✓	✓	✓	✓	✓

KEY: ✓ = Working × = Not working I = Intermittent N/A = Not Applicable

see Table 4.1 for the location of coil pairs A, B and C.

Table 5.1 Status of the strain coils and pressure cells, Spring 1990

The pressure cells proved to be slightly less robust with a survival rate to the Spring of 1990 of approximately 60% and even fewer were operating in the Spring of 1991. Of those that survived most required some form of remedial work to function correctly. This normally entailed addition of high stability resistors, externally to the strain gauge Wheatstone Bridge , in order to re-balance the cell. The addition of resistors over 5000 Ohms was considered not to affect the calibration of the cells. Those which required balancing resistors of less than 5000 Ohms were considered to be unusable. This was partly due to concern that the initial calibration would no longer be valid and partly due to the fact that pressure cells requiring the addition of low value resistors were unlikely to prove stable over time.

At the end of the trial several of those pressure cells that were not functioning correctly were retrieved for examination. It was found that, despite the efforts taken to protect the cells from the effects of moisture, some corrosion had occurred on the fine wires inside the cell. It is possible that the moisture was able to enter the cell through the cable wall. P.V.C., which was used to sheath the cable, is not water proof and over long periods of time a small quantity of water will pass through the casing and into the wire. This moisture will travel down the wire, by capillary action, into the cell where fine wires are easily corroded.

5.5.2 Strain coils

The strain coils were calibrated using the "Bison" system, but were read using "Emu" equipment developed at Nottingham University. A cross calibration between the different units was performed, and a prediction of the actual coil spacing given any Emu output can be made, using the calibration curves from the Bison, to within an accuracy of 1%. Because, in this application, it is strains, or coil movement, that is of principle interest and as the error in predicting the coil spacing is constant for any coil pair, the error in determining the absolute spacing leads to very small errors in the measurement of permanent deformation (change in spacing). Similarly the cross-calibration errors in transient strains were found to be small as the transient response is a function of the spacing.

Transient strains of the geosynthetic, aggregate and subgrade were monitored using the "dynamic" output of the Emu and recorded, via an analog to digital converter, to a personal computer. An example of a result is shown in Figure 5.3 and the strain

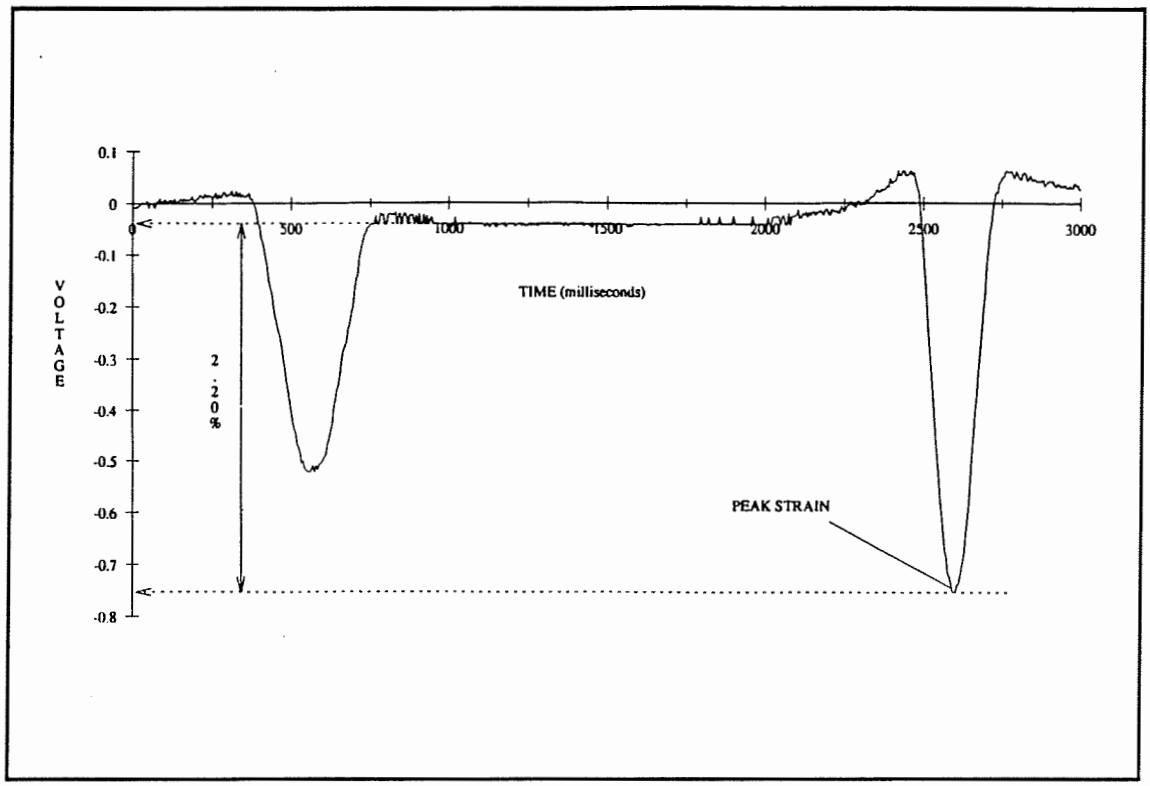

Figure 5.3 Example of the Dynamic Output from the Emu Device

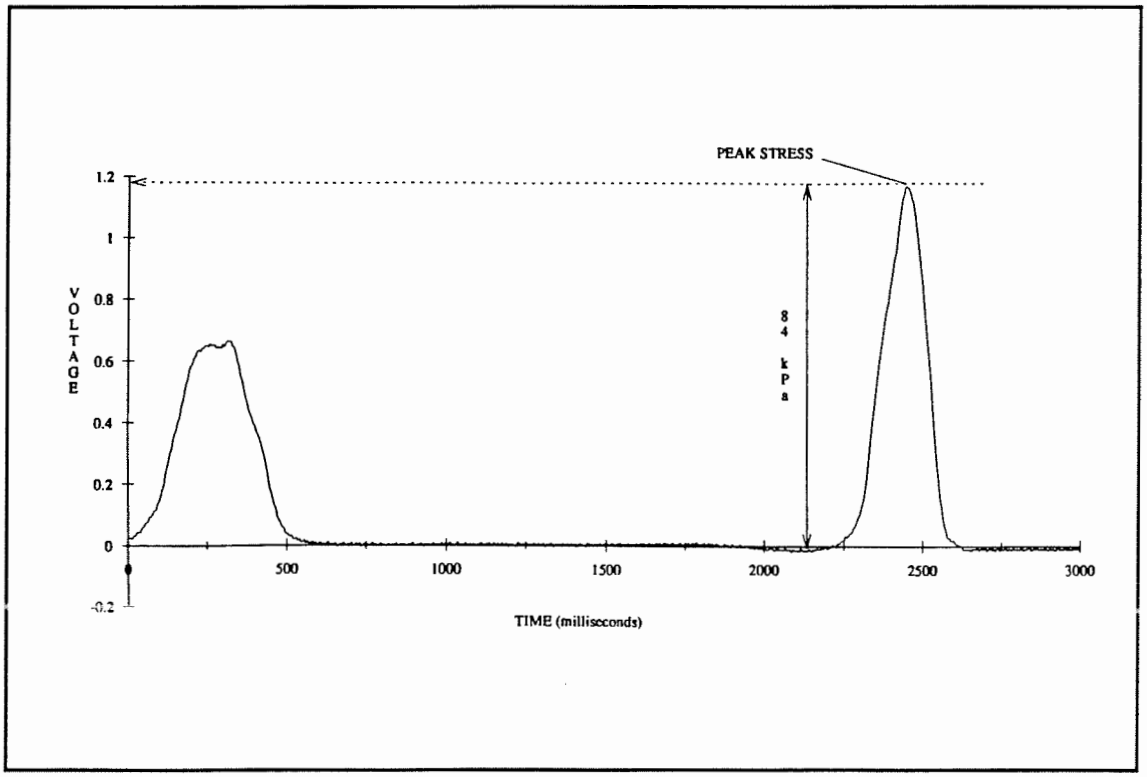

Figure 5.4 Example of the Amplified Output from a Pressure Cell

obtained from the calibration has been added. The signal to noise ratio in this example is fairly high. However, the measured transient response is a function of the size of the strain involved, the initial proximity of the strain coils and the amplification applied to the measured signal by the monitoring unit. Therefore, for strain coils where the strains were small, or the initial spacing of the strain coils was large, the results have been lost due to noise in the system. It is unfortunate that strain coils are, by their very nature, good aerials and hence pick up a large range of noise signals. This noise was particularly problematic for those strain coils that were attached to the geosynthetics in a position remote from the wheel path. Thus, the quality of the signal generated by the strain coil pairs attached to the geosynthetic deteriorate from the pair beneath the wheel load to the remotest coil pair.

5.5.3 Pressure cells

The transient response of the pressure cells, due to traffic loading, was amplified using a rack of strain gauge amplifiers. In a similar manner to the signal from the Emu devices the amplified, out of balance signal was recorded on a personal computer via an analog to digital converter. An example of a raw result is shown in Figure 5.4 with stresses obtained from the calibration added. The balance of the Wheatstone Bridge within the pressure cell wanders slightly over time and therefore there can be no measure of permanent, or locked in, vertical stresses

5.5.4 Vertical inspection tubes

The vertical inspection tubes were designed to gain access to the level of the geosynthetics by levelling the top of a 1m long bar. The top of the tubes were plugged in an attempt to prevent the tubes being filled with stones. However, often the plugs would become dislodged and the tubes would fill with stones carried by the lorry's tyres, or the plugs would be pushed into the tube by loose stones and would then be impossible to remove. None of the inspection tubes have generated reasonable results because the deformations at the interface were often small and uncertainty in the quantity of materials that may be in the tubes leads to a low degree of confidence in the readings obtained.

5.5.5 Horizontal Extensometers

The horizontal extensometers were not sensitive enough for monitoring the small lateral deformations that occurred in most sections. The resolution of the read-out unit was probably around ± 2mm and over a gauge length of 400mm this represents ± 0.5% strain. In those sections where the deformations were large, close to failure, the instruments recorded some movement, however, these movements were small and often the magnet holders pinched the extensometer tube preventing the sond from travelling the length of the instrument.

5.5.6 Piezometers

The position of the ground water level determines the suctions that are present near to the surface of the subgrade. Piezometers were installed in the subgrade to measure this suction at a depth of 200mm below the surface. Normally, piezometers are permanently connected, via an arrangement of taps, to a pressure transducer. This is done to exclude air from the system. Because air expands and contracts under differing pressures, the ingress of air will cause water to flow from the piezometer tip into the surrounding subgrade thus destroying the suctions that have developed.

However, the size of the site was such that it was not possible to permanently connect all of the piezometers to a read-out unit. A portable system was developed which contained a supply of de-aired water and a measuring unit. This could be coupled to each piezometer in turn via a tap which was permanently attached to each instrument. However, it was found that on each occasion that the unit was connected to the piezometers, a small amount of air entered the system thus destroying the suctions that the unit was attempting to measure. In order for the suctions to develop again the portable unit was left attached overnight. However, it was still not possible to obtain stable readings and so, unfortunately, subgrade suctions have to be estimated from the ground water levels.

5.5.7 Standpipes

Pore water pressures can be estimated if the position of the water table is known. For this purpose standpipes were installed next to Sections A, F, H and P. Four pipes at

each location were driven vertically into the ground near to the side of the pavements to depths of 0.5, 1, 1.5 and 2m below ground level. Each pipe was equipped with a conical tip which was pushed clear of the end of the pipe after installation. The water level in the pipes was left to reach equilibrium for three months before the trafficking in the Spring of 1991. The level of the standing water was then monitored by passing a sond, which responded to the water level, down the pipe. This appeared to be a quick, easy and reliable method of determining the ground water level and the results are shown in Chapter 6.9.

5.5.8 Thermocouples

Thermocouples were installed in some of the sections and were monitored throughout the two trafficking periods. The welded tips all survived the construction and trafficking processes and gave sensible readings of the temperature of the geosynthetics. Generally it was found that during the trafficking period, the temperature of the geosynthetics remained relatively constant at around 11 to 15°C.

CHAPTER SIX

RESULTS

It is intended in this Chapter to present a summary of the results obtained from the full-scale trials at Bothkennar. Further results, where applicable, are presented in Appendix C but even so this only represents a fraction of the available data. Little (1992) has presented a full data base in spread sheet formats.

6.1 RUT DEPTHS

6.1.1 Definition of Rut Depth and Vertical Depression

The rut depth is defined as the vertical distance between the highest and the lowest point across the instrumented half of the pavement. In order to take account of any initial unevenness in the pavements' transverse profiles, the rut depth readings were adjusted to show the movement away from the initial profile. The rut depth was measured at six places on each section, three around each reading location, periodically during the first 1000 passes. These readings were supplemented by an additional three readings at the central part of each section, for passes 1000 to 2115. In order to correlate the two sets of readings the assumption has been made that the rut depth at the central location at pass 1000 was the mean of the rut which had developed previously at the reading locations during the initial 1000 passes. Ruts were measured transversely across the pavement using a level, 2m long straight edge. Table 6.1 shows the final rut depths recorded after 2115 passes.

The vertical depression is defined as the downward movement of the aggregate surface as measured in the centre of the wheel path. The vertical depression is one component of the rut depth, the other being hog in the structure away from the wheel path. The vertical depression was measured by recording the levels of the aggregate, wheel path surface during the trials and by calculating the movement away from the initial value.

6.1.2 Rut Depth Development

An example of the development of rut depth with passes for a typical section is shown in Figure 6.1 and for all sections in Appendix C. It should be noted that large rut depths developed in Sections I and J. Also, it should be noted that in Section J, Reading Location J1 performed very differently to Reading Location J2 (see Appendix C). One of the principal reasons for the poor performance of the pavement at this point is that segregation of the aggregate occurred in the layer during construction, as highlighted by the density of the aggregate at J1 shown in Table 3.6. Excavation at the end of the trials of Section I and Section J showed that the geosynthetic had ruptured. It would be sensible to assume that this rupture occurred when the slope of the rut depth/passes curve increased. This happened shortly after the higher axle load was applied. Because in the post-failure pavement a different type of deformation behaviour occurs, the rutting data obtained in the range from 1000 to 2115 passes for these two sections must be treated with caution.

In most sections the first two measurements of rut depth, taken at passes 1 and 3, exhibit a high rate of rut depth development per pass. This high deformation in the first few passes is mirrored by the high axial deformations recorded in the first few cycles of repeated triaxial testing of aggregates (Thom (1988)). Figure 6.2 shows the general relationship between shear stress and shear strain for a granular material subjected to repeated triaxial loading. It may be seen that the graph shows an initial monotonic loading curve followed by a series of load/unload curves which lead to progressively smaller incremental plastic strains. Under the first pass of the axle load the stress-strain response may be expected to move up the monotonic loading line, large strains being generated. Subsequent loadings will then yield smaller values of strain - as can be seen from the figure.

Given that this initial rutting may not be regarded as being indicative of the general pavement performance and that this early rut depth development is probably an aggregate related phenomena, it is unlikely to be useful in indicating the geosynthetic performance. Therefore, it would appear wise to examine more closely the development of rutting with passes. As the development of ruts in the first few passes has, in some cases, contributed significantly to the overall rut depth, the data was analysed both in terms of the total rut depth for each pavement, and the rate of accumulation of rutting per pass for each axle loading excluding the high initial values. By using the rut development rate, measured in

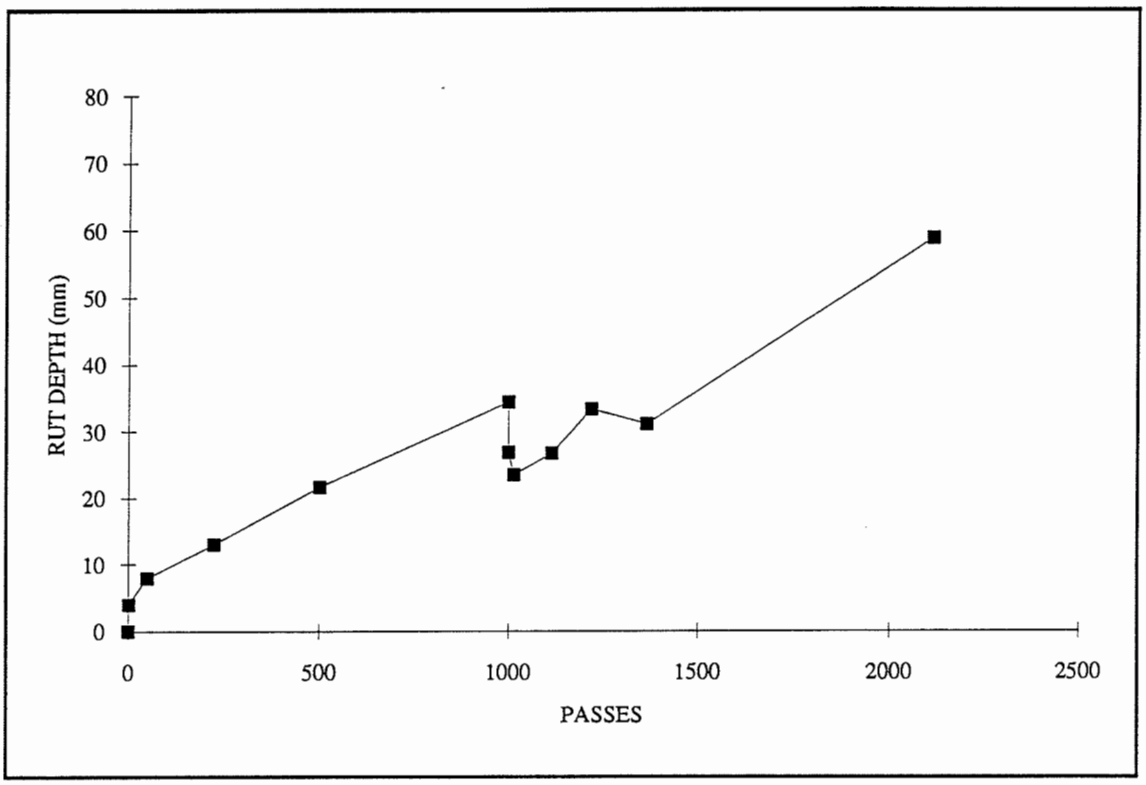

Figure 6.1 Typical Rut Depth Development for an Upper-bound Pavement at Bothkennar

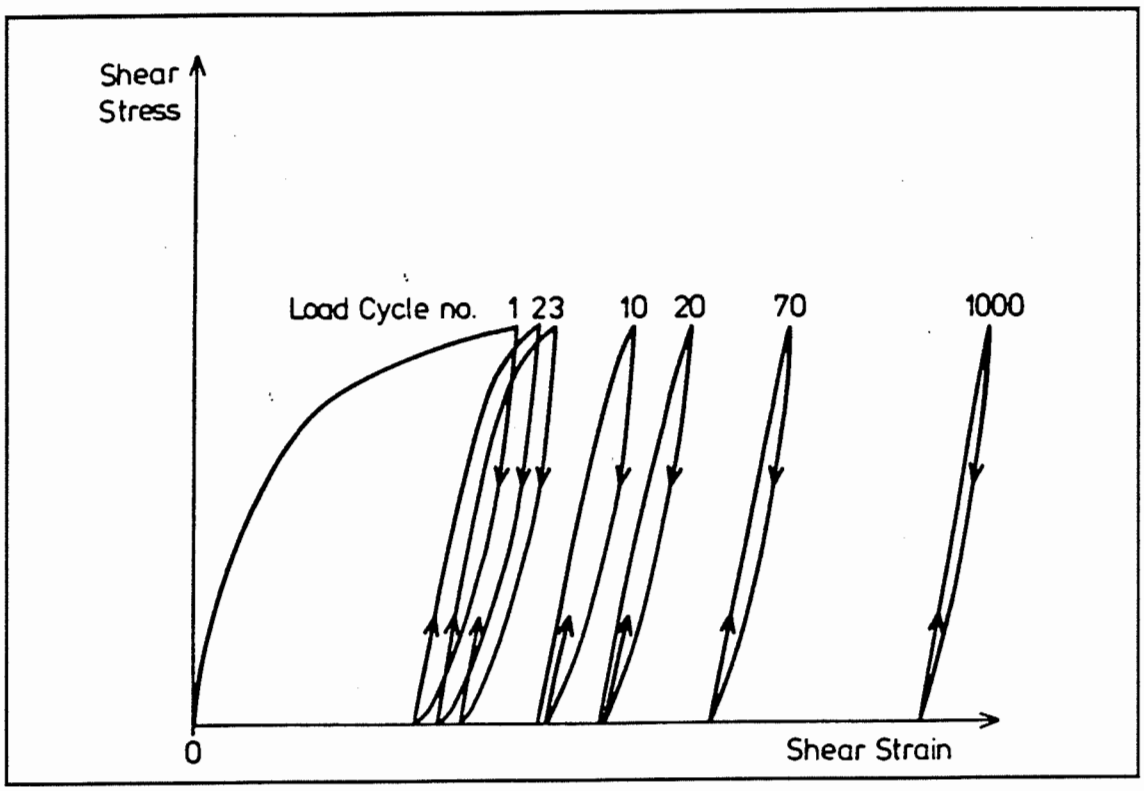

Figure 6.2 Shear Stress and Shear Strain for Granular Materials in a Triaxial Test - After Thom (1988)

mm per pass, as the comparative measure between pavements, "start-up" errors caused by local variations in the aggregate layer are eliminated.

The rate of rut depth development with passes, excluding Sections I and J1, has been calculated and is shown in Table 6.1. It can be seen that the increases in rut depth per pass was, on average, 43% higher for passes 1115 to 2115 (the 126kN axle load range) compared to passes 50 to 1000 (the 80kN axle load range).

Section	Final total rut depth (mm)	"Start-up" rut depth (mm)	rut development per pass. passes 50-1000	rut development per pass. passes 1115-2115
A	59	4	0.027	0.032
B	71	10	0.035	0.034
C	33	5	0.016	0.013
D	35	8	0.008	0.013
E	28	6	0.008	0.009
F	40	7	0.012	0.021
H	44	8	0.009	0.017
I	175+	6	0.018	0.201
J1	160*	8	0.053	0.102
J2	72	7	0.023	0.037
K	33	16	0.004	0.012
L	38	4	0.014	0.011
M	32	6	0.024	0.008
N	48	8	0.015	0.018
O	62	12	0.020	0.040
P	55	6	0.016	0.027

+ failure at 1850 passes

* failure at 1448 passes

Table 6.1 Rut depth development

6.2 LONGITUDINAL PROFILE

The longitudinal profile of each instrumented wheel path was recorded using an automatic level and staff. Readings were taken at the same number of passes as the rut depth measurements and consisted of readings taken at 0.5m intervals from 1m before the first reading location to 1m past the second reading location for each section and the vertical displacements from the initial levels were calculated. An example of the development of the vertical displacement along a typical section after 1000 and 2115 passes is shown in Figure 6.3, and full details are given in Appendix C.

It can be seen that in many sections the development of vertical displacement is not constant along the length of the section. It would be a fair assumption that the vertical deformation is related to the rut depth, especially within any given section. Plainly, the values of the rut depths shown in Table 6.1 are dependent on whether the location of the measurements is at a low or a high point along the longitudinal profile. Therefore, for each section, the nine individual final measures of rut depth (three at each of the two reading locations and three at the centre) and the final vertical depression at those points was compared. The rut depth was then corrected in proportion to the difference between the mean value of vertical displacement along the whole section and the vertical depression at the selected points. These results are shown in Table 6.2.

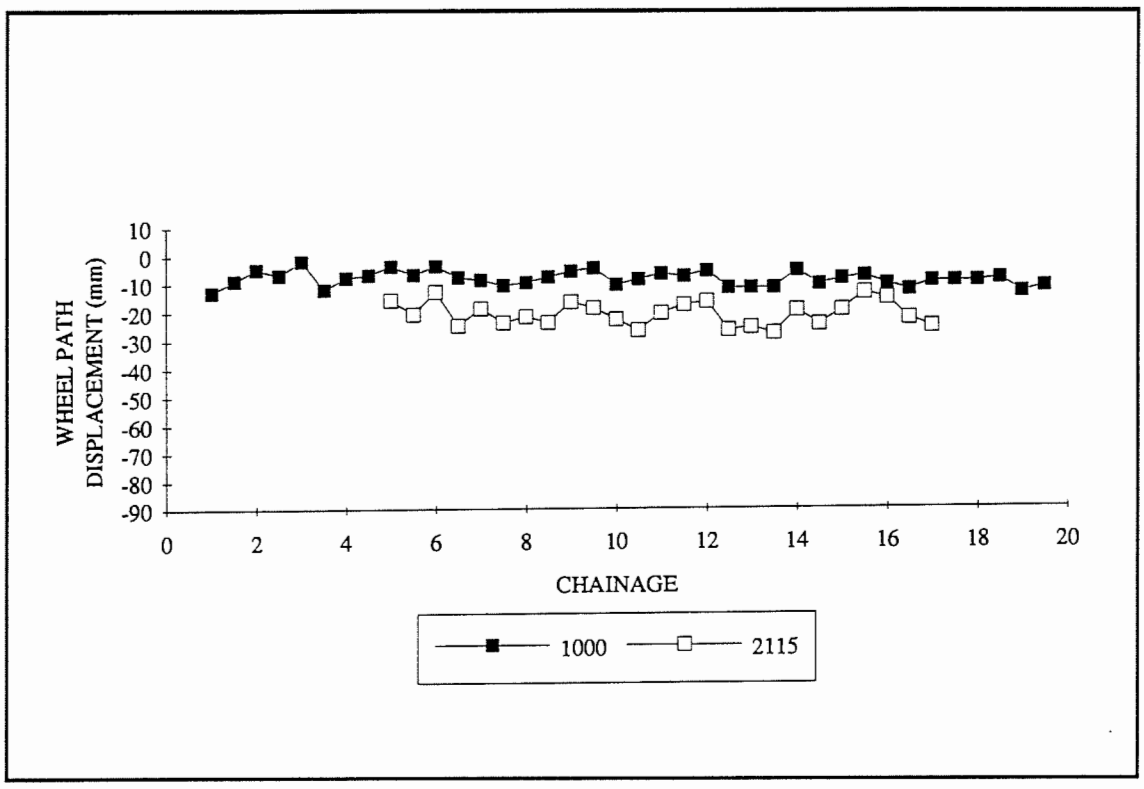

Figure 6.3 The Development of Vertical Aggregate Displacement with Passes - for a Typical Section at Bothkennar

Section	Mean Reading Location Rut Depth (mm)	Reading Location Vertical Displacement (mm)	Rut Depth/ Vertical Displacement	Vertical Displacement Mean Value (mm)	Estimated mean rut depth (mm)
A	59	50	1.18	43.2	51.0
B	66	40	1.65	40.1	66.2
C	33	33	1	32.0	32.0
D	32	26	1.23	21.8	26.8
E	24	28	0.86	29.0	24.9
F	38	39	0.97	40.5	39.3
H	42	19	2.21	21.2	46.9
I	failed	failed	-		
J	failed	failed	-		
K	28	22	1.27	19.5	24.8
L	35	28	1.25	28.0	35.0
M	32	21	1.52	17.6	26.7
N	44	17	2.59	21.2	54.9
O	68	32	2.13	28.7	61.1
P	56	49	1.14	32.7	37.3

Table 6.2 Estimate of the mean section rut depth after 2115 passes

6.3 VERTICAL STRESSES

The transient vertical stresses were measured using strain-gauged diaphragm pressure cells and, as was seen from Figure 5.4, the generated signal was relatively free of noise. By considerations of vertical equilibrium it is believed that, except possibly at large rut depths, the vertical stresses measured at the base of the aggregate layer and at the top of the subgrade are largely unaffected by the inclusion of a geosynthetic. The scatter in the data in Table 6.3 is largely caused by the inherent variation due to differences in installation and to the variation in thickness of the aggregate layer, both due to design and construction. The mean value of a number of pressure cells, installed in the same environment, would generate a reliable value. However, the degree of redundancy required is so high that, for this project, the costs of manufacture and the time required for installation were prohibitive. Thus, individual measurements of absolute stress should be treated with caution, whereas percentage changes in stress readings are likely to be more reliable.

	PASSES 0-1000		PASSES 1115-2115		PERCENTAGE INCREASE	
Section	Aggregate stress (kPa)	Subgrade stress (kPa)	Aggregate stress (kPa)	Subgrade stress (kPa)	Aggregate	Subgrade
A	-	-	139	82	-	-
B	52	-	-	-	-	-
C	-	110	-	173	-	57
D	52	55	80	76	54	38
E	81	76	94	90	16	18
F	73	69	82	-	12	-
I	169	117	127	134	-25	14
J	185	126	160	139	-14	-13
K	75	-	176	122	134	-
L	46	80	35	74	-24	-7
M	62	63	81	77	31	22
N	64	98	116	124	81	27
O	82	117	131	-	60	-
P	111	83	-	-	-	-

Table 6.3 Mean aggregate and subgrade vertical stresses

During the trials in the Spring of 1991 the tyre pressures on the lorry, and therefore presumably the pavement contact stress, was raised from 500kPa to 650kPa. However, it is an accepted principle that, at depth, the vertical stress is dependent on the magnitude of the load rather than the contact stress. An examination of the measured vertical transient stresses, before and after this increase, imply that these changes in contact stress did not increase the vertical stresses at the base of the pavements. However, insufficient data from these trials exist for a full examination of the effects of contact stress on pavement stresses. Therefore, it is assumed in the analysis of the results that the stresses are purely dependent on the load magnitude.

It was noted that the increase in the vertical stresses, as measured at the base of the aggregate layer and the top of the subgrade, generated by the passage of the 126kN axle load, as opposed to the 80kN axle load, were less than might have been expected. The

58% increase in load led, on average, to a 32% increase in vertical stress at the base of the aggregate layer and a 20% increase in the vertical stress at the top of the subgrade.

By knowing the time lag between the pulses of the pressure cells, generated by the two axles of the lorry, and knowing the distance between the the axles, it is possible to calculate the speed of the lorry and therefore convert the time before and after the peak readings into longitudinal distance of the rear axle from the cell. The longitudinal stress distribution can be calculated from such an analysis and is shown in Figure 6.4. The vertical stress distribution within the pavement structure may be different in the longitudinal and transverse directions, especially in the sections with geosynthetics which have notably different properties in each direction and in those sections which have rutted. However, Figure 6.4 was generated from a section early in the trials, before significant rut depths had developed, and therefore the longitudinal stress distribution shown is probably also a fair indication of the transverse stress distribution.

6.4 TRANSIENT STRAINS

The mean transient strains observed in the wheel path at the base of the aggregate, the geosynthetic and the top of the subgrade are shown in Table 6.4. In a similar manner to the the vertical stresses, it is observed that the transient strains did not increase linearly with the increase in axle load. The 58% increase in load has led, on average, to a 22% increase in transient vertical aggregate strain, a 43% increase in transient vertical subgrade strain and a 31% increase in transient transverse geosynthetic strain.

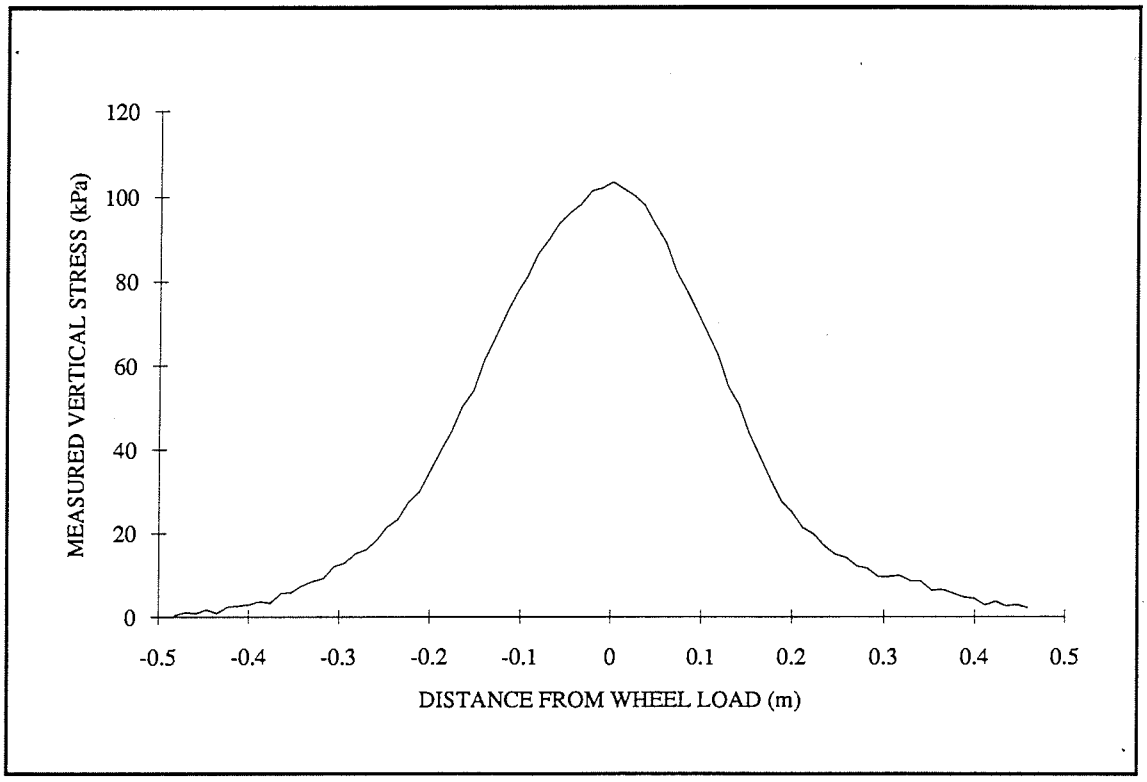

Figure 6.4 Longitudinal Stress Distribution for a Typical Section at Bothkennar

	PASSES 0 - 1000			PASSES 115 - 2115		
Section	Vertical Aggregate strain (με)	Vertical Subgrade strain (με)	Transverse Geosynthetic strain (με)	Vertical Aggregate strain (με)	Vertical Subgrade strain (με)	Transverse Geosynthetic strain (με)
A	3100	7500	-1800	4300	10000	-3000
B	2500	6200	-	3100	7000	-
C	2400	4400	-2000	2800	5100	-2300
D	2000	2800	-	2900	3800	-800 *
E	1600	4000	-1100	1800	6000	-1700
F	2800	6700	-2400	3100	8800	-3700
I	4200	12600	-	7600	36300	-9500
J	12300	29800	-5500	10200	35700	-4600
K	4600	10600	-3300*	4900	13400	-3300*
L	3900	12200	-2900	3600	16600	-3100
M	2600	8900	-2900	500	10300	-3300
N	6700	12700	-3500	12200	18100	-6500
O	3700	14800	-4700	5200	21200	-4800
P	5600	14600	-3700	10600	21800	-5700

* Control section, the value shown is the horizontal subgrade surface strain

Table 6.4 Transient Strains

Multi-layer elastic analysis (Peutz et al (1968)) implies that, for a typical lower-bound section, (350mm thick and stiffness values taken from soil testing results) transient elastic strains of 900με could be expected at the base of the aggregate layer and 1300με at the top of the subgrade. For this type of analysis, these strains are calculated to increase in both aggregate and subgrade layers by 56% for a 58% increase in load. The non-linear model FENLAP (Almeida et al (1991)) suggests that transient elastic strains of 800με could be expected at the base of the aggregate layer and 1000με at the top of the subgrade. The increase in these strains caused by the increase in loading are calculated to be of the order of 22% at the base of the aggregate layer and 33% at the top of the subgrade.

It was found during the analysis that strains on the geosynthetic outside the loaded area (as defined by the widely held concept of a load spread angle), exhibited small transient strains. Indeed, for many sections, the strain induced in the geosynthetic, away from the

wheel path, was below the noise threshold of the strain coils. Figure 6.5 shows how the transient geosynthetic strains dissipate with distance from the wheel path. It is interesting to note that the transient transverse strains tend to become compressive at a distance from the load.

6.5 PERMANENT STRAINS

The application of 2115 passes has generated permanent deformations in the aggregate geosynthetic and subgrade. The permanent strains, directly under the wheel path, at the base of the aggregate layer, the top of the subgrade and the geosynthetic are shown in Table 6.5 and, where possible or sensible, the results are the mean of the two reading locations.

Geosynthetic strain coils, remote from the wheel path, showed little or no permanent strain as shown in Figure 6.6. This is hardly surprising given that they exhibited little or no transient strain. It should be noted that although the transient strains were higher at the top of the subgrade than at the base of the aggregate layer, the permanent deformations are generally more pronounced in the aggregate layer.

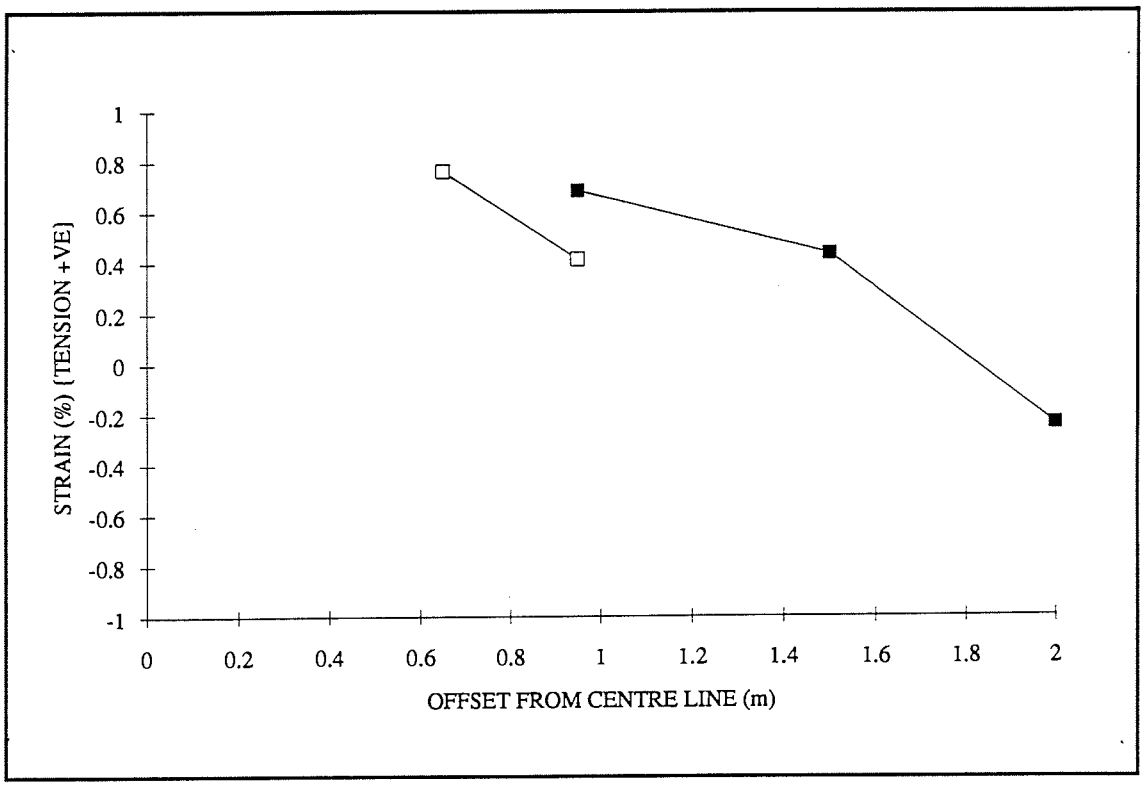

Figure 6.5 Transient Geosynthetic Strain Away from the Wheel Path for a Typical Section at Bothkennar

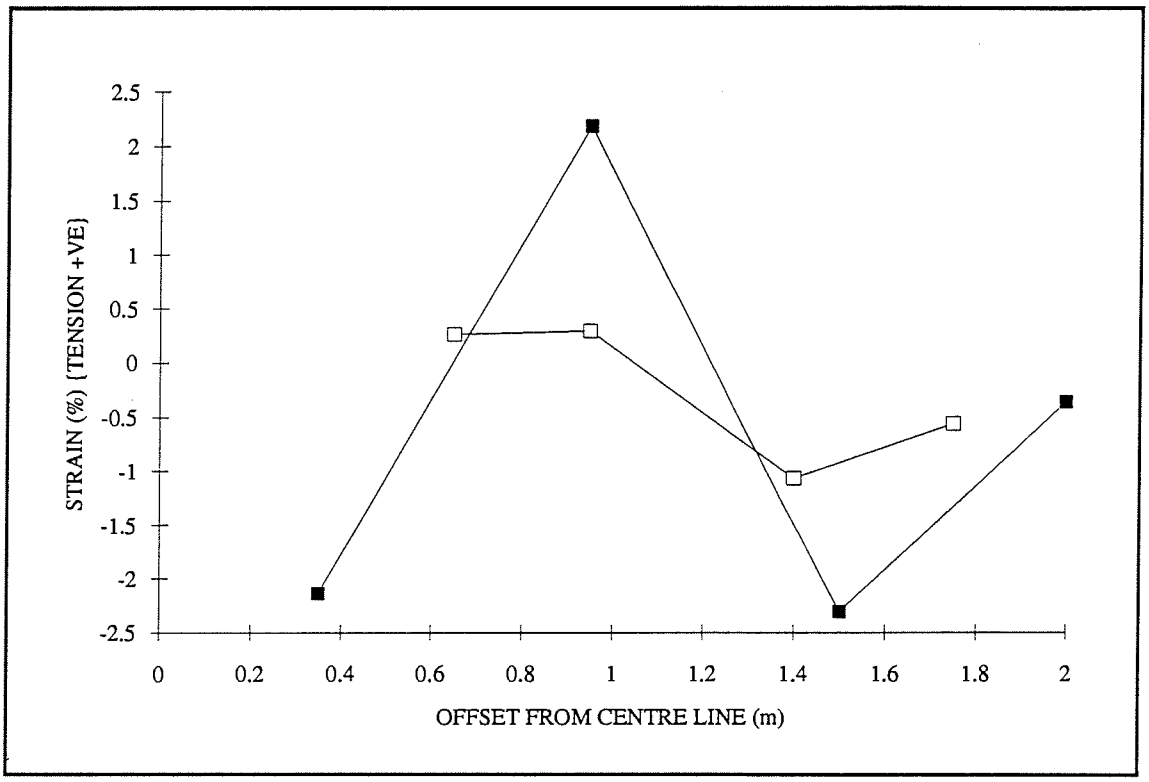

Figure 6.6 Permanent Geosynthetic Strain Away from the Wheel Path for a Typical Section at Bothkennar

Section	Vertical Aggregate strain (με)	Vertical Subgrade strain (με)	Transverse Geosynthetic strain (με)
A	18800	7600	-11800
B	19700	11800	-
C	15800	2900	-2500
D	16400	-2300	-
E	8800	4400	0
F	30800	18900	-
I	48000	21900	-
J1	97300	44000	-7400
J2	-	12700	-
K	14800	5100	-700*
L	24400	9000	-4600
M	5200	6800	0
N	8500	15600	-4300
O	24600	25700	-2500
P	21800	19100	-10700

* Control section, the value shown is the transverse subgrade surface strain (compression positive)

Table 6.5 Mean Accumulated Permanent Wheel Path Strain After 2115 Passes

6.6 AGGREGATE THICKNESS

The initial thickness of the aggregate layer can be calculated from the levels that were taken of the subgrade and those of the final aggregate surface. Each were levelled in a 0.5m grid and by superimposing the data, a large number of determinations can be found. Table 6.6 shows the aggregate thickness for the sections as a whole and the values that relate to the instrumented wheel path. From an examination of the longitudinal profile and the changes in the longitudinal thickness it is inferred that the small variations in pavement thickness are not mirrored in changes of the longitudinal vertical depression measurements and therefore, presumably, in the rut depth.

	Instrumented Wheel Path Thickness (mm)		Pavement Thickness (mm)		Design Thickness
Section	Mean	Standard Deviation	Mean	Standard Deviation	(mm)
A	430	16.5	430	18.0	400
B	495	33.4	493	32.3	450
C	527	23.6	526	26.9	500
D	580	33.5	580	33.7	550
E	536	23.4	541	28.5	490
F	436	16.8	428	20.8	400
H	428	12.7	431	21.3	400
I	350	29.3	342	28.1	300
J	262	13.9	265	12.6	340
K	394	29.4	397	25.1	400
L	354	23.4	352	26.0	350
M	372	16.3	372	17.2	350
N	332	30.9	340	28.4	300
O	366	22.9	366	21.4	350
P	360	18.8	368	20.8	350

Table 6.6 Aggregate Thickness

6.7 EXCAVATED CROSS SECTIONS

Recovery of the geosynthetics for analysis at the University of Strathclyde enabled an examination of the post trafficking cross-section profiles, a typical example of which is shown in Figure 6.7 and the full results are shown in Appendix C. An overall measurement of aggregate strain in the wheel path was determined from the initial and final thicknesses. It should be noted that two years elapsed between the measurements of thickness and the method of measurement, with a level and staff, is not conducive to a high degree of accuracy. This probably explains the observation that no strain has occurred within the fill in Section M, whilst the aggregate strain coil reading in Table 6.5 shows a compressive permanent strain. Generally, it is interesting to note that the strains measured by the strain coils at the base of the aggregate layer are significantly lower than the overall aggregate

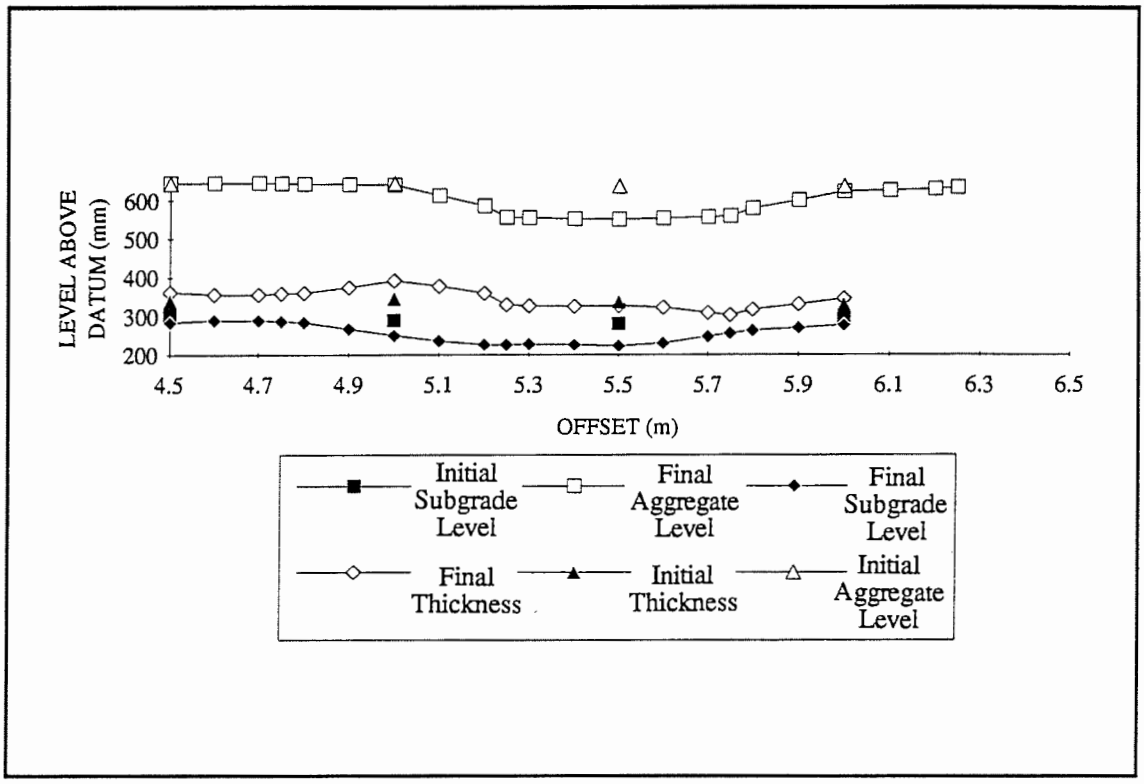

Figure 6.7 Post Trafficking Cross-section for a Typical Section at Bothkennar

strain. As could have been predicted, the majority of the strain must therefore occur near to the surface of the pavement, where the stresses imposed by the wheel load are greatest.

Examination of the eight excavated sections at Bothkennar indicate that deformation within the aggregate layer makes up between 0% and 42% to the total surface rut depth, with a mean of 21%, the remainder being the result of subgrade deformation.

6.8 SUBGRADE SHEAR STRENGTH

The subgrade shear strength was tested at intervals during the course of the trials, using a hand held shear vane, and the shear strength of the subgrade was found to remain constant throughout the period of trafficking. The mean surface shear strength of the subgrade was calculated during the two trafficking periods and it was found to be around 85kPa on both occasions. There is an inherent variability in the results obtained from such an instrument due to both the operator and the fact that the vane tests a small, local sample. Thus, the results shown in Figure 6.8 from the vane show a high degree of scatter, but mean values are probably reasonably accurate.

The shear strength profile with depth shows a strength reducing markedly with depth. The crust of firmer material on the site is caused by evaporation, which in turn causes pore-water suctions which leads to the soil being slightly over-consolidated and gives a drier, stiffer material. The shape of the profile obtained from the shear vane matches closely the one reported by Paul et al (1991) which shows a shear strength of 80kPa near to the surface decreasing to 20kPa at a depth of 2m (see Figure 3.1). However, this inversion of the shear strength profile makes numerical analysis difficult because most programs assume a linear increase in strength with depth.

After trafficking the subgrade was exposed in many of the sections either to recover post-trafficking geosynthetic samples or defective pressure cells. These excavations presented an opportunity to determine the shear strength of the surface of the formation using the hand held shear vane. Four determinations of shear strength were made of each exposed formation and the results are shown in Table 6.7. Only surface values were recorded as it was expected that the shear strength at depth was unlikely top change significantly from the values as shown in Figure 6.8 By reducing the number of data points that are considered,

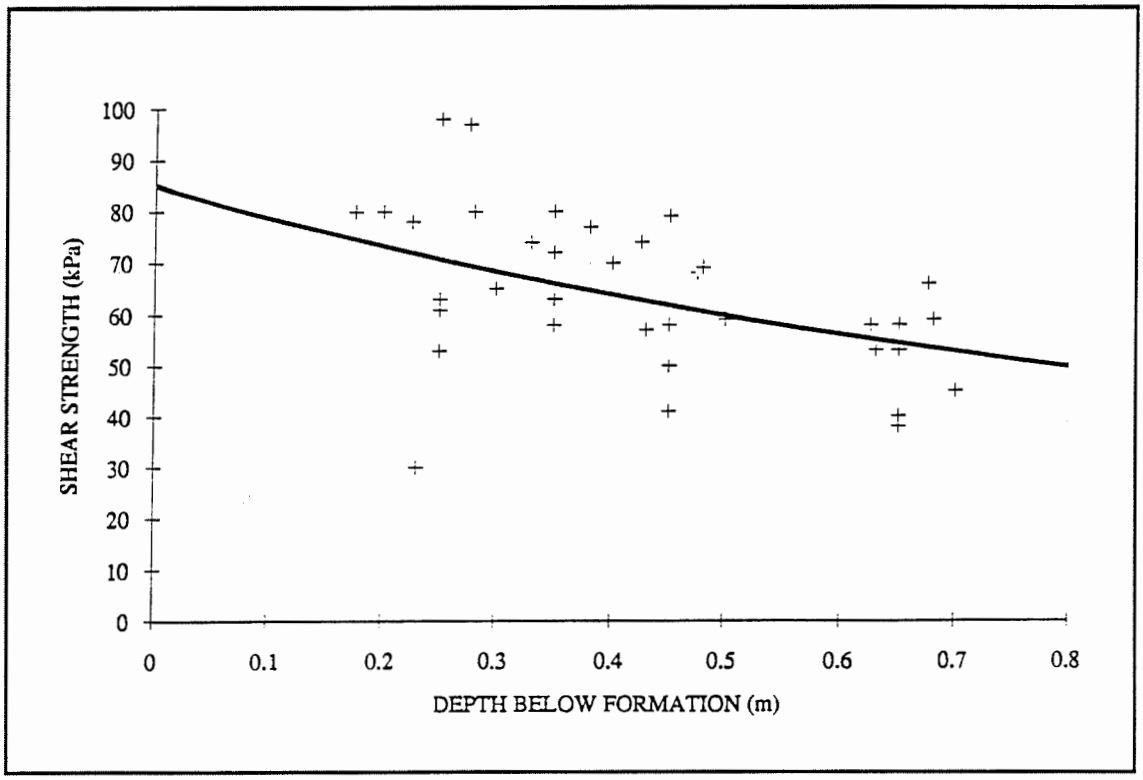

Figure 6.8 Subgrade Shear Strength Profile

the mean value of the shear strength for each section can not be determined with the same degree of confidence that can be done for the site as a whole. It might be argued from the results presented in Table 6.7 that the thicker sections (A to F) have a higher mean surface shear strength and, if that is indeed the case, it might be attributable to the slightly larger overburden stresses causing a small amount of subgrade consolidation.

Section	Mean surface shear strength (kPa)
A	105
B	90
C	90
E	96
F	75
H	81
I	77
J	98
K	90
L	74
M	82
N	82
O	82
P	77

Table 6.6 Formation level shear strength

6.9 WATER TABLE

The water table on the site was determined by using the standpipes which were installed in January 1991. Generally it was found that the water table level was between 0.2 and 0.7m below the formation level of the pavements, as shown in Table 6.8. Because the site was next to the tidal Firth of Forth, it was thought that the water table might be affected by the nearby tidal movement. It was found, by monitoring the water table level over a 12 hour period, that the water table on the site was stable.

Depth below site surface (Formation + 300mm)				
Section	15 April	24 April	30 April	7 May
A	0.70	0.80	0.83	0.84
F	0.02	0.07	0.29	0.71
H	0.49	0.70	0.64	0.62
P	0.99	0.73	0.75	0.75

Table 6.8 Water table level in m below formation level.

As can be seen from Table 6.8, the ground water level fell steadily during the course of the trials. It had been raining heavily prior to the trials commencing and water was standing on the surface near to Section F, which is in a slight hollow. This surface water probably raised the ground water levels near to Section F at the start of the trials and during the course of the trials these came to equilibrium with the rest of the site as the surface water filtered into the site. During the course of the trials the weather was mainly dry and overcast, which explains the gradual fall in the ground water levels.

CHAPTER SEVEN

DISCUSSION

The full-scale trials have generated some interesting results and it is intended, within this Chapter, to highlight those that appear to be of value. Some of the common assumptions made in the design of unpaved roads are examined.

7.1 RUT FORMATION

7.1.1 Early rut formation

The aggregate surface of the haul road was given a final roll with the roller before the start of trafficking in order to ensure that there was no looseness of the surface of the aggregate which might affect the results. After a few passes it was possible to see the path that the lorry had taken and it was initially thought that a small amount of surface compaction had occurred. However, on analysis, it became apparent that all sections had undergone varying and sometimes large amounts of deformation between the first and third pass. It is considered that this "start-up" rut was due to the aggregate and that the variation in the start-up ruts was caused by small differences in the aggregate layer. This initial deformation is unrelated to the performance of either the pavement in general or of the geosynthetic in particular.

This high deformation in the first few passes is mirrored in the high deformations recorded in the first few cycles of cyclic triaxial testing of aggregates (Thom (1988)). If monotonic loading was undertaken, it would be expected that large strains would occur as the load passes from zero to the equivalent of the axle load. If the material is then unloaded, the unloading stress/strain curve will be steeper than the loading curve and, upon unloading, permanent deformation will occur, as shown in Figure 6.2, reproduced here as Figure 7.1. In subsequent cycles the stress path moves up and down the load/unload curve generating little permanent deformation. The permanent strain on the first cycle is difficult to predict because it depends on the stress history of the sample. In theory, aggregates which have undergone the same construction and compaction processes should deform by the same amount in the first cycle. However, small variations is these processes appear to have a disproportional effect on the

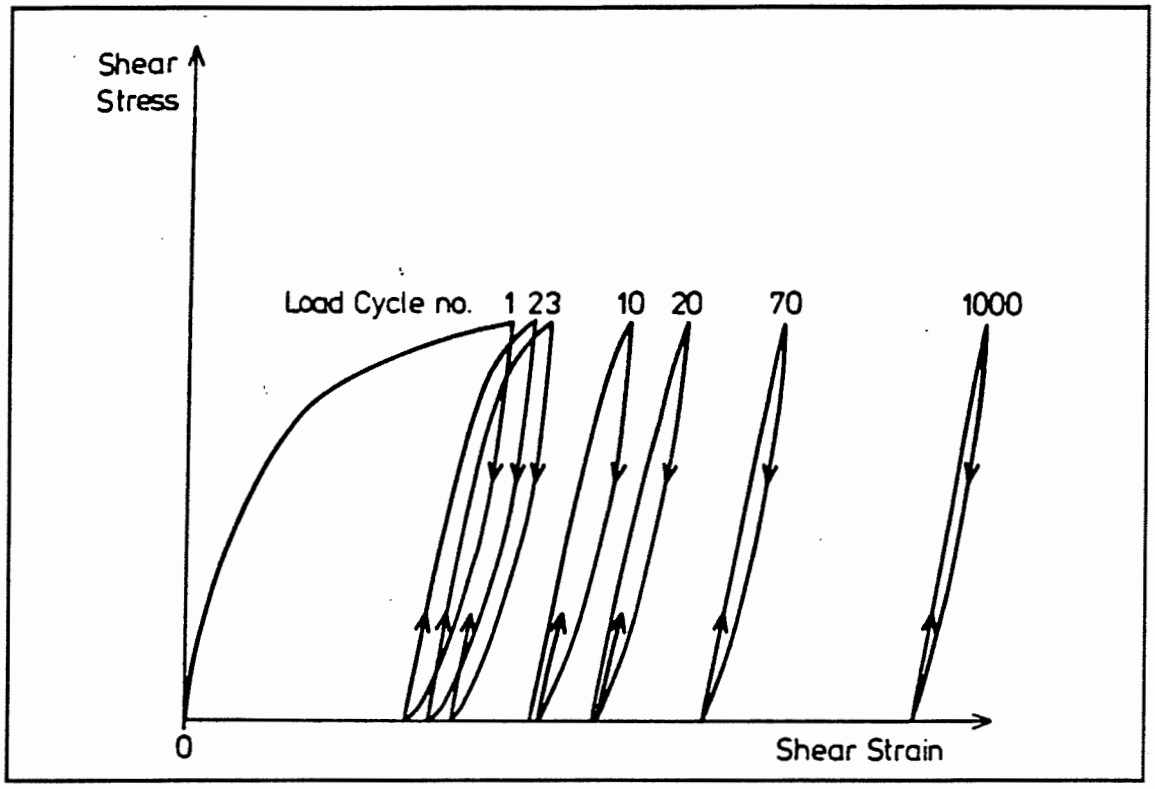

Figure 7.1 Development of Permanent Strain Under Cyclic Loading of an Aggregate Triaxial Sample - After Thom (1988)

properties of the aggregate in this first cycle. Thus, it is difficult to predict how any one aggregate is likely to behave in the first cycle of loading.

7.1.2 Rut depth and passes

The rate at which rutting develops and the ultimate rut depth, are functions of many criteria. Not least of these functions are: the axle load, number of passes and contact stress of the loading vehicles; the separation, filtration and reinforcement characteristics of the geosynthetics; the aggregate thickness, strength and stiffness; and the shear strength of the subgrade. Thus, direct comparison between the performance of two sections is not truly valid, as the rut depths measured are controlled by many factors which are not constant from section to section. To compare the performance of two different sections directly, the expected rut depth should be calculated, for each section, by a design method incorporating all of the above factors. The full-scale trials were planned so that all the sections should perform the same - according to each manufacturer's design methods - and that, as far as possible, the non-geosynthetic variables remained constant.

Allowing for experimental scatter, the relationship between rut depth and passes appears to be linear for each of the two axle loadings. This may change for sites where the subgrade is softer and a fuller range of the unpaved road's life is utilised. There appears to be a change of gradient, occurring at the point where the axle load was increased, which is more pronounced on some sections than others. The assumption that deformation of unpaved roads is proportional to the logarithm of the number of passes arises from bituminous pavement design (Karkhovan and Dormon (1953)) where the life expectancy is often measured in millions of standard axles. Its application to unpaved road design is a little arbitrary given that haul road life expectancy is often measured in hundreds or thousands of passes. Re-plotting the results of Webster and Watkins (1977) and Webster and Alford (1978) and the model tests of Fannin (1986), show that a relationship with the number of passes would be more appropriate (see Figures 2.9, 2.10 and 2.12).

7.1.3 Rut depth and axle load

7.1.3.1 Common Assumptions

The trials at Bothkennar incorporated the use of two axle loads (80 and 126kN) and it is a common assumption that the data relating to different axle loads can be reduced to an equivalent number of standard axles. It is often assumed that some form of power relationship exists, relating non-standard axle loads to a standard one. For example:

$$\frac{N_S}{N_i} = \left(\frac{P_S}{P_i}\right)^{\alpha} \tag{7.1}$$

where: N = number of passes
P = axle load
s = standard axle
i = non-standard axle
$\alpha = 3.95$ (Giroud & Noiray (1981))
or $\alpha = 6.12$ (De Groot et al (1982))

It is also often assumed that a succession of non-standard and standard loadings may be treated as the sum of their equivalent loadings (using Equation 7.1) regardless of order of application. Mathematically, this is expressed as:

$$N_S = \Sigma\left[N_i \left(\frac{P_S}{P_i}\right)^{\alpha}\right] \tag{7.2}$$

7.1.3.2 Examination of Assumptions

Assuming that damage is proportional to the logarithm of the number of passes and that a power law is appropriate , and that

$P_i = 142kN$
$P_S = 80kN$
$\alpha = 4$

then $N_i = N_S \left(\frac{142}{80}\right)^4 = 10N_S$

Therefore after 10 standard axle passes the damage done to the pavement would be the same as done by 1 pass of the non-standard axle, 100 standard axles are equivalent to the damage done by 10 non-standard and 1000 standard equivalent to 100 non-standard. Therefore, as can be seen from Figure 7.2, the two relationships are parallel, when plotted in log space.

Consider the case where 1000 passes of a standard load is followed by passes of a 142kN load. The equivalency, as determined by the power law, leads to the prediction that each pass of the 142kN axle has the same effect as 10 of the standard axle. The assumption of Equation 7.2 implies that the damage done by 1000 passes of a standard axle, plus 100 passes of the high axle load, would generate the same amount of deformation as the equivalent 2000 passes of the standard load. Plotting this assumption for each additional pass of the higher axle load generates a curve as shown in Figure 7.3.

It should be noted that initially, in log space, there is an increase in the rate at which the rut depth develops which is expected from the change of loading rate on the pavement. Also it should be noted that the combined effect is asymptotic to the high axle load/deformation line which is also expected as, at a high number of passes, the relative influence of the initial 1000 passes must reduce.

The measured deformations at Bothkennar can be made to fit such a format and the power law deduced. An example is shown in Figure 7.4, which relates to the performance of Section P. The value of α (the power) has been adjusted in order to obtain the best 'least squares' fit.

Unfortunately, in order to get the best fit, α is found to be 16 in this case. In the analysis of the other sections, the fit between the predicted and measured deformations is not as good as for Section P. However, the analysis for the other sections shows that the best fit occurs for values of α in the range of 8 to 20. Thus, the experimental data leads to values of the power, α, that are not reasonable because to suggest that the power should be twenty means that doubling the axle load would yield an approximate equivalency of 1 to 1 million which, in turn, would predict immediate pavement failure upon trafficking. Further doubt on the validity of this approach is that there is a large degree of scatter in the results, especially when it is considered that only one aggregate and subgrade condition was considered.

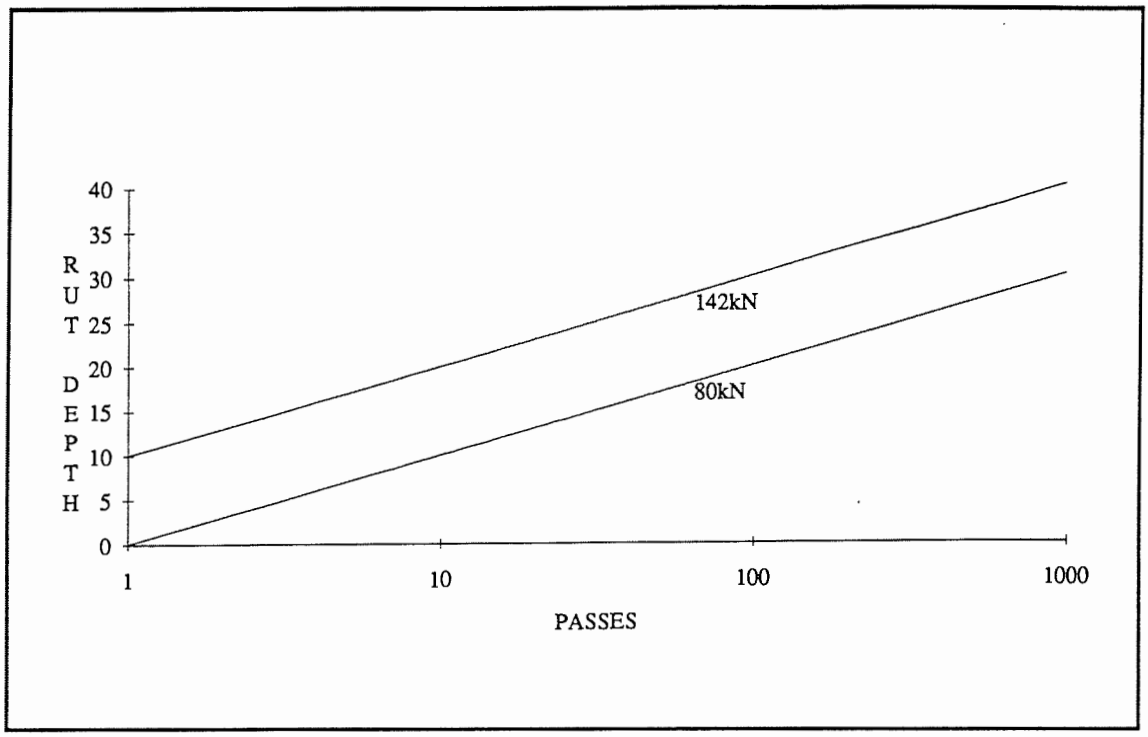

Figure 7.2 Predicted Deformation of a Pavement Subjected to Either One of Two Different Loads

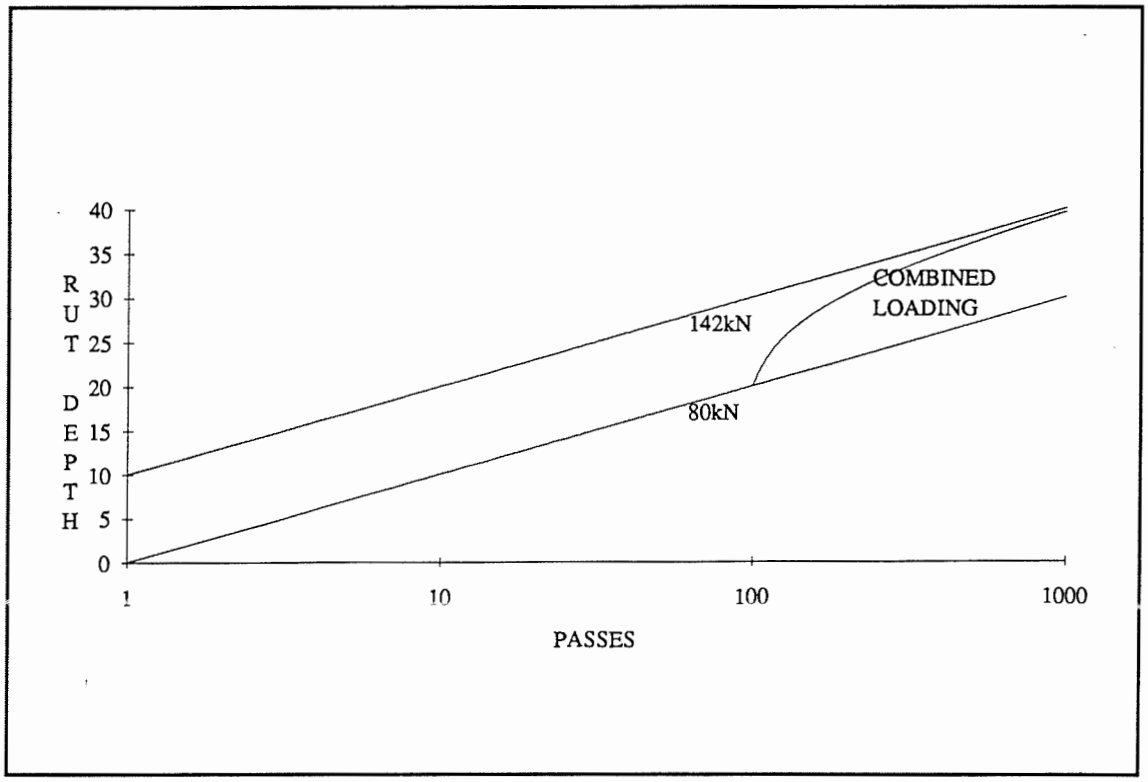

Figure 7.3 The Effect on Deformation of a Change in Loading

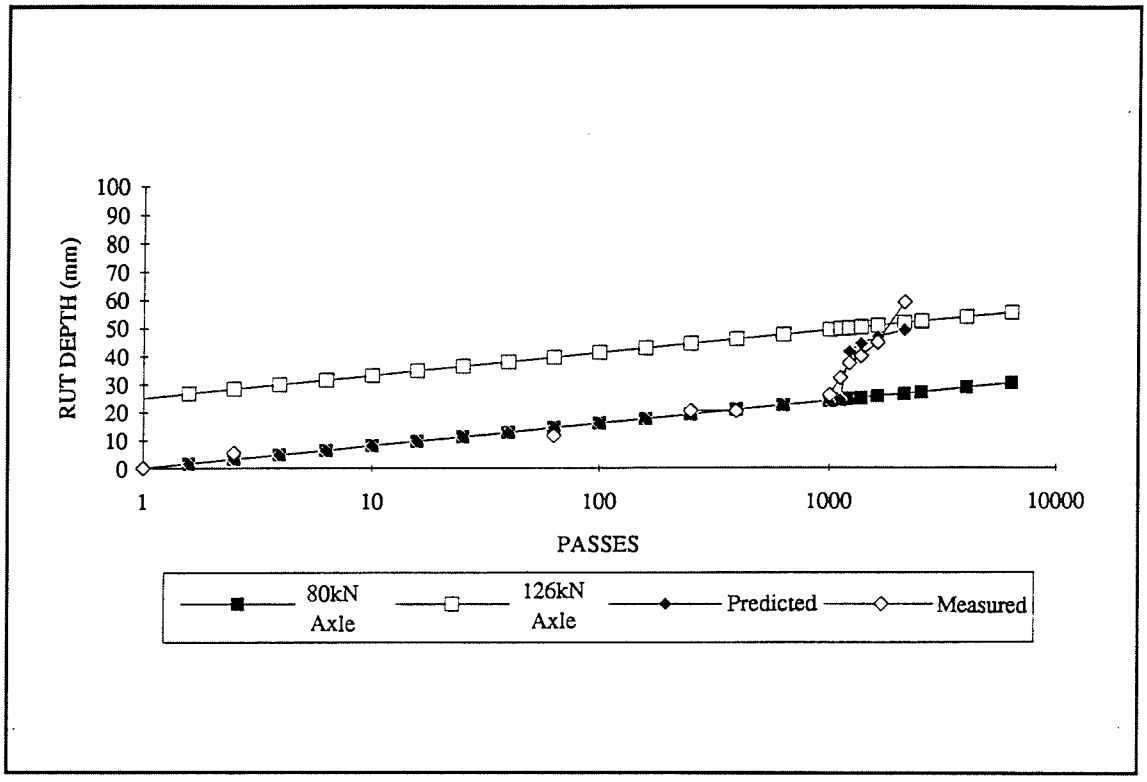

Figure 7.4 Observed and Measured Deformation of Section P

On this basis, the initial premise that a fourth power law is applicable to unpaved roads has not been proven. De Groot et al (1982) based their recommendations for geosynthetic reinforced roads on the results of a few pavements. The trend observed at Bothkennar is, as noticed by De Groot, that the power, if it is appropriate, should be increased above the value 4 which is commonly assumed. However, the observations at Bothkennar suggests that it is not possible to generate sensible or consistent power values. Therefore, the applicability of the law to unbound pavements must itself be called in question.

7.1.3.3 Alternative Relationship

Extensive trials on unreinforced, unpaved roads were undertaken by Hammitt (1970). A relationship was developed which predicted the number of passes, of any given axle load, which would generate a 75mm rut and this work was discussed more fully in Chapter 2.1. Based on 59 sections and various axle loadings, Hammitt (1970) predicted that the number of passes was a function of $\sqrt{\text{axle load - contact area.}}$ This appears to be based on a larger number of sections than De Groot et al (1982) and, because both relationships are empirical, it appears that the larger number of sections considered by Hammitt leads to a more sound basis for prediction. Thus, a relationship for non-standard axle loads is probably more correctly defined by reference to Hammitt (1970) than from more arbitrary use of a power law.

7.1.4 Rut depth and pavement thickness

7.1.4.1 Control of Aggregate Deformation

Sections A, B, C & D performed less well than their equivalent lower-bound counterparts. Indeed Section E may have only out-performed Section J because of the much reduced thickness of Section J and Section F may have out-performed Section I because the geogrid may have failed prematurely in Section I. It is possible that the increase in the upper-bound pavement deformation was caused by the lorry, as it came down off the hard standing area onto the pavements, inducing higher local stresses in the first section and continuing to bounce along the upper-bound pavements. Thus, Section A faired least well, with subsequent sections progressively suffering less severely. However, the speed of the lorry was, at most, 10m/s and it is felt that

although the effects mentioned above might have had some bearing on the performance of Section A, it is unlikely that it continued to affect the pavements further down the series. Examination of the longitudinal profile of Section A shows that the vertical depression of the wheel path varies with a wavelength of 5m and a noticeable depression was noted before the start of Section A approximately 5m before the first measured depression. These observations are consistent with the lorry bouncing. Although there may be some evidence that this effect is still apparent in Section B, it is no longer evident in Section C (as can be seen from Figures C16, 17 and 18 in Appendix C) and so another explanation for the poor performance of the upper-bound sections must be found.

If the performance of these sections can not be attributable to the influence of unstable loading then another explanation may be that the aggregate layer is making a larger contribution to the overall rut depth by straining internally. The thicker pavements of the upper-bound sections are preventing the geosynthetic from working efficiently as they are too low in the pavement structure. Conventional wisdom for the reinforcement of static foundations implies that the reinforcement works at its most efficient when placed at approximately ⅓ of the footing width below the footing, as reviewed by Lee (1989). Assuming that the wheel print has an effective width of 600mm, geosynthetics will thus probably perform to their maximum advantage at a depth of 200mm into the pavement structure.

It would appear that there is a maximum working thickness for singly reinforced pavements and that if the design dictates that larger thicknesses are required, then inclusions within the fill have to be considered.

Examination of the vertical strains monitored at the base of the aggregate layer shows that, although the transient strains are of a similar magnitude in the upper and lower-bound cases, in the reinforced cases, the permanent strains are higher in the upper-bound. This unusual observation might be explained by examining the vertical and horizontal stresses. The transient vertical strains are probably of a similar order of magnitude because the differences in pavement thickness between the upper and lower-bound pavements is small. In the thinner pavements however, the geosynthetic is in greater tension than in the thicker ones and this geosynthetic force increases the horizontal confining stress within the aggregate layer. Thus in the thicker pavements the deviator stress at the base of the pavement, is greater than in the thinner one and it is

known that, loosely, the permanent deformation is a function of the magnitude of this stress (Loach (1987)).

7.1.4.2 Local Variation of Thickness

Small variations in the level of the subgrade and aggregate surface during construction produces a variation in the thickness aggregate within any one section. A comparison of the small differences in the thickness of the aggregate layer and the vertical depression, measured every 0.5m along the length of each section, implies that rutting is not too sensitive to local variations in the thickness of the layer. As can be seen from Figure 7.5, there is little correlation between vertical depression and pavement thickness. It might appear therefore that the performance of the haul roads is not sensitive to the thickness of the layer. However, experience on the site has shown that the control sections have performed as well as some of the reinforced sections and commonly, there is only 50mm between the design thicknesses. This observation implies that the pavements are sensitive to small changes in design thickness, which finding is supported by examination of the empirical design charts (Figure 7.6). The development of rutting appears, therefore, to be sensitive to changes in the design thickness but not to small local variations. In the area over which the load is spread a range of thickness of the layer exist. This means that local deficiencies in the aggregate layer thickness are averaged over a number of measurements, reducing the importance of local variations. Alternatively, or additionally, the rut depth is more sensitive to other local factors such as variations in the shear strength of the subgrade and in the aggregate stiffness. This would imply that changes in the rut depth caused by local variations in thickness, are small in comparison to changes due to the other variables.

7.2 GEOSYNTHETIC RUPTURE

The expected geosynthetic strains at a surface rut depth of 150mm, assuming that the deformed shape at formation is parabolic (after Giroud and Noiray (1981)), is in the region of 4%. However, the trials at Bothkennar have shown that geosynthetic rupture occurs at strains well below the wide-width tensile test values as determined from the site delivered samples. The testing at Strathclyde University (Yeo (1992)) has shown that the effect of construction and trafficking on the stress/strain characteristics of the

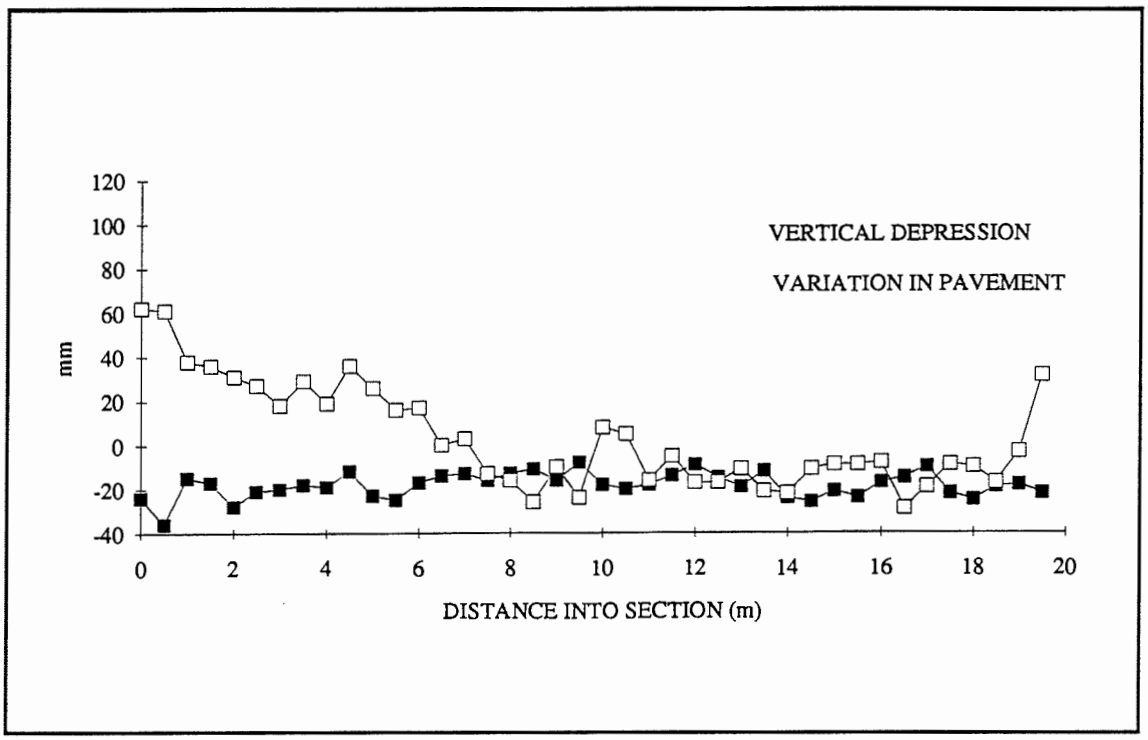

Figure 7.5 Vertical Depression After 2115 Passes and Initial Pavement Thickness For a Typical Lower-bound Section

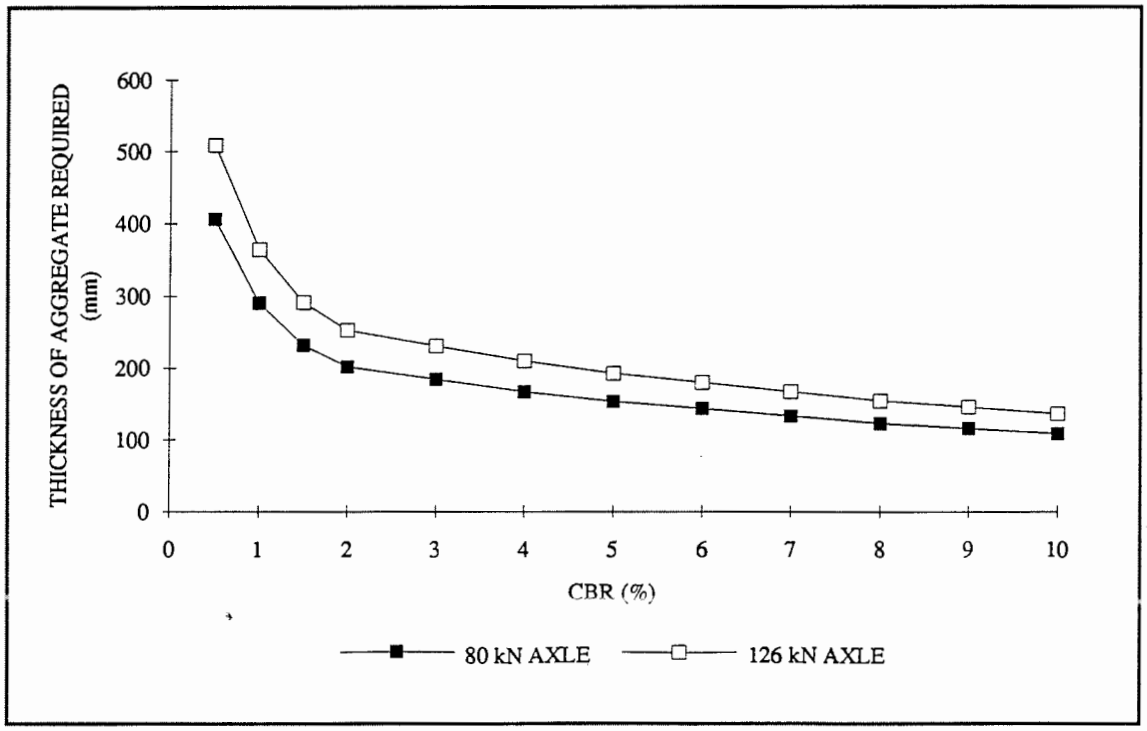

Figure 7.6 Empyrical Design Chart of Thickness of Aggregate Required to Resist Deformation

geosynthetics is to make them more brittle, reducing the strain at failure (see Appendix A).

Two of the pavements examined at Bothkennar, Sections I and J, suffered geosynthetic rupture. The onset of geosynthetic rupture was marked by a noticeable change in gradient of the rut depth v passes plot and it led to the pavement's rapid deterioration. The rupture of the geosynthetic is catastrophic to the serviceability of the pavement as the rate of rut depth development becomes very large. It was found that filling the ruts in a pavement, where geosynthetic rupture had occurred, did not lead to a slowing in the rate of deformation.

7.3 NON-LINEAR BEHAVIOUR

A multi-layer, linear elastic analysis of the stress distribution throughout the pavement structure using the BISTRO program (Peutz et al (1968)) leads to the expectation that a 58% increase in the axle load would lead to a similar percentage increase in the vertical stresses at the base of the aggregate layer and at the top of the subgrade. Such an analysis for a typical lower-bound section at Bothkennar was performed. It included a standard axle load, an aggregate stiffness of 100 MPa and a subgrade stiffness of 30MPa (as determined on site by FWD testing), and a contact stress of 500 kPa. The program predicted that the vertical stresses 50mm above the base of the aggregate layer and 20mm below the surface of the subgrade will be 69.4kPa and 56.2kPa respectively. These stresses are of a similar magnitude to the mean values observed at Bothkennar under the 80kN axle load.

The increase in the observed peak vertical stresses generated when the axle load increased from 80kN to 126kN was less than may have been expected from the multi-layered, linear-elastic analysis. The 58% increase in load led, on average, to an observed increase of 32% in the vertical stress at the base of the aggregate layer and a 20% increase in the vertical stress at the top of the subgrade. The fact that the observed values did not increase by the amount predicted by multi-layered, linear elastic analysis is a result of the non-linear-elastic behaviour of the aggregate and subgrade materials.

The non-linear behaviour of clays and aggregates is a well-known phenomena and many models exist to predict the stress/strain relationships for both granular and cohesive materials. FENLAP is a finite element programme developed by Almeida et al

(1991) primarily as a tool to calibrate the back-analysis programs which estimate the stiffness of pavement layers from falling weight deflectometer data. FENLAP was used with a "k theta model" (Hicks and Monnismith (1971)) for the aggregate layer and a subgrade model described by Brown (1979) to analyse the non-linearity of the aggregate and subgrade. The constraints required for the models were obtained by examining on-site FWD data. A FENLAP analysis predicts that the 58% increase in load applied at Bothkennar should generate a 37% increase in the vertical stress at the base of the aggregate layer and a 33% increase in the vertical stress at the top of the subgrade, which are closer to the observed values.

Therefore, the vertical stresses and strains as measured in the pavement can be predicted, in the standard axle loading case, by the use of multi-layered, linear-elastic analysis provided that an appropriate stiffness for the aggregate and soil has been adopted. Changes in the stress condition at the base of the aggregate layer and at the top of the subgrade due to a changing loading are not accurately modelled by linear-elastic analysis in which the same material stiffnesses are used. However non-linear analysis has produced some explanation for the stresses observed.

7.4 STRESS DISTRIBUTION

It is a widely held concept that the vertical stress distribution with depth, or in this case at the base of the aggregate layer, can be determined using a load spread angle. This, in turn, gives a rectangular, stepped vertical stress distribution at any given depth which is convenient for analysis. However, it is known that the concept of the load spread angle is an approximation, and that the true vertical stress distribution is more bell shaped. Many of the analytical methods only consider the case of plane strain limiting themselves to stress and strain within a transverse section of the pavement. Even those which are axisymmetric do not consider the manner in which the rut depth or the geosynthetic properties may alter the stress distribution in the pavement structure.

Stress distribution across the pavement is not available from these trials but the longitudinal stress distribution is likely to be a better approximation to the transverse stress distribution than the concept of a load spreading angle. The longitudinal vertical stresses may be approximated by study of the change in the measured vertical stress at the base of the aggregate layer as the load approaches the instrument, as shown in Figure 6.4 and reproduced here as Figure 7.7. Although the vertical stresses were

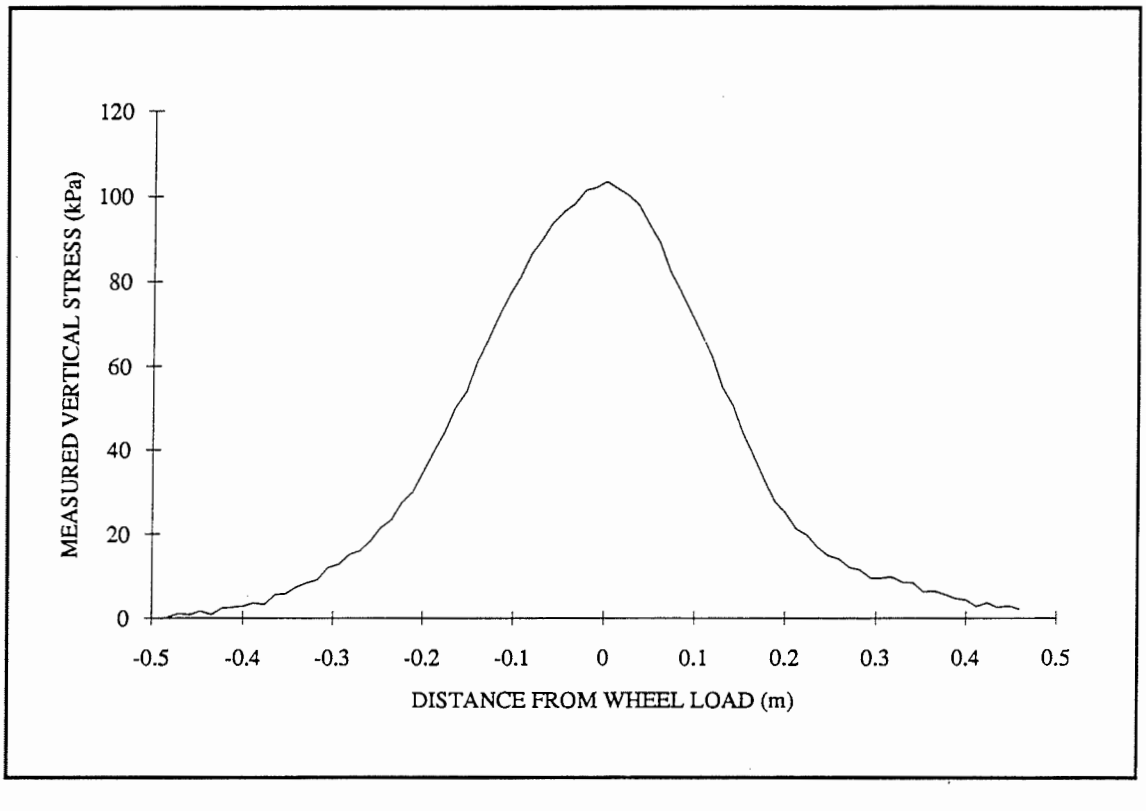

Figure 7.7 Subgrade Longitudinal Stress Distribution - Section P

measured on a time basis, it is possible to convert from time to distance because the wheel base of the lorry is known and the time lag between the pulse generated by the front and rear axles can be used to determine its speed of travel. To perform analysis on the basis of the stress profile shown in Figure 7.7 would add a complication to the calculations. Finite Element calculations by Brocklehurst (in print) suggests that the errors, generated as a result of using a load spread angle approximation, are small.

As far as transient stresses are concerned, the axisymmetric assumption is probably valid, and so the transverse stress equals the longitudinal stress. There is no evidence that the inclusions alter the vertical stress distribution within the pavement structure. However, it is possible that they affect the horizontal stress state, as discussed in 7.1.4.1.

7.5 ANCHORAGE OF THE GEOSYNTHETICS

The transient strains observed on the geosynthetic decay rapidly from peak values under the wheel path, as shown in Figure 7.8. Outside the loaded area of the geosynthetic, as calculated assuming that the aggregate performs load spreading with an angle $\tan\alpha = 0.6$, the strains induced in the inclusion by the wheel load are small, tending to zero. This leads to the conclusion that the geosynthetic is not working outside this area, and so, for transient loading, is not in need of anchorage. The observation that the geosynthetic transient strains tend to zero or even tend to the compressive, at remote positions to the wheel path, suggests that the aggregate is pushing the geosynthetic away from the loaded area, as predicted by Milligan et al (1989a) and Brocklehurst (in print).

The accumulation of permanent deformation also tends to suggest that the tensile strains tend to zero away from the wheel path, as can be seen in Figure 7.9. This implies that for permanent strains the use of anchorage is not necessary. However, it must be pointed out that these trials were carried out on clay that was much stiffer than may be the case for many such roads and the high strength of the subgrade may be the reason why anchorage is not required.

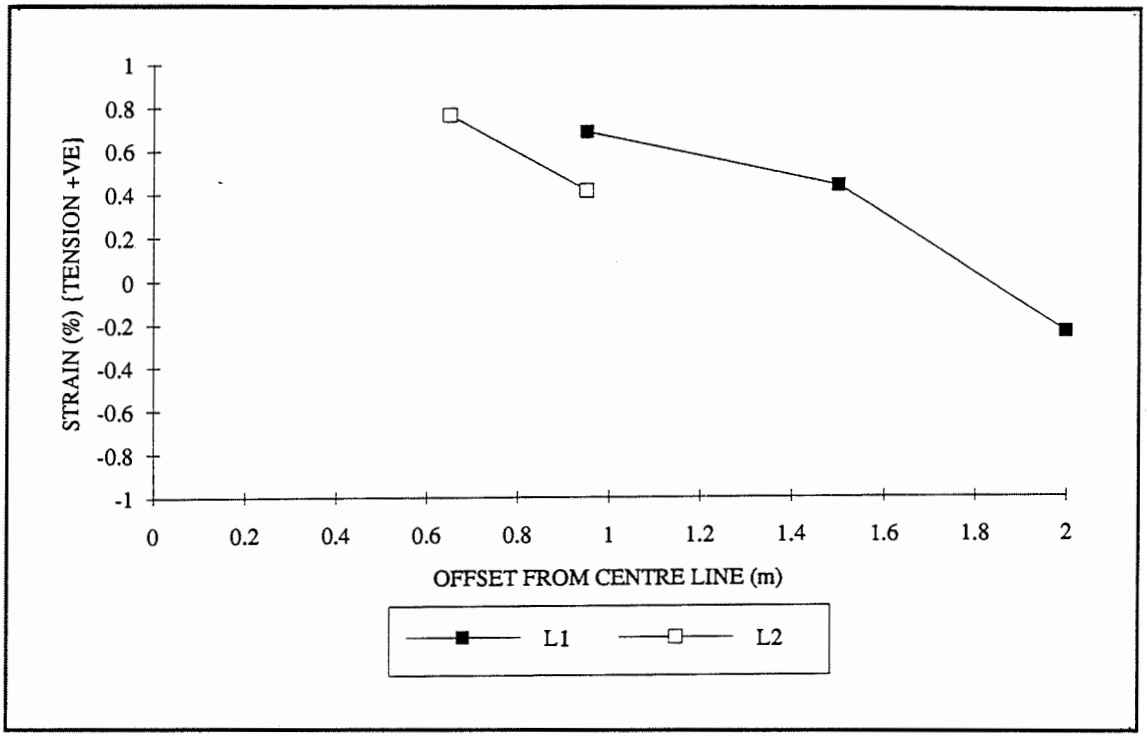

Figure 7.8 Transient Transverse Geosynthetic Strain Distribution - Section L

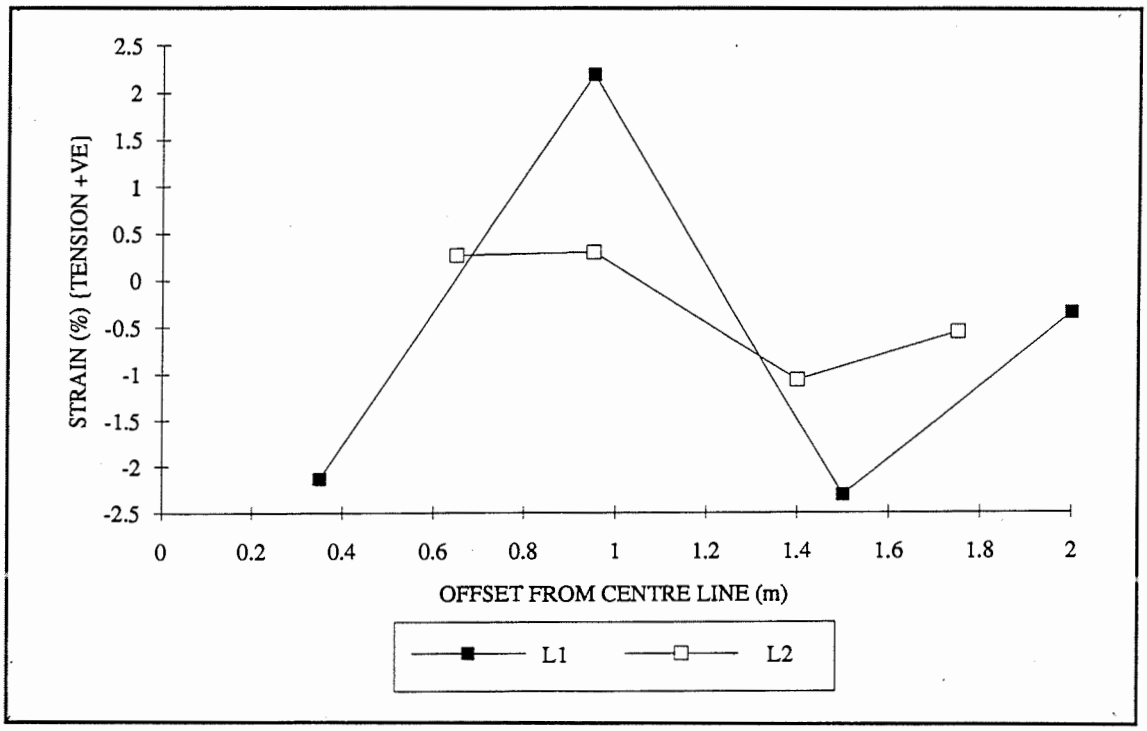

Figure 7.9 Permanent Transverse Geosynthetic Strain Distribution - Section L

CHAPTER EIGHT

CALIBRATION OF DESIGN METHODS

The objective of this chapter is to critically examine, in turn, each design method and in particular to examine the actual performance, of the relevant section, to that which could have been expected from the design method. Where possible the "as built" material properties are used as the inputs to the design. Where it is felt that the design method is lacking or could be improved, in the light of the results, then this will be highlighted.

8.1 GIROUD & NOIRAY (1981)

8.1.1 Unreinforced pavements

8.1.1.1 Static loading - required pavement thickness

The design method proposed by Giroud & Noiray (1981) consists of a static analysis of the vertical stresses in the reinforced pavements. In the unreinforced analysis, the vertical stress imposed upon the subgrade is limited by the elastic bearing capacity πS_u. Thus, the thickness of the pavement required to resist an application of one pass of a wheel load in the unreinforced case, h_o, is given by Equation 2.13:

$$\pi S_u = \frac{P}{(W + 2h_o\tan\alpha)\,(L + 2h_o\tan\alpha)} + \gamma h_o \qquad (2.13)$$

For the case at Bothkennar, it is assumed that

S_u = 85kPa, W = 0.4m, L = 0.283m, $\tan\alpha$ = 0.6, γ = 21kN/m^3, P = 80kN

The concept of a load spread angle, $\tan\alpha$, was discussed in Chapter 7 and it is assumed here to be a fair approximation to the imposed vertical stress distribution on the subgrade. The value of $\tan\alpha$ suggested by Giroud and Noiray is 0.6, as above

$$85\pi = \frac{80}{2(0.4 + 1.2h_o)\,(0.283 + 1.2h_o)} + 2h_o$$

Thus $h_o = 0.042m$

It should be noted that $h_o = 0$ when $S_u = 112.5kPa$, that is direct static loading of the subgrade by a standard axle would be possible without exceeding the elastic bearing capacity.

8.1.2 Reinforced pavements

8.1.2.1 Static loading - required pavement thickness

In the static analysis of reinforced pavements, as proposed by Giroud and Noiray (1981), it should be noted that the vertical stress which can be imposed on the subgrade is limited by the plastic bearing capacity, $(2 + \pi)S_u$. This vertical stress is modified by the contribution made by the geosynthetic due to the membrane effect. Under standard axle loading, the thickness of aggregate required to resist the application of one pass of a wheel load in the reinforced case, h, is given by Equation 2.21:

$$(2 + \pi)S_u = \frac{P}{(W + 2h\tan\alpha)\,(L+2h\tan\alpha)} - p_r \qquad (2.21)$$

where p_r is the reduction in vertical subgrade stress attributable to the membrane effect. If the contribution of the membrane effect is assumed to be zero and the following values apply:

$P = 80kN$, $W = 0.4m$, $L = 0.283m$, $\tan\alpha = 0.6$ and $p_r = 0kPa$,

then $h = 0m$ when $S_u = 68.7kPa$.

An analysis making no allowance for the effects of the membrane effect, p_r, will yield $h = 0m$ at subgrade undrained shear strengths above 68.7kPa, that is direct static loading of the geosynthetic, by a standard axle, would be possible without exceeding the plastic bearing capacity.

At subgrade shear strengths above 68.7kPa, less if the membrane effect contribution is to be considered, the static analysis for reinforced pavements would yield a negative

requirement for the thickness of aggregate. This appears to be nonsense and the conclusion may be drawn that the method is not suitable for subgrade shear strengths above this level.

However, the analysis is somewhat arbitrary, in that it is the difference in aggregate thickness between the reinforced and the unreinforced cases that is of interest. This saving of aggregate is applied to an unreinforced, empirical design. Therefore, although negative thickness requirements at higher subgrade shear strengths may bring into question the applicability of the design, it is possible to generate some form of design for these shear strengths. The use of questionable, negative required thicknesses is likely to generate more sensible answers than the alternative assumption which is that at subgrade shear strengths above 68.7kPa the static, reinforced case thickness required equals zero as this will not take into account the effects of repeated loading.

8.1.1.2 The vertical, central displacement of the membrane

For the geogrid pavement at Bothkennar, h = 0.30m and after 1000 passes of an 80kN axle, a rut depth of 0.023m had developed.

Therefore, if $\tan\alpha = 0.6$ and W = 0.4m the ½ width of the subgrade subject to vertical stress is given by the following equation

$$a = \frac{W}{2} + h\tan\alpha = 0.38$$

and $a' = 0.95 - 0.38m = 0.57m$

where a is the ½ length of the loaded area and a' is the ½ length between the loaded areas,

As a' > a , Giroud and Noiray suggest that by considering the volumetric equilibrium that must occur during the deformation of the subgrade, the vertical depression at the surface of the subgrade is given by Equation 2.16.

$$s = \frac{ra'}{a + a'} = 0.014m \qquad (2.16)$$

The vertical depression under the wheel paths is not the full rut depth, which depends on vertical depression plus heave away from the wheel path. Equation 2.16 predicts the contribution to the rut depth due to the vertical depression of the subgrade by making the assumption that the subgrade is incompressible and therefore the volume of material displaced from beneath the loaded area must be equal to that contributing to the area of heave. Equation 2.16 is formed by assuming that the convex and concave profiles of the post trafficking subgrade are parabolic and by equating the depression and heave areas.

In this case the vertical depression at the surface of the subgrade, s, is 60% of that of the rut at the surface of the aggregate and this varies depending on a' and a, ie for any wheel loading, the ratio of s to r is related to the thickness of the aggregate layer and the load spread angle, tanα, considered applicable. For any given load spreading function, tanα, and rut depth, r, increasing the pavement thickness yields a smaller ratio of vertical subgrade depression, s, to the rut depth, r. Because the analysis assumes that the aggregate layer deforms without changing its thickness, the subgrade vertical depression is assumed to be equal to the vertical depression of the surface of the aggregate. However, this is not the case because some deformation occurs within the aggregate layer and thus the vertical depression at the surface of the subgrade is less than is calculated above.

It can be seen from Figure 8.1 that, at least for Bothkennar, the ratio of the surface rut depth to the surface vertical depression is approximately 0.70 for all sections regardless of the pavement thickness. Part of the scatter seen in Figure 8.1 is due to variations in the amount of internal aggregate deformation that occurs which also explains why the actual ratio between s and r is higher than predicted.

8.1.1.3 Geosynthetic strains

Assuming that the deformation of the subgrade is parabolic, and the length of the initial and final soil/aggregate interface profiles under the loaded area is a and b, then the strain is given by the following equation

$$\frac{b}{a} - 1 = \tfrac{1}{2}\left[\sqrt{1 + \left(\frac{2s}{a}\right)^2} + \frac{a}{2s}\ln\left(\frac{2s}{a} + \sqrt{1 + \left(\frac{2s}{a}\right)^2}\right) - 2\right] \qquad (2.21a)$$

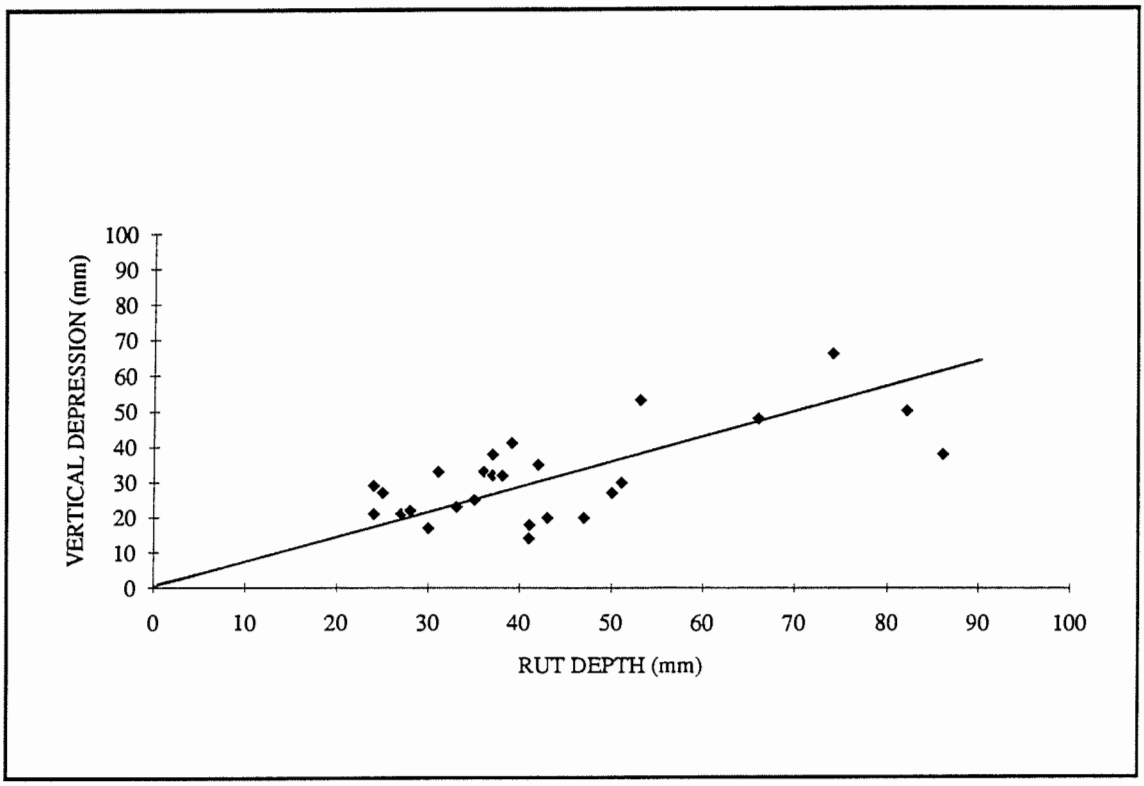

Figure 8.1 Rut Depth and Vertical Depression for the Pavements at Bothkennar

giving a linear strain in the loaded area of 0.07%. Therefore the length of the final profile under the loaded area, b, is 0.3803m.

The initial and final length of the subgrade profile between the loaded area, a' and b', is given by the following equation

$$\frac{b'}{a'} - 1 = \tfrac{1}{2}\left[\sqrt{1+\left(\frac{2(r-s)}{a'}\right)^2} + \frac{a'}{2(r-s)} \ln\left(\frac{2(r-s)}{a'} + \sqrt{1+\left(\frac{2(r-s)}{a'}\right)^2}\right) - 2\right]$$

The initial length,of a', was 0.57m and therefore the length of the final profile between the load area, b', is 0.5701m giving a linear strain in the unloaded area of 0.02%.

The membrane effect assumes that the geosynthetic is pulled towards the wheel path as a result of the deformation. Furthermore, it assumes that the overburden vertical stress between the wheel path is insufficient to resist, by friction, the forces generated and so slipping occurs. Therefore, the strain is assumed to be constant across the pavement and is defined by this Equation 2.18:-

$$\varepsilon = \frac{b + b'}{a + a'} - 1 = 0.05\% \qquad (2.18)$$

The validity of the assumption that the geosynthetic strain is even across the width of the pavement is common in many membrane effect design methods (Giroud & Noiray (1981)), Neiuwenhuis (1977)) and indeed, if the geosynthetic is to transfer significant vertical forces to the area of the subgrade between the load areas, it is a pre-requisite that the strains induced in the geosynthetic out-side the load area are large. This has not been observed at Bothkennar where the transverse geosynthetic strain distribution is far from constant, reducing rapidly away from the wheel path. This observation is confirmed by evidence from the Sandheath trials (CIRIA (1986)), where the geosynthetics were seen to go into compression away from the wheel loads.

8.1.1.4 Vertical subgrade stress reduction

The membrane effect of the design method predicts that there will be a reduction in the vertical stress applied to the subgrade. Again, assuming that the subgrade deformation is parabolic, the reduction in vertical stress is given by Equation 2.20

$$p_r = \frac{k\varepsilon}{a\sqrt{1 + \left(\frac{a}{2s}\right)^2}} \qquad (2.20)$$

Where k is the stiffness of the geosynthetic. Geosynthetics do not demonstrate linear stress/strain relationships and, although it is not specified within the design method, it appears to be sensible to assume a value for k at the strain level of interest. Also, geosynthetic stiffness is a function of the rate of loading and although some type of creep stiffnesses may be the most correct value to use, the BS 6906 part 1 (1987) test is the most readily available data.

For the example from Bothkennar, the strain induced in the geogrid by a surface rut depth of 0.023 is 0.05 percent. Results from Strathclyde University (Yeo (1992)) imply that at this strain level, in the standard index test, the force, $k\varepsilon$, that could be expected in the geogrid is

0.20 kN/m for the post compaction sample and
0.22 kN/m for the post trafficking sample

assuming that the stiffness is constant from 0 to 5% strain.
Thus after 1000 passes of an 80kN axle, the force at this strain level might be 0.22kN/m and the value p_r can then be calculated to be 0.02kPa.

8.1.1.5 Aggregate saving

The thickness of aggregate required to withstand the application of an 80kN axle load in this example if given by Equation.2.21:-

$$(2 + \pi)\, S_u = \frac{P}{2(W + 2h\tan\alpha)\,(L + 2h\tan\alpha)} - p_r \qquad (2.21)$$

If S_u = 85kPa, P = 40kN, W = 0.4m, L = 0.283m, tanα = 0.6 and p_r = 0.02kPa, then h = 0.028m.

As predicted h is negative so the value of the saving of aggregate is a little unclear. However, the saving in aggregate may be considered as

$$\Delta h = h_o - h = 0.042 - - 0.028 = 0.070m$$

8.1.3 Comparison of design and performance

The saving in the thickness of the aggregate, as calculated by the two phases of the quasi-static analysis, is applied to an unreinforced pavement design. For the purpose of calibration, the rut depth expected after 1,000 passes in the example above is calculated below. A "forward calculation" as opposed to this "back calculation" is shown in Chapter 2.4.3.

The thickness reduction possible as a result of the inclusion, as shown above, is 0.070m. The actual thickness of the pavement constructed at Bothkennar is 300mm which implies that the pavement is equivalent to an unreinforced pavement of thickness 300 + Δh mm.

Giroud and Noiray (1981) suggest that unreinforced road design is governed by Equation 2.6

$$h' = \frac{119.24 \log N + 470.98 \log P - 279.01r - 2283.34}{S_u^{0.63}} \qquad (2.6)$$

h', being 300 + Δh = 0.370m log N = 3, log P = 4.903, S_u = 85,000Pa.

Therefore the rut depth, r, as calculated by this method should be - 316mm and in fact was found to be 23mm.

The design method assumes that a fourth power law is applicable and therefore, according to this design method, passes of the 126kN axle applied at Bothkennar are equivalent to 6.15 passes of an 80kN axle. It is possible to perform a calibration calculation on the design method using the rut depth generated after 2115 passes of the combined axle loads by using the fourth power relation. However, there are

reservations about the applicability of the fourth power law to unsurfaced low-volume roads, as discussed in Chapter 2. It would be possible to revert to Hammitt (1970) for an analysis of the effects of trafficking by simply replacing Equation 2.6 with Equation 2.12. The combined loading applied at Bothkennar has been reduced to standard axles by the fourth power relation and for the constants h, S_u and P in Equation 2.6, the expected rut depth, r, is plotted for a variety of values of N and this is shown in Figure 8.2. It can be seen that the prediction of the development of rutting is very poor because, as shown in Chapter 2, at low rut depths and high subgrade shear strengths negative rut depths are required to satisfy Equation 2.6. This is plainly unsatisfactory.

8.1.4 Comments on the design method

The design method presented is, like many design methods, a static analysis and as such the controlling parameters relate to static failure. Rut depth development however, is not generally a single loading phenomenon, but is a result of an accumulation of small plastic deformations caused by the repetition of vertical stresses well below the failure values. However, analytical design methods rely on static analysis and it is a generally accepted method to extrapolate designs on the basis of empirical data because simple repeated loading models, predicting permanent deformations within the system, have yet to be developed.

The low rut depths encountered in the trials have led to low geosynthetic strains and low stress reductions on the subgrade due to the membrane effect. It is thus apparent that the principle reason for the improvement in performance that is predicted by this design method is the change of the subgrade bearing capacity from elastic failure to general plastic failure. However, this change is not justified within the method and, even so, is not realistic (as shown in Chapter 9). The vertical stresses imposed upon the subgrade are, at least at low rut depths, are not affected by the inclusion of a geosynthetic, because the membrane effect can only make significant contributions at high rut depths. Therefore, the vertical stress imposed on the subgrade by each application of load, is generally the same in both the reinforced and unreinforced cases and is well below the failure stresses.

Milligan et al (1989a) have shown that an improvement in bearing capacity may be possible with a reinforcing inclusion. Giroud and Noiray's (1981) shift in bearing

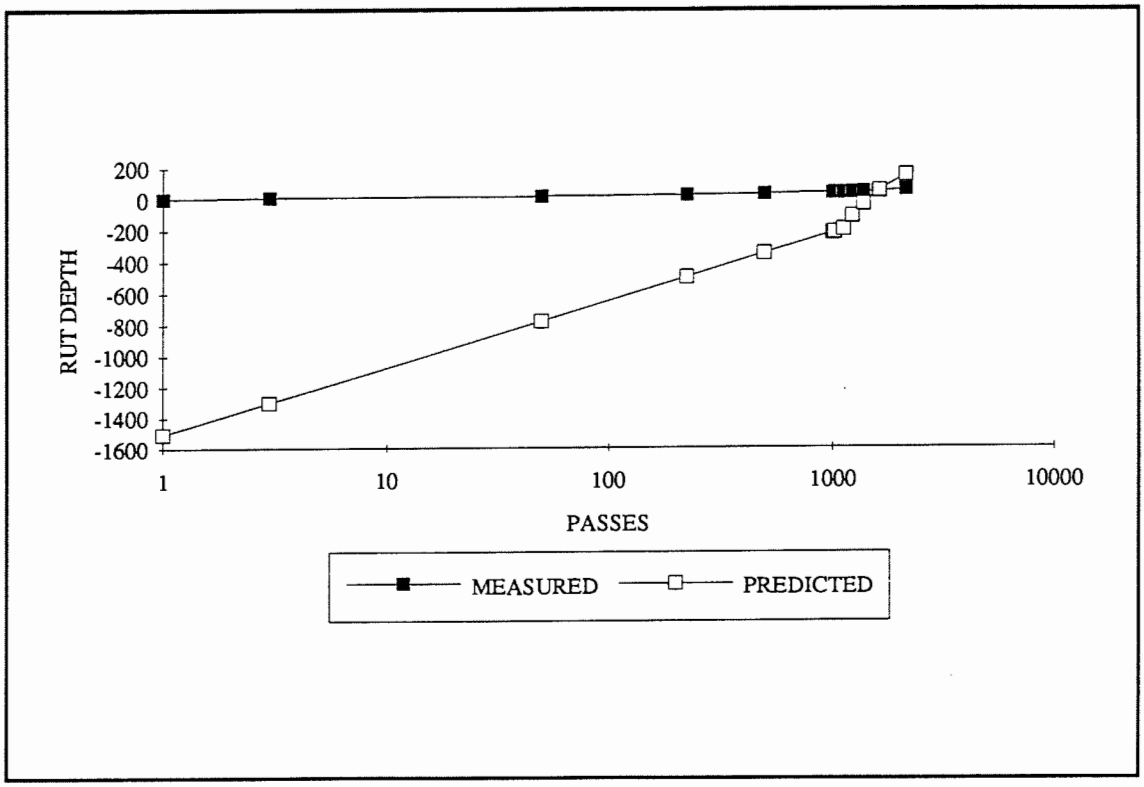

Figure 8.2 Measured and Predicted Deformation of the Section Designed by a Giroud and Noiray (1981) Approach

capacity from πS_u to $(2 + \pi)S_u$ for the unreinforced to the reinforced case can be shown to be a reasonable assumption in certain cases however a range of possible values exist which might make these assumptions optimistic or pessimistic.

The assumption that the strain in the geosynthetic is constant across the pavement must be viewed critically. Experimental data from Bothkennar shows that the transient strains decay with distance away from the wheel path. This observation questions the validity of the membrane effect which assumes that the inclusion is pulled towards the wheel path as a result of the deformation. This would produce larger strains in the geosynthetic away from the loaded area than were observed. The membrane effect relies upon significant geosynthetic forces, and therefore strains, outside of the loaded area in order to transfer vertical loading to the area between the wheel paths.

In summary, the method proposed by Giroud and Noiray (1981) appears to be a membrane effect type of design method but, in fact, generates most of the benefit by an arbitrary change in bearing capacity. This change in bearing capacity could be justified (Milligan et al (1989a)) for a fully reinforced analysis. However, static analysis is a poor model as, in fact, deformations are caused by multiple applications of stresses well below failure.

The development of permanent deformation is loosely related to the proximity of the applied cyclic stress to the failure stress (Loach (1987)). Although the actual vertical stresses on the subgrade are the same for the unreinforced and reinforced cases at small rut depths, the confining stresses in the reinforced case are probably higher than in the unreinforced as a result of the tension within the geosynthetic. Thus the development of permanent deformation may well be less in the reinforced case.

The concept of the membrane effect has not been supported by the experimental data. Even at reasonably large rut depths, the computed contribution it makes to the stress distribution is small and so is probably not worth considering. For standard wheel loadings the analysis requires a negative thickness of aggregate, to resist a single application, when the subgrade shear strength exceeds 68.7kPa and, as such, should be considered as a limitation of the design.

Giroud and Noiray (1981) provides an easy to follow method which, within limitations, gives reasonable results. However, it does so by making many assumptions that in many cases will be invalid.

8.2 MILLIGAN ET AL (1989 a & b)

The design method proposed by Milligan et al (1989 a & b) considers the equilibrium of a block of aggregate below the wheel as shown in Figure 8.3. Active forces within the aggregate under the wheel are resisted by passive forces away from the loaded area and because of the difference in vertical stresses in the two areas, the active forces are greater than the passive. Horizontal resolution of the forces is made possible by shear forces at the interface. In the unreinforced case these shear forces are applied to the surface of the subgrade which can reduce its bearing capacity to as low as $\left(1 + \frac{\pi}{2}\right) S_u$. In the fully-reinforced case all of the shear forces are transferred to the geosynthetic, enabling purely vertical loading to be applied to the subgrade which enables a bearing capacity of $(2 + \pi)\ S_u$ to be generated. However, a range of cases must exist between the fully-reinforced and the unreinforced cases depending upon the stiffness of the geosynthetic.

8.2.1 Static analysis

The analysis can be performed either as an axisymmetric or as a plain strain analysis. It is possible to perform the plane strain analysis by hand, whereas the axisymmetric analysis requires the aid of a computer. The distribution of stress (and strain) away from the centre will be different in the two cases and so the two methods will generate slightly different results in terms of the actual thickness required and thus in the aggregate saving. The plane strain case is more conservative but in order to examine the concepts behind the design method plane strain analysis will be considered in further detail.

The section designed by the Milligan et al (1989a) method at Bothkennar consisted of 300mm of sand and gravel overlying a lightweight polypropylene geogrid. If the loaded half footing width, $\frac{W}{2}$ is 0.2m and $\tan\alpha = 0.6$ then the half width loaded area at subgrade level is:

$$\frac{W}{2} + h\tan\alpha = 0.2 + 0.3 \times 0.6 = 0.38m$$

It was found in the 280mm diameter triaxial tests that the angle of internal friction of the sand and gravel was 58° (Appendix D)

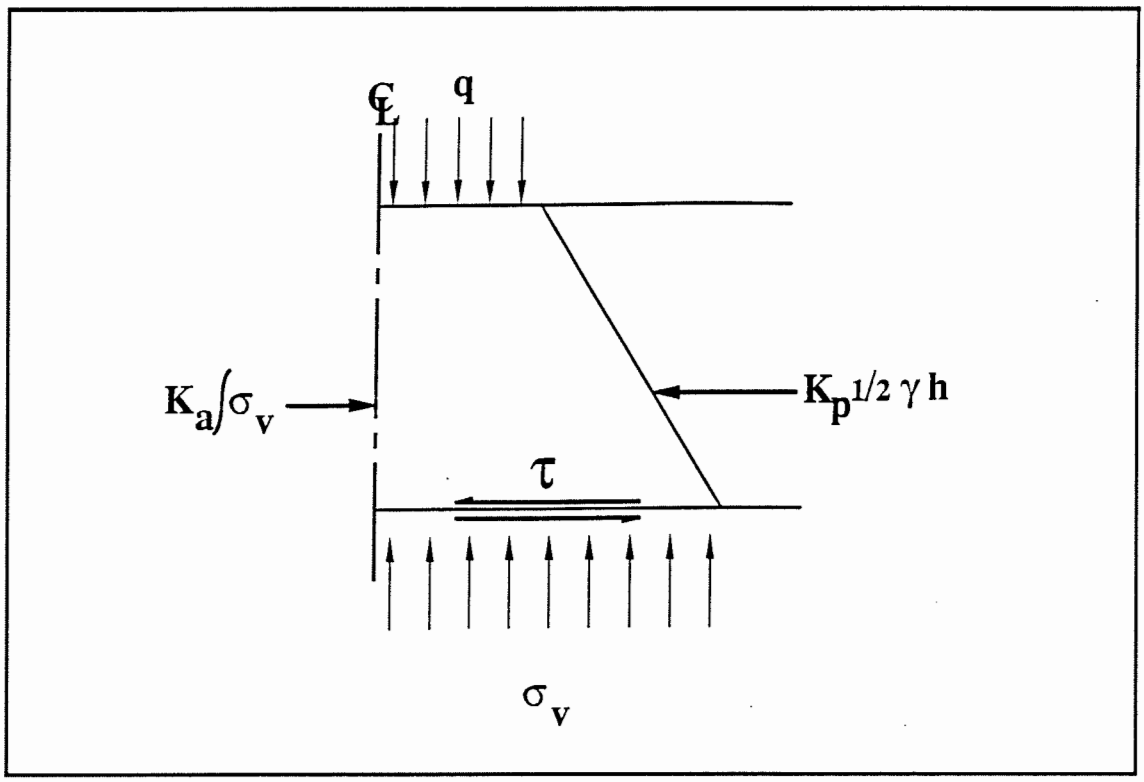

Figure 8.3 The Equilibrium of a Block of Aggregate Under a Load After Milligan et al (1989a)

The active earth pressure coefficient, K_a, is such that,

$$K_a = \frac{1 + \sin\phi}{1 - \sin\phi} = 0.08$$

and the passive earth pressure coefficient, K_p, is such that

$$K_p = \frac{1}{K_a} = 12.16$$

The non-dimensional parameter $\psi \left(= \frac{\tau}{S_u} \right)$ is related to the bearing capacity, N_c, by Equation 2.26.

$$\psi = \tfrac{1}{2} (K_a - K_p) \frac{\gamma h^2}{S_u (\frac{W}{2} + h\tan\alpha)} + N_c \left[\frac{K_a}{\tan\alpha} \ln \left(\frac{(\frac{W}{2} + h\tan\alpha)}{\frac{W}{2}} \right) \right] \quad (2.26)$$

when $h = 0.3m$, $\tan\alpha = 0.6$, $\gamma = 21kN/m^3$ and $S_u = 85kPa$

then in this case

$$\psi = - 0.353 + 0.088N_c$$

which is the line GCH in Figure 8.4.

The intercept of the line GCH with the available envelope yields the value $N_c = 5.0097$

Substitution of this value of N_c into Equation 2.27

$$q_s = N_c S_u \left(\frac{\frac{W}{2} + h\tan\alpha}{\frac{W}{2}} \right) = 809kPa$$

where q_s is the static stress required to reduce soil failure.

The design also does not produce any predictions for the development of rut depth. Milligan et al (1989b) suggests that this static analysis be extended to the trafficking case by reference to De Groot et al (1982) who suggested that for reinforced roads

$$\frac{P_s}{P_n} = N^{0.16} \quad (8.1)$$

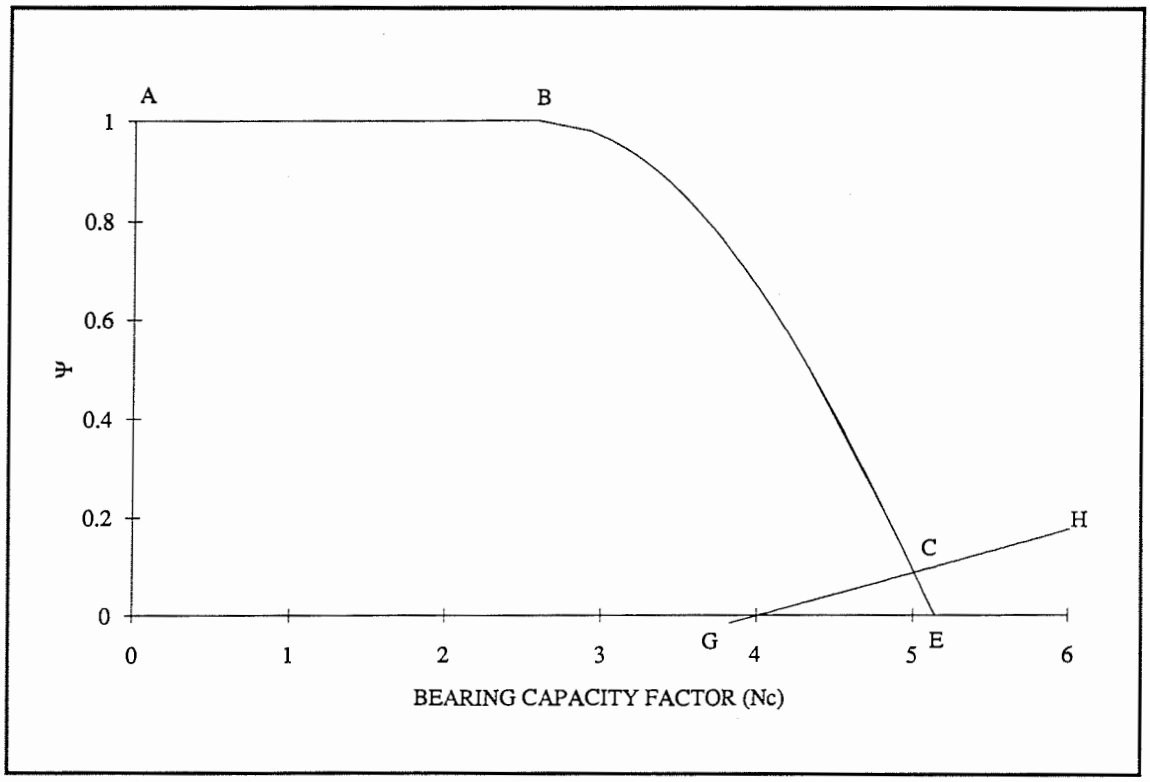

Figure 8.4 The Available and Required Bearing Capacities of a Loaded Subgrade - After Milligan et al (1989a)

The actual contact stresses, q_n, applied at Bothkennar were around 500 kPa and so $\frac{q_s}{q_n}$ $= \frac{809}{500} = 1.618$ and hence N = 20 passes.

In the plane strain case the permissible static stress P_s is only slightly more than the actual applied stress P_n and so, by reference to De Groot et al (1982), this appears to be an unsatisfactory design. However, if an unreinforced and reinforced analysis are compared, a saving in aggregate can be calculated which can then be applied to an unreinforced design such as Hammitt (1970). This approach would also yield a method of predicting the rut depth that is likely to develop.

This design consists mainly of a static analysis of failure, whereas pavements fail as a result of repeated loading at stresses well below failure. Although no model exists for accurately predicting subgrade deformation with passes, Brown and Dawson (1992) suggest that as long as a threshold value of deviator stress is not exceeded then gross deformations will not occur.

In the reinforced case $N_c = 5.14$ and so if the allowable surface contact stress remains constant in the two cases the contact stress 809kPa above equates to a thickness of aggregate by Equation 2.27.

$$809 = 5.14 S_u \left(\frac{\frac{W}{2} + h\tan\alpha}{\frac{W}{2}} \right)$$

which implies h = 0.283m.

Thus, a fully reinforced pavement will, in this case, generate an aggregate saving of 17mm.

The axisymmetric analysis possible with the program "Roadsolver" (Houlsby and Jewell (1987)) generates permissible surface contact stresses of 1641kPa in the unreinforced case and 1722kPa in the reinforced case. These values are above the contact stresses applied at Bothkennar. Milligan et al (1986b) suggest that the De Groot et al (1982) power law relationship (Equation 8.1) for varying axle loads, should be applied to determine how repeated, low contact stress loading can be converted to an equivalent load of a single axle application. However, the design method as such does not predict the rut depth that might be expected and, as Equation 8.1 is being used to allow for trafficking, it would appear more sensible to apply the work of Hammitt

(1970) to the axisymmetric case in the same manner as was suggested for the plane strain case.

Axisymmetric analysis suggests that the reinforced thickness is equivalent, for monotonic loading, to an unreinforced pavement thickness of 315mm. Based on the work of Hammitt (1970), and the observations on that work in Chapter 2, the development of rut depth with passes for an unreinforced pavement of this thickness is shown in Figure 8.5. Also plotted in this figure is the actual development of rut depth with passes. As can be seen, the predicted rate of deformation was much higher than the actual, which would imply that the aggregate saving calculation is not generous enough. This is probably due to the fact that no benefit is placed, within the design method, on the value of geosynthetic as separators.

8.3 EMPIRICAL DESIGN METHODS

8.3.1 Tonus et al (undated) - an empirical design

In the method proposed by Tonus et al (undated) the thickness of aggregate required to resist 1000 applications of an 80kN load is dependent upon the CBR of the subgrade and the geosynthetic inclusion. Such a thickness required versus CBR plot is shown in Figure 8.6, taken from Tonus et al (undated). The expected rut depth is one third of the thickness of the pavement, and therefore the design is a little inconvenient to the user, who tends to specify pavement performance by the rut depth which is permitted after a specified number and size of loadings. Such an analysis is possible using Tonus et al (undated) however some assumptions, not mentioned in the method, have to be made and some iteration is required.

Back-calculation, to compare actual and predicted performance, is possible provided that some assumptions, not stated within the method, are made.

For the trials at Bothkennar, the subgrade had an undrained shear strength of 85kPa. Figure 8.6 requires the subgrade to be described in as CBR and so the equivalency of $CBR = \frac{S_u}{23}$ will be used. Thus, 85kPa is equivalent to 3.7% CBR and therefore from Figure 8.6 it can be seen that the thickness of aggregate required to resist 1000 applications of the load, h, is 175mm. It is expected that after these applications, the rut depth that would develop would be a third of the thickness of the pavement, 58mm.

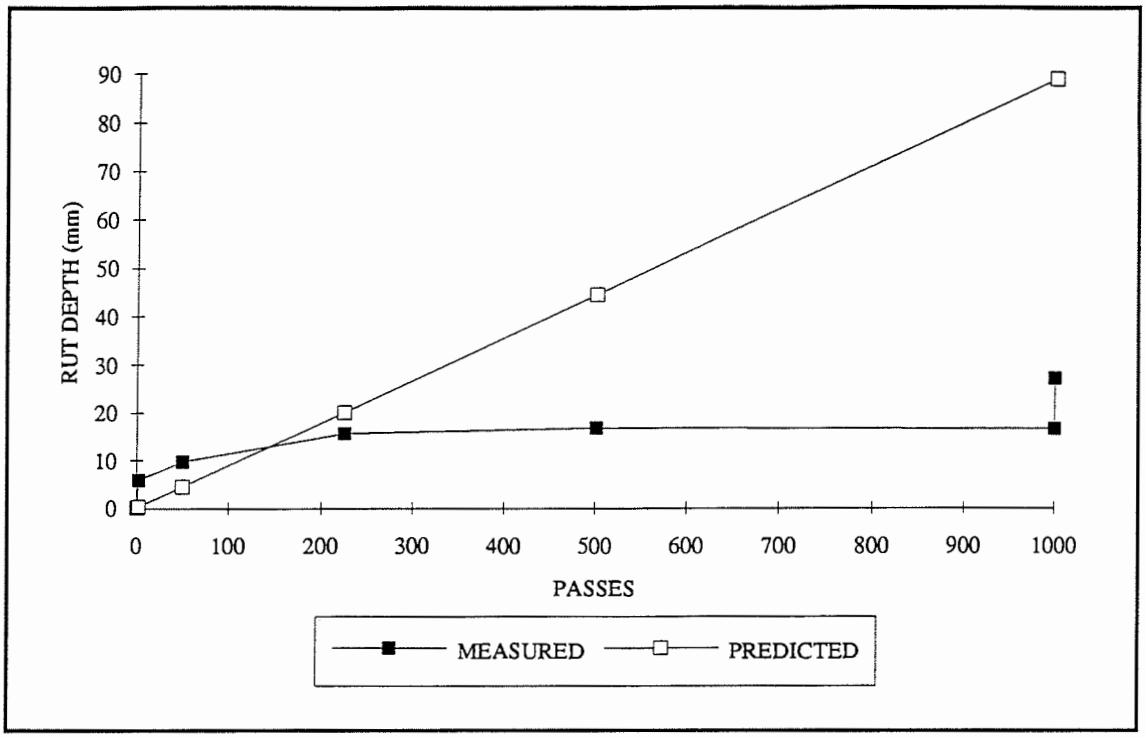

Figure 8.5 Measured and Predicted Rut Depth Development for the Section Designed According to Milligan et al (1989a)

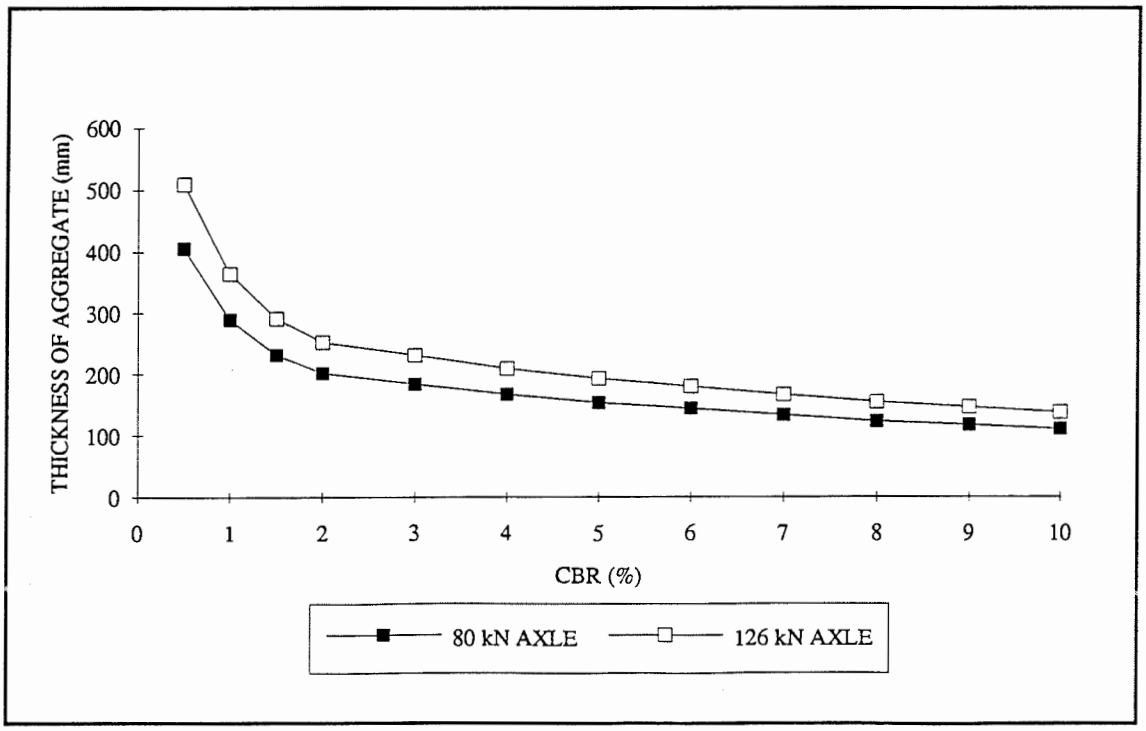

Figure 8.6 Thickness of Aggregate to Resist 1,000 Passes of a 90kN Axle - After Tonus et al (undated)

The design method makes some common assumptions about the effects of trafficking, namely that non-standard axles can be related to standard axles by the use of a "fourth power law", $\left(\frac{N_s}{N_i}\right)=\left(\frac{P_i}{P_s}\right)^4$, that a variety of axle loads can be expressed as the sum of their equivalents, $N_s = \Sigma[N_i \left(\frac{P_i}{P_s}\right)^4]$ and that the trafficking damage is a function of the logarithm of the number of passes, as shown in Figure 8.7 where the traffic influence factor is derived from the work of Hammitt (1970) and is given in Equation 8.2.

$$f = 0.27 \log N + 0.19. \qquad (8.2)$$

where f is the traffic influence factor

The actual thickness of the pavement at Bothkennar was 350mm and therefore from Figure 8.7 the traffic influence factor, f, must be $\frac{350}{175} = 0.27\log N + 0.19$.

ie $\log N = 6.70$.

Using the assumptions made above, the variety of axle loadings can be reduced to an equivalency of 7,125 passes of an 80kN axle and $\log 7{,}125 = 3.85$.

Thus a 350mm thick pavement is expected to rut to one third of its depth, ie 117mm, after $\log N = 6.70$ passes. Continuing with the assumption in Equation.8.2, that rut depth development is dependent on the logarithm of the number of load applications, the rut depth expected at the end of trafficking is $\frac{3.85}{6.70} \times 117 = 67$mm. The actual, final rut depth was 32mm.

The design method does not attempt to predict any savings of aggregate that might be possible by incorporating the product, although comparison with Hammitt (1970) would be possible. The prediction of rut depth development between the reinforced and unreinforced pavements of the same thickness is compared to the actual in Figure 8.8. As can be seen from the figure, the design method underestimates the performance of the pavement by a factor of about 2. The unreinforced case would be expected to generate more deformation because it is not taking into account the separation and reinforcement benefits of the inclusion.

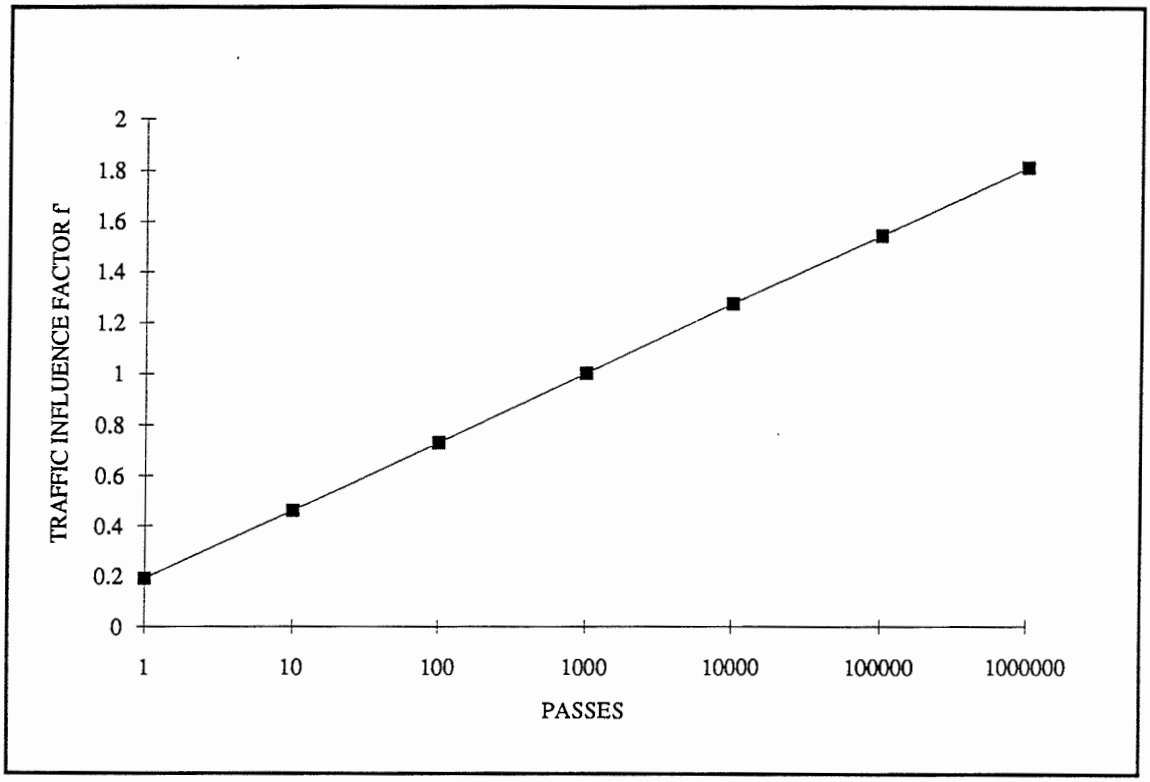

Figure 8.7 Traffic Influence Factor After Tonus et al (undated)

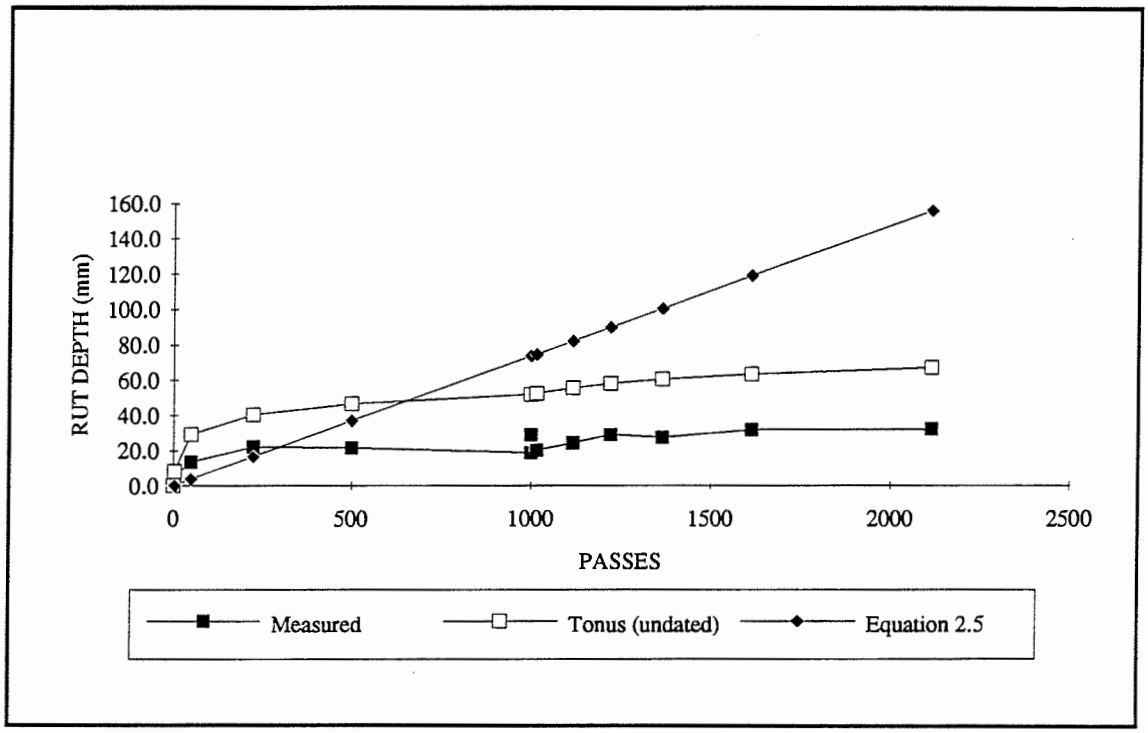

Figure 8.8 Measured and Predicted Deformation of the Section Designed According to Tonus et al (undated)

8.3.2 Needle-punched geosynthetic - empirical designs

Two needle-punched geosynthetics were used in the trials, a polypropylene based product and a polyester one. The polyester fabric was designed by reference to the publication by the Comité Français des Geotextiles (1981) which specified that for HGV loading, at a density of 10-100 passes per day, good fill, an allowable rut depth of 15cm, and a subgrade CBR between 2 and 5%, then 350 to 450mm of aggregate was required. The design method does not predict how the rut depth develops The wide range of possible subgrade CBR's that are permitted for any one design does not fit with the observation that most analytical and empirical designs are sensitive to small changes in CBR. So, if the number of CBR intervals could be increased, the design method may have some useful function. This type of design method is very difficult to calibrate and in relation to the trials at Bothkennar. However, it was be observed that the rut depth developed by the 2115 passes applied was 38mm, less than the 150mm expected.

The section including the polypropylene geosynthetic was designed according to Polyfelt (undated). It is a similar method to that described in Chapter 8.3.1, in that a thickness of aggregate required to resist failure, in this case static failure, is calculated and that thickness is adjusted to take account of trafficking and the acceptable rut depth.

The design method is empirical and experimental data supporting such design methods cannot cover all eventualities. The thickness of aggregate required to resist static failure, as shown in Figure 8.9, can be determined for two axle loads and two qualities of fill. The axle load 90kN is approximately equal to the lower axle load applied at Bothkennar, and the 135kN load nearer to the higher load applied. The aggregate at Bothkennar had an angle of internal friction of 54º and Figure 8.9 relates to aggregates with an internal angle of friction of 45º. For the case at Bothkennar, in order to assess the method, one must assume that 80kN axle load and 54º fill is approximately equivalent to 90kN axle loads and 45º fill. This generates a required thickness of aggregate, to resist static failure, of 65mm.The actual thickness of aggregate used in the trials was 350mm and a rut depth of 50mm occurred after approximately 1115 passes of an 80kN axle together with 800 passes of a 126kN axle.

The trafficking influence factor must be equal to $\frac{350}{65} = 5.38$ and, as can be seen from Figure 8.10, a rut depth of 50mm would be expected after many millions of passes. It appears that the design is over optimistic as the predicted number of passes to produce a

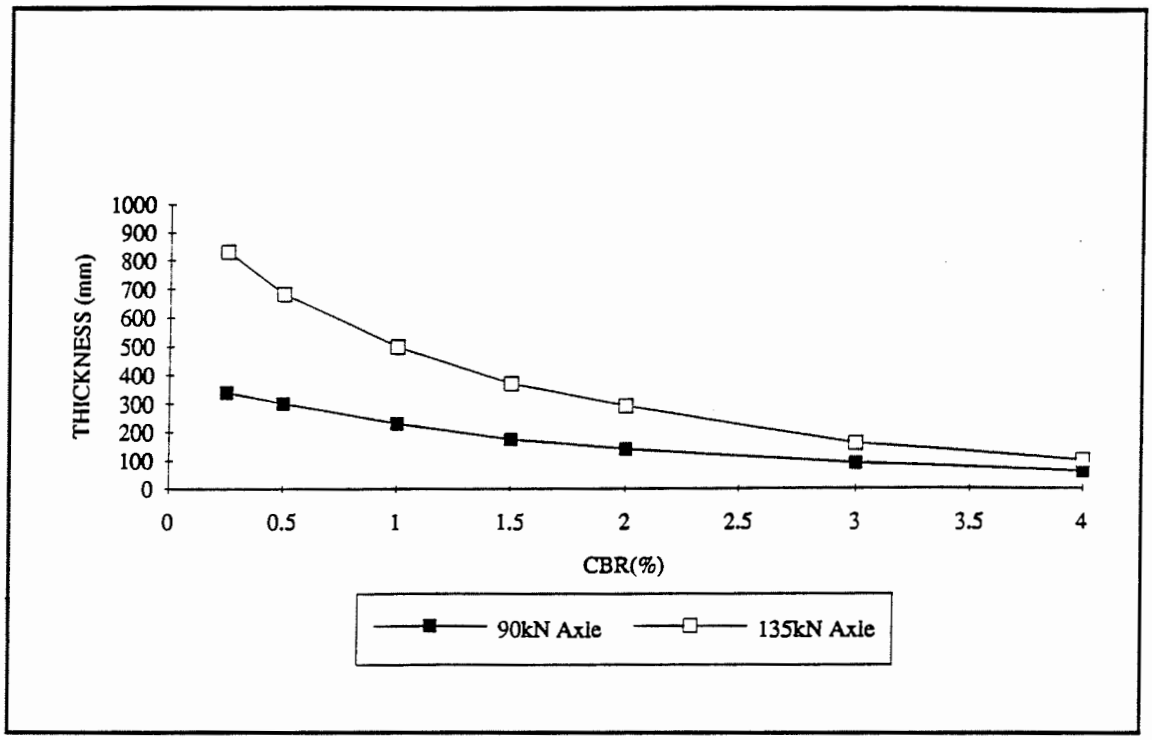

Figure 8.9 The Thickness of Aggregate Required to Resist 1,000 passes of a 90kN Axle After Polyfelt (undated)

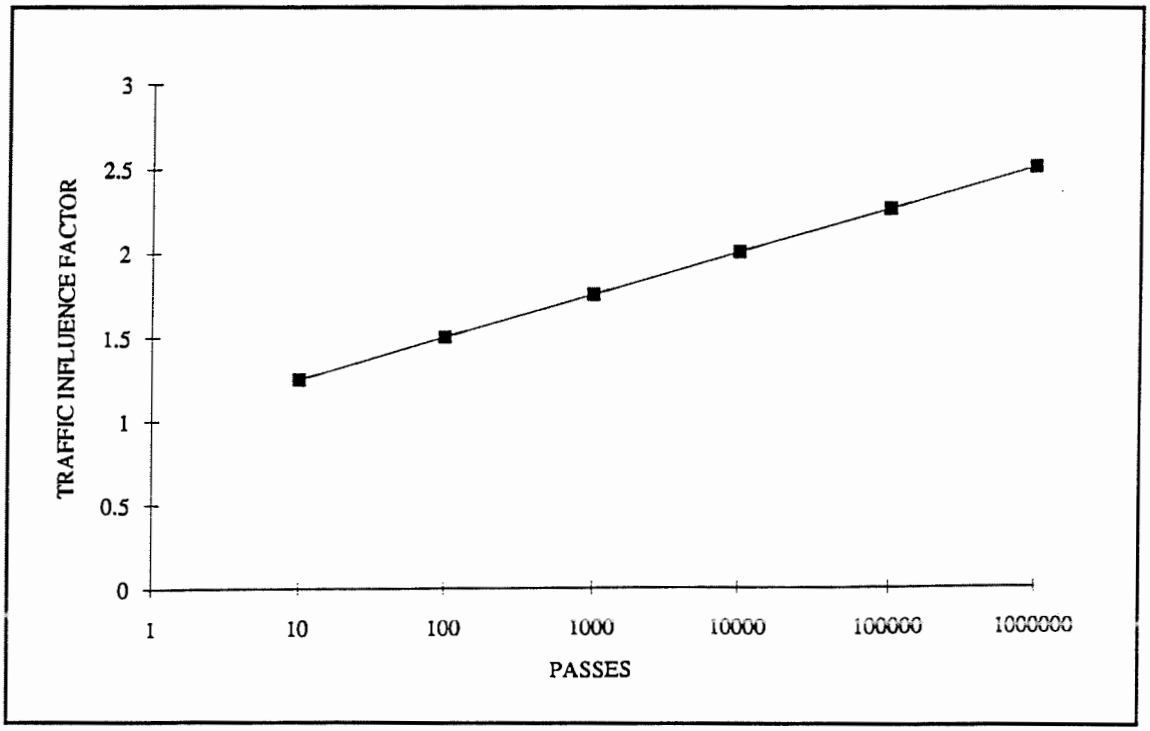

Figure 8.10 Traffic Influence Factor fof a Rut Depth of 50mm - After Polyfelt (undated)

50mm rut depth is much greater than the observed. However, Figure 8.9 has been extrapolated from the figure in Polyfelt (undated) and the pavement at Bothkennar is therefore outside the published limits of the design method. This highlights one of the problems with empirical approaches to design.

CHAPTER NINE

TOWARDS A NEW DESIGN METHOD

In this chapter the existing design methods will be re-examined and the parts of those methods which are of value will be highlighted. These will then be incorporated, along with some other observations, in a new proposed design method.

9.1 MECHANISM

9.1.1 Membrane effect

The membrane effect was considered for many years to be the principal mechanism behind the reinforcement of unpaved roads. However calculations of the reduction in applied vertical stresses on the surface of the subgrade attributable to the membrane effect was calculated for a typical pavement after Giroud & Noiray (1981). The depth of aggregate was taken to be 350mm and tanα, the load spread angle, to be 0.6. The deformation of the subgrade was assumed to be parabolic in nature and that the subgrade was incompressible. The calculated reduction in vertical subgrade stress for a range of rut depths up to 200mm is shown in Figure 9.1. At low rut depths it can be seen that the predicted decrease in subgrade stress as a result of the membrane effect is small and that even at higher rut depths the decrease is not large. Therefore, because of the doubts expressed about the validity of the mechanism resulting from the inability of the method to predict the observed geosynthetic strain distribution, and because the decrease in applied vertical stress attributable to the membrane effect is small, it is probably not the principal mechanism in geosynthetic reinforcement of unsurfaced pavements.

However, some concepts proposed by Giroud & Noiray (1981) are of value, notably that the bearing capacity of the subgrade changes between the reinforced and unreinforced case. Although this change in the bearing capacity was not properly justified, later work by Milligan et al (1989a) demonstrated mechanisms by which it could be obtained. The suggestion that a design method should calculate a saving of aggregate by a static analysis which is then applied to an empirical relationship for trafficking damage, such as Hammitt (1970), is also of value. Indeed, because at this time no reliable, simple models exist to accurately predict permanent deformations

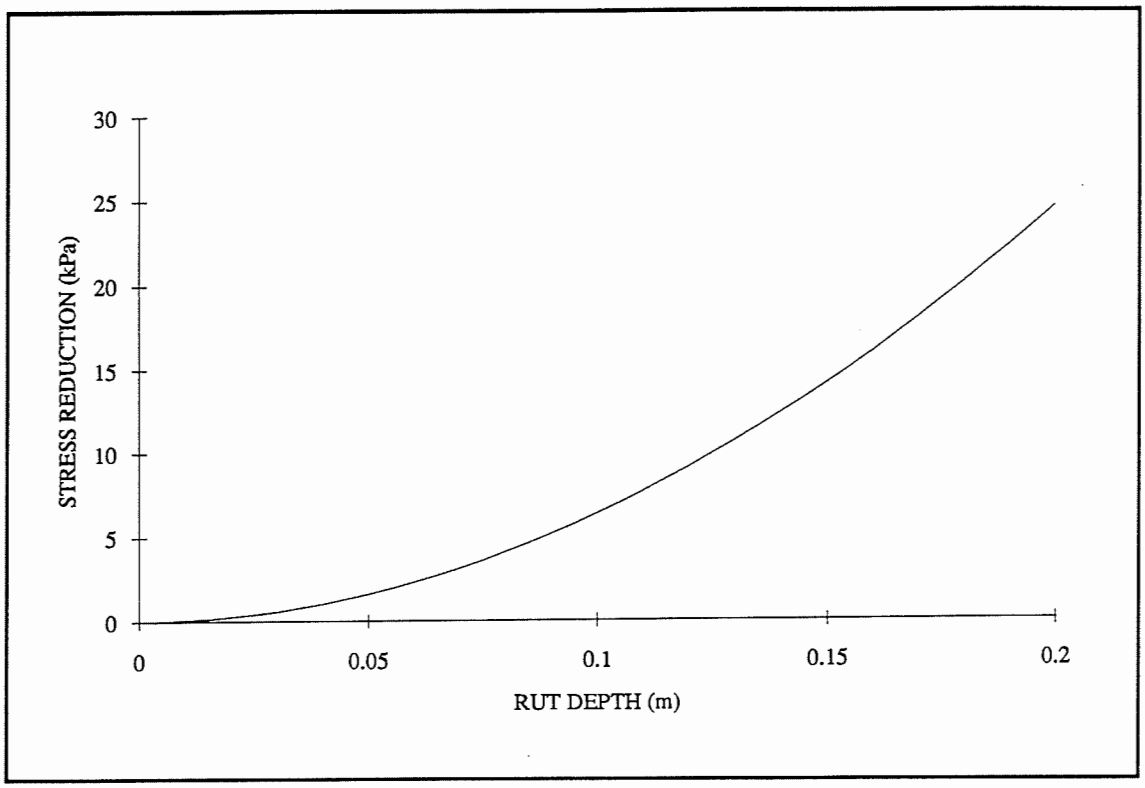

Figure 9.1 The Calculated Reduction in Vertical Subgrade Stress as a Result of the Membrane Effect - After Giroud and Noiray (1981)

resulting from the repeated loading of soils and granular materials, it may be the only sensible method of modelling these effects.

9.1.2 Slab effect

A slab effect type of design method such as that proposed by Sellmeijer (1990) might on first inspection appear to be promising. It is the only currently available design method which directly incorporates a stiffness property of the aggregate and it also recognises the fact that, unless slippage occurs at the interfaces, strain compatibility must occur. The elastic deformations are predicted by considering that the load applied is resisted by the shear modulus of the aggregate, assisted by the plastic bearing capacity of the subgrade in the reinforced case and the elastic in the unreinforced. However, the elastic deformations are not helpful in determining the permanent deformations that are likely to occur. As with other methods, it may be possible to generate aggregate savings based on the elastic deformation response of reinforced and unreinforced pavements and to apply these to an empirical permanent deformation model.

However, the slab effect design method is principally concerned with maintaining the integrity of the aggregate layer. The horizontal forces within the aggregate are calculated and great importance is placed on the maximum passive resistance of the aggregate not being exceeded. Plainly, within any one load application, it is undesirable for the aggregate to fail. However, this type of aggregate failure was observed at Bothkennar after many passes of the load, principally in the Oxford section (I), and the Polyfelt/Bamboo section (O), but was associated with geosynthetic rupture and bamboo failure respectively.

The passive failure of aggregate is likely to occur at large strains and these will only occur at large rut depths. Thus, it is possible that pavements will fail serviceability requirements before passive aggregate failure.

The slab effect relies upon the fact that the horizontal strains at the base of the aggregate layer are the same as that in the geosynthetic. This concept of strain compatibility between the aggregate and geosynthetic is important. It determines the strain within the inclusion and, as such, the forces generated in the geosynthetic. However, because slipping between the aggregate and the geosynthetic is considered not to occur, as

demonstrated in the 300mm shear box tests, and because the geosynthetic stiffness is low in comparison to that of the aggregate (Sellmeijer 1990), the geosynthetic strain is governed by the aggregate strain.

Two concepts appear to be of value in the Sellmeijer (1990) model. Firstly, that the aggregate plays a role in the control of at least the elastic or transient deformations and also possibly of the permanent deformations. Secondly, that there must be strain compatibility between the aggregate and geosynthetic and, for any given geosynthetic, this second concept will determine the forces generated in the inclusion.

9.1.3 Aggregate base restraint

An aggregate base restraint method such as proposed by Milligan et al (1989a) demonstrates the value of the geosynthetic in reducing the shear stress at the subgrade surface and thus improving the bearing capacity of the reinforced system. The low remote geosynthetic strains away from the wheel path observed from the experimental data from Bothkennar implies that the assumption made by Milligan et al (1989a), that the aggregate pushes away from the loaded area leading to tensions within the geosynthetic, is valid. Finite Element calculations (Brocklehurst (in print)) suggest that the improvement in the load carrying capacity of the system does not increase significantly when the geosynthetic is extended to an area that is normally considered as outside the load spread angle area of influence. The fact that little strain, either transient or permanent, was measured outside this area suggests that this analysis is more realistic than the constant-tension, membrane type of model which would predict non-decreasing strains in the geosynthetic away from the wheel path.

However, the papers by Milligan et al (1989 a & b) only consider either fully unreinforced or fully reinforced analyses. Plainly, there must be a range of cases between the two values depending, presumably, upon stiffness of the geosynthetic. Less stiff geosynthetics will relieve the subgrade of less of the shear forces at the interface so having some influence on the bearing capacity of the subgrade but not as much as in the fully reinforced case. Trials have shown (Sellmeijer et al (1982)) that the inclusion of stiffer fabrics results in continuing improvement in performance with stiffness. As a limiting geosynthetic stiffness has yet to have been demonstrated, it is reasonable to conclude that all current geosynthetics perform a partial reinforcement of the system. As can be seen from Figure 9.2, the ψ/N_{ca} curve is steeper nearer to the

fully reinforced condition than the unreinforced case. Therefore, small changes in the shear stresses imposed upon the subgrade, resulting from the change from the unreinforced to the partially reinforced, will have a more significant effect than the same amount of change from the partially reinforced to the fully-reinforced. Thus, even though the amount of shear stress relieved by the geosynthetic is proportional to its stiffness, the improvement in the bearing capacity of the system is not proportional to the same.

The method proposed by Milligan et al (1989 a & b) does not predict deformations, it considers only failure. A thickness saving of aggregate from the unreinforced case to the reinforced case can be calculated and applied to the empirical method of Hammitt (1970), as suggested in Chapter 8. This approach relies upon the assumption that, if the failure loadings suggest that an aggregate saving of, say, 100mm is possible, then a reinforced pavement can expect to perform as well as an unreinforced one 100mm thicker. This may not be the case as the mechanisms of static failure and of serviceability failure, caused by repeated loading, are different. However, it is a common assumption and it may be difficult to improve on this type of aggregate saving calculation.

The treatment of the subgrade properties in this method appears to be valid and the mechanism by which forces are dissipated within the structure appears to be sound. However, the method proposed by Milligan et al (1989 a & b) requires modification for partial reinforcement and a method of predicting rut depths.

9.2 KEY ELEMENTS

The concept proposed by Milligan et al (1989 a & b) of the aggregate moving outwards from the wheel path restricted by the passive forces within the aggregate and shear forces at the interface appears to be validated by the examination of the strain profile of the geosynthetic across the pavement. The method also demonstrates how the bearing capacity of the subgrade changes as shear forces are removed from the surface of the subgrade and thus, is probably the most realistic treatment for the subgrade currently available. However, the method requires modification because it currently assumes the reinforced pavements are fully reinforced and it is obvious that a range of partial reinforcement is possible.

It is possible to modify the model proposed by Milligan et al (1989 a & b) to include the idea of partial reinforcement, by taking note of the observation made by Sellmeijer (1990) that there must be strain compatibility at the interface. It is proposed here that if the stiffness of the aggregate layer is greater than the stiffness of the geosynthetics, as suggested by Sellmeijer (1990), then the strain in the geosynthetic, and hence the forces in it, are going to be governed by the horizontal strain at the base of the aggregate layer. This geosynthetic force is controlled by the stiffness of the geosynthetic and so it is possible to determine the remainder of the shear forces that need to be carried by the subgrade. The stiffness of the geosynthetics is, among other things, strain-rate dependent and two different cases need to be considered for the pavement. Fast rates of strain occur under transient loading and slow rates of strain occur with permanent pavement deformation (by a stress relaxation effect). The index test for stiffness, the wide width tensile test, represents neither of these two cases.

The inclusion of geosynthetics in unpaved roads will also prevent the loss of aggregate particles into the subgrade as long as the geosynthetic survives the installation and trafficking process. The saving of aggregate that is attributable to separation may be significant, but unfortunately no current method exists to predict the amount of aggregate expected to be "lost" as a result of a specified number of load repetitions on a pavement founded upon a subgrade with a specified shear strength.

Models predicting permanent deformation of soils and granular materials as a result of repeated loading, are not easily applicable to this type of analysis. Davies & Bridle (1990) appear to have had some success in this field by considering the work done within the system. However, it is beyond the scope of the research to propose or validate new models of this nature. The simplest method for predicting the deformation as a result of repeated loading is by referral to empirical data. Little high quality data exists for this type of pavement construction and so it may be necessary to rely upon modified data obtained from unreinforced trials.

9.3 CALCULATION OF HORIZONTAL, TRANSIENT AGGREGATE STRAIN.

The horizontal transient strain at the base of the aggregate layer can be calculated using linear elastic theory for the aggregate layer. This implies that the horizontal transient strain is as shown in Equation 9.1.

$$\varepsilon_{transient} = \frac{1}{M_r}[\Delta\sigma_h - \nu(\Delta\sigma_v + \Delta\sigma_h) \quad (9.1)$$

if it is assumed that the horizontal stress in the aggregate is equal in both directions and where $\Delta\sigma_h$ and $\Delta\sigma_v$ are the additional stresses imposed by the wheel load. The vertical transient stress, $\Delta\sigma_v$, can be calculated using the concept of a load spread angle and $\Delta\sigma_h$ can be estimated from the expression

$$\Delta\sigma_h = \left(\frac{\nu}{1-\nu}\right)\Delta\sigma_v \quad (9.2)$$

The resilient modulus M_r can be determined by laboratory testing of aggregate samples, or a value of 100MPa might be assumed for a well compacted crushed rock (Brown and Pappin (1985)), although a higher value for directly trafficked aggregate might be applicable (Brown and Dawson (1992)). Assuming that Poissons ratio is 0.35 and that M_r = 100MPa, Figure 9.2 shows some agreement between Equation 9.1 and the observed transient horizontal, geosynthetic strains. Equation 9.1 assumes that the properties granular layer are unaffected by the layers below, ie it is an infinite layer, and it assumes that the aggregate acts in a linear elastic manner. Both of these assumptions can be improved upon by computer programs which can calculate the effects of multi-layered elastic systems and/or incorporate some model for the non-linear elastic behaviour of the layers. FENLAP (Almeida et al (1991)) is one such program which would lead to a refinement of the design.

9.4 CALCULATION OF GEOSYNTHETIC TENSILE FORCES

Since it is assumed that strain compatibility occurs, the geosynthetic will strain to the same degree as the aggregate. Therefore, it is a simple matter to estimate the forces being taken by the geosynthetic by reference to the manufacturers stiffness data. However, the actual forces in the geosynthetic are likely to be somewhat different. The rate of loading in the transient case is very fast which would yield higher transient stresses in the geosynthetic than might be calculated by reference to the index tests. Permanent deformation of the system will lead to long term tension of the geosynthetic and creep induced stress relaxation would cause the forces in the geosynthetic to be over-estimated by reference to the index tests. To complicate the picture even further, trials at Bothkennar and by Watts & Brady (1990) show that the properties of the geosynthetic change after installation and, from Bothkennar, that they change further

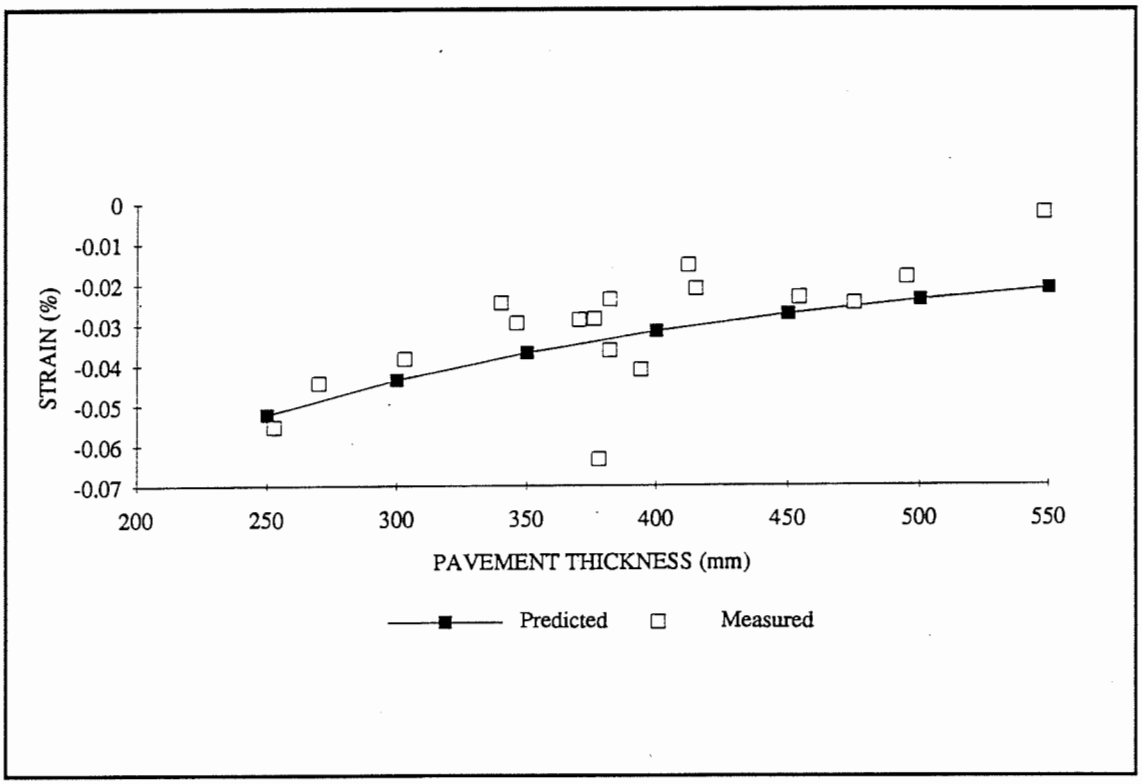

Figure 9.2 Predicted and Measured Horizontal Aggregate Strain

during the trafficking process. No standard test covers these observed phenomena and so it is difficult to apply any index test to the stress/strain characteristics of the in-situ material. It will be assumed in the following analysis that the standard index test applies in the determination of the stress/strain relationship of the inclusion, however it is recognised that this is a simplification.

9.5 CALCULATION OF THE SUBGRADE BEARING CAPACITY

In the unreinforced case the bearing capacity of the subgrade is controlled by the shear stresses imposed at the aggregate/subgrade interface. The available bearing capacity curve is shown in Figure 9.3 and a typical required bearing capacity line, G C H, is shown which is calculated from Equation 2.26 as discussed in 2.5.2.1.

In the partially reinforced case, some of the applied shear stress at the interface is transferred to the geosynthetic, reducing the size of the shear stress imposed upon the surface of the subgrade, and this reduces the value ψ ($= \tau/S_u$). Thus, the reinforced case generates a change in bearing capacity because, as a result of the change in ψ caused by $\Delta\tau$, a new required bearing capacity line GEF is formed (Figure 9.3).

$\Delta\tau$ = geosynthetic force (kN/m)

The changes in the bearing capacity of the system from the unreinforced to the reinforced case enables calculations of the permissible surface contact stress. In order for the contact stresses in the two cases to be the same, the reinforced pavement must be constructed with a thinner layer of aggregate. Thus, from the bearing capacity calculations, a saving of aggregate, as a result of reinforcement, can be calculated.

9.6 PREDICTION OF RUT DEPTH DEVELOPMENT

The lack of a simple and easily applicable model for the permanent deformation characteristics of the aggregate and subgrade subjected to repeated loading, leads to it being necessary to revert to empirical data to predict how rut depths will develop with passes. It has been observed at Bothkennar that a significant contribution to the rut depth occurs within the aggregate layer by deformation and compaction within the layer itself. Only 80% of the rut depth occurred, on average, within the subgrade (Figure

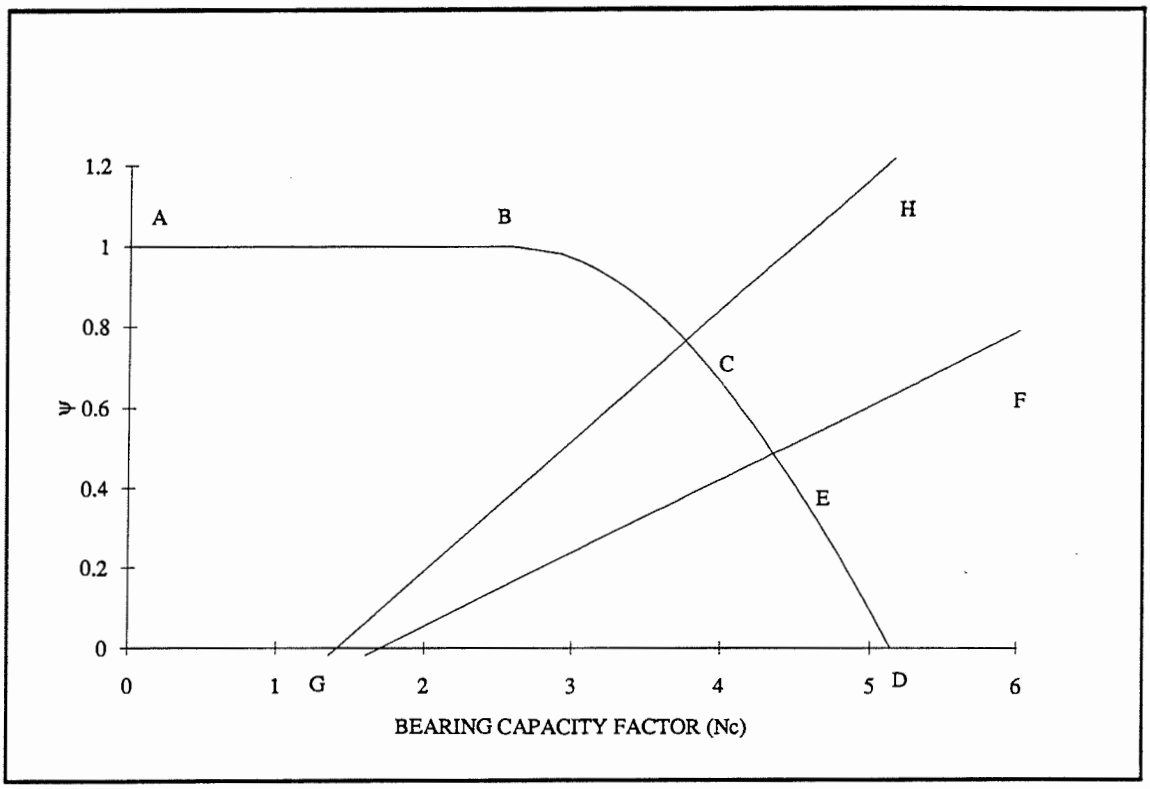

Figure 9.3 The Available and Required Bearing Capacity Factors of the Subgrade - After Milligan et al (1989a)

6.7) and so a sophisticated model would consist of a deformation model for both the aggregate's and subgrade's contribution to the surface deformation.

The expected number of passes required to generate a rut depth of 75mm in an unreinforced pavement can be found from Hammitt (1970). It has been shown that the rate of development of rutting is linear with passes, at least for the relatively few cycles that a haul road is expected to be designed for. Thus, the number of passes required to generate rut depths not equal to the 75mm can also be estimated in the unreinforced case using Equation 2.9. For the reinforced pavement design, the empirical data is rather sparse and, even so, the effect of wide variations in geosynthetic stiffness would hinder its interpretation in a manner similar to that of Hammitt (1970). It is therefore necessary to estimate the rut depth development rate for the reinforced pavements by examination of unreinforced data. It is an inherent assumption, in any "aggregate saving" method of reinforced road design, that a reinforced road consisting of, for example, 300mm of fill is "equivalent" to an unreinforced one consisting of, say, 350mm of fill. Therefore, the aggregate saving assumption implies that the thicker unreinforced pavement will deform at the same rate as the thinner reinforced one. However, there is little or no evidence for or against this assertion and further examples of reinforced pavement performance are required to validate this assumption.

9.7 WORKED EXAMPLE

The approach described above is best explained in detail by reference to the following worked example:

Required inputs

Number of passes to generate 75mm rut depth, N_{75}	= 1000 passes
Wheel load, P	= 40kN
Contact area, A	= 0.08m^2
Angle of internal friction for aggregate	= 55°
Load spread angle, tanα	= 0.6
Bulk density of aggregate, γ	= 21kN/m^3
Thickness of aggregate, h	= 0.34m
Subgrade shear strength, S_u	= 85kPa

continued over ....

Rut depth, r = 75mm
Actual contact stress, q = 500kPa
Poissons ratio, ν = 0.35
Resilient modulus of aggregate (M_r) = 100MPa
Force in geosynthetic at 5% strain = 20kN/m

9.7.1 Design of unreinforced pavements

Equation 2.1 enables a prediction of the thickness of aggregate required to allow a rut depth of 75mm to develop given the number of passes, wheel load and contact area.

$$h = (0.000493N_{75} + 0.352)\sqrt{\frac{P}{56CBR} - \frac{A}{\pi}} \qquad (2.1)$$

$$= 0.34m$$

Thus, in the unreinforced case, the thickness of aggregate required for a wheel load of 40kN, 1000 passes and a rut depth of 75mm can be calculated. For cases where the rut depth (r) is required to be another value other than 75mm, then Equation 2.9 enables Equation 2.1 to be modified accordingly.

$$\frac{r}{75} = \frac{N}{N_{75}} \qquad (2.9)$$

If the permissible rut depth is 150mm at 1,000 passes, then a rut depth of 75mm is expected to occur after 500 passes and therefore N_{75} = 500 is put into Equation 2.1.

9.7.2 Base aggregate strain

The horizontal transient strains expected at the base of the aggregate layer were discussed in Part 9.3 and can be determined from the following equation.

$$\varepsilon_{transient} = \frac{1}{M_r}\left(\Delta\sigma_h - \nu\,(\Delta\sigma_v - \Delta\sigma_h)\right) \qquad (9.1)$$

Assuming that the contact area, A, is 0.08m^2, then the radius of the equivalent contact area is 0.160m and, assuming axisymmetric stress distribution, the increase in vertical stress, $\Delta\sigma_v$ is given by Equation 2.22.

$$\Delta\sigma_v = q\left(\frac{W/2}{(W/2 + h\tan\alpha)}\right)^2 \qquad (2.22)$$

$$\Delta\sigma_v = 97\text{kPa}$$

The relationship between the increase in vertical stress, $\Delta\sigma_v$, and the increase in horizontal stress, $\Delta\sigma_h$, is given by Equation (9.2)

$$\Delta\sigma_h = \left(\frac{\nu}{1-\nu}\right)\Delta\sigma_v \qquad (9.2)$$

$$\Delta\sigma_h = \left(\frac{0.35}{0.65}\right) \text{x } 97 = 52\text{kPa}$$

Thus, the base horizontal aggregate strain is:

$$\varepsilon_{transient} = \frac{1}{M_r}(\sigma_h - \nu\,(\Delta\sigma_v - \Delta\sigma_h)) \qquad (9.1)$$

$$= \frac{1}{100000}\ (52 - 0.35\ (97 - 52))$$

$$= 0.036\%$$

9.7.3 Tension generated in geosynthetic

9.7.3.1 Estimate of the stiffness of the geosynthetic

The tension generated in the geosynthetic will be a function of the strain imposed upon it and the stiffness that one assumes for it, which is dependent upon the time of loading, sample history and temperature amongst other parameters. The change in stiffness between the transient and permanent deformations is going to be caused by changes in the time of loading. Isochronous strain curves may well generate accurate values of the stiffness that should be used. However, such data is not readily available from the

manufacturers and so it is suggested here that the BS6906 Part 1 (1987) standard test is used as a first approximation to the required values of the stiffness at 5% strain. For the purpose of this worked example, it is assumed that the load carried by the geosynthetic at 5% strain is 20kN/m a typical value for a geogrid.

9.7.3.2 Estimate of strain in the geosynthetic

The strains induced in the geosynthetic as a result of the trafficking have two components, the transient and the permanent. Assuming that there is no slipping at the aggregate/geosynthetic interface, the transient strain at the base of the aggregate must be equal to the transient strain in the geosynthetic calculated in 9.7.2. The accumulation of many small permanent deformations will cause some locked-in stress in the geosynthetic. If there is no slip within the system, then the permanent geosynthetic strain must be caused by the deformation of the system.

The assumption that the deformed shape of the pavement is parabolic was made by Giroud & Noiray (1981) and no evidence exists to contradict this assumption. Finite element analysis by Brocklehurst (in print) suggests that the geosynthetic is only working in the wheel path which in turn, suggests that the membrane is not in tension between the wheel paths. Furthermore, observations from Bothkennar suggest that, on average, 20% of the surface rut depth is a result of deformation within the fill. Thus a rut at the surface of the pavement of 75mm probably translates to a subgrade rut depth of 60mm. Thus, the permanent geosynthetic strain can be calculated from the equation below. Assuming that if the thickness of the pavement, h,= 0.34m, the load spreading angle α is such that $\tan\alpha = 0.6$, and the loaded length at the interface, a, = 0.364m, then if the rut depth at the subgrade is 0.06m, the vertical depression of the subgrade, s, will be 0.037m as determined by Equation 2.16.

$$\varepsilon_{permanent} = 0.5 \left[\left(\sqrt{1 + \left(\frac{2s}{a}\right)^2} + \frac{a}{2s} \ln\left(\frac{2}{a} + \sqrt{1 + \left(\frac{2s}{a}\right)^2} \right) \right) - 2 \right] \quad (2.21a)$$

thus $\varepsilon_{permanent} = 0.678\%$

It can be seen that the permanent strain is, in this case, twenty times the size of the transient value. Because the permanent strain is far more significant, the stiffness chosen for the geosynthetic should be weighted towards the slow rate of strain values.

Total geosynthetic strain = 0.678 + 0.036% = 0.714%

Assuming a plane strain analysis, and that the geosynthetic stiffness is linear over the range 0 -5% strain, then the force generated by a strain of 0.714% is given by:

$$\frac{0.714}{5} \times 20 = 2.856 \text{ kN/m}$$

9.7.4 Bearing capacity calculations

As was shown by Milligan et al (1989a) the available bearing capacity envelope is described by Equation (2.18a).

$$N_{ca} = 1 + \frac{\pi}{2} + \cos^{-1}\psi + \sqrt{1 - \psi^2} \qquad (2.18a)$$

This expression is represented by the line ABCD in Figure 9.4.

The required bearing capacity in the unreinforced case is given by Equation 2.26

$$\psi = \frac{1}{2}(K_a - K_p)\frac{\gamma h^2}{S_u (W + h\tan\alpha)} + N_{cr}\left[\frac{K_a}{\tan\alpha} \ln\left(\frac{W + h\tan\alpha}{W}\right)\right] \qquad (2.26)$$

This expression is represented by the line GCH in Figure 9.4.

As can be seen from the graph, or computer interpolation the intersection point C occurs at N = 4.746 ψ = 0.256 which implies that the shear stress at the top of the subgrade in the unreinforced case is such that $\frac{\tau}{S_u}$ = 0.256, and as S_u = 85kPa, τ = 21.726kPa.

In the reinforced case the shear stress imposed upon the subgrade, τ, is reduced, not removed as suggested by Milligan et al (1989a), by the forces induced by the strain in the geosynthetic. Thus the shear stress applied to the surface of the subgrade is reduced by the transient and permanent induced stresses in the geosynthetic.

$$\tau = 21.726 - 2.856 = 18.870\text{kPa}$$

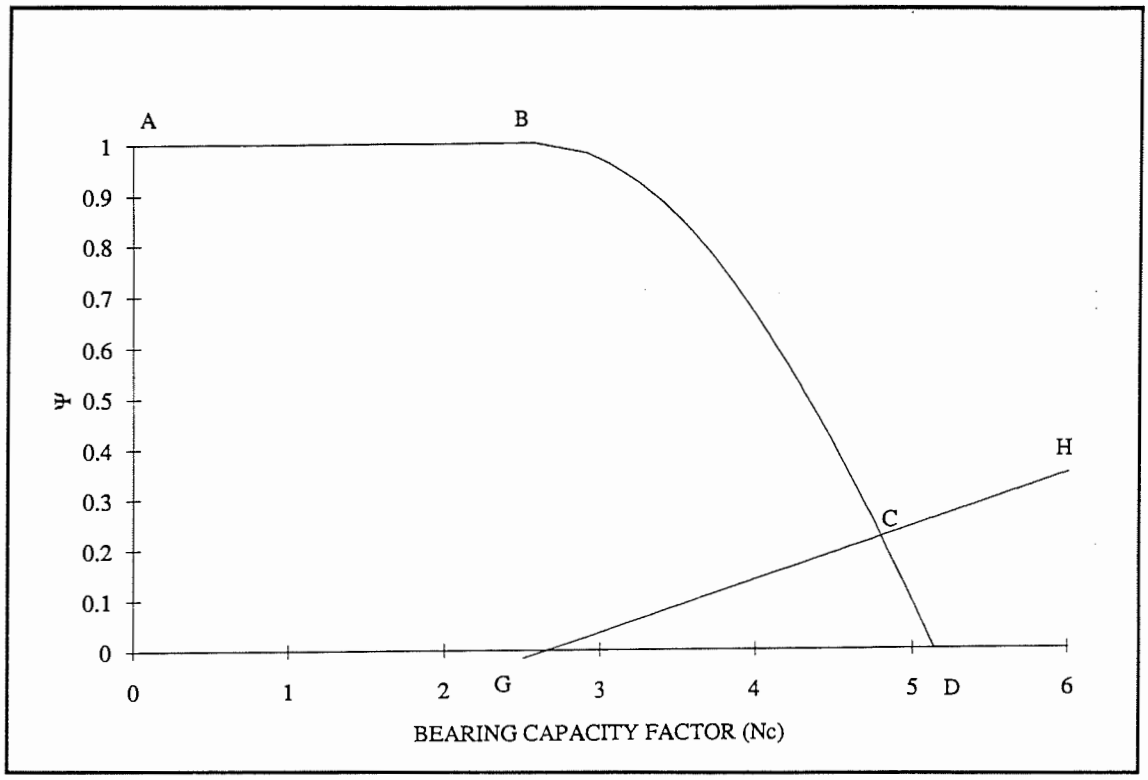

Figure 9.4 Bearing Capacity Interaction Diagram for the Worked Example - After Milligan et (1989a)

The value of ψ in the reinforced case can now be determined:

$$\psi \left(= \frac{\tau}{S_u}\right) = \frac{18.870}{85} = 0.222$$

By substitution in Equation 2.26 it can be seen that when $\psi = 0.222$, $N_c = 4.800$.

Thus the appropriate bearing capacity in the unreinforced case $N_c = 4.746$ and in the reinforced case $N_c = 4.800$.

9.7.5 Aggregate saving

In the unreinforced pavement the thickness of fill required, by a modified Hammitt (1970) approach was 0.34m. Bearing capacity analysis suggests that in the unreinforced case the permissible surface contact stress is determined by Equation (2.27).

$$q = N_c S_u \left(\frac{W/2 + h\tan\alpha}{W/2}\right) \qquad (2.27)$$

$$q = 4.746\, S_u \left(\frac{0.16 + 0.34 \times 0.6}{0.16}\right)$$

$$q = 917.7\text{kPa}$$

In the reinforced case N_c is increased and if the contact stress, q, is the same, the reinforced thickness required is determined by rearranging Equation (2.27).

$$h = \left(\frac{q}{N_c S_u} - 1\right)\frac{W}{2\tan\alpha} = 0.333\text{m}$$

Therefore the thickness saving is 7mm, as a result of the reinforcement effects. To this should be added a saving for separation which currently cannot be estimated with any accuracy (although observations from Bothkennar, to which this worked example approximates, suggest separation savings could be greater than this direct reinforcement amount).

9.8 WORKED EXAMPLE FOR SOFT SUBGRADE CONDITIONS

The saving of aggregate calculated is small, but given the high subgrade shear strengths at Bothkennar, this could be expected. All the manufacturers design manuals show that the savings of aggregate increase as the shear strength of the subgrade reduces. Normally, it is not considered economical to use geosynthetics at high subgrade shear strengths and to demonstrate the same approach for a more realistic situation, an example calculation for lower subgrade shear strengths follows.

Altered Inputs

Su= 46kPa r = 150 N = 1000 N_{75} = 500 $\phi = 45°$

Unreinforced thickness

From Equation 2.5, it is possible to calculate the unreinforced design thickness

$$h_o = (0.000493 \times 500 + 0.352)\sqrt{\frac{40}{56 \times 2} - \frac{0.08}{\pi}} = 0.342m \qquad (2.5)$$

Aggregate stresses

The vertical stress imposed upon the subgrade is given by Equation 2.22

$$\Delta\sigma_v = 500\left(\frac{0.16}{0.16 + 0.342 \times 0.6}\right)^2 = 96kPa \qquad (2.22)$$

The horizontal aggregate stress at the base of the layer is given by Equation 9.2

$$\Delta\sigma_h = \frac{0.35}{(1 - 0.35)}\Delta\sigma_v = 51kPa \qquad (9.2)$$

Interface strains

Equation 9.1 enables the transient geosynthetic strain to be calculated

$$\varepsilon_{transient} = \frac{1}{100000}\left(\Delta\sigma_h - \nu\,(\Delta\sigma_v - \Delta\sigma_h)\right) = 0.035\% \qquad (9.1)$$

$$\varepsilon_{permanent} = \frac{1}{2}\left[\left(\sqrt{1+\left(\frac{2s}{a}\right)^2} + \frac{a}{2s}\ln\left(\frac{2s}{a}+\sqrt{1+\left(\frac{2s}{a}\right)^2}\right) - 2\right)\right] \quad (2.21a)$$

$$= 2.664\%$$

$$\varepsilon_{Total} = 2.699\%$$

Load in geosynthetic $\frac{2.699}{5}$ x 20 = 10.80kN/m

Unreinforced Bearing Capacity

From Figure 9.5, it can be seen that

$N_c = 4.183$ and ψ 0.5737

$\frac{\tau}{S_u} = 0.5737$ thus $\tau = 26.39$kN/m

Reinforced Bearing Capacity

The shear stress applied to the surface of the subgrade is reduced by the geosynthetic tension

$\tau = 26.39 - 10.80 = 15.59$kN/m

thus $\psi = 0.346$ and so from Figure 9.5, it can be seen that $N_c = 4.597$

Aggregate saving

From Equation 2.27, it can be seen that in the unreinforced case, the maximum permissible contact stress, q, is such that:

$$q = N_c S_u \left(\frac{W/2 + h\tan\alpha}{W/2}\right) \quad (2.27)$$

$$q = 4.183 \times 46 \left(\frac{0.16 + 0.342 \times 0.6}{0.16}\right) = 439\text{kPa}$$

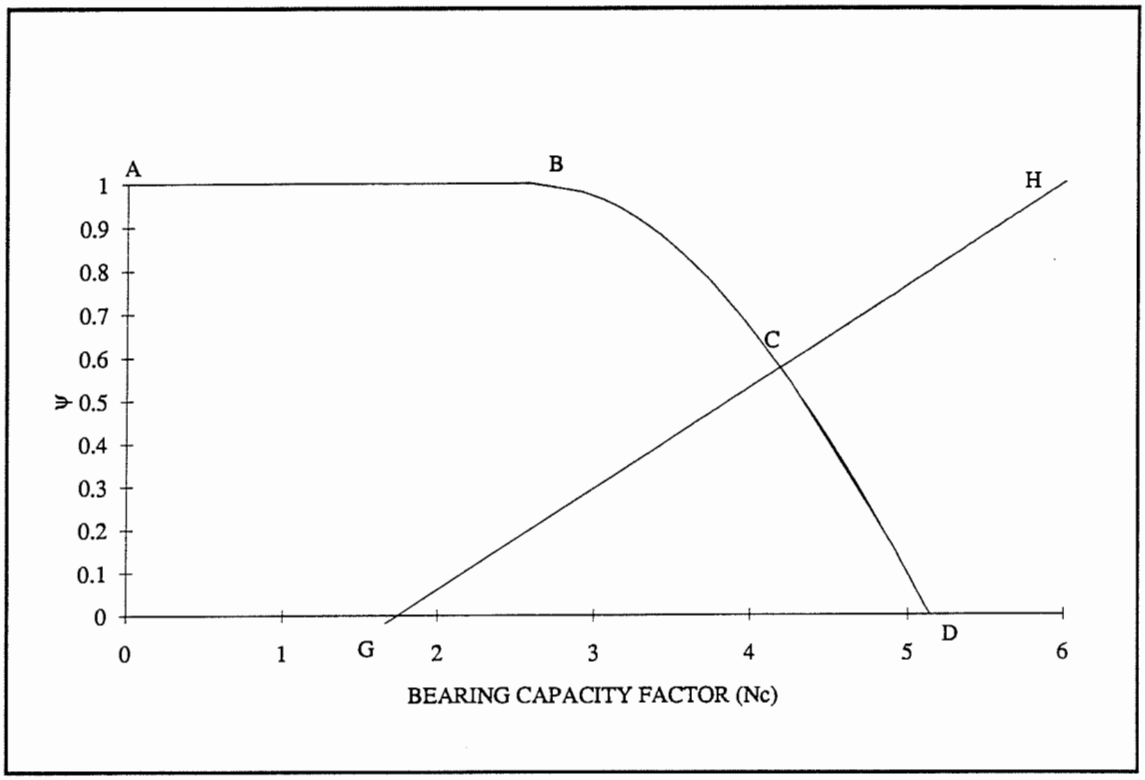

Figure 9.5 Bearing Capacity Interaction Diagram for the Second Worked Example - After Milligan et (1989a)

By re-arranging 2.27 and substituting the reinforced, as opposed to the unreinforced bearing capacity, it can be seen that

$$h = \frac{\left(\frac{439}{4.597 \times 46} - 1\right) 0.16}{0.6} = 0.287\text{m}$$

Saving = 55mm

plus an allowance for the separation function performed by the geosynthetic.

9.9 OBSERVATIONS ON THE PROPOSED NEW METHOD

The proposed method is a static analysis, which generates a saving in the thickness of aggregate required. It takes the best available concepts of all the existing methods, rigourous calculation of the subgrade bearing capacity and internal forces based on the deformed profile and strain compatibility. It shows that for moderately stiff geosynthetics, a reinforcement benefit can be obtained which would improve with increasing stiffness.

The calculations have shown that, at higher values of subgrade shear strength, the savings in aggregate that can be obtained, even by relatively stiff reinforcements, are modest. At lower subgrade shear strength, the savings are larger but still not as significant as the manufacturers would claim. This difference is caused by the separation function, which is common to all of the geosynthetics. The value of savings that are attributable to the separation cannot yet be determined, however it is clear that this needs to be resolved if a fuller understanding of how geosynthetics improve pavements is to be made.

CHAPTER TEN

CONCLUSIONS & RECOMMENDATIONS FOR FUTURE WORK

The previous chapters have shown that the study has brought some important findings to light. These are now summarized in the following sections.

10.1 BOTHKENNAR AND THE TRIALS

The Bothkennar Soft Clay Research site has superb office facilities equipped to a very high standard by the Science and Engineering Research Council. As time progresses, the engineering properties of the clay becomes better defined and the uniformity of the deposit makes it an ideal location for research into the behaviour of soft clays.

The site however, has a firm crust (Figure 3.1) which was problematic for these trials. Pavement foundations are essentially controlled by shallow soil mechanics and so, although at depth the site was soft, geosynthetic reinforcement of unpaved roads is not normally considered to be economically viable for surface subgrade shear strengths of the magnitude encountered at Bothkennar. As a consequence it has been shown, in this case, that the savings of aggregate possible by including geosynthetics are small and hence the absolute value of the products, in this instance, is marginal. However, the instrumentation of the pavements was generally successful as it enabled a study of the mechanisms involved in this type of pavement leading to a new understanding of how geosynthetics perform in this application.

10.2 RUT DEPTH DEVELOPMENT

At Bothkennar it was found that there was a relatively large amount of deformation which occurred in the first pass. Most of this initial deformation occured within the aggregate layer, an observation also made by other authors in repeated triaxial tests on the aggregates. It gives little or no indication as to the performance of the pavement. It was found that, as long as the geosynthetic did not rupture, the development of rutting, after the initial settling of the pavement, was linear with the number of passes of the

axle. Other data (Webster & Watkins (1977), Webster & Alford ((1978) and others) was replotted on a linear passes scale and found to be in good agreement with a concept of a linear development of rut depth with passes.

The rate of the accumulation of rut depth with passes increases rapidly upon rupture of the geosynthetic and filling the ruts with extra material does not prevent further rutting developing. The failure is, in this sense, brittle and so rupture of the geosynthetic should therefore be avoided as once this has occurred the deterioration of the pavement is more rapid than if no geosynthetic was present.

No evidence was found to support the commonly held assumption that unpaved roads conform with the concept that non-standard loads can be related to the standard loads by the means of a power law. This finding contradicted the proposal of De Groot et al (1986) for a large power law. In these trials the increase in axle load led to a small increase in the rate of development of rut depth and this is more in keeping with the earlier work of Hammitt (1977) than later, power law-type, calculations.

Some of the thicker pavements in the trial had a higher rate of rut depth development than their thinner counterparts. One most important functions of the geosynthetic is to pick-up the shear forces induced in the aggregate by the wheel load. In thicker pavements the geosynthetic may be too low in the pavement structure, where the shear stresses are low, to be effective to the system. The maximum aggregate shear force, in thick pavements, will occur within the aggregate layer and thus, in these pavements, internal aggregate deformation will contribute significantly to the overall rut depth. The evidence from the thinner pavements suggests that this internal shearing of the aggregate can be prevented by putting the geosynthetic higher in the pavement structure - in accord with the proposals of Bathurst et al (1986) and this should be considered if the pavement thickness is to exceed 350mm.

It was found that even in pavements of approximately this thickness a significant amount of the surface rut depth was caused by internal aggregate deformations, and in these trials that was, on average, 20%.

10.3 GEOSYNTHETIC PROPERTIES

The stiffness properties of the geosynthetic are important to the design of the unpaved roads, especially if significant benefits are to be obtained from reinforcement. The value of the stiffness is dependent upon the time of loading: in the transient conditions under the wheel path, the rate of loading is very fast, under the permanent deformation conditions the rate of loading is very slow. In the trials at Bothkennar, the rate of loading could be measured in tens of per cent per minute in the transient loading case and in per cent per annum in the permanent deformation case.

The calculations presented in Chapter 9 show that, while the stiffness of the geosynthetics under transient loading might be very high, the strains are very small. More importantly, the permanent deformation induces much larger strains in the geosynthetic and this plays a major role in the reinforcement of the pavement. Therefore, if the geosynthetic is to be a good reinforcing element the geosynthetic properties required are not only that it is stiff, but that it has a good resistance to creep.

None of the geosynthetics tested in the 300mm shear box exhibited any slipping between the components of the system. Thus, it is concluded that shear resistance within the system is governed not by the geosynthetic but by the shear strength of the soil and the angle of aggregate internal friction.

All of the sections tested showed that geosynthetics act as good separators. From tentative observations and the calculations shown in Chapter 9 the separation function may be as valuable to the performance of the pavement as reinforcement. Of course, geosynthetics designed as reinforcement elements also act as separators.

10.4 REINFORCEMENT MECHANISM

Evidence was found to suggest that anchorage of geosynthetics was not required in order for them to be effective. The geosynthetic strains away from the wheel path were found to be small and tending towards the compressive which agrees with finite element parametric studies undertaken by Brocklehurst (in print) and with earlier studies (CIRIA (1986)).

The transverse geosynthetic strain distribution across the pavement also leads to the observation that a constant tension membrane approach to design is not appropriate. This is backed-up by the calculation that, even at large rut-depths, the reduction in the vertical stresses applied to the subgrade as a result of any type of membrane effect is small.

These observations suggest that the base restraint mechanism proposed in detail by Milligan et al (1989a) is a more realistic method of analysis than the concept of the tensioned membrane.

10.5 A NEW DESIGN METHOD

A new design method has been proposed which is founded on a base restraint approach adopted by Milligan et al (1989a) but modified to take into account the geosynthetic stiffness and the concept of strain compatibility between the components of the soil-geosynthetic-aggregate system. The approach has been further modified to enable a prediction of the rate and quantity of deformation that can be expected.

The proposed method shows that the benefits of including geosynthetics in pavements founded upon stiff subgrades are small whereas, at lower subgrade stiffnesses, the benefits could be substantial. It shows that stiff geosynthetics produce more benefit than their less stiff counterparts as supported by the observation of Sellmeijer et al (1982). However, the reinforcing characteristics of geosynthetics are only part of the benefit that their inclusion generates. Separation, leading to the prolonging of the original pavement thickness by the prevention of the intermixing of aggregate and subgrade layers, might well provide a more significant contribution to the pavement's performance. No model is presented to give an analytical method of predicting how effective geosynthetics are at this function, but, if such a method were available, it would show that all geosynthetics would exhibit some additional, perhaps large, benefit over that due to reinforcement alone.

10.6 RECOMMENDATIONS FOR FUTURE WORK

Further full-scale or model trials on a variety of subgrade types and stiffness are required to validate further the new proposed design method in particular for softer soil.

Non-linear analysis of the aggregate and subgrade components needs to be included within the design method which currently utilises linear elastic theory to predict the strains that are expected at the interface.

The empirical nature of the prediction of permanent deformation is far from satisfactory. An analytical, permanent deformation model is required for the whole system of aggregate, subgrade and geosynthetic. It needs to be able to predict the increments of permanent deformation attributable to large and mainly elastic deformations. An analysis based on the work done by the system may be a possible avenue of exploration.

The value of separation may well be larger than the reinforcement characteristics of the geosynthetics. A separation model would demonstrate a "base advantage" of using geosynthetics, with stiffer products enabling larger savings as a result of their higher reinforcement capabilities. The relative merits of different fabrics could then be assessed on a financial basis of commercial viability.

REFERENCES

Almeida J, Brunton J M and Brown S F (1991), "Structural Evaluation of Pavements". Nottingham University, Second Progress Report Submitted to TRRL.

Ahlvin R G (1959), "Developing a Set of CBR Design Curves". Instruction Report No 4, US Army Engineer Waterways Experimental Station, Vicksburg, Mississippi, USA.

Bathurst R J and Raymond G P and Jarrett P M (1986), "Performance of Geogrid-Reinforced Ballast Railroad Track Support". Third International Conference on Geotextiles, Vienna, pp 43-48.

Bender D A and Barenberg E J (1978), "Design and Behaviour of Soil-Fabric-Aggregate Systems". Transport Research Record 671 pp 64-67, TRB, Washington, USA.

Borrosson I and Erikson L (1986), "Long-term Properties of Geotextiles and their Function as a Separator in Road Construction". Third International Conference on Geotextiles, Vienna, pp 93-98.

Boyce J R Cobbe M I and Fleming P R (1989), "Technical Note - Development of a Prototype Variable Impact Apparatus". Unbound Aggregates in Roads, Butterworths pp 397-407.

Brocklehurst C (in print), "Finite Element Studies of Reinforced & Unreinforced Two-Layer Soil Systems". D.Phil, Oxford University.

Brown S F (1979), "The Characterisation of Cohesive Soils for Flexible Pavement Design". Proceedings of the 7th European Conference on Soil Mechanics and Foundation Engineering, Vol 2 pp 15-22.

Brown S F and Dawson A R (1992), "Two Stage Mechanistic Approach to Asphalt Pavement Design". Seventh International Conference on Alsphalt Pavements Nottingham.

Brown S F and Pappin J W (1985), "Modelling of Granular Materials in Pavements". Transportation Research Record 1022 pp 45-51.

Brunton J M and Ackroyd P M (1990), "Monitoring the Performance of a Full Scale Experimental Pavement". Third International Conference on the Bearing Capacity of Roads and Airfields. pp585-594.

BS 812 (1975), "Methods for sampling and testing of mineral aggregates, sands and fillers". British Standards Institution.

BS 1377 (1975), "Methods of Test for Soils for Civil Engineering Purposes". British Standards Institution.

BS 6906 Part 1 (1987), "British Standards Methods of Test for Geotextiles. Determination of the Tensile Properties using a Wide Width Strip". British Standards Institution.

BS 6906 Part 4 (1989), "British Standards Methods of Test for Geotextiles. Determination of the Puncture Resistance (CBR Puncture Test)". British Standards Institution.

BS 6906 Part 6 (1990), "British Standards Methods of Test for Geotextiles. Determination for Resistance to Perforation (Cone Drop Test)". British Standards Institution.

BS 6906 Part 8 (1991), "British Standards Methods of Test for Geotextiles. Determination of Sand-Geotextile Frictional Behaviour by Direct Shear". British Standards Institution.

Chueng L-W and Dawson A R (1991), "Research to Improve Road Foundation Design (2nd Year Report)". Report No PR91040 submitted to TRRL.

Comité Français des Géotextiles (1981), "Recommendations Pour L'emploi des Géotextiles dans les Voies de Circulation Brovisoire, les Voies à Faible Trafic et les Couches de Forme". Document du Ministere des Transports, Direction des Routes et de la Circulation Routière.

Construction Industry Research & Information Association (1986), "The Construction and Performance Under Traffic of a Full-scale Experimental Road Incorporating Geotextiles". Technical Note 126.

Davies M C R & Bridle R J (1990), "Predicting the Pavement Deformation of Reinforced Flexible Pavements Subject to Repeated Loading". Proceedings of the B.G.S. International Reinforced Soil Conference, Strathclyde University.

Dawson A R, PhD Thesis submitted to the University of Nottingham, (in print).

Dawson A R & Brown S F (1984), "Geotextiles in Road Foundations". Submitted to ICI Fibres, Geotextile Division. University of Nottingham, September 1984.

Department of Transport (1986), "Specification for Highway Works, Part 3". HMSO.

De Groot M, Janse E, Maagdenberg T A C & Van Den Berg C (1986), "Design Method and Guidlines for Geotextile Application in Road Construction". Third International Conference of Geotextiles, Vienna, pp 741-746.

Fannin (1986), "Geogrid Reinforcement of Granular Layers on Soft Clay". PhD Thesis, Department of Engineering Science, Oxford University.

Giroud J P & Noiray L (1981), "Geotextile Reinforced Unpaved Road Design". Proc ASCE Journal, Geotech. Eng. Div, No 1 107, No GT9, pp 1233-1254.

Gostelow T P and Browne M A E (1986), "Engineering Geology of the Upper Forth Esturary". British Geological Survey, Vol 16 : No 8.

Hammitt G M (1970), "Thickness Requirements for Unsurfaced Roads & Airfields Bare Base Support". Technical Report S-70-5, US Army Engineer Waterways Experimental Station, Vicksburg, Mississippi, USA.

Hausmann M R (1987), "Geotextiles for Unpaved Roads - A Review of Design Procedures". Geotextiles & Geomembranes 5, pp 201-233.

Hicks R G and Monismith C L (1971), "Factors Influencing the Resilient Responses of Granular Materials". Highway Research Record 345, Highway Research Board, Washington DC.

Houlsby GT and Jewell RA (1989), "Road Solver - Design of Unreinforced and Reinforced Unpaved Roads on Soft Clay". Oxford Geotechnical Software.

Jagielski K (1991), "Western European Geotextile Market Report". Geotextile Fabrics Report, October 1991, pp 24-25.

Karkhoven R E and Dormon G M (1953), "Some Considerations on the Californian Bearing Ratio Method for the Design of Flexible Pavements". Shell International Petroleum Co Ltd, London.

King G (1990), Personal Correspondence Relating to the Results from the ODIN Device at Bothkennar.

Lee R G (1989), "Grid Reinforced Soil Foundations". Phd Thesis, University of Nottingham.

Little P H (1990), "Construction of Experimental Haul Road at Bothkennar, Airth, Scotland". University of Nottingham Department of Civil Engineering, Report No PR90005.

Little P H (1992), "Data Obtained from Full-Scale Trials at Bothkennar, Airth, Scotland". University of Nottingham Department of Civil Engineering, Report No PR92015, May 1992.

Loach S L (1987), "Repeated Loading of Fine Grain Soils for Pavement Design". PhD Thesis Nottingham University.

McGown A, Andrews K Z, Werner G and Yusuf Z (1990), "Bending and Tensile Reinforcement of Unbound Roads". Fourth International Conference on Geotextiles Geomembranes and Related Products, The Hague, pp 239-246.

Milligan G W E, Jewel R A, Houlsby G T & Burd H J (1989a), "A New Approach to the Design of Unpaved Roads Part I". Ground Engineering, April 1989, pp 25-29.

Milligan G W E, Jewel R A, Houlsby G T & Burd H J (1989b), "A New Approach to the Design of Unpaved Roads Part II". Ground Engineering, November 1989 pp 37-42.

Nash D F T, Hawkins A B and Lloyd I (1985), "Location and Investigation of Test Bed Site on Soft Clay - Progress Report". University of Bristol, Department of Civil Engineering.

Nieuwenhuis J D (1977), "Membranes and the Bearing Capacity of Roadbases". International Conference on the use of Fabrics in Geotechnics, Vol 1 pp 3-8.

Paul M A, Peacock J D and Wood B F (1991), "The Engineering Geology of the Soft Clay at the National Soft Clay Research Site, Bothkennar". Heriot-Watt University.

Peutz M G F, Von Kempem H P M and Jones A (1968), "Layered Systems Under Normal Surface Load - Computer Program BISTRO". Koninklijke/Shell-Laboratorium, Amsterdam.

Prandtl (1920), "Uber die Harte Plastischer Korper". Nachr. Kgl. Ges. Wiss. Gottingen, Math-Phys. KL.

Resl S & Werner G (1980), "Influence of Non-Woven Needle Punched Geotextiles on Ultimate Bearing Capacity of the Subgrade". Third International Conference on Geotextiles, Vienna. pp 129-135.

Sand & Gravel Association (undated), "Gravel Sub-base Materials : Type IG".

Sellmeijer J B (1990), "Design of Geotextile Reinforced Paved Roads & Parking Areas". Fourth International Conference on Geotextiles, Geomembranes and Related Products, The Hague, Vol 1 pp 177-182.

Steward J E, Williams R and Mahoney J (1977), "Guidelines for use of Fabrics in Construction and Maintenance of Low-Volume Roads". USDA Forest Serv, Portland, Oregon, USA. Report No FHWA-TS-78-205.

Tam W S (1987), "Pavement Evaluation and Overlay Design". PhD Thesis, University of Nottingham.

Thom N H (1988), "Design of Road Foundations". Phd Thesis, University of Nottingham.

Van Den Berg C, & Kenter C (1984), "Design Method and Guidelines for Geotextile Application in Unpaved Low Volume Roads". Geotextile Technology 1984.

Watts G R A & Brady K C (1990), "Site Damage Trials on Geotextiles". Fourth International Conference on Geotextile Geomembranes and Related Products", The Hague, Vol 2, pp 603-607.

Webster S L & Alford S J (1978), "Investigation of Construction Concepts of Pavements Across Soft Ground". Technical Report S-78-6, US Army Engineer Waterways Experimental Station, Vicksburg, Mississippi, USA.

Webster S L & Watkins J E (1977), "Investigation of Construction Techniques for Tactical Bridge Approach Roads Across Soft Ground". Technical Report S-77-1, US Army Engineer Waterways Experimental Station, Vicksburg, Mississippi, USA.

Yeo K (1992), "Results of Geosynthetic Index Testing of Samples from Bothkennar". Personal Correspondance.

APPENDIX A

GEOSYNTHETIC INDEX TEST RESULTS

GEOSYNTHETIC	CONDITION	LOAD AT 5% STRAIN (kN)	MAX LOAD (kN)	MAX STRAIN (%)
BIDIM M/D	CONTROL	0.53	8.86	54.38
	BURIED	1.28	4.212	35.40
	TRAFFIC DAMAGED	2.70	4.12	10.04
BIDIM X-M/D	CONTROL	0.32	7.38	61.20
	BURIED	1.29	5.29	41.50
	TRAFFIC DAMAGED	0.846	5.431	32.25
WOVEN M/D	CONTROL	8.86	54.75	16.08
	BURIED	9.02	33.77	11.33
	TRAFFIC DAMAGED	8.48	16.16	7.93
WOVEN X-M/D	CONTROL	32.20	48.35	7.89
	BURIED	32.10	49.24	8.04
	TRAFFIC DAMAGED	13.80	3.77	10.44
TYPAR M/D	CONTROL	3.53	6.79	35.40
	BURIED	3.34	5.65	21.75
	TRAFFIC DAMAGED	3.22	4.64	13.85
TYPAR X-M/D	CONTROL	3.44	7.86	40.65
	BURIED	3.31	6.72	27.1
	TRAFFIC DAMAGED	3.33	4.60	13.25
POLYFELT M/D	CONTROL	0.70	9.02	75.15
	BURIED	1.48	8.39	58.85
	TRAFFIC DAMAGED	3.16	7.36	17.94
POLYFELT X-M/D	CONTROL	1.94	9.80	36.6
	BURIED	2.74	8.334	25.63
	TRAFFIC DAMAGED	2.97	7.57	22.34
TENSAR SS1 M/D	CONTROL	9.63	12.64	8.942
	BURIED	10.26	14.64	17.761
	TRAFFIC DAMAGED	14.25	20.252	10.10
TENSAR SS1 X-M/D	CONTROL	16.90	32.77	9.66
	BURIED	14.23	19.73	10.36
	TRAFFIC DAMAGED	fail at 3.51%	11.07	3.514
TENSAR SS2 M/D	CONTROL	20.11	28.62	7.68
	BURIED			
	TRAFFIC DAMAGED	22.10	28.45	8.067
TENSAR SS2 X-M/D	CONTROL			
	BURIED	13.84	19.69	16.27
	TRAFFIC DAMAGED	12.11	15.74	8.131

Table 1

Geosynthetic Wide Width Tensile Strengths (after BS6906 part 1 1987)

		MASS UNIT AREA
BIDIM	CONTROL BURIED TRAFFIC DAMAGED	144.34 462.51 721.67
WOVEN	CONTROL BURIED TRAFFIC DAMAGED	265.24 490.62 456.67
TYPAR	CONTROL BURIED TRAFFIC DAMAGED	133.76 380.96 346.67
POLYFELT	CONTROL BURIED TRAFFIC DAMAGED	142.43 374.46 862.50

Table 2 Geosynthetic Mass per Unit Area

		2KPa	20KPa	200KPa
BIDIM	CONTROL BURIED TRAFFIC DAMAGED	1.36 2.33 3.78	1.04 1.86 3.44	0.54 0.94 1.98
WOVEN	CONTROL BURIED TRAFFIC DAMAGED	0.87 1.21 1.19	0.80 1.03 1.10	0.67 0.86 0.81
TYPAR	CONTROL BURIED TRAFFIC DAMAGED	0.44 1.13 2.16	0.41 0.96 1.89	0.35 0.67 1.35
POLYFELT	CONTROL BURIED TRAFFIC DAMAGED	1.2 1.58 0.95	0.93 1.30 0.78	0.60 0.87 0.53

Table 3 Geosynthetic Thickness

		FORCE (KN)	DISPLACEMENT (mm)
BIDIM	CONTROL	1.70	61.8
	BURIED	1.31	47.9
	TRAFFIC DAMAGED	1.21	47.3
WOVEN	CONTROL	6.43	36.6
	BURIED	5.11	33.6
	TRAFFIC DAMAGED	4.51	37.3
TYPAR	CONTROL	1.35	48.0
	BURIED	1.17	44.4
	TRAFFIC DAMAGED	1.12	41.6
POLYFELT	CONTROL	1.63	49.2
	BURIED	1.43	43.3
	TRAFFIC DAMAGED	1.59	45.7

Table 4 Geosynthetic CBR Plunger Test (after BS6906 part 4, 1989)

GEOTEXTILE	CONDITION	CONE PENETRATION	ROD DEFLECTION
BIDIM	CONTROL	33.7	55.4
	BURIED	34.0	51.3
	TRAFFIC DAMAGED	35.8	57.9
WOVEN	CONTROL	9.5	29.2
	BURIED	12.2	24.0
	TRAFFIC DAMAGED	9.8	28.5
TYPAR	CONTROL	33.1	43.0
	BURIED	36.2	46.1
	TRAFFIC DAMAGED	37.1	48.4
POLYFELT	CONTROL	33.8	49.4
	BURIED	34.4	46.5
	TRAFFIC DAMAGED	34.5	48.8

Table 5 Geosynthetic Cone Drop Tests (after BS6906 part 6, 1990).

APPENDIX B

CONSTRUCTION DATA SUMMARY

SECTION A

Materials

Constructed with Tensar SS2 and 400mm of Type1 aggregate.

Dates Constructed

11/7/89 - 14/7/89

Shear Vane Readings (kPa)

Depth (mm)	Reading Location 1				Reading Location 2	
30	Off-scale	Off-scale	114	74	Off-scale	Off-scale
200	89	78	72	80	87	86
300	69	79	58	95	102	96
400	67	68	62	75	81	82
500	51	58	53	55	70	76
800	42	53	45	62	65	69

Clegg Hammer Subgrade Readings

Reading Location 1 Average Value = 11.6
Reading Location 2 Average Value = 13.1

Cone Penetrometer Subrade Readings

Reading Location 1 Average Value = 6.86 = 143 kPa
Reading Location 2 Average Value = 7.36 = 154 kPa

Subgrade Moisture Content (%)

Depth (mm)	Reading Location 1	Reading Location 2
surface	14.8	7.4
200	27.0	31.1
350	31.9	32.9

SECTION B

Materials

Contstructed with Typar 3407 and 450mm of Type1 aggregate.

Dates Constructed

17/7/89 - 19/7/89

Shear Vane Readings (kPa)

Depth (mm)	Reading Location 1			Reading Location 2		
30	118	94	Off-scale	Off-scale	88	Off-scale
200	98	52	102	Off-scale	114	88
300	98	78	88	Off-scale	119	92
400	77	59	74	122	82	64
500	58	48	70	76	74	54
800	42	43	44	61	43	48

Clegg Hammer Subgrade Readings

Reading Location 1 Average Value = 9.7
Reading Location 2 Average Value = 14.8

Cone Penetrometer Subrade Readings

Reading Location 1 Average Value = 6.13 = 128kPa
Reading Location 2 Average Value = 6.70 = 140 kPa

Subgrade Moisture Content (%)

Depth (mm)	Reading Location 1	Reading Location 2
surface	17.6	17.3
200	33.6	25.9
350	32.4	40.4

SECTION C

Materials

Constructed with Bidim B2 and 500mm of Type1 aggregate.

Dates Constructed

19/7/89 - 20/7/89

Shear Vane Readings (kPa)

Depth (mm)	Reading Location 1			Reading Location 2		
30	Off-scale	95	126	Off-scale	Off-scale	Off-scale
200	Off-scale	105	93	Off-scale	Off-scale	Off-scale
300	115	96	102	Off-scale	107	106
400	102	69	80	97	87	65
500	92	64	57	60	88	40
800	42	52	53	50	56	43

Clegg Hammer Subgrade Readings

Reading Location 1 Average Value = 13.8
Reading Location 2 Average Value = 12.1

Cone Penetrometer Subrade Readings

Reading Location 1 Average Value = 6.02 = 126kPa
Reading Location 2 Average Value = 6.01 = 126kPa

Subgrade Moisture Content (%)

Depth (mm)	Reading Location 1	Reading Location 2
surface	20.8	9.6
200	32.8	27.6
350	37.5	34.1

SECTION D

Materials

Control section constructed with 550mm of Type1 aggregate.

Date Constructed

21/7/89

Shear Vane Readings (kPa)

Depth (mm)	Reading Location 1			Reading Location 2		
30	Off-scale	110	122	Off-scale	102	Off-scale
200	Off-scale	110	Off-scale	Off-scale	112	110
300	118	106	124	Off-scale	95	86
400	94	82	91	92	77	68
500	62	70	72	66	61	50
800	54	62	45	54	53	45

Clegg Hammer Subgrade Readings

Reading Location 1 Average Value = 13.5
Reading Location 2 Average Value = 11.0

Cone Penetrometer Subrade Readings

Reading Location 1 Average Value = 5.15 = 108kPa
Reading Location 2 Average Value = 4.66 = 94kPa

Subgrade Moisture Content (%)

Depth (mm)	Reading Location 1	Reading Location 2
surface	20.8	24.3
200	30.2	38.6
350	33.4	28.0

SECTION E

Materials

Constructed with a woven Geosynthetic and 490mm of Type1 aggregate.

Dates Constructed

5/9/89 - 6/9/89

Shear Vane Readings (kPa)

Depth (mm)	Reading Location 1			Reading Location 2		
30	46	Off-scale	126	81	102	124
200	62	85	90	82	104	106
300	66	96	118	78	94	104
400	51	64	76	67	73	72
500	45	54	66	58	60	58
800	38	54	48	49	49	50

Clegg Hammer Subgrade Readings

Reading Location 1 Average Value = 7.6
Reading Location 2 Average Value = 7.6

Cone Penetrometer Subrade Readings

Reading Location 1 Average Value = 4.86 = 102kPa
Reading Location 2 Average Value = 4.30 = 90kPa

Subgrade Moisture Content (%)

Depth (mm)	Reading Location 1	Reading Location 2
surface	21.7	33.3
200	43.9	35.0
350	36.4	35.4

SECTION F

Materials

Constructed with Tensar SS1 and 400mm of Sand and Gravel.

Dates Constructed

8/9/89 - 12/9/89

Shear Vane Readings (kPa)

Depth (mm)	Reading Location 1			Reading Location 2		
30	Off-scale	102	89	Off-scale	113	107
200	121	112	87	112	113	122
300	121	102	84	Off-scale	Off-scale	117
400	75	70	61	80	77	84
500	72	60	62	72	64	59
800	45	58	46	53	46	41

Clegg Hammer Subgrade Readings

Reading Location 1 Average Value = 8.2
Reading Location 2 Average Value = 9.9

Cone Penetrometer Subrade Readings

Reading Location 1 Average Value = 5.82 = 122kPa
Reading Location 2 Average Value = 7.53 = 157kPa

Subgrade Moisture Content (%)

Depth (mm)	Reading Location 1	Reading Location 2
surface	29.0	19.0
200	28.7	31.4
350	37.5	39.4

SECTION I

Materials

Construced with Tensar SS1 and 400mm of Sand and Gravel.

Dates Constructed

12/9/89 - 14/9/89

Shear Vane Readings (kPa)

Depth (mm)	Reading Location 1			Reading Location 2		
30	78	62	63	76	61	72
200	96	83	98	90	104	78
300	100	118	108	110	115	108
400	95	89	94	106	94	86
500	82	93	81	78	65	72
800	65	72	62	54	62	55

Clegg Hammer Subgrade Readings

Reading Location 1 Average Value = 6.8
Reading Location 2 Average Value = 4.6

Cone Penetrometer Subrade Readings

Reading Location 1 Average Value = 3.81 = 80kPa
Reading Location 2 Average Value = 3.45 = 72kPa

Subgrade Moisture Content (%)

Depth (mm)	Reading Location 1	Reading Location 2
surface	35.8	32.8
200	38.1	34.3
350	31.7	32.3

SECTION J

Materials

Constructed with a woven geosynthetic and (notionally) 340mm of Type1 aggregate.

Dates Constructed

11/9/89 - 12/9/89

Shear Vane Readings (kPa)

Depth (mm)	Reading Location 1			Reading Location 2		
30	72	94	80	74	82	86
200	80	82	88	88	76	94
300	96	88	102	106	91	110
400	82	77	76	92	80	90
500	66	58	62	74	72	75
800	58	69	52	60	62	65

Clegg Hammer Subgrade Readings

Reading Location 1 Average Value = 4.9
Reading Location 2 Average Value = 6.0

Cone Penetrometer Subrade Readings

Reading Location 1 Average Value = 2.68 = 56kPa
Reading Location 2 Average Value = 3.41 = 71kPa

Subgrade Moisture Content (%)

Depth (mm)	Reading Location 1	Reading Location 2
surface	32.1	30.5
200	32.4	32.4
350	33.5	32.0

SECTION K

Materials

Control section constructed with 400mm of Type1 aggregate.

Dates Constructed

2/10/89 - 3/10/89

Shear Vane Readings (kPa)

Depth (mm)	Reading Location 1			Reading Location 2		
30	78	80	81	108	84	83
200	95	89	102	94	94	106
300	100	108	Off-scale	116	123	112
400	98	100	116	106	92	105
500	78	78	85	74	70	75
800	62	65	70	74	65	60

Clegg Hammer Subgrade Readings

Reading Location 1 Average Value = 7.9
Reading Location 2 Average Value = 7.3

Cone Penetrometer Subrade Readings

Reading Location 1 Average Value = 5.00 = 105kPa
Reading Location 2 Average Value = 5.47 = 114kPa

Subgrade Moisture Content (%)

Depth (mm)	Reading Location 1	Reading Location 2
surface	28.0	25.1
200	37.2	32.3
350	31.9	31.0

SECTION L

Materials

Constructed with Bidim B2 and 350mm of Type1 aggregate.

Dates Constructed

26/9/89 - 27/9/89

Shear Vane Readings (kPa)

Depth (mm)	Reading Location 1			Reading Location 2		
30	60	68	68	38	54	60
200	86	100	104	76	86	66
300	112	108	118	73	90	84
400	74	84	94	71	77	64
500	60	75	72	66	56	56
800	62	58	56	56	64	55

Clegg Hammer Subgrade Readings

Reading Location 1 Average Value = Clegg Hammer Faulty
Reading Location 2 Average Value = No Readings Available

Cone Penetrometer Subrade Readings

Reading Location 1 Average Value = 2.83 = 59kPa
Reading Location 2 Average Value = 2.13 = 45kPa

Subgrade Moisture Content (%)

Depth (mm)	Reading Location 1	Reading Location 2
surface	34.1	34.7
200	38.5	33.3
350	36.0	38.8

SECTION M

Materials

Constructed with Typar 3407 and 350mm of Type1 aggregate.

Dates Constructed

28/9/89 - 29/9/89

Shear Vane Readings (kPa)

Depth (mm)	Reading Location 1			Reading Location 2		
30	81	82	105	92	76	78
200	83	87	78	94	94	96
300	104	104	94	102	94	90
400	76	72	74	74	74	69
500	61	58	60	55	60	58
800	70	60	54	62	52	64

Clegg Hammer Subgrade Readings

Reading Location 1 Average Value = 6.9
Reading Location 2 Average Value = 6.4

Cone Penetrometer Subrade Readings

Reading Location 1 Average Value = 4.43 = 93kPa
Reading Location 2 Average Value = 4.27 = 89kPa

Subgrade Moisture Content (%)

Depth (mm)	Reading Location 1	Reading Location 2
surface	30.8	33.0
200	36.8	29.3
350	38.1	37.5

SECTION N

Materials

Constructed with Tensar SS2 and 300mm of Type1 aggregate.

Dates Constructed

4/10/89 - 5/10/89

Shear Vane Readings (kPa)

Depth (mm)	Reading Location 1			Reading Location 2		
30	78	99	95	72	108	93
200	84	98	88	104	102	88
300	76	79	75	75	99	85
400	64	60	62	62	71	71
500	52	55	47	54	62	54
800	45	44	60	47	42	53

Clegg Hammer Subgrade Readings

Reading Location 1 Average Value = 9.3
Reading Location 2 Average Value = 8.0

Cone Penetrometer Subrade Readings

Reading Location 1 Average Value = 6.02 = 126kPa
Reading Location 2 Average Value = 6.88 = 144kPa

Subgrade Moisture Content (%)

Depth (mm)	Reading Location 1	Reading Location 2
surface	27.5	26.3
200	31.6	34.2
350	41.7	41.3

SECTION O

Materials

Constructed with Polyfelt TS500, 60/65mm diameter bamboo and 350mm of Type1 aggregate.

Dates Constructed

23/10/89 - 25/10/89

Shear Vane Readings (kPa)

Depth (mm)	Reading Location 1			Reading Location 2		
30	126	78	92	86	112	72
200	61	66	74	87	86	77
300	68	70	73	82	76	83
400	54	64	59	69	68	66
500	47	46	52	66	58	64
800	46	44	44	56	48	38

Clegg Hammer Subgrade Readings

Reading Location 1 Average Value = 7.0
Reading Location 2 Average Value = 5.7

Cone Penetrometer Subrade Readings

Reading Location 1 Average Value = 5.92 = 124kPa
Reading Location 2 Average Value = 4.02 = 84kPa

Subgrade Moisture Content (%)

Depth (mm)	Reading Location 1	Reading Location 2
surface	31.7	29.1
200	34.1	44.6
350	44.8	42.2

SECTION P

Materials

Constructed with Polyfelt TS500 and 350mm of Type1 aggregate.

Dates Constructed

26/10/89 - 28/10/89

Shear Vane Readings (kPa)

Depth (mm)	Reading Location 1			Reading Location 2		
30	62	83	70	32	13	36
200	94	100	108	48	52	69
300	102	100	96	71	58	69
400	74	84	72	50	49	66
500	68	74	74	55	43	52
800	54	44	46	42	35	43

Clegg Hammer Subgrade Readings

Reading Location 1 Average Value = 7.2
Reading Location 2 Average Value = 4.7

Cone Penetrometer Subrade Readings

Reading Location 1 Average Value = 3.66 = 76kPa
Reading Location 2 Average Value = 1.28 = 27kPa

Subgrade Moisture Content (%)

Depth (mm)	Reading Location 1	Reading Location 2
surface	42.2	38.1
200	30.1	34.7
350	37.3	39.2

APPENDIX C

TRAFFICKING RESULTS

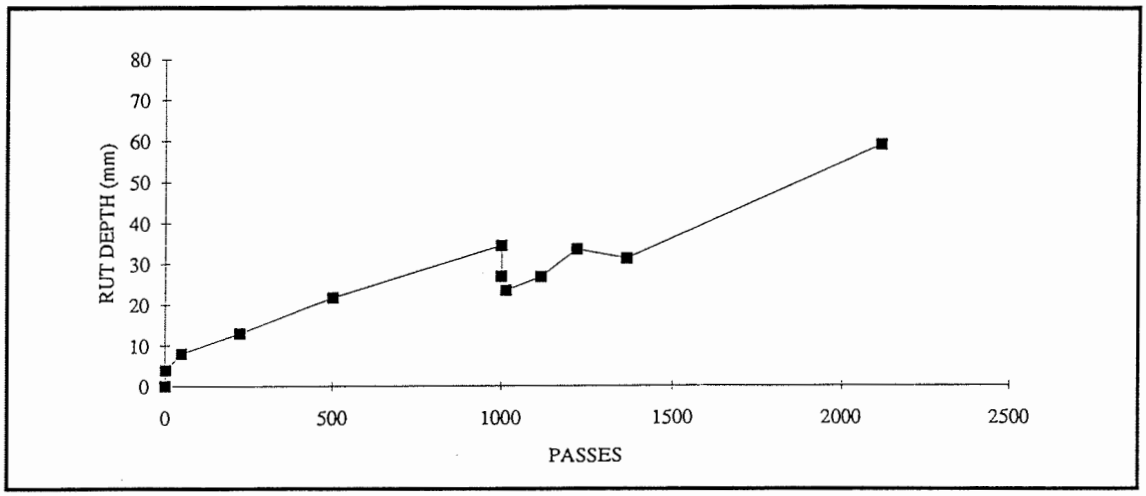

Figure C1 Rut Depth Development - Section A

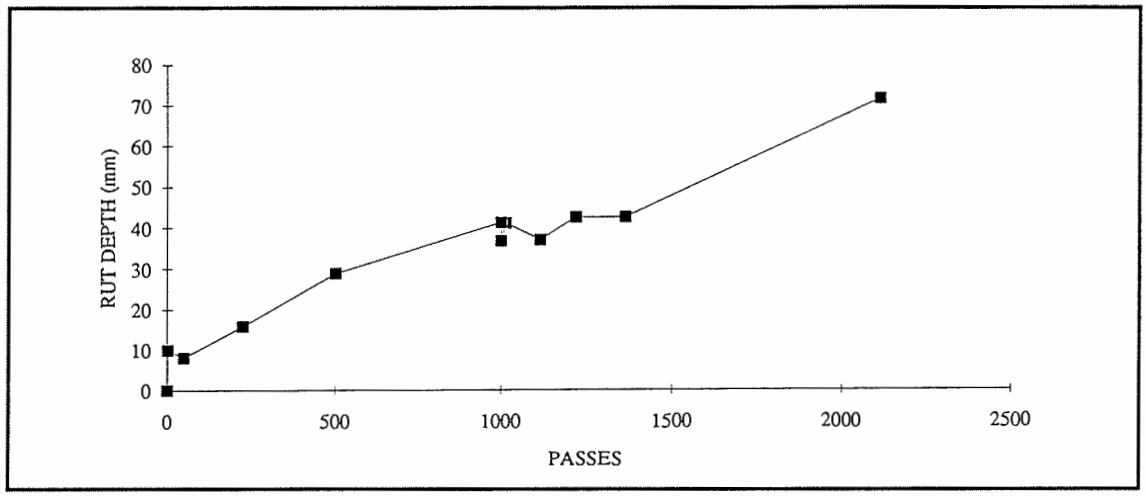

Figure C2 Rut Depth Development - Section B

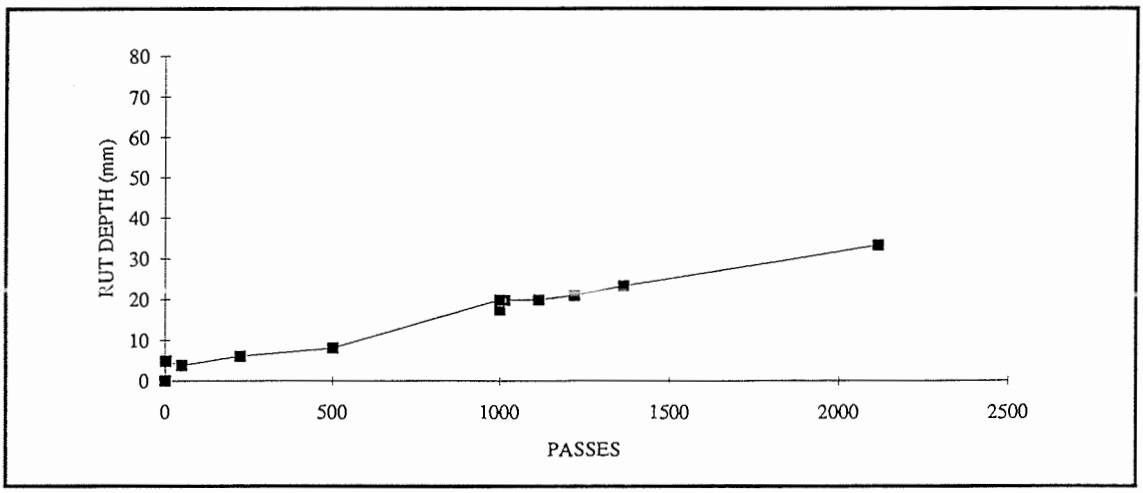

Figure C3 Rut Depth Development - Section C

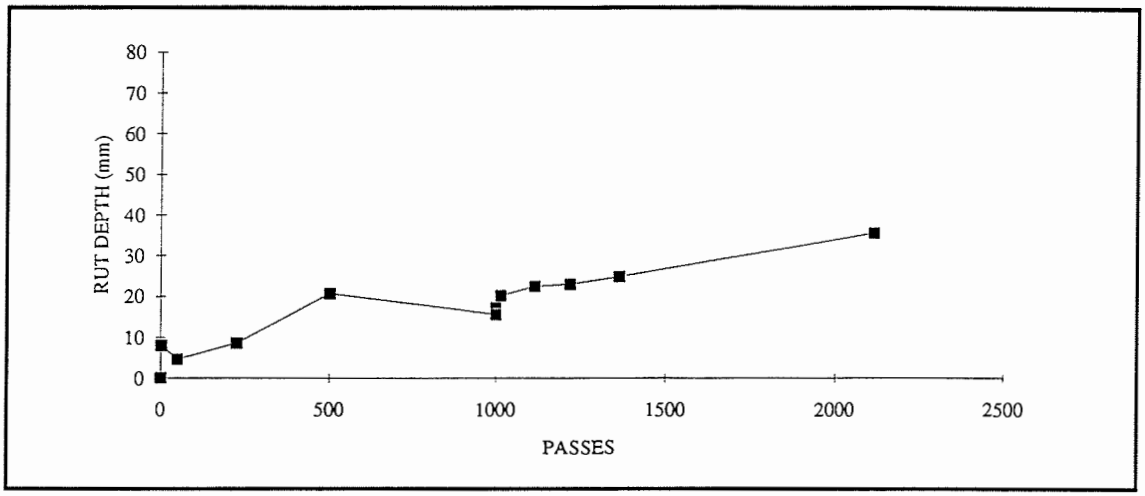

Figure C4 Rut Depth Development - Section D

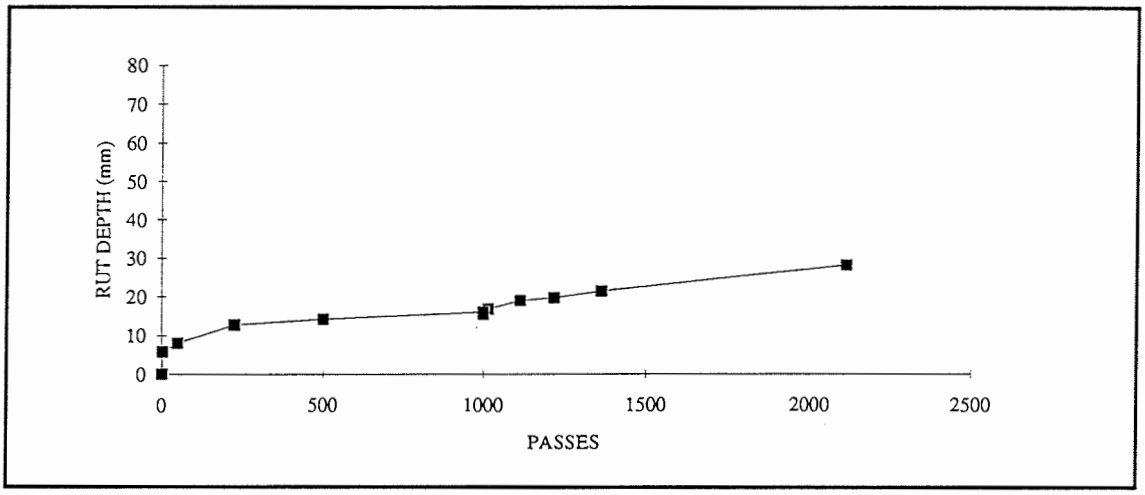

Figure C5 Rut Depth Development - Section E

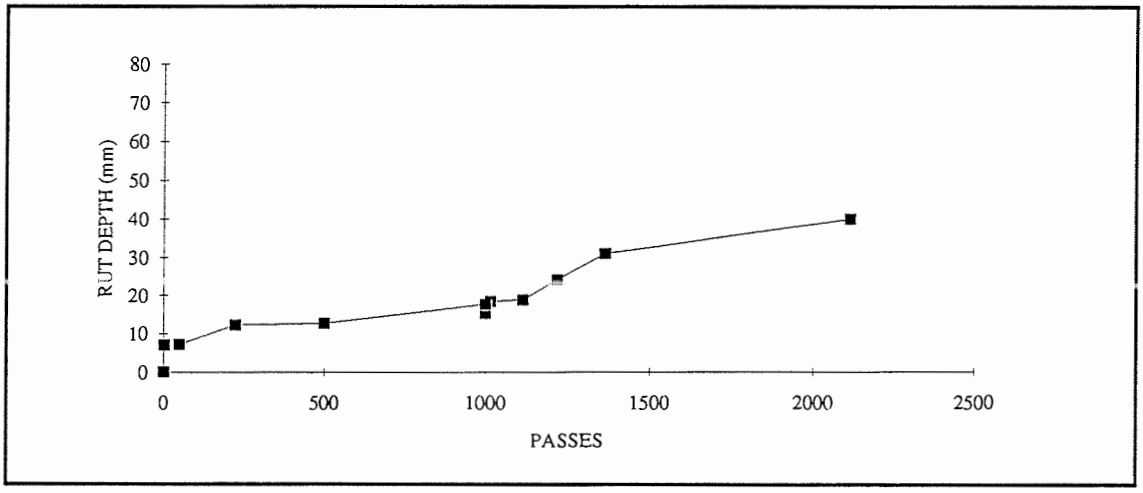

Figure C6 Rut Depth Development - Section F

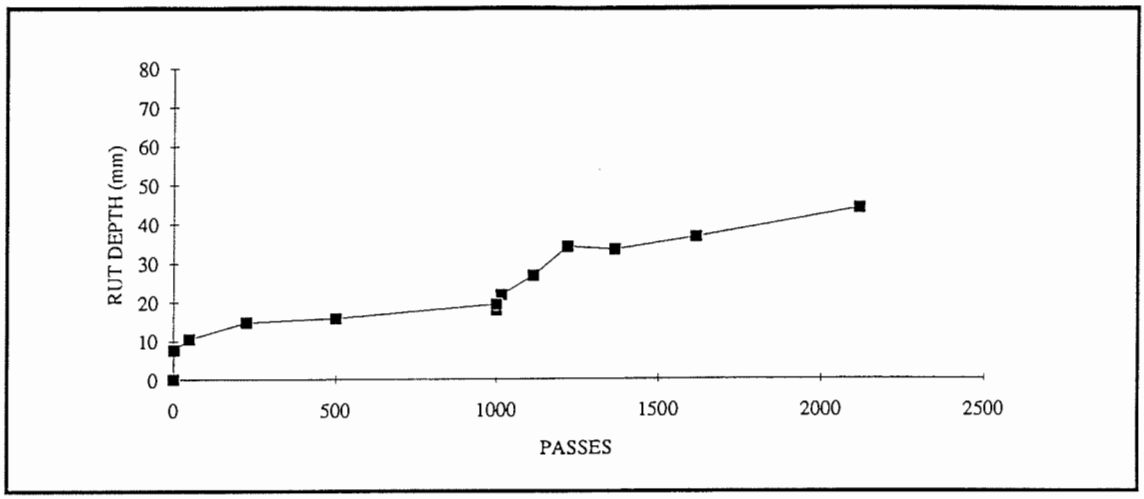

Figure C7 Rut Depth Development - Section H

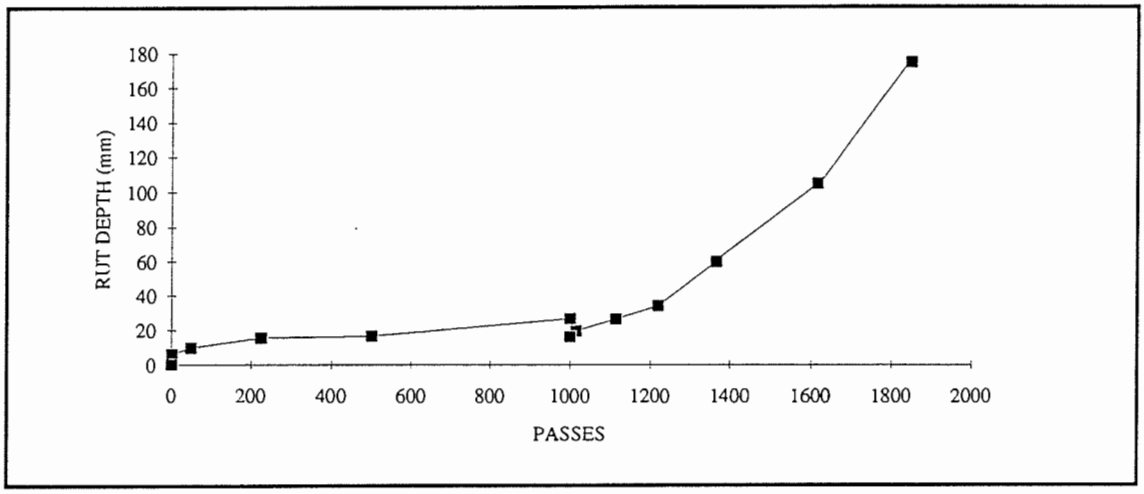

Figure C8 Rut Depth Development - Section I

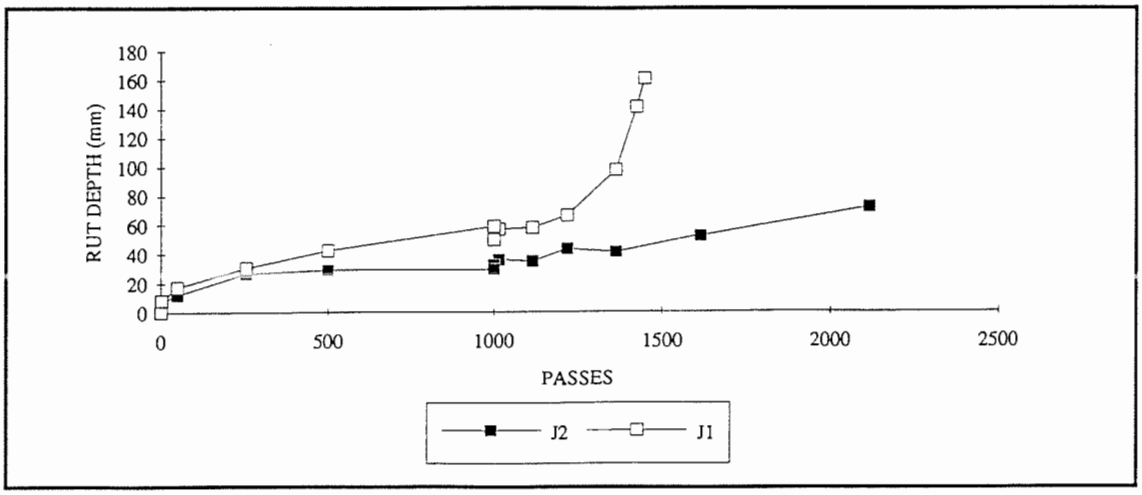

Figure C9 Rut Depth Development - Section J

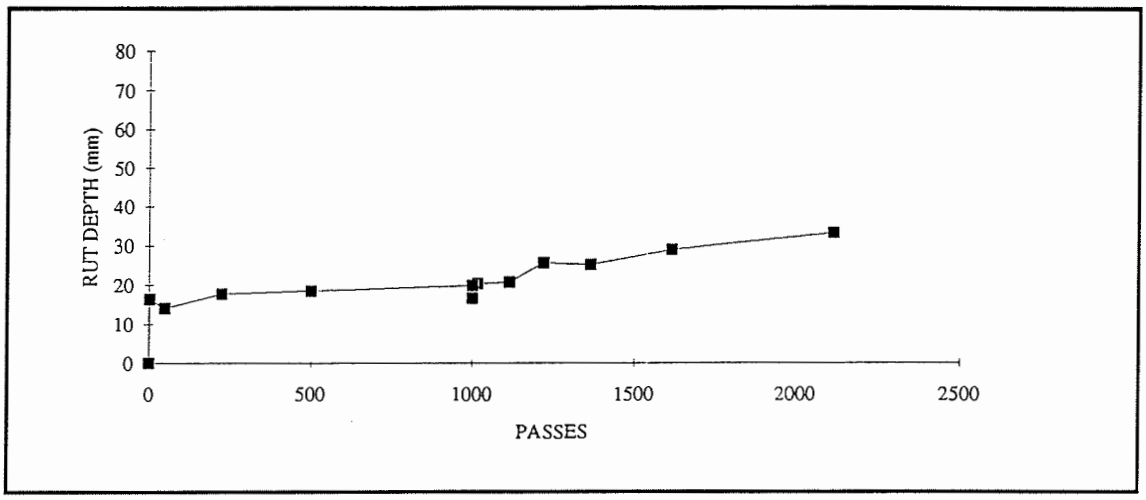

Figure C10 Rut Depth Development - Section K

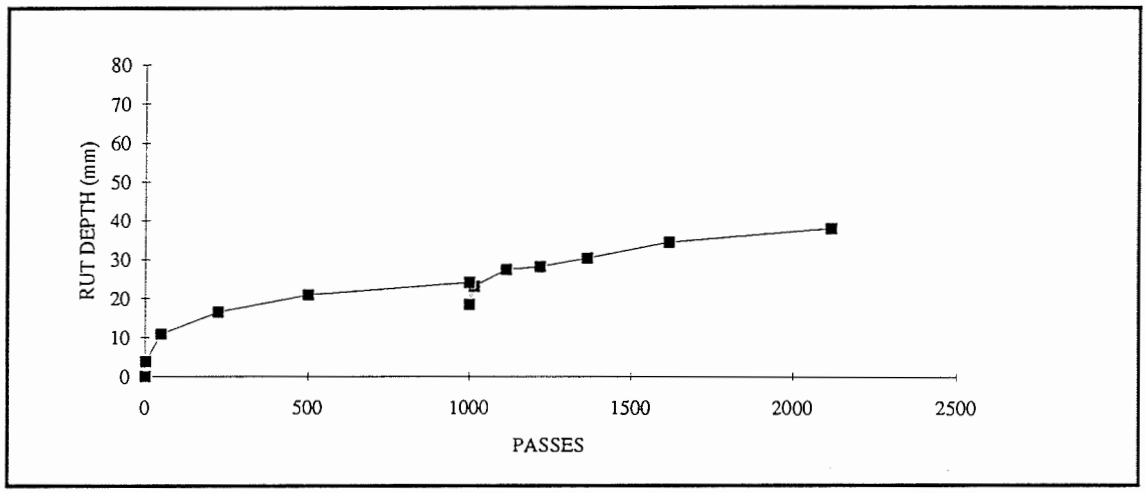

Figure C11 Rut Depth Development - Section L

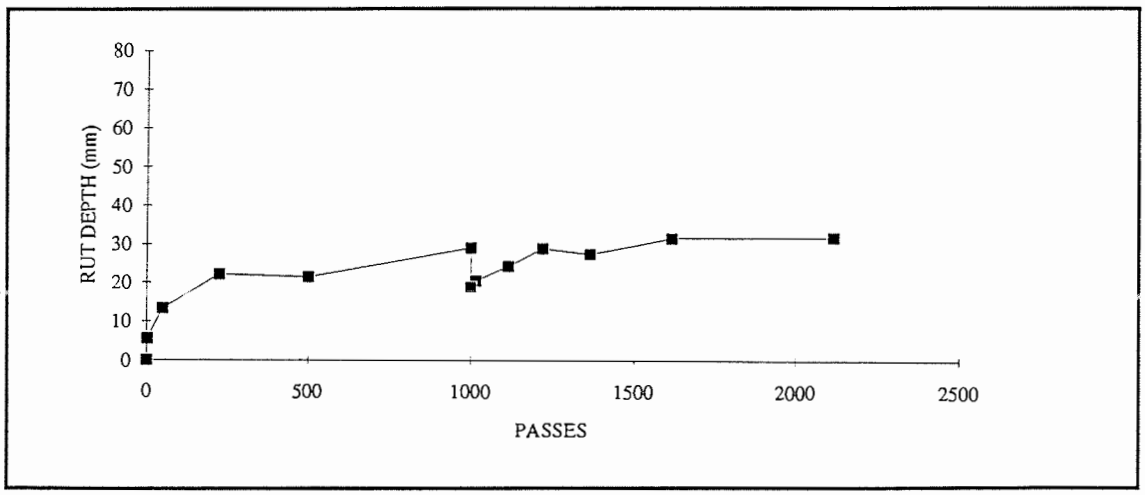

Figure C12 Rut Depth Development - Section M

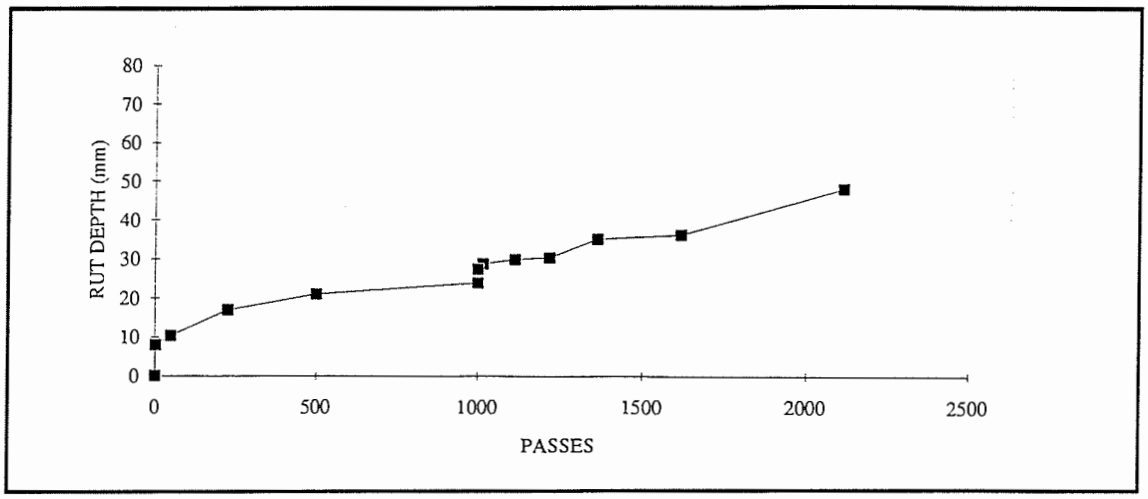

Figure C13 Rut Depth Development - Section N

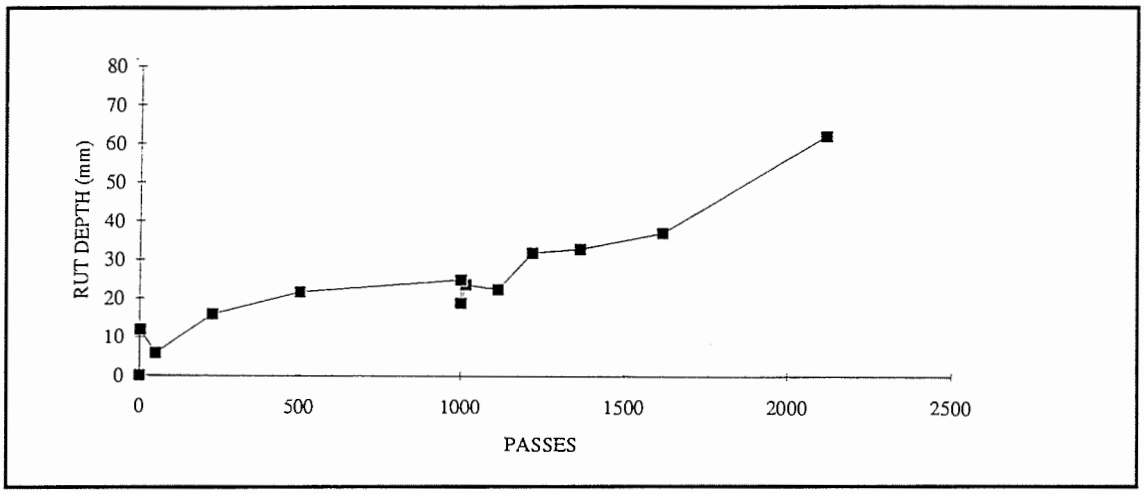

Figure C14 Rut Depth Development - Section O

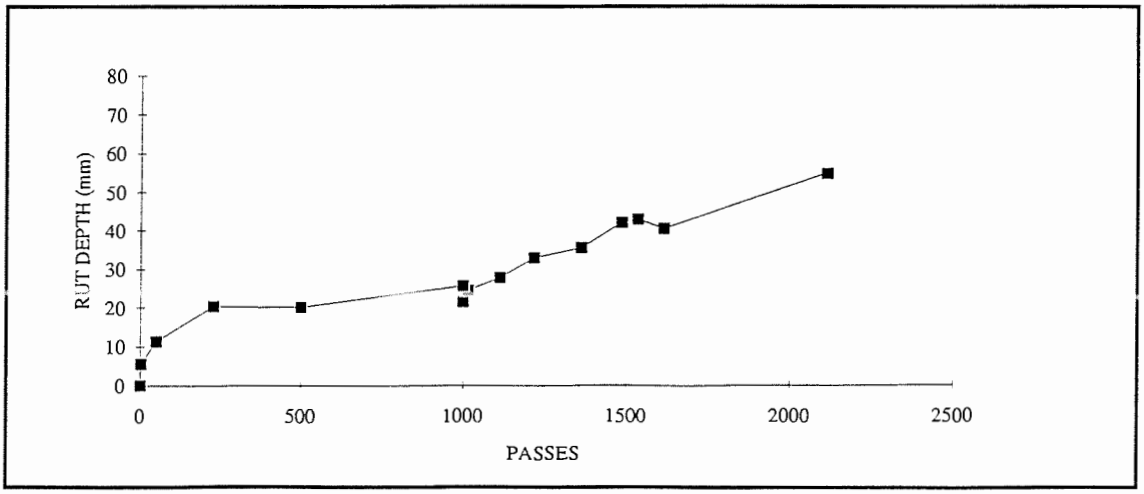

Figure C15 Rut Depth Development - Section P

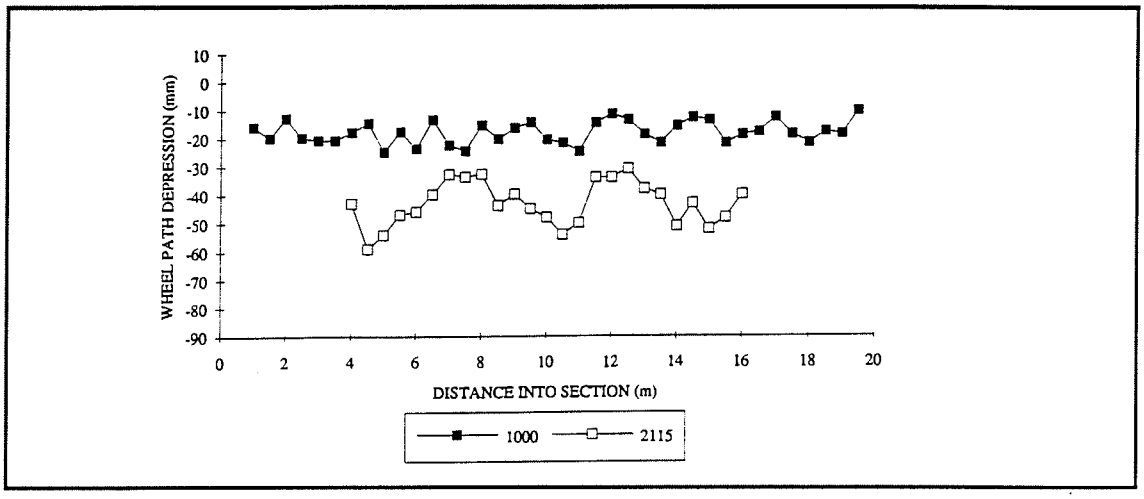

Figure C16 Vertical Depression of the Aggregate Surface after 1000 and 2115 Passes - Section A

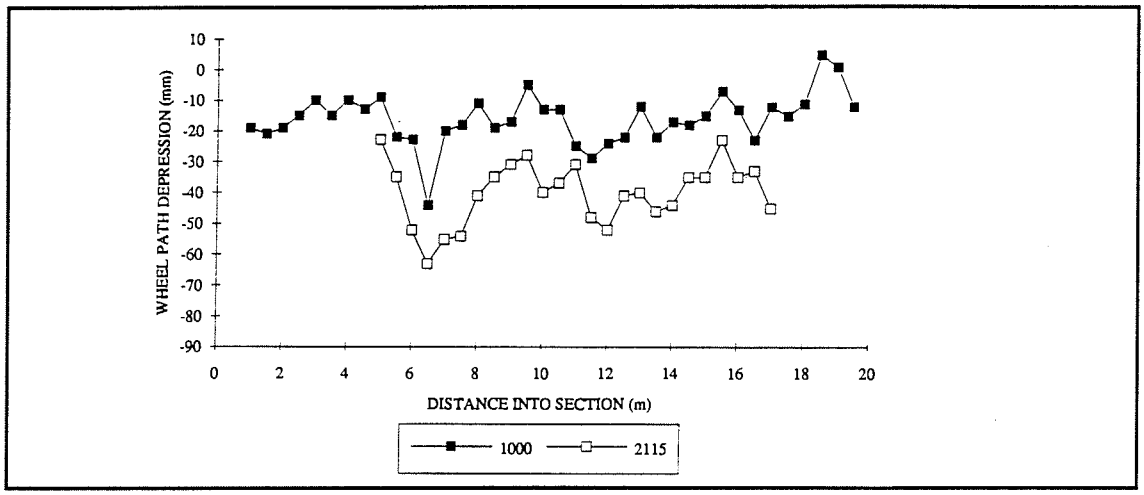

Figure C17 Vertical Depression of the Aggregate Surface after 1000 and 2115 Passes - Section B

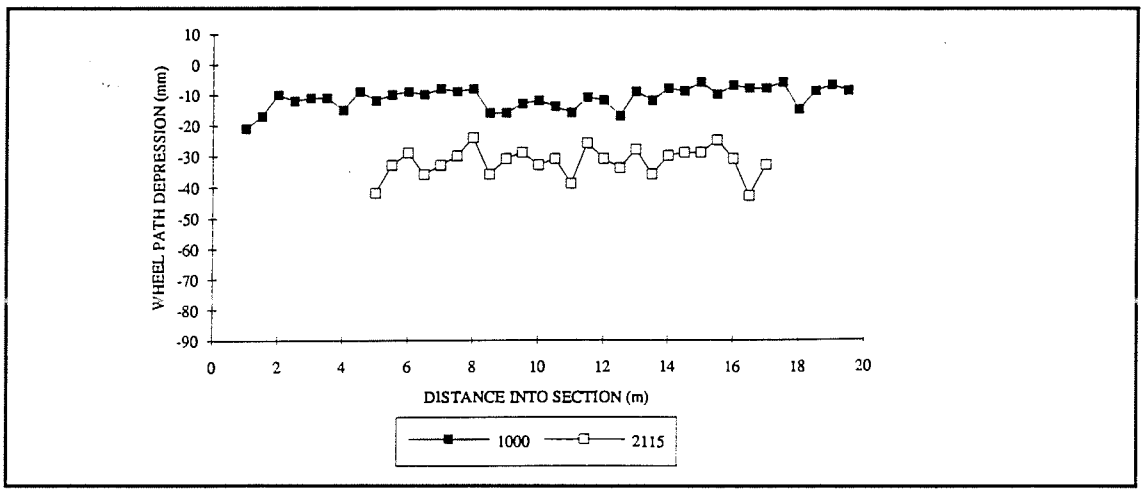

Figure C18 Vertical Depression of the Aggregate Surface after 1000 and 2115 Passes - Section C

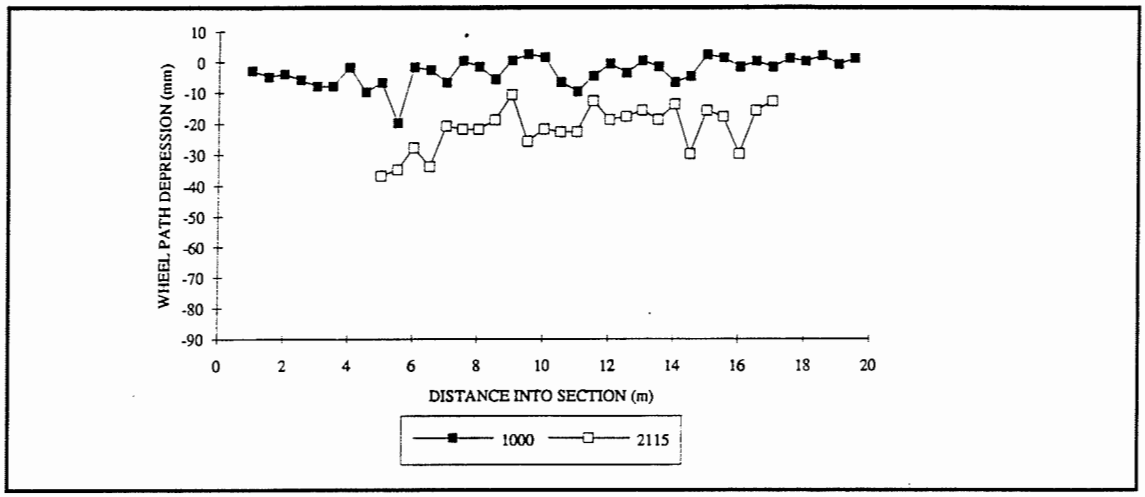

Figure C19 Vertical Depression of the Aggregate Surface after 1000 and 2115 Passes - Section D

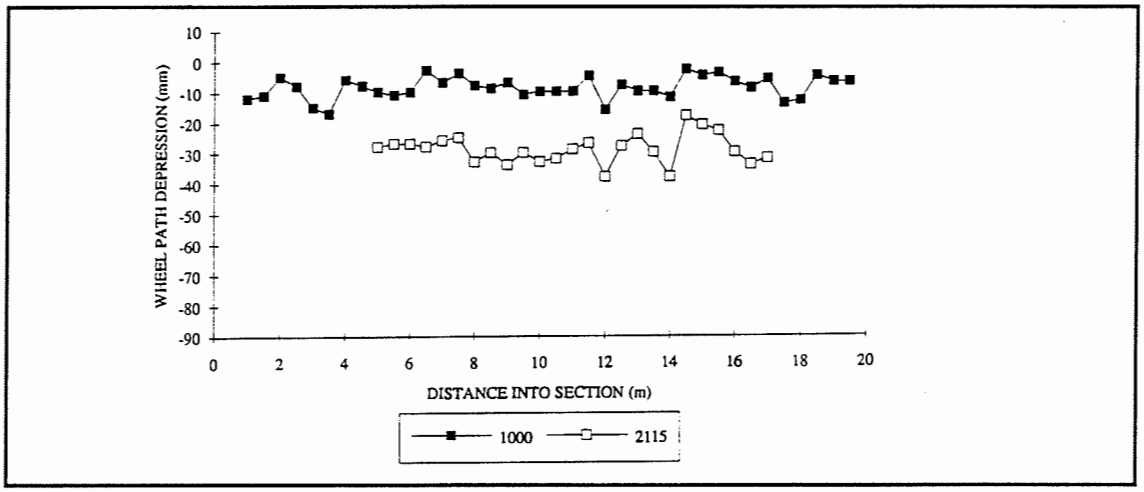

Figure C20 Vertical Depression of the Aggregate Surface after 1000 and 2115 Passes - Section E

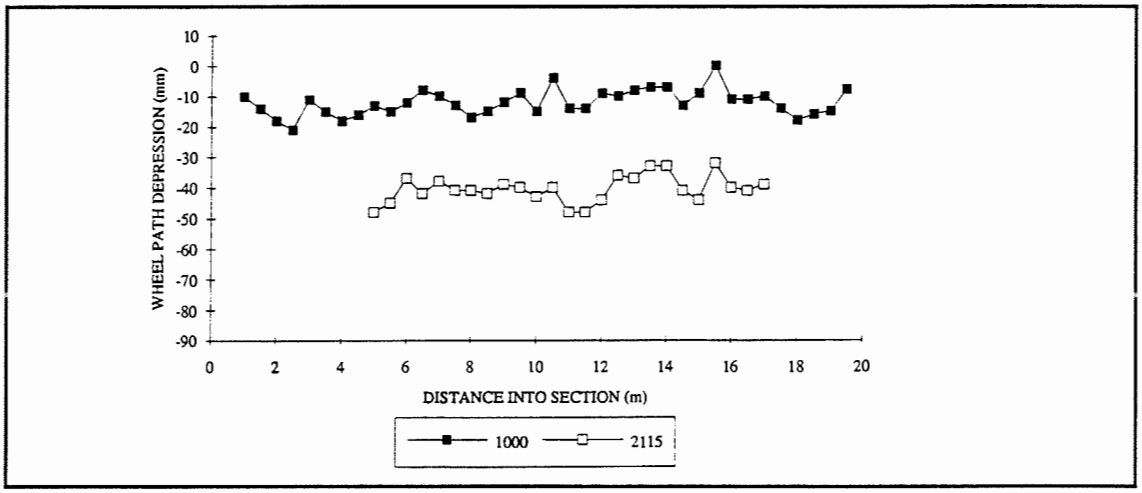

Figure C21 Vertical Depression of the Aggregate Surface after 1000 and 2115 Passes - Section F

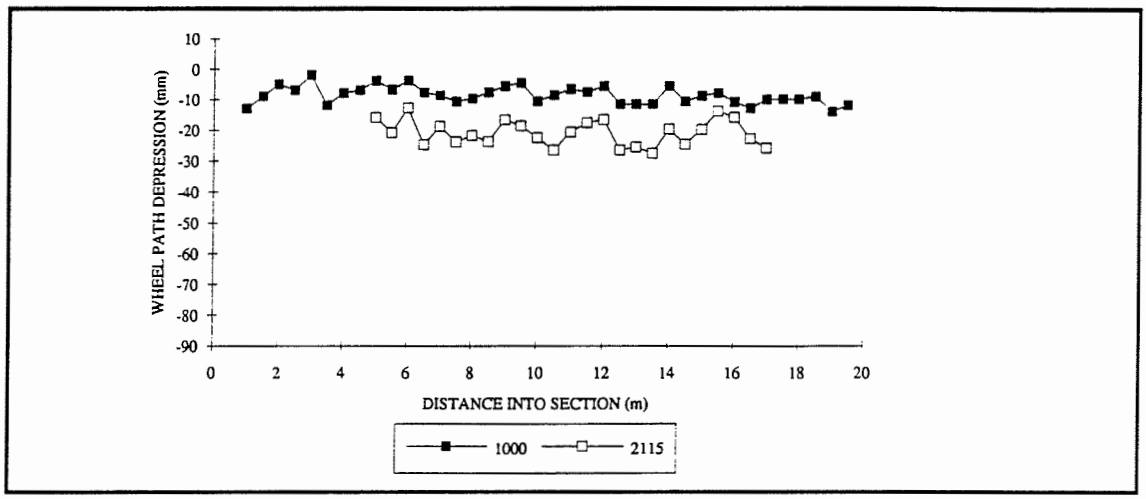

Figure C 22 Vertical Depression of the Aggregate Surface after 1000 and 2115 Passes - Section H

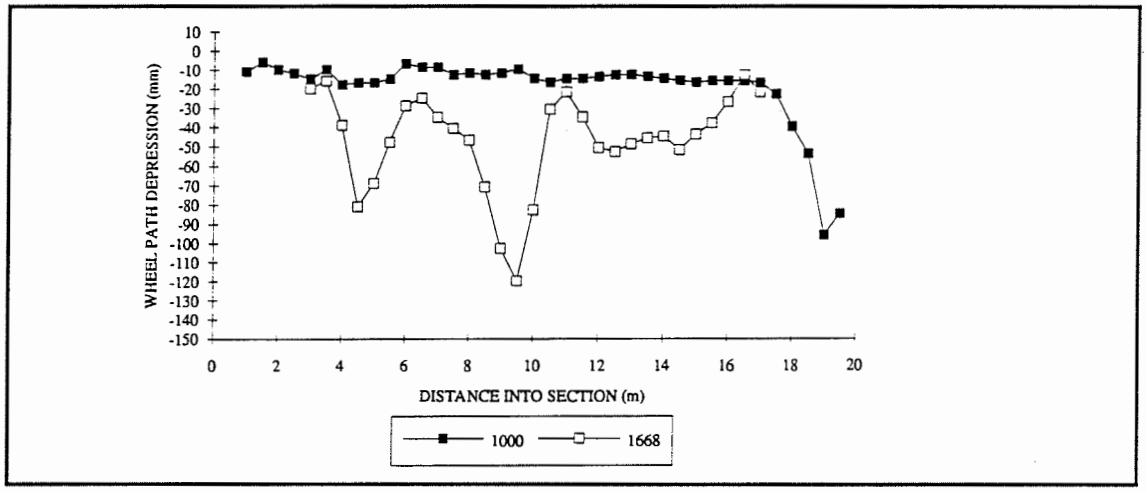

Figure C23 Vertical Depression of the Aggregate Surface after 1000 and 1668 Passes - Section I

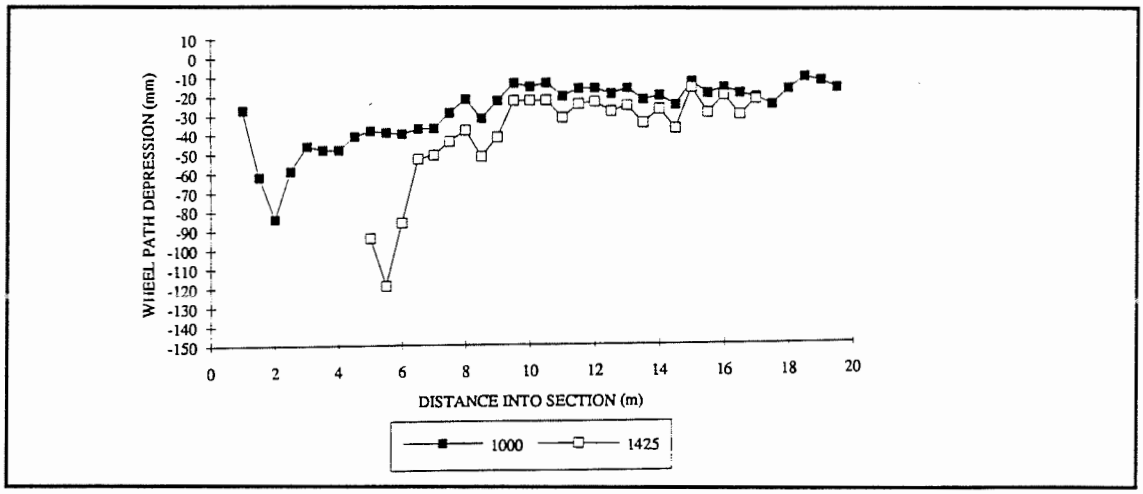

Figure C24 Vertical Depression of the Aggregate Surface after 1000 and 1425 Passes - Section J

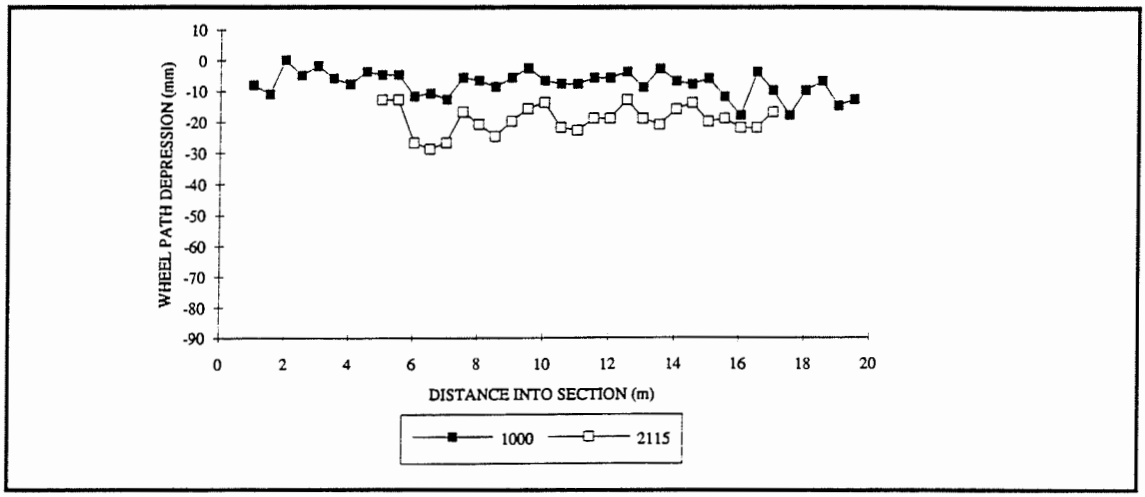

Figure C25 Vertical Depression of the Aggregate Surface after 1000 and 2115 Passes - Section K

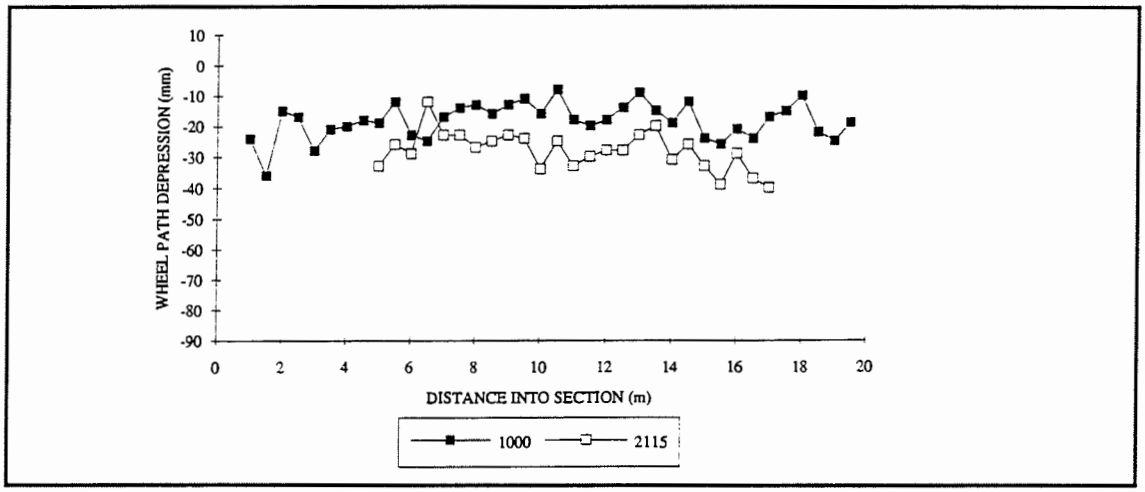

Figure C26 Vertical Depression of the Aggregate Surface after 1000 and 2115 Passes - Section L

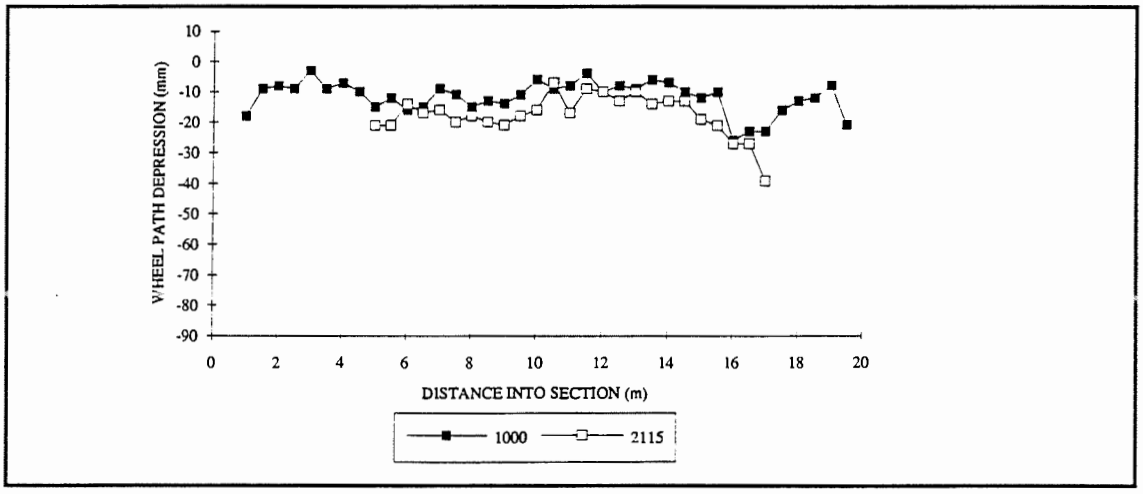

Figure C27 Vertical Depression of the Aggregate Surface after 1000 and 2115 Passes - Section M

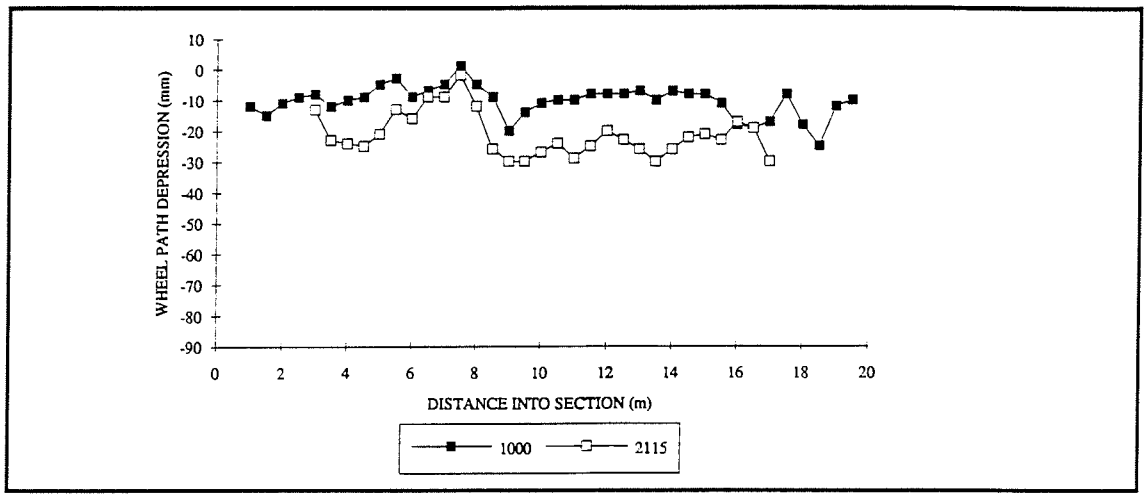

Figure C28 Vertical Depression of the Aggregate Surface after 1000 and 2115 Passes - Section N

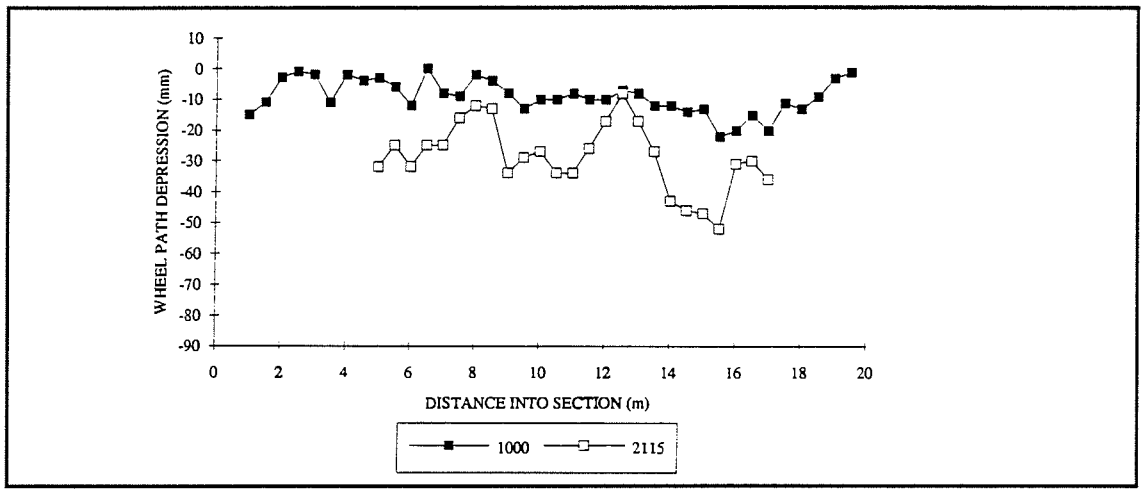

Figure C29 Vertical Depression of the Aggregate Surface after 1000 and 2115 Passes - Section O

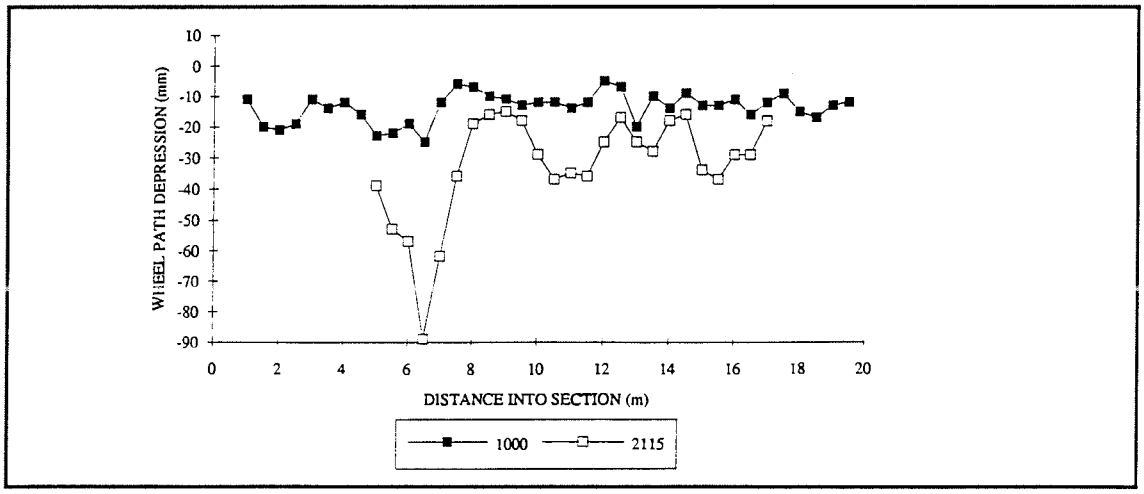

Figure C30 Vertical Depression of the Aggregate Surface after 1000 and 2115 Passes - Section P

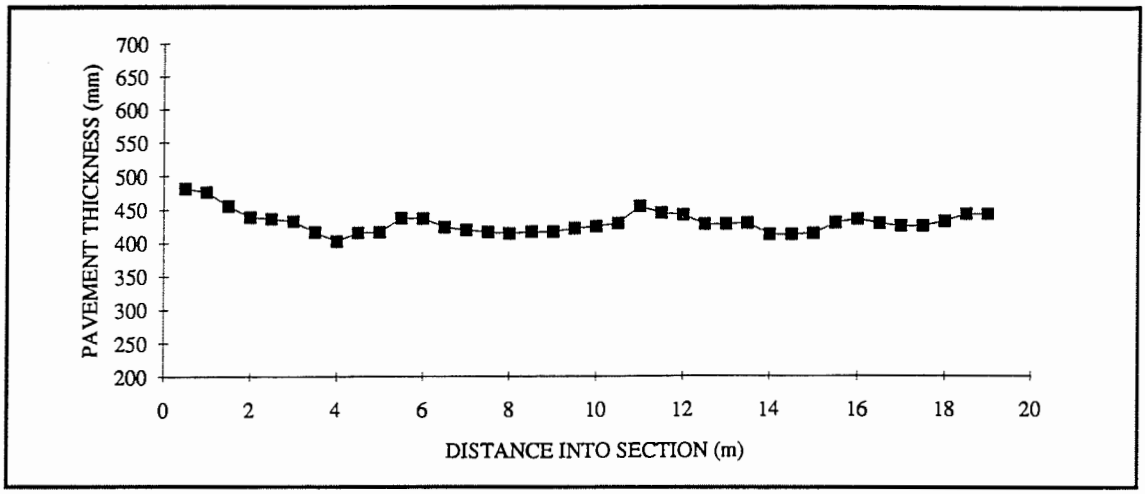

Figure C31 Pavement Thickness - Section A, Instrumented Wheel Path

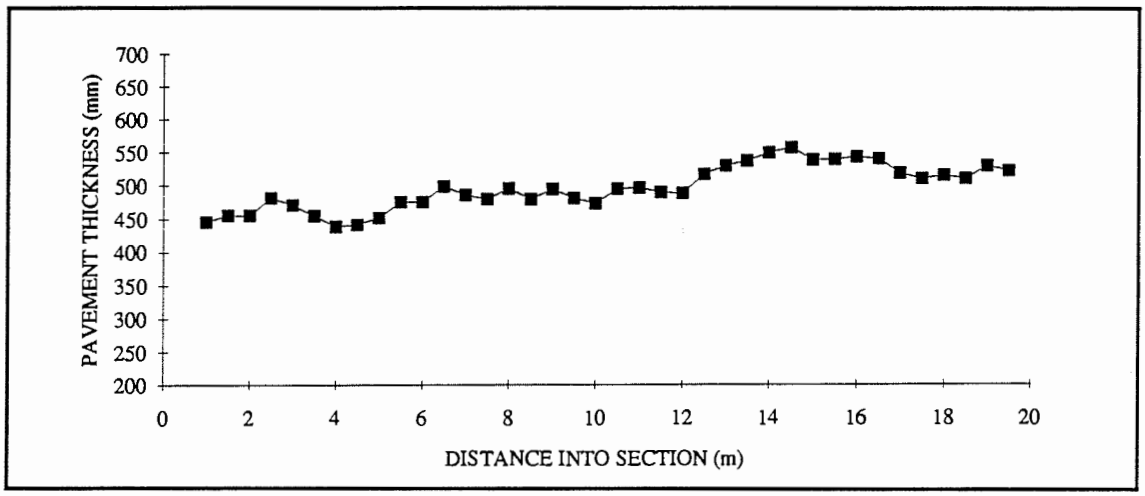

Figure C32 Pavement Thickness - Section B, Instrumented Wheel Path

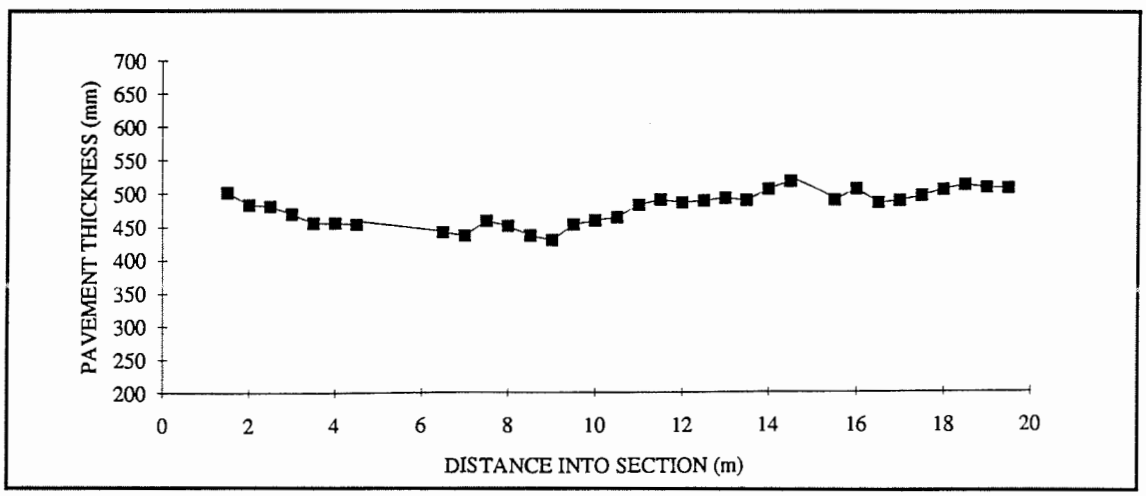

Figure C33 Pavement Thickness - Section C, Instrumented Wheel Path

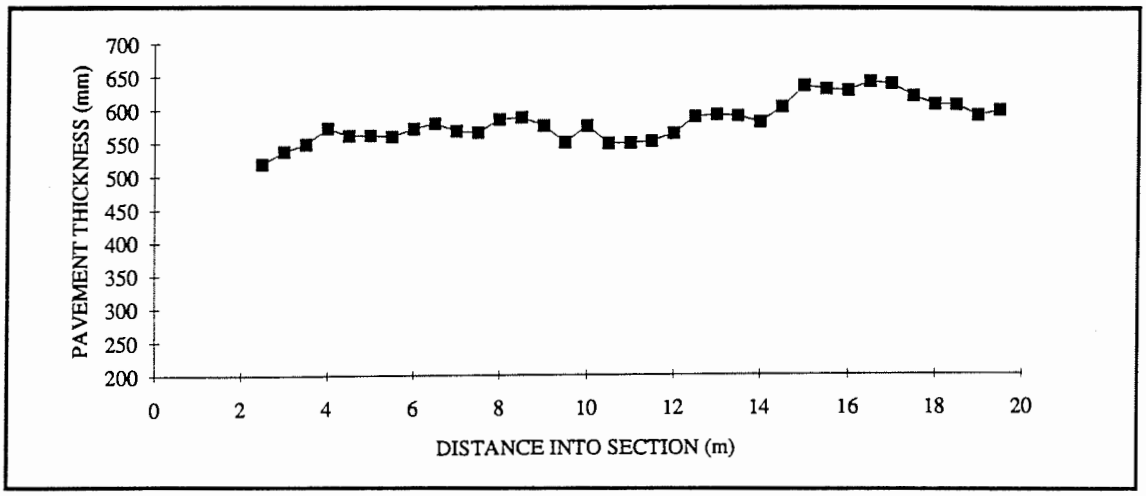

Figure C34 Pavement Thickness - Section D, Instrumented Wheel Path

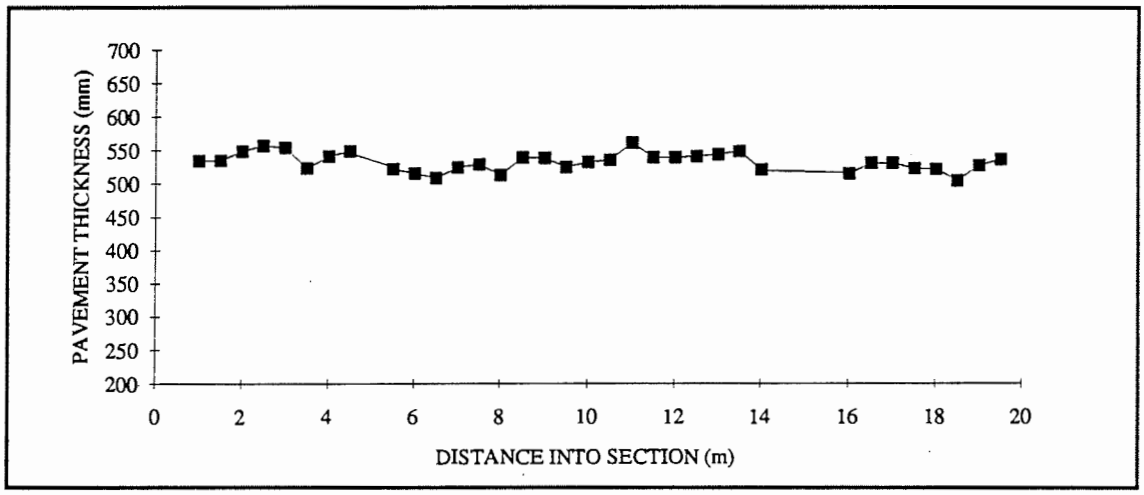

Figure C35 Pavement Thickness - Section E, Instrumented Wheel Path

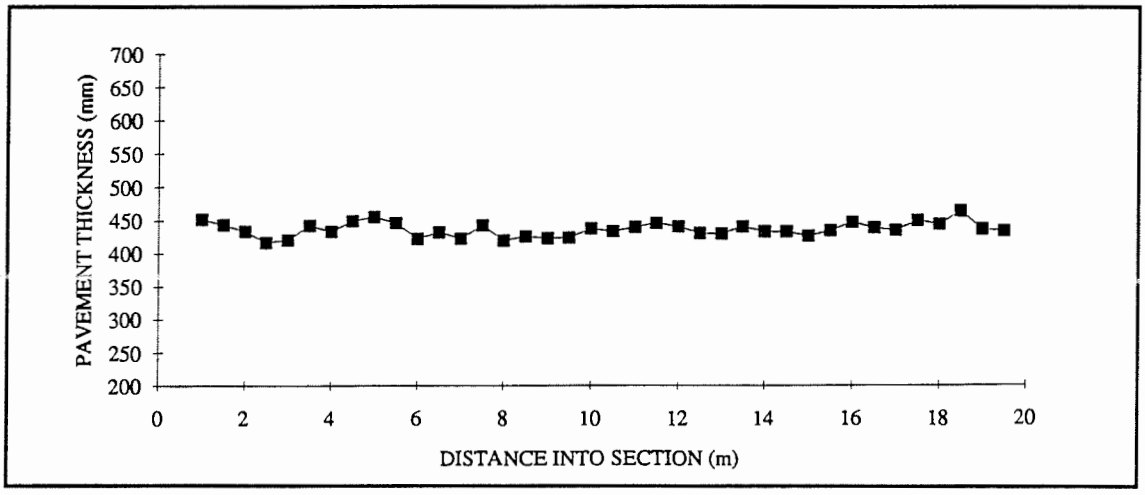

Figure C36 Pavement Thickness - Section F, Instrumented Wheel Path

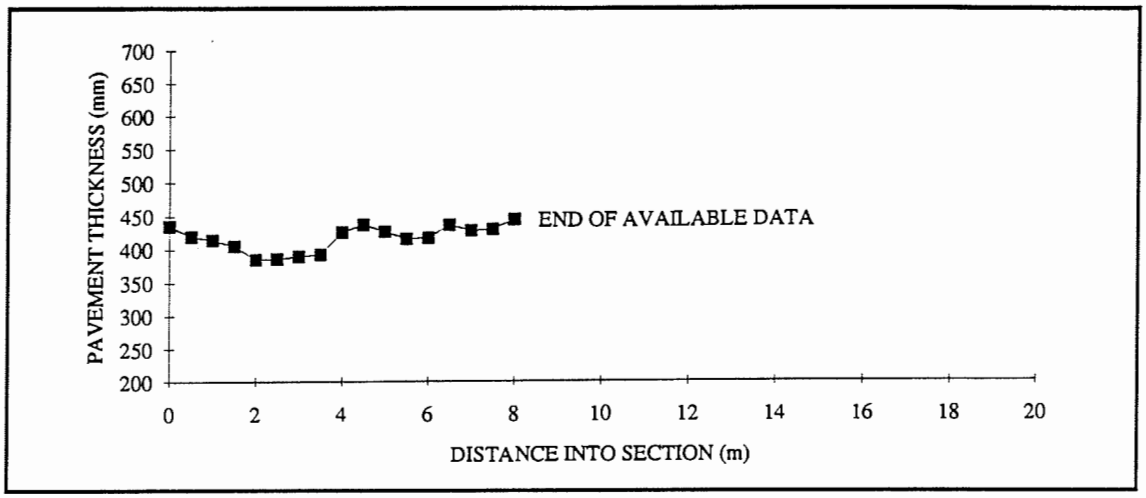

Figure C37 Pavement Thickness - Section H, Instrumented Wheel Path

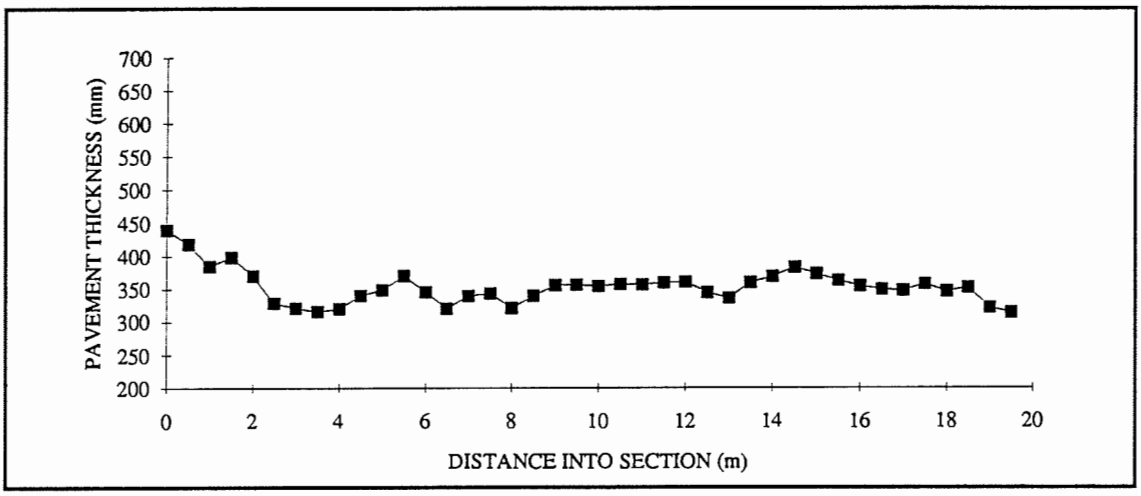

Figure C38 Pavement Thickness - Section I, Instrumented Wheel Path

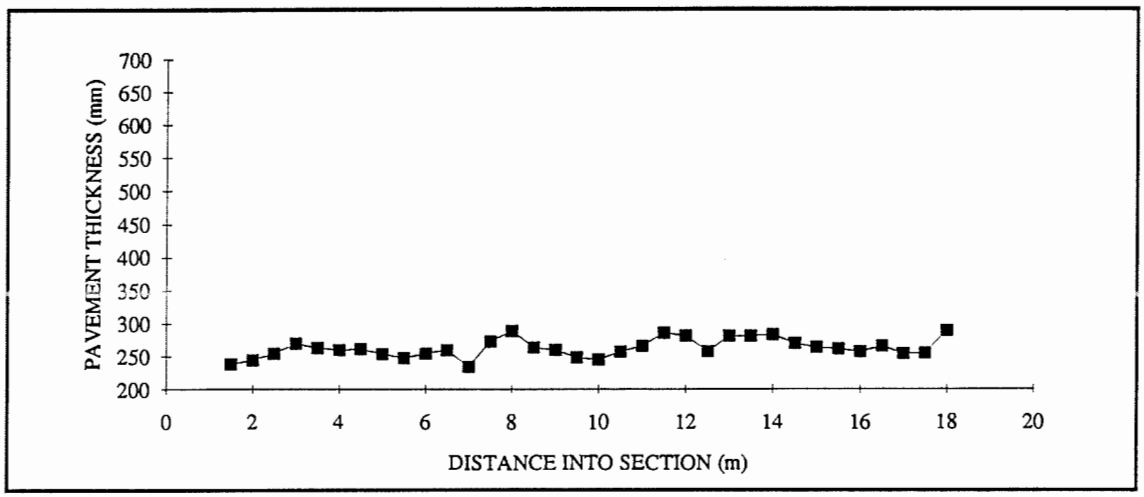

Figure C39 Pavement Thickness - Section J, Instrumented Wheel Path

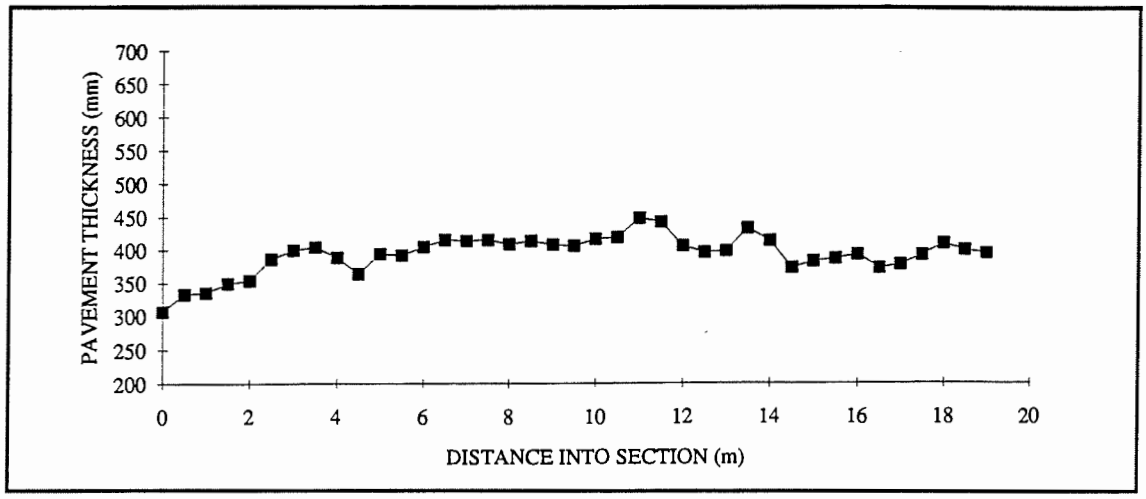

Figure C40 Pavement Thickness - Section K, Instrumented Wheel Path

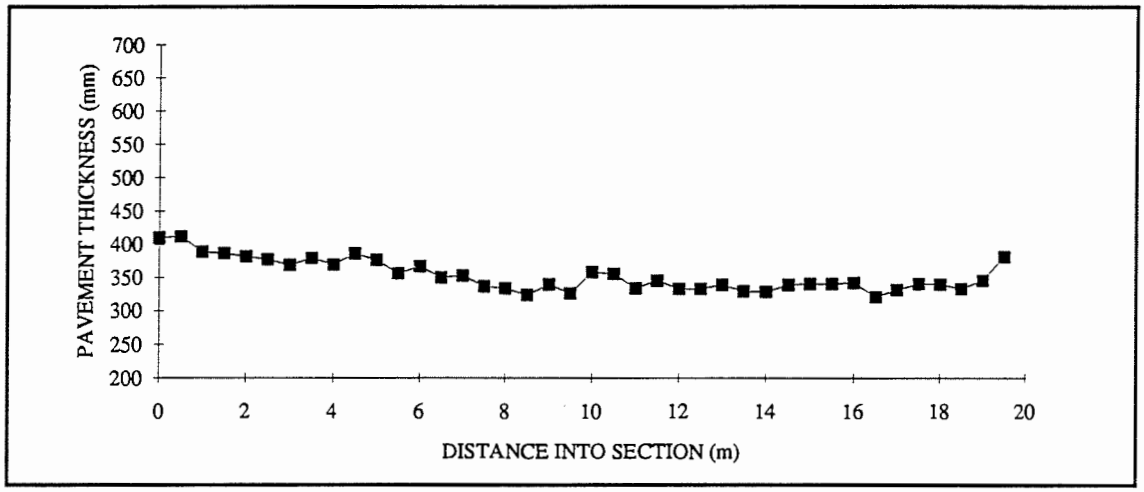

Figure C41 Pavement Thickness - Section L, Instrumented Wheel Path

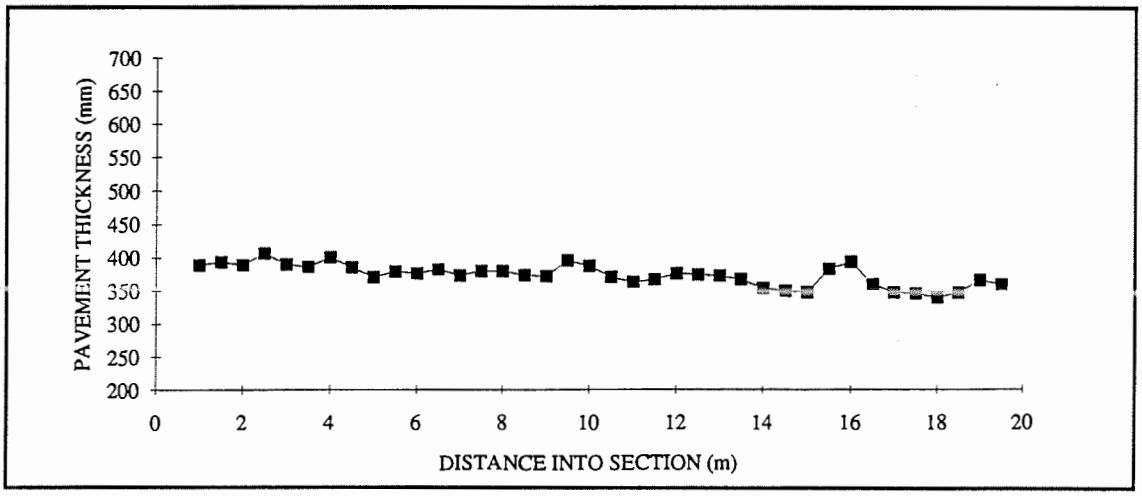

Figure C42 Pavement Thickness - Section M, Instrumented Wheel Path

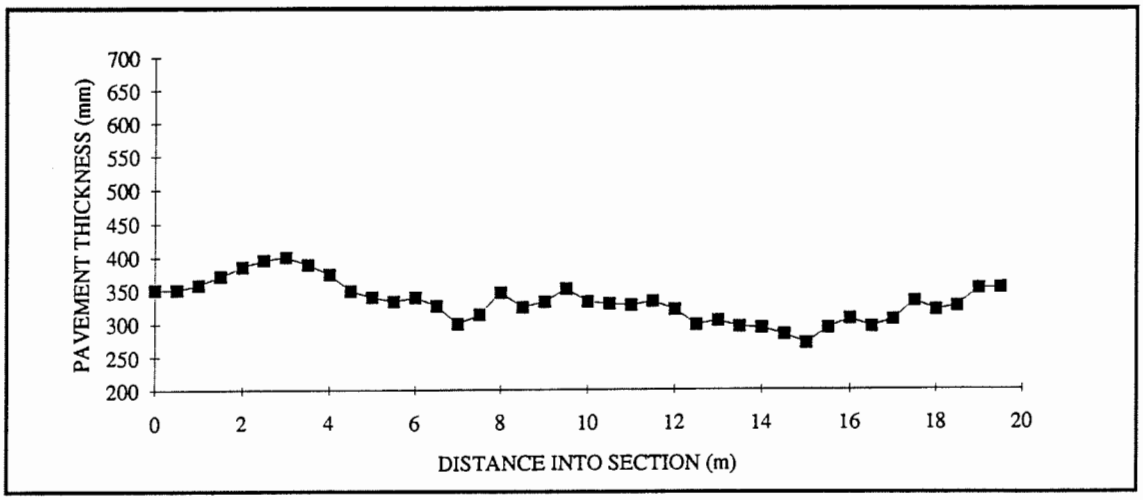

Figure C43 Pavement Thickness - Section N, Instrumented Wheel Path

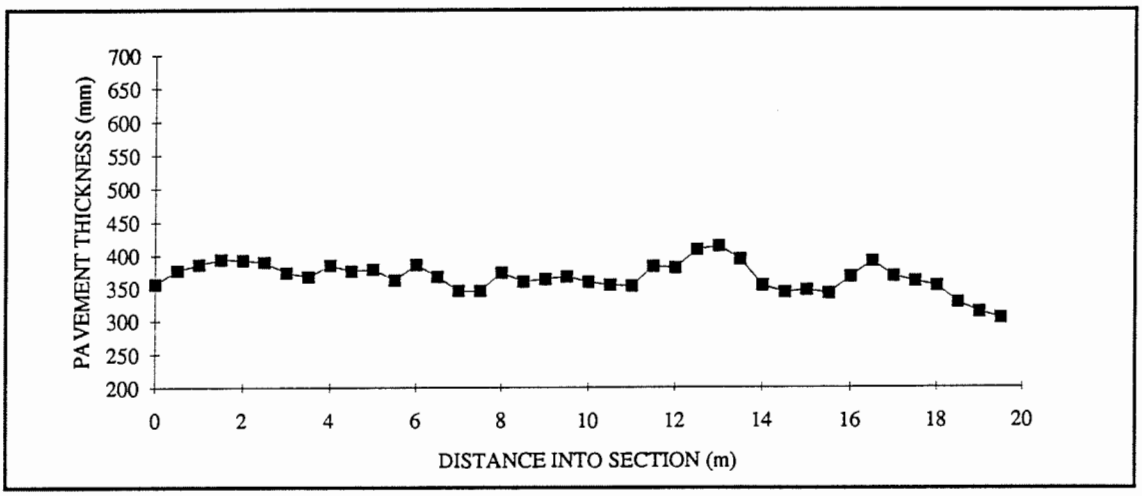

Figure C44 Pavement Thickness - Section O, Instrumented Wheel Path

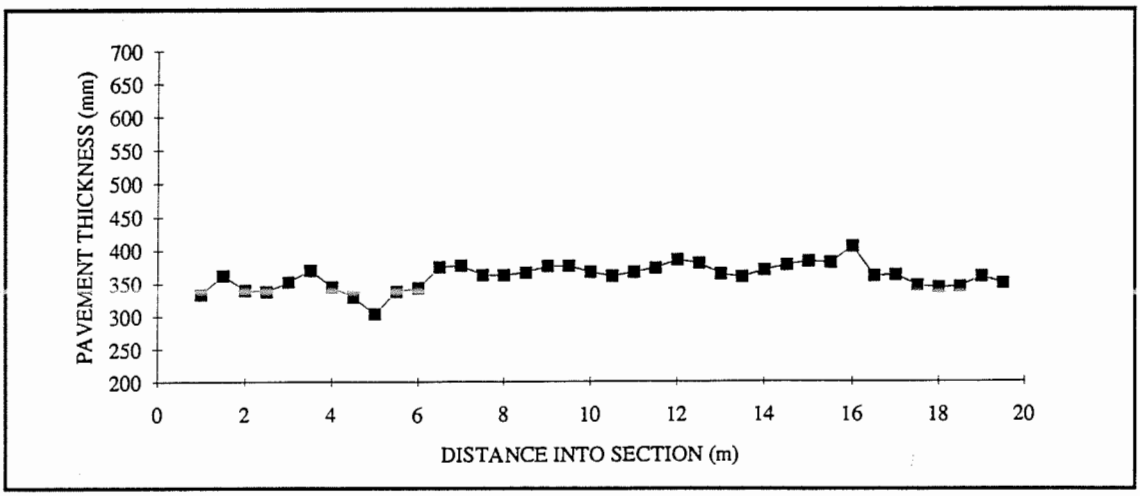

Figure C45 Pavement Thickness - Section P, Instrumented Wheel Path

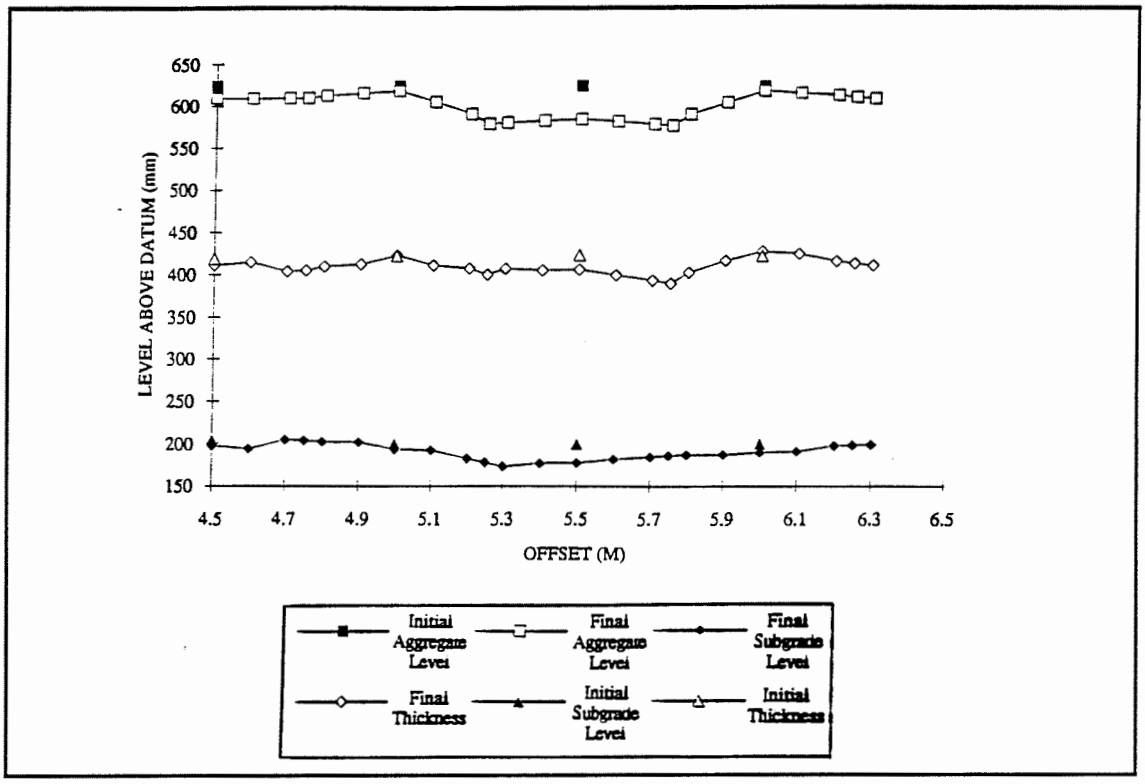

Figure C46 Post-Trafficking Transverse Cross-Section - Section F

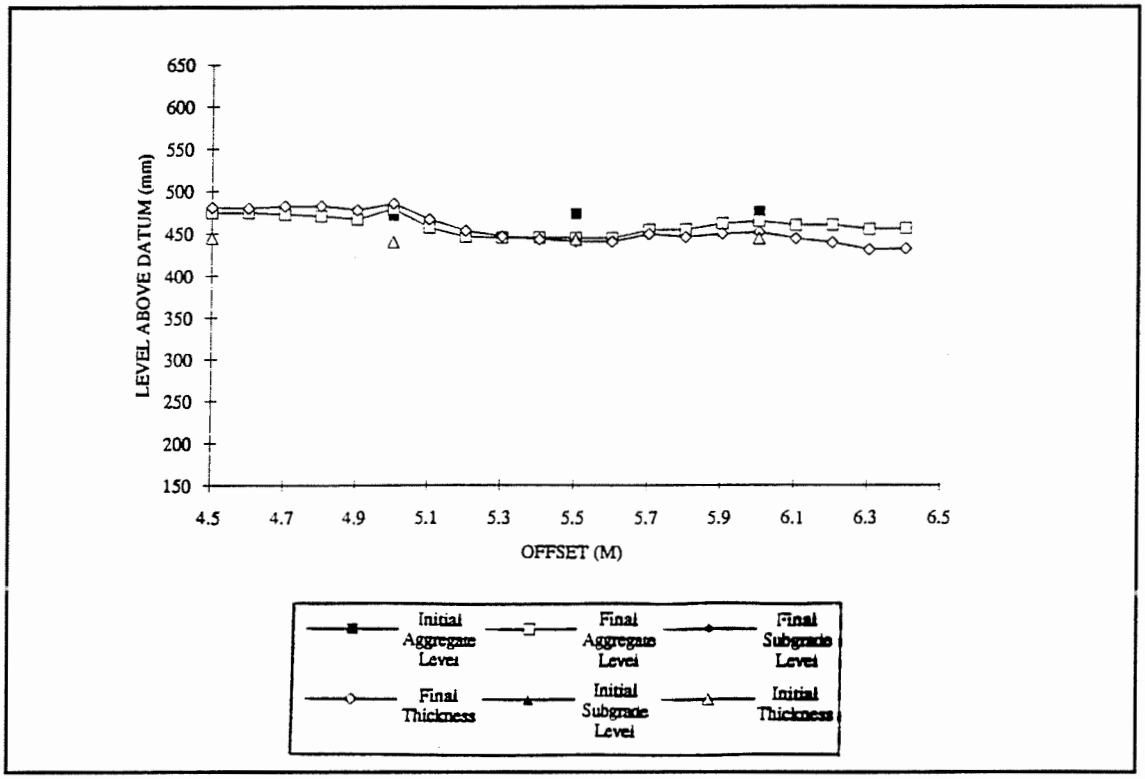

Figure C47 Post-Trafficking Transverse Cross-Section - Section H

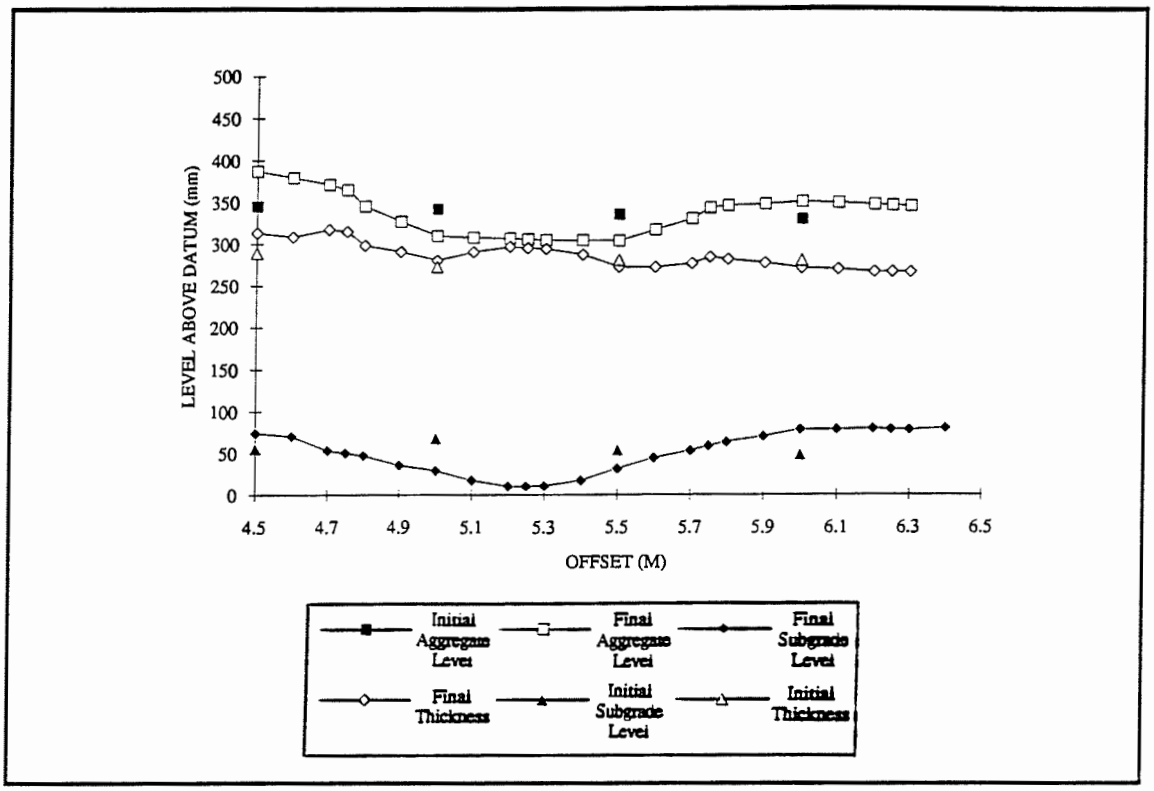

Figure C48 Post-Trafficking Transverse Cross-Section - Section J

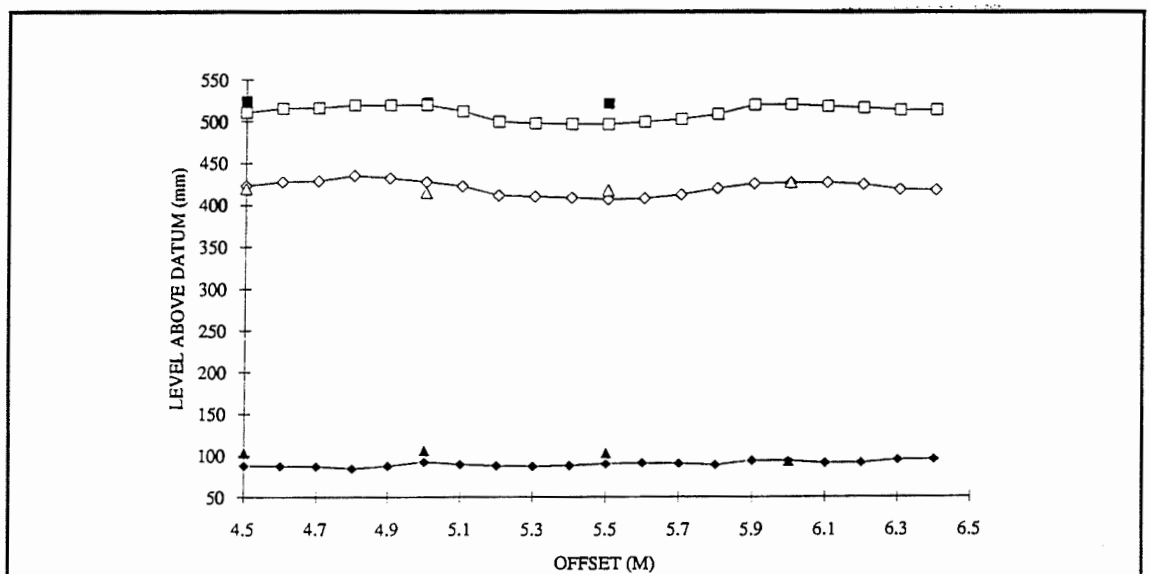

Figure C49 Post-Trafficking Transverse Cross-Section - Section K

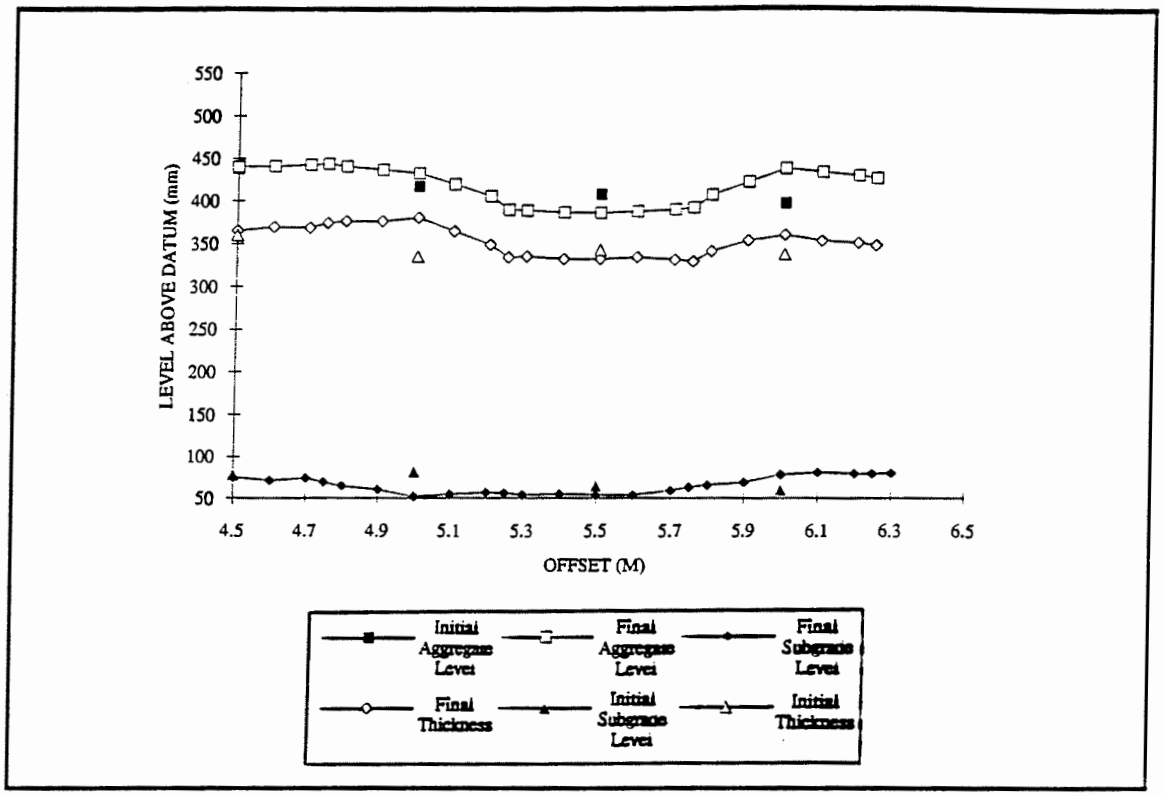

Figure C50 Post-Trafficking Transverse Cross-Section - Section L

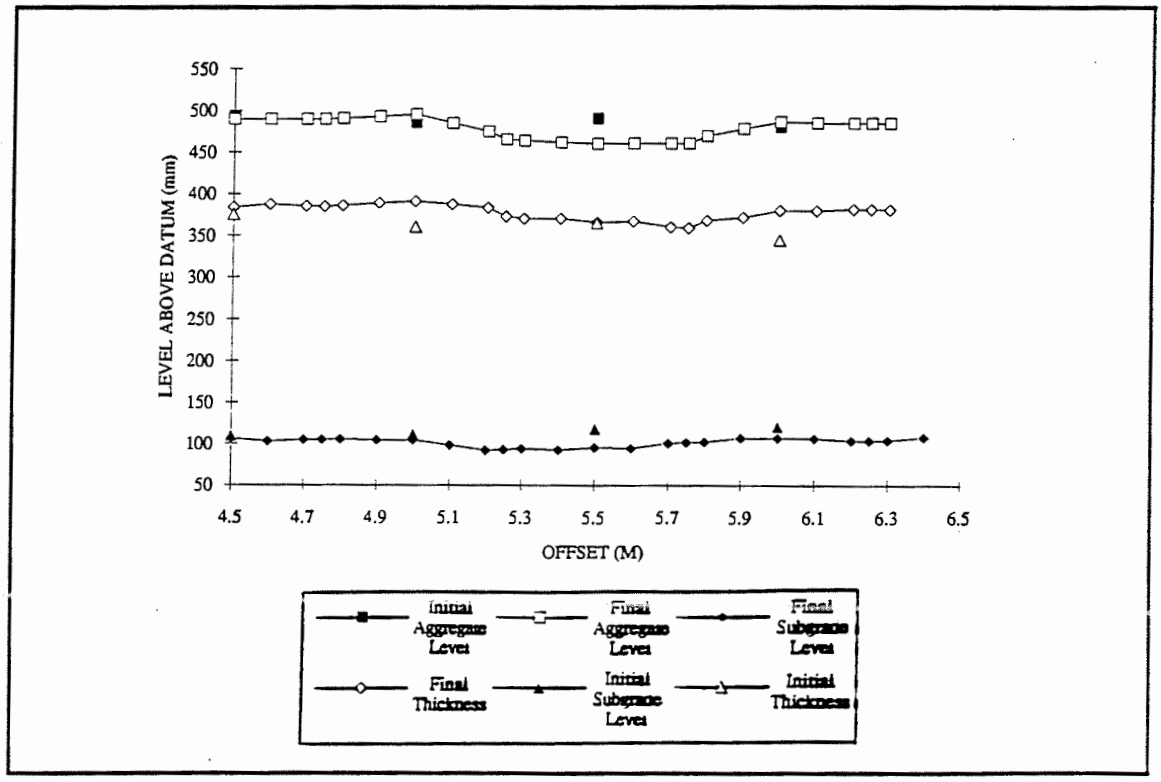

Figure C51 Post-Trafficking Transverse Cross-Section - Section M

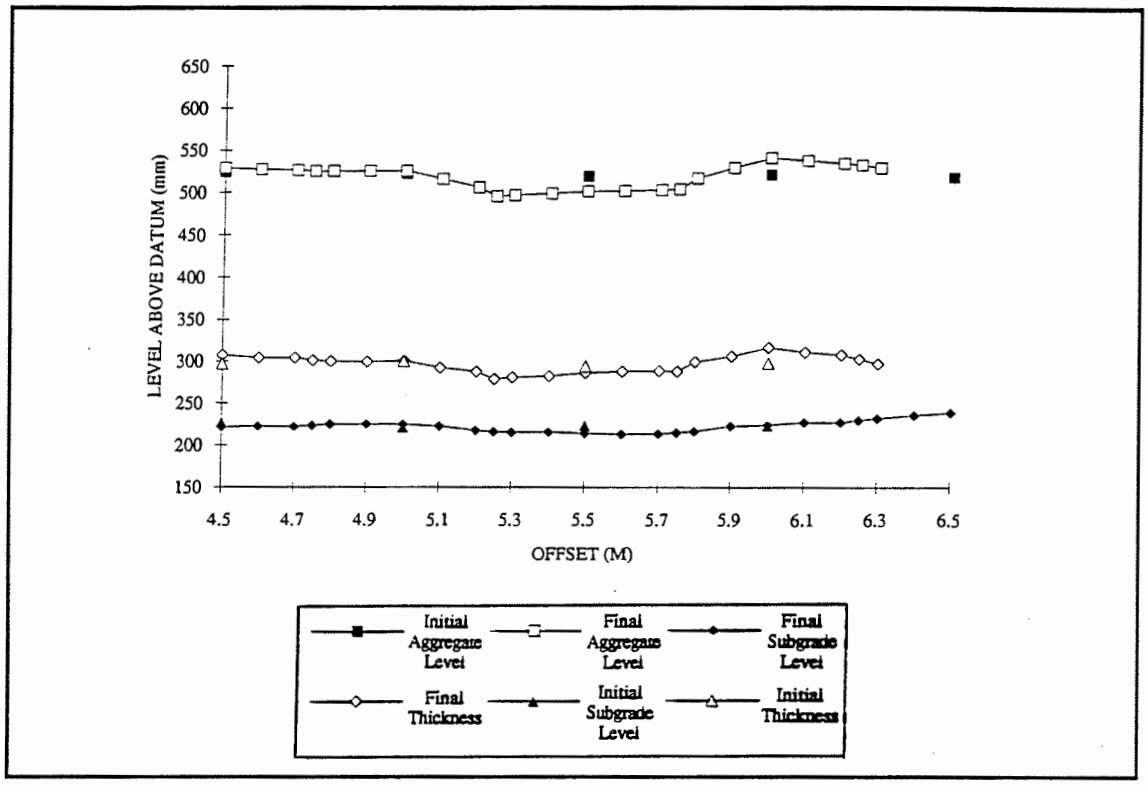

Figure C52 Post-Trafficking Transverse Cross-Section - Section N

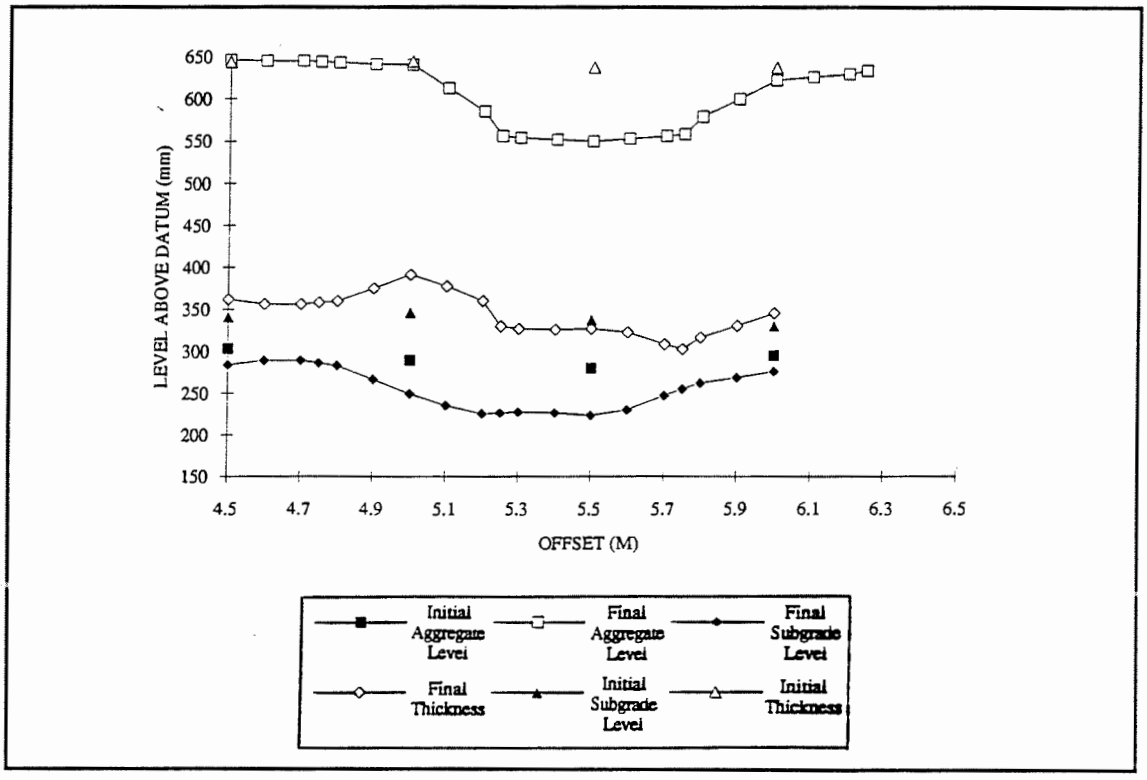

Figure C53 Post-Trafficking Transverse Cross-Section - Section P

APPENDIX D

MISCELLANEOUS TESTING

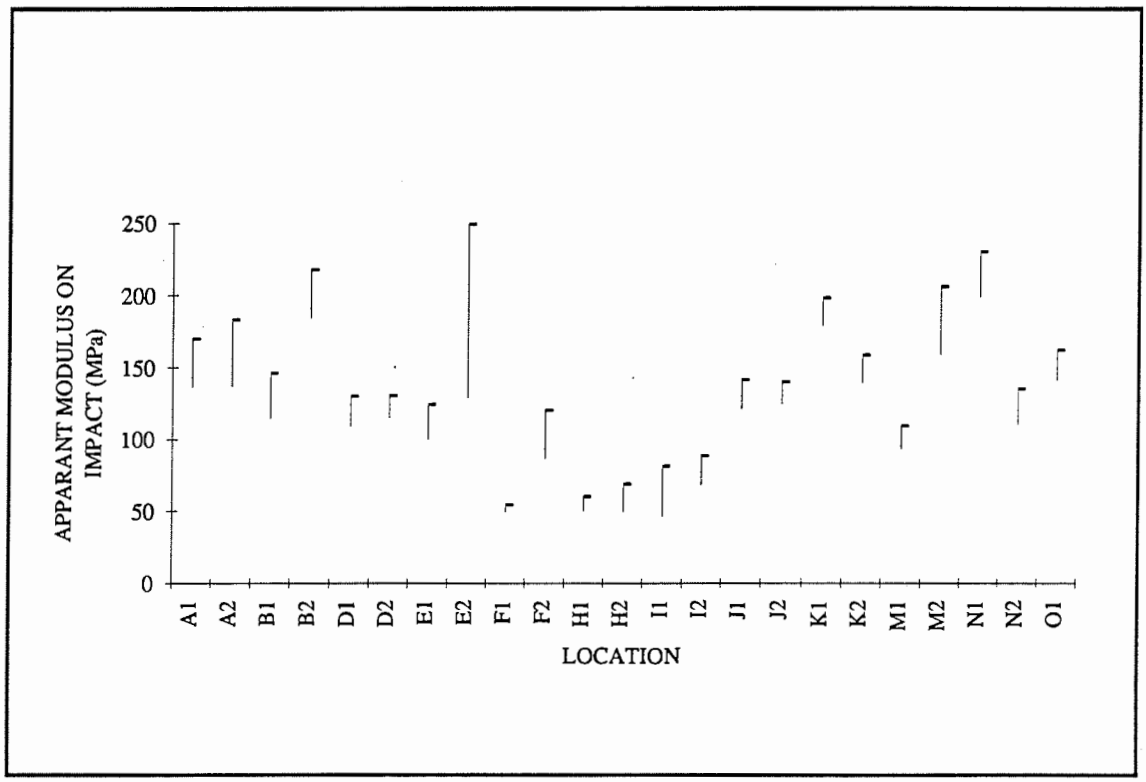

Figure D1 The Range of Results Obtained with the ODIN Device

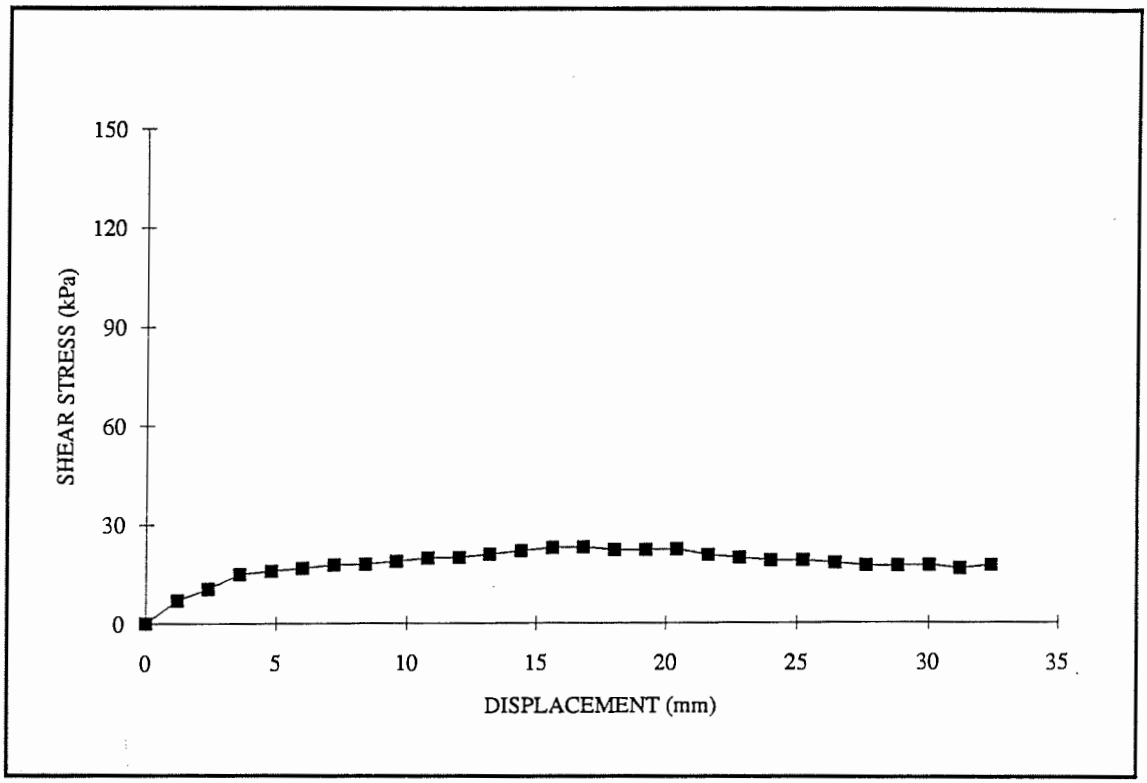

Figure D2 Aggregate/Typar Shear Box Test - Confining Stress 103kPa

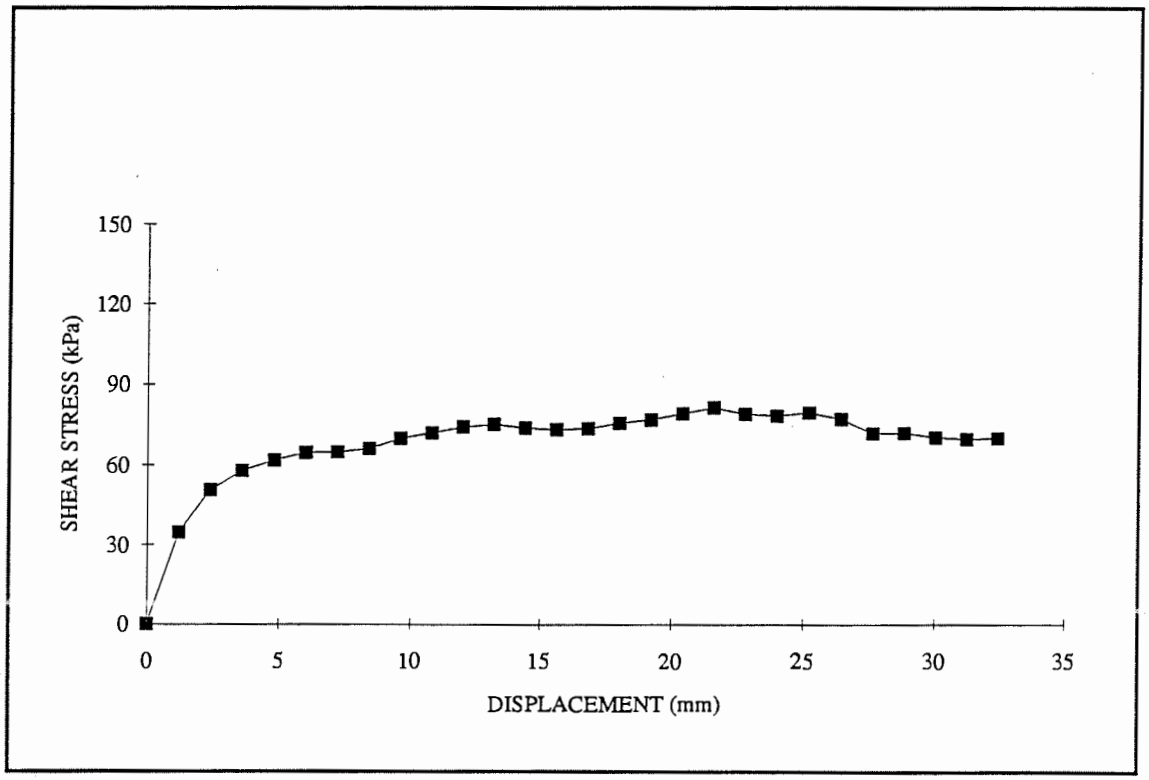

Figure D3 Aggregate/Typar Shear Box Test - Confining Stress 54kPa

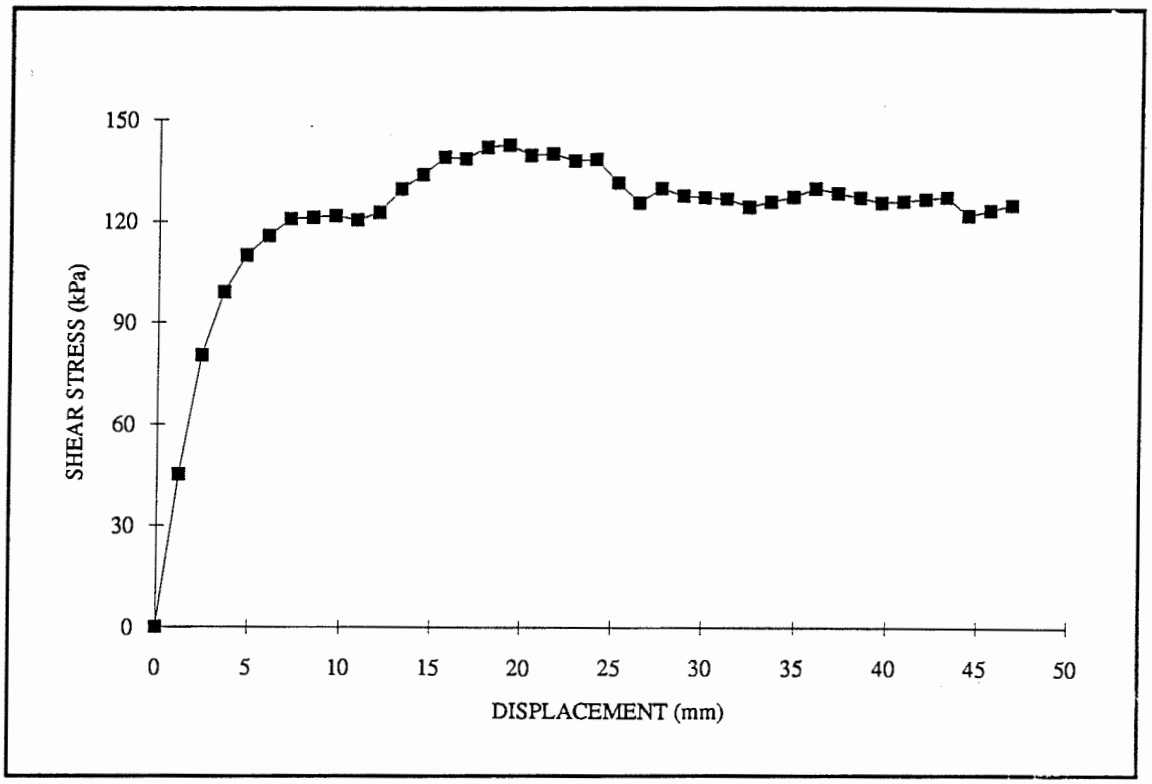

Figure D4 Aggregate/Typar Shear Box Test - Confining Stress 11kPa

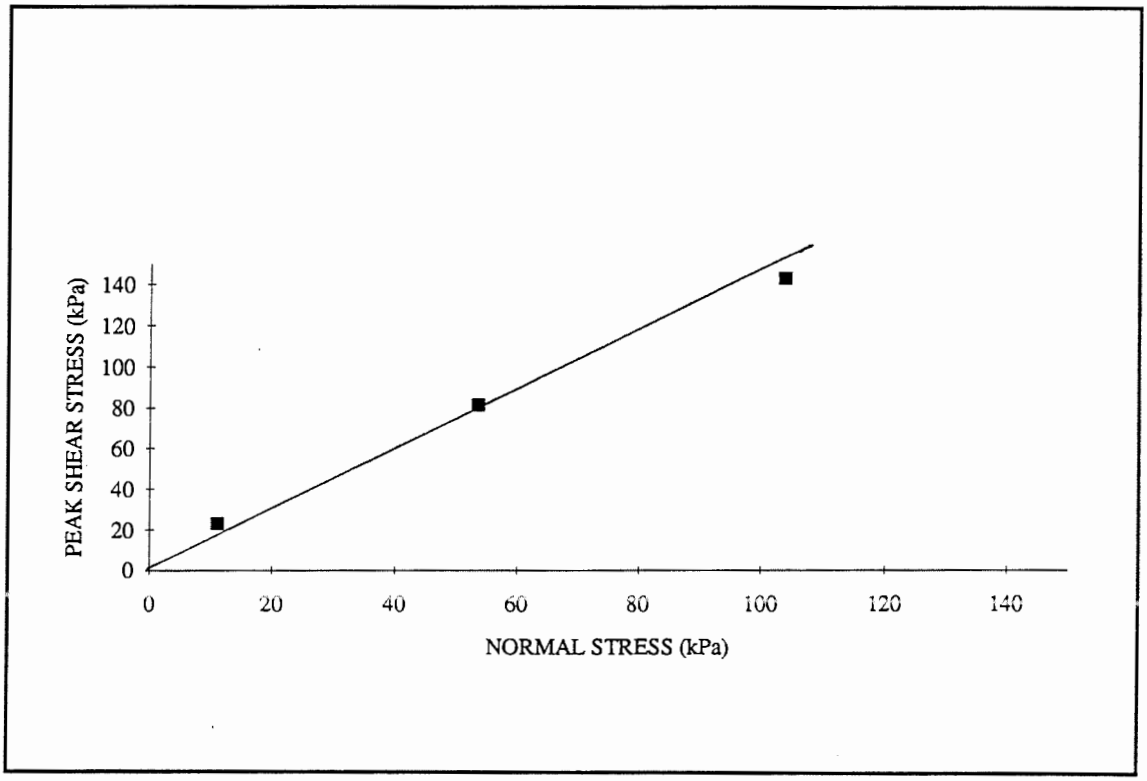

Figure D5 Angle of Frictional Resistance - Aggregate/Typar

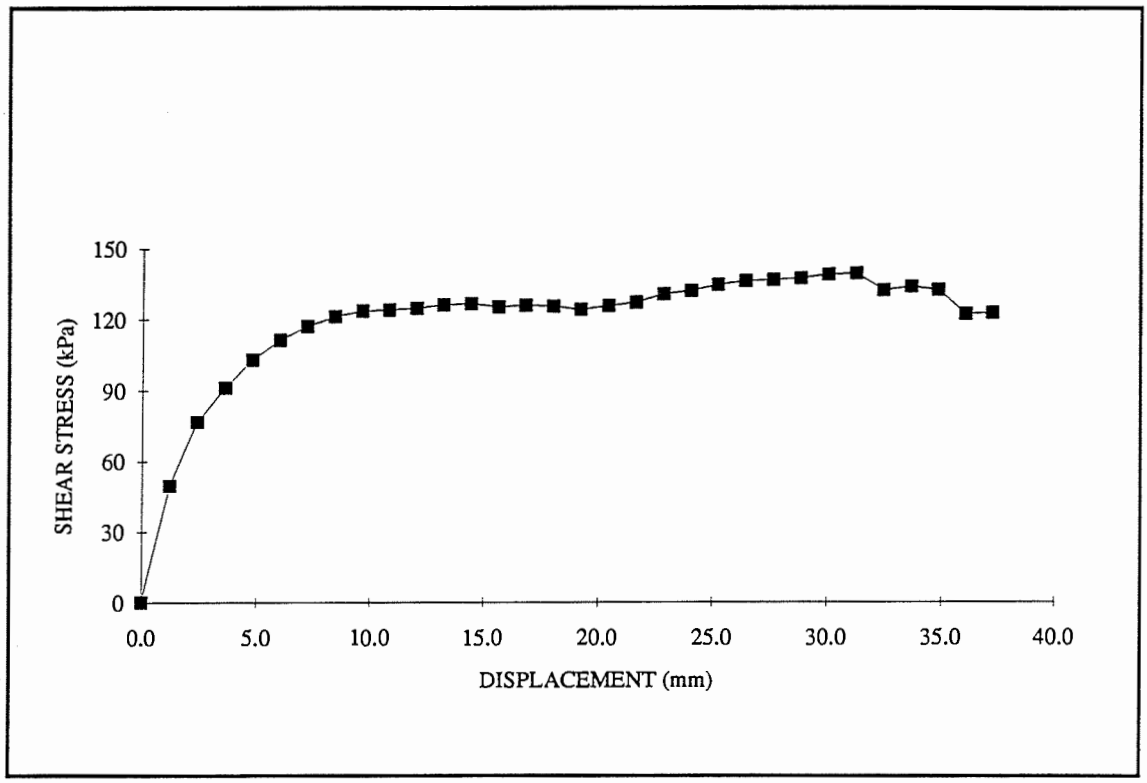

Figure D6 Aggregate/Bidim Shear Box Test - Confining Stress 103kPa

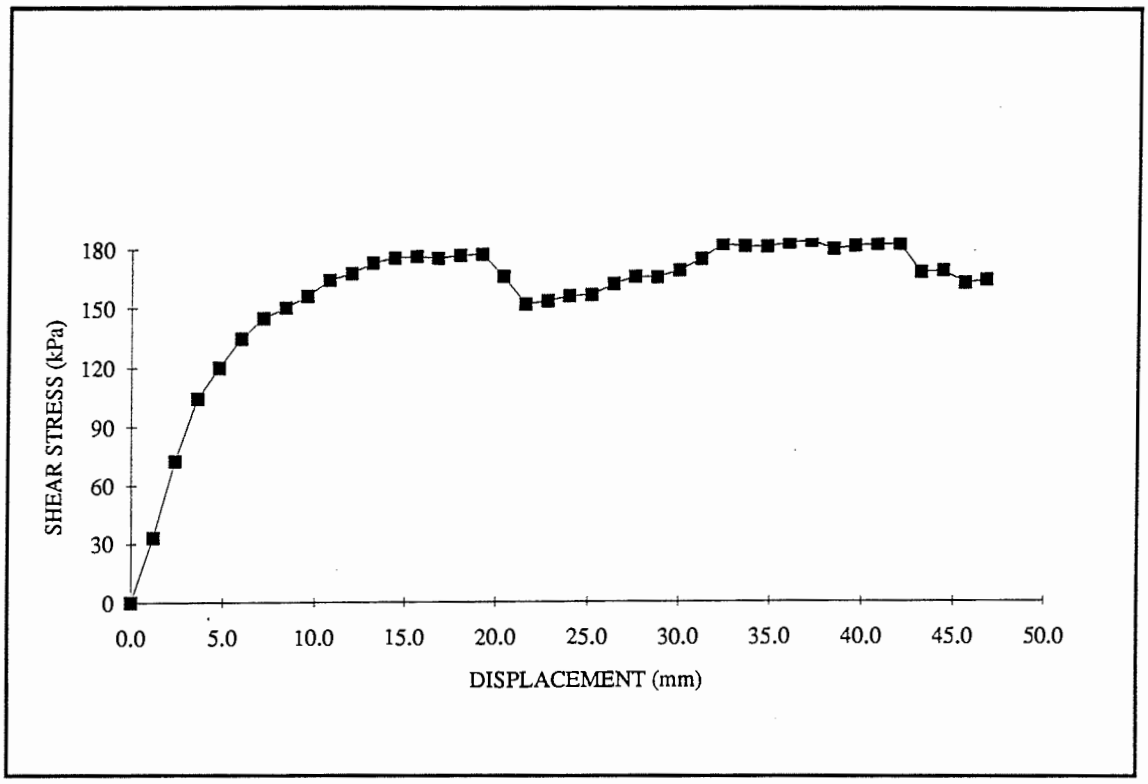

Figure D7 Clay Sheared over Aggregate - Confining Stress 100kPa

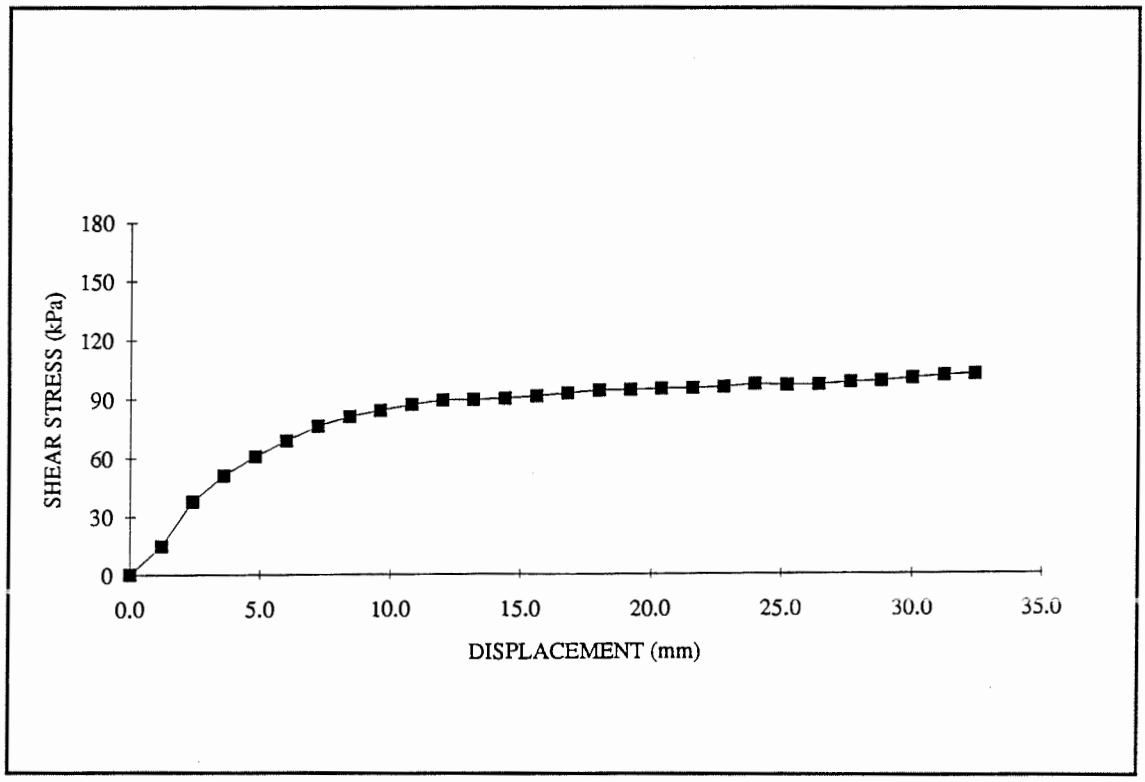

Figure D8 Clay Sheared over Bidim - Confining Stress 100kPa

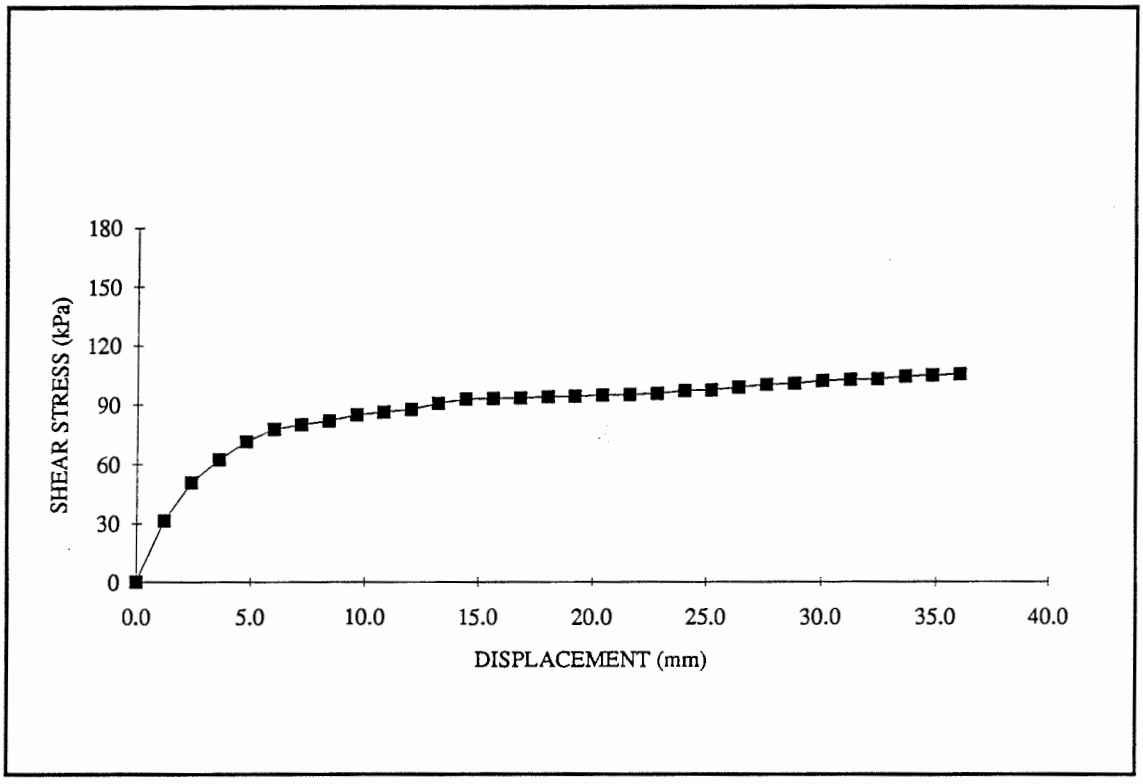

Figure D9 Clay Sheared over Typar - Confining Stress 100kPa

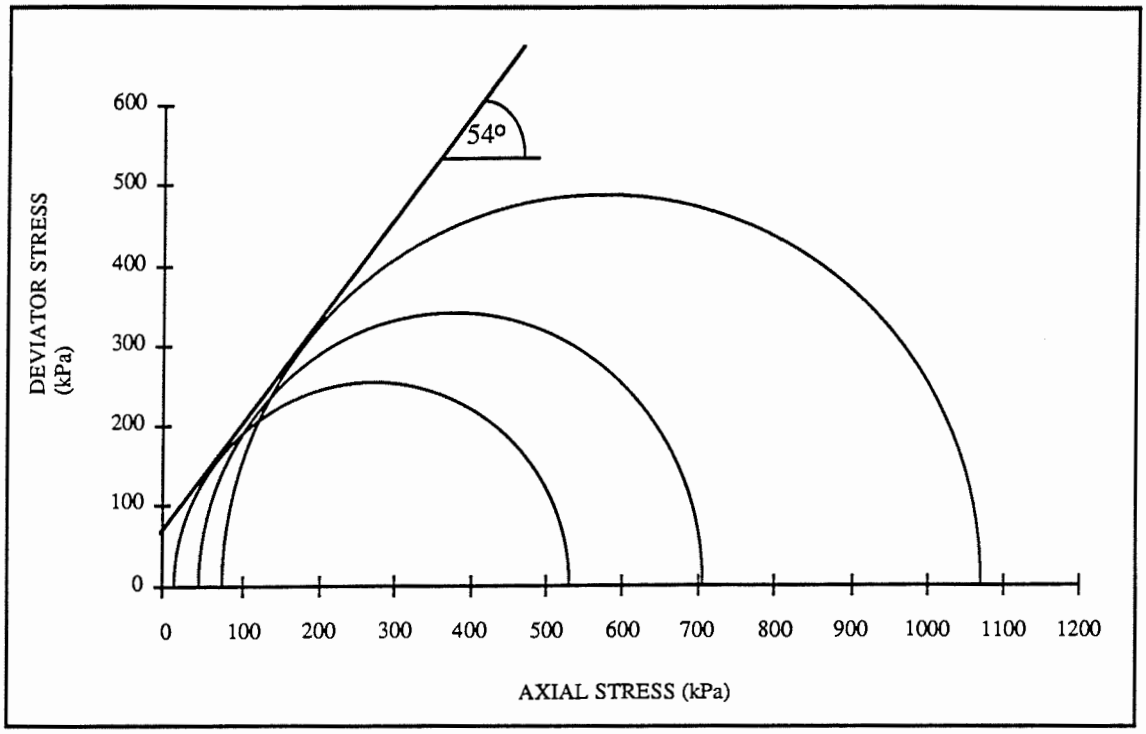

Figure D10 Multi-Stage 280mm Diameter Triaxial Test - Type1 Sample

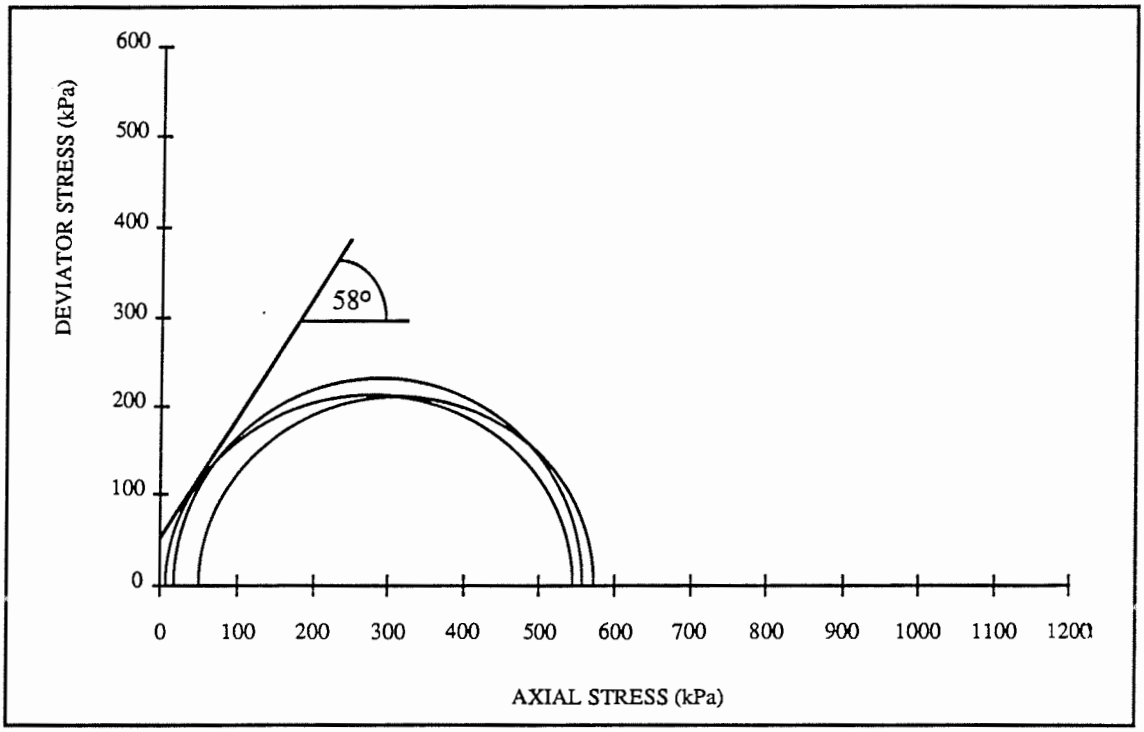

Figure D11 Multi-Stage 280mm Diameter Triaxial Test - Sand and Gravel Sample

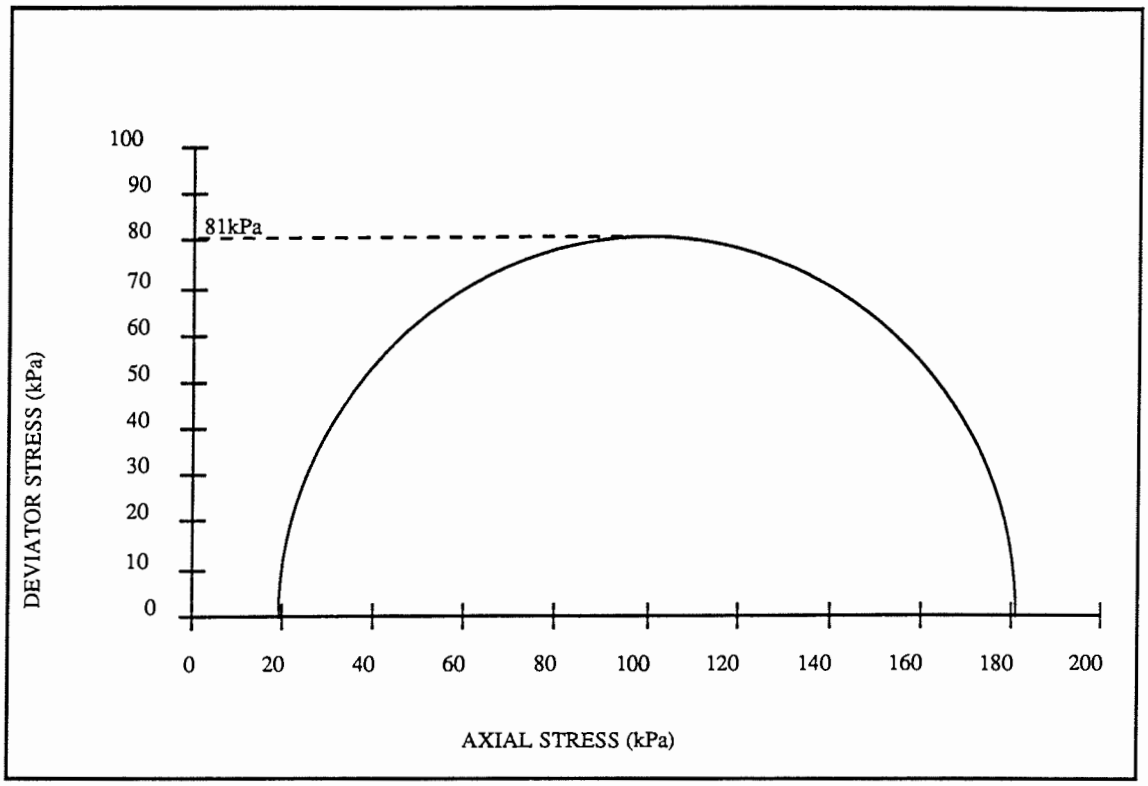

Figure D12 Quick Undrained 76mm Diameter Triaxial Test - Section H

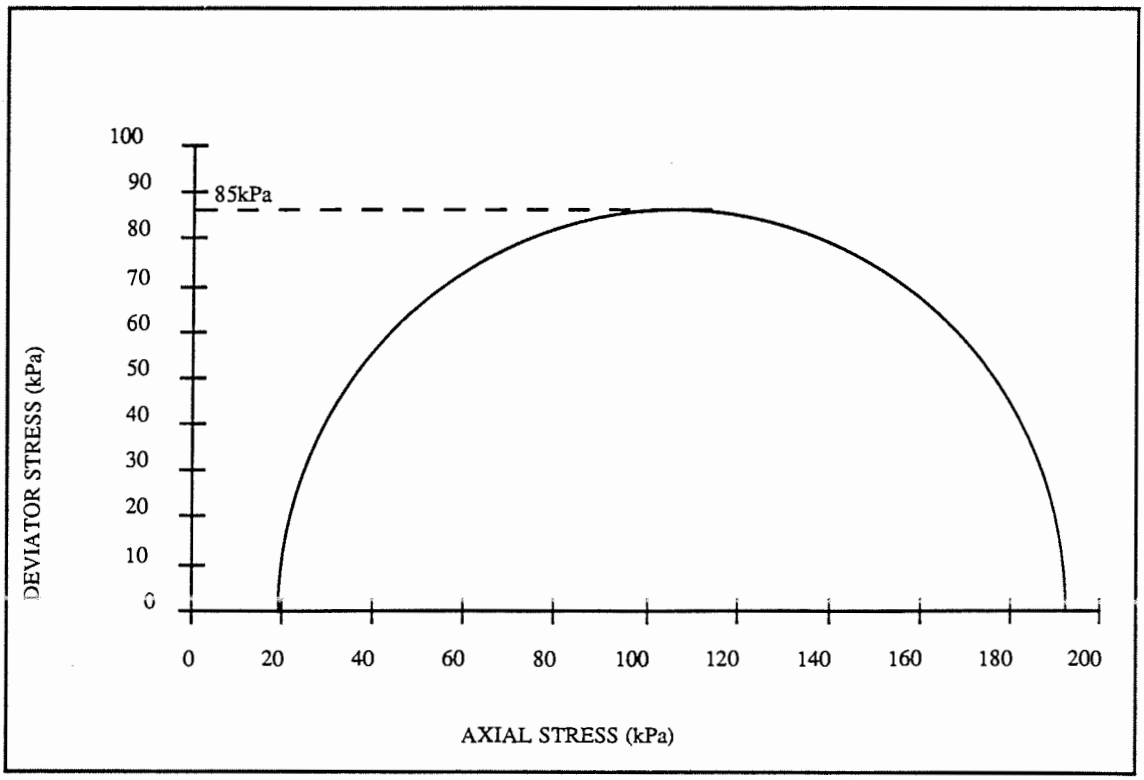

Figure D13 Quick Undrained 76mm Diameter Triaxial Test - Section L

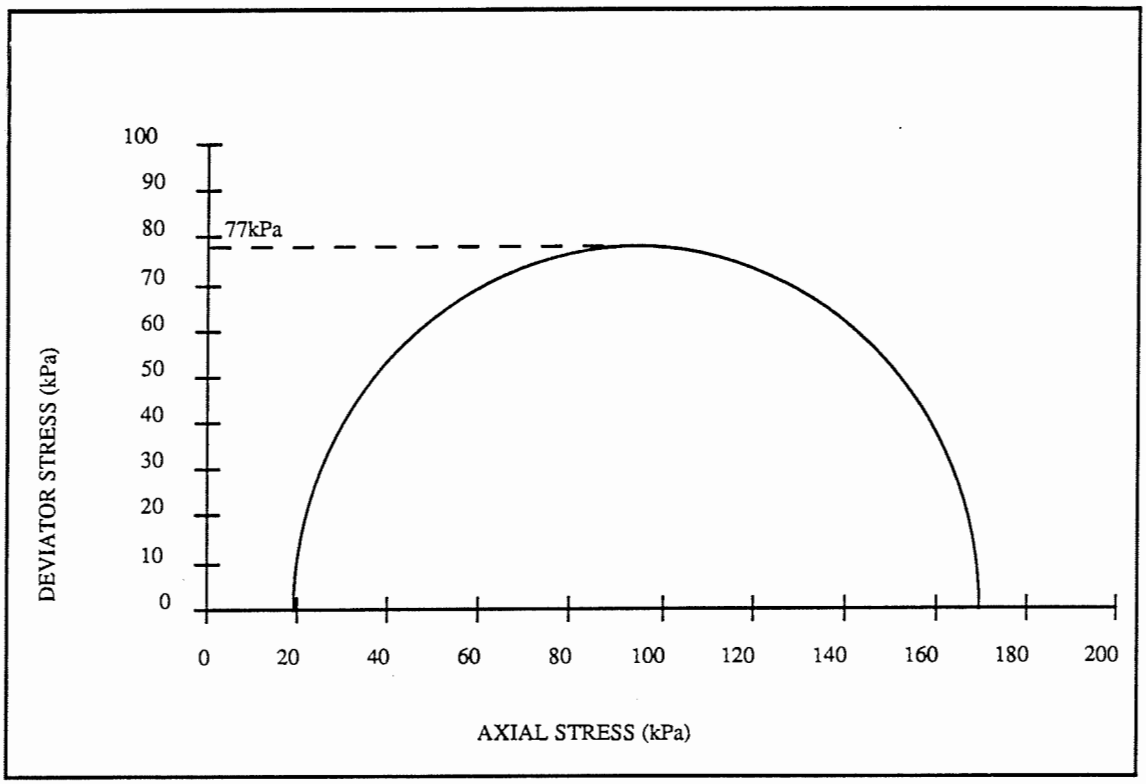

Figure D14 Quick Undrained 76mm Diameter Triaxial Test - Section P

APPENDIX E

INSTRUMENT CALIBRATIONS

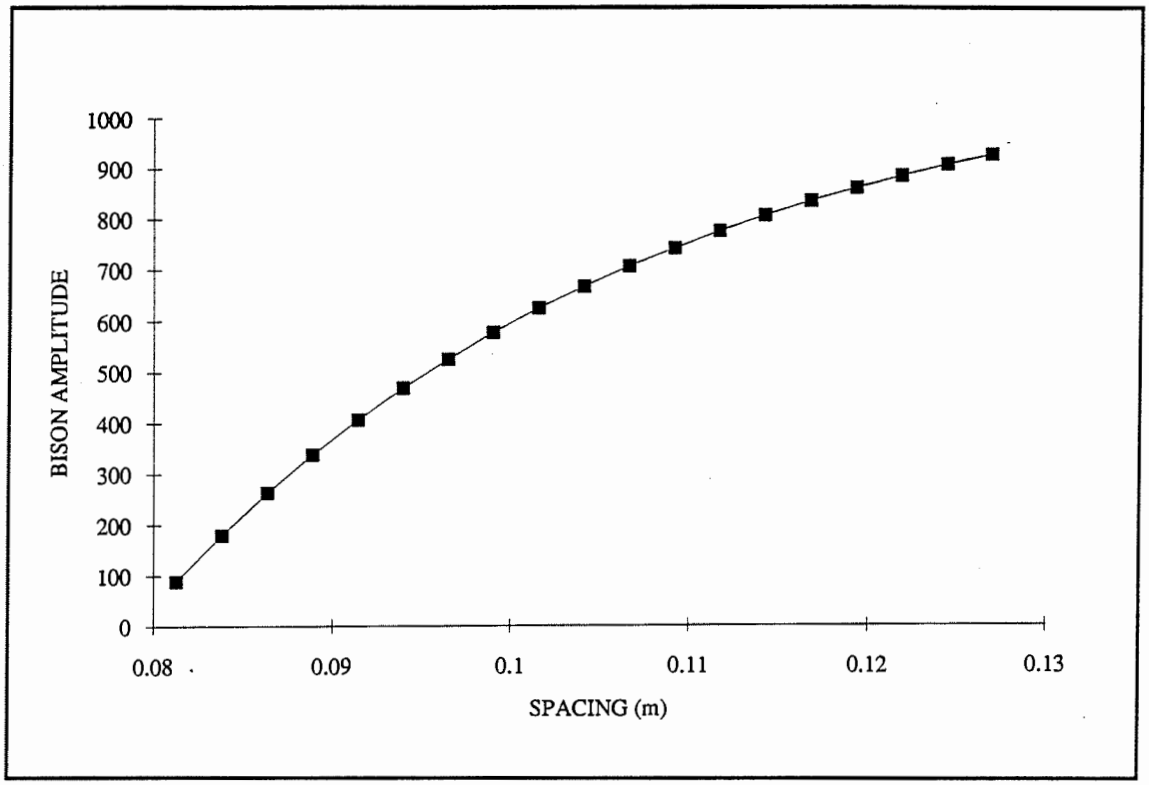

Figure E1 Typical Coaxial Strain Coil Calibration

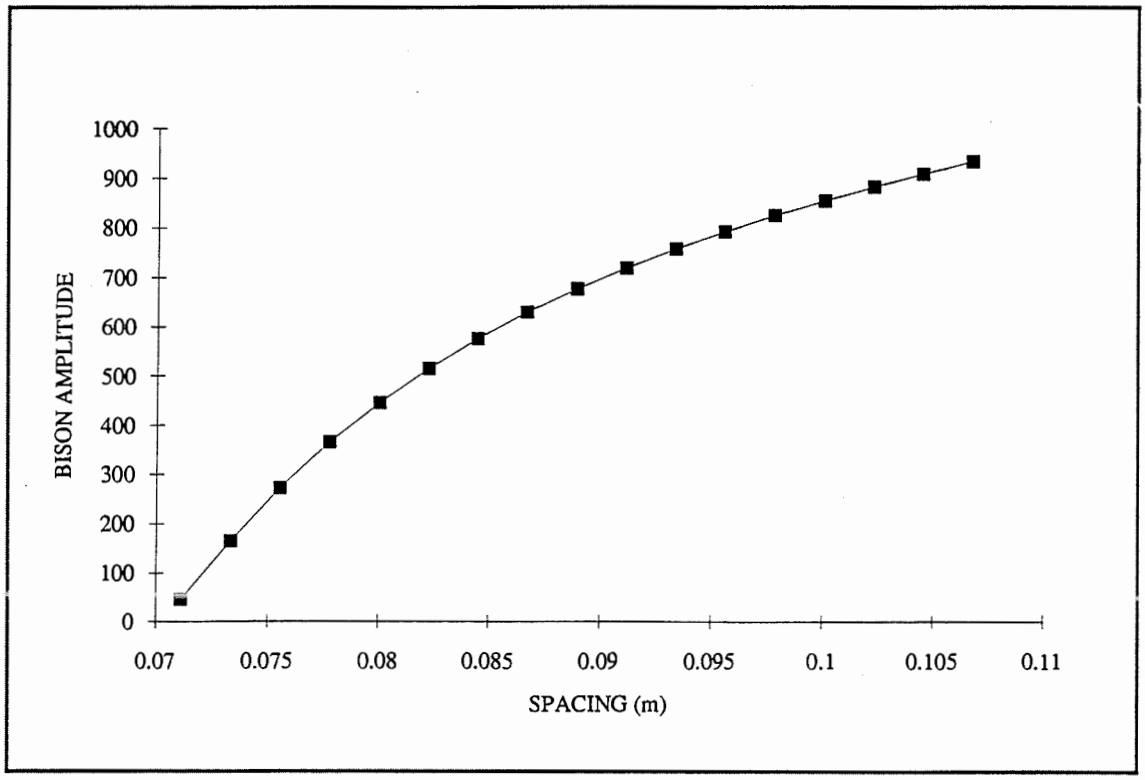

Figure E2 Typical Co-planar Strain Coil Calibration

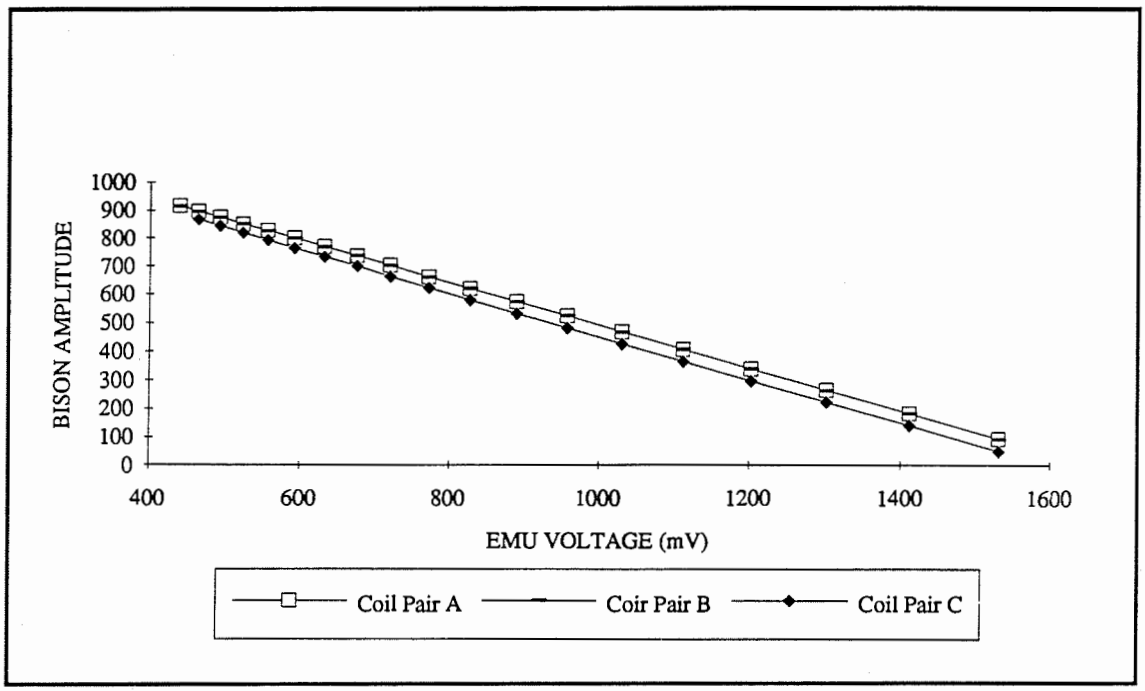

Figure E3 Bison/Emu Static Cross Calibration
Emu reading x 0.737 + 1237 = Bison reading

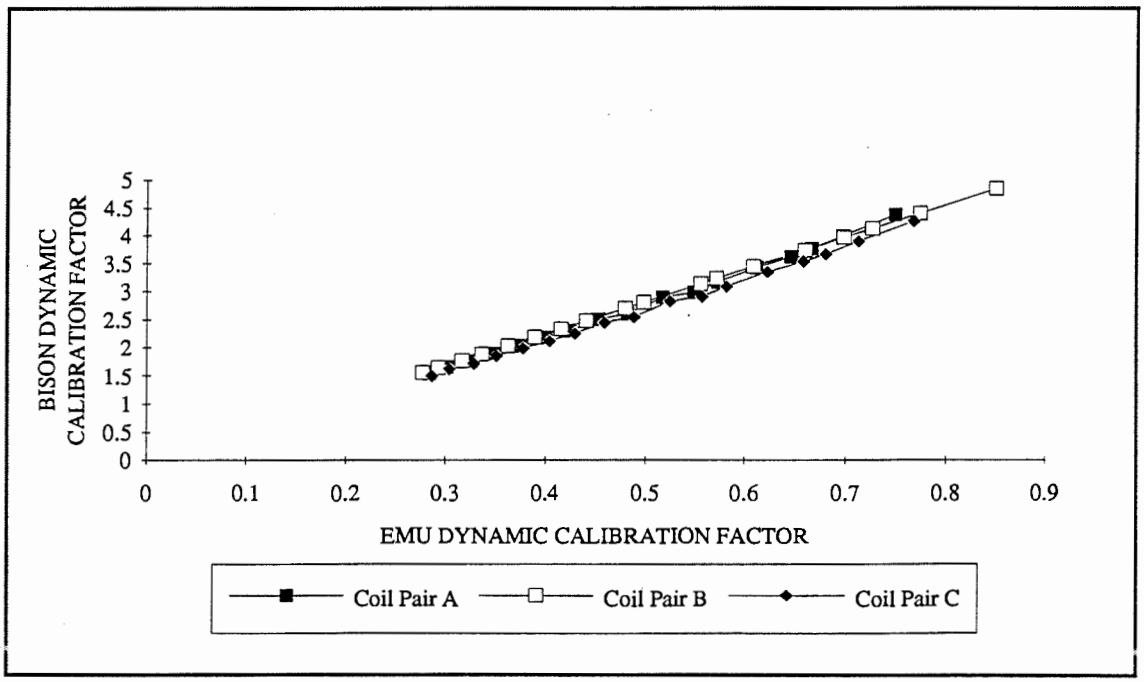

Figure E4 Bison/Emu Dynamic Cross Calibration
Emu reading / 0.17 = Bison reading

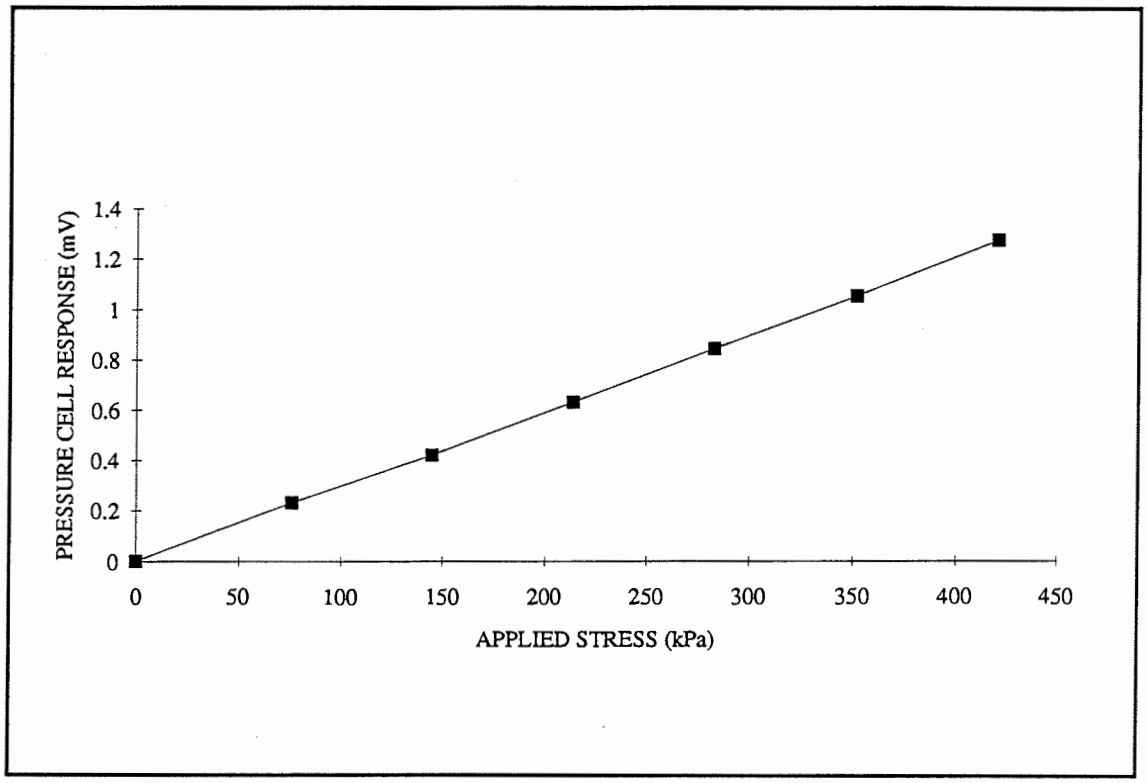

Figure E5 Typical Pressure Cell Calibration

APPENDIX F

SELLMEIJER (1990) DERIVATION OF EQUATIONS AND WORKED EXAMPLE

Derivation of Equation 2.28

From Figure 2.18 it can be seen that:

$$d\tau = \{p - \tan\beta\, p\tan\Phi - q - \gamma h\}\, dx \quad (1)$$

$$dN = \{p\tan\beta + p\tan\Phi\}\, dx \quad (2)$$

$$dT = \{\sec\beta\, (S_u + h\tan\varphi + p\tan\Phi)\}\, dx \quad (3)$$

when Φ is the aggregate/geosynthetic friction angle and φ is the subgrade/geosynthetic friction angle.

If G is the shear modulus of the aggregate under the wheel imposed stress, then it is clear that the relationship between shear force and deflection is given by:

$$\frac{\tau}{h} = G\tan\beta \quad (4)$$

ie $$\frac{d\tau}{dh} = Gh\,\frac{d(\tan\beta)}{dx}$$

If the deflections are small then $\tan\beta = 0$ and $p = \sigma_v$

so re-writing Equations 1to 4

$$\frac{dT}{dx} = S_u + \sigma_v\ (\tan\varphi + \tan\Phi) \quad (5)$$

$$\frac{dN}{dx} = \sigma_v \tan\Phi \quad (6)$$

$$Gh\,\frac{d(\tan\beta)}{dx} = \Delta\sigma_v - q \quad (7)$$

It can be seen that Equation 7 is the deformation equation. However, as $\tan\beta$ is the rate of change of vertical displacement (y) with respect to x, $\frac{dy}{dx}$, then $\frac{d\tan\beta}{dx}$ can be re-written $\frac{d^2y}{dx^2}$.

Thus $Gh\frac{d^2y}{dx^2} = \Delta\sigma_v - q$ (2.28)

Derivation of Equation 2.31

The maximum hoizontal stress can be calculated by examining the Mohr's circle as shown in Figure 2.21.

From Figure 2.21 it can be seen that:

$$x = \sqrt{\left(\frac{T}{h}\right)^2 + \left(\frac{1}{2}\left(\frac{1}{2}\left(\Delta\sigma_v + q\right) - \frac{\sigma_h}{h}\right)\right)^2} \quad (8)$$

$$y = \frac{1}{2}\left(\frac{1}{2}\left(\Delta\sigma_v + q\right) + \frac{\sigma_h}{h}\right) \quad (9)$$

$$\sin\phi = \frac{x}{y} = \frac{\sqrt{4T^2_m + \left(h\frac{1}{2}\left(\sigma_v + q\right) - \sigma_h\right)^2}}{\frac{1}{2}h\left(\Delta\sigma_v + q\right) + \sigma_h} \quad (10)$$

Re-arranging Equation 10 yields:

$$\sigma_h = (\sec^2\phi - \tfrac{1}{2})(\sigma_v+q)h - \sec\phi\sqrt{\{(\sigma_v+q)h\}^2\tan^2\phi - (\Delta\sigma_v{}^2 -)\,(b-W)^2} \quad (2.31)$$

Calculation of Geosynthetic Forces

The geosynthetic force (T) is a maximum under the wheel load and reduces away from it. The force T can be described as:

$T = T_m$ - in Section 3 (10)

$T = T_m + (x - \frac{1}{2}(b-W)\,(S_u+\sigma_v(\tan\varphi + \tan\Phi))$ - in Section 2 (11)

$T = T_m - \frac{1}{2}(b-W)\,(S_u+\sigma_v(\tan\varphi + \tan\Phi)) + x\gamma h\,(\tan\varphi + \tan\Phi)$

- in Section 1 (12)

$$T_m = \sigma_{hmax} - \sigma_h + \tfrac{1}{2}((B-A)-b)\,(S_u + \gamma h \tan\varphi) + \tfrac{1}{2}(b-W)\,(S_u + \sigma_v \tan\varphi) \qquad (13)$$

The length over which T acts is controlled by:

$$\frac{T_m - \tfrac{1}{2}(b - W)\,(S_u + \Delta\sigma_v\,(\tan\phi + \tan\Phi))}{-\,(S_u + \gamma h\,(\tan\phi + \tan\Phi))} \qquad (14)$$

Derivation of the Strain Compatability Equations - after Sellmiejer (1990)

$$\varepsilon_{agg} = \sigma_v h - \frac{(1 - \nu)\sigma_h}{2Gh} \qquad (15)$$

$$2Ghu = \int_0^{\frac{B}{2}} \nu\sigma_v h\,dx - \int_0^{\frac{B}{2}} (1 - \nu)\sigma_h\,dx \qquad (16)$$

$$\int_0^{\frac{B}{2}} \sigma_v h\,dx = \nu h \left(\frac{B}{4}\gamma h + Wq\right) \qquad (17)$$

$$(1-\nu)\int_0^{\frac{B}{2}} (1-\nu)\left[\tfrac{1}{8}\{(B-A-W)^2 + (A-W)^2\}\sigma_v \tan\Phi - \tfrac{1}{2}B\sigma_{hmax} - \tfrac{1}{8}\{(B-A-b)^2 + (A-b)^2\}\,(\sigma_v - \gamma h)\tan\Phi\right] \qquad (18)$$

Therefore:

$$2Ghu = \nu h\left(\frac{B}{4}\gamma h + Wq\right) + \left[\tfrac{1}{8}\{(B-A-W)^2 + (A-W)^2\}\sigma_v \tan\Phi - \tfrac{1}{2}B\sigma_{hmax} - \tfrac{1}{8}\{(B-A-b)^2 + (A-b)^2\}\,(\sigma_v - \gamma h)\tan\Phi\right] \qquad (19)$$

$$\varepsilon_{geosynthetic} = \frac{T}{E}$$

$$Eu = \int T\,dx \qquad (20)$$

$$Eu = \tfrac{1}{2}BT_{max} - \tfrac{1}{8}\{(B-A-W)^2 + (A-W)^2\}\ \{S_u + \sigma_v(\tan\Phi + \tan\varphi)\}$$

$$+ \tfrac{1}{8}\{B-A-b)^2 + (A-b)2\}\ (\sigma_v - \gamma h)\ (\tan\Phi + \tan\varphi) \qquad (21)$$

Equating Equations 19 and 21 the elongation, u, required can be calculated, and hence E.

EXAMPLE CALCULATION - AFTER SELLMIEJER (1990)

Assumptions

The aggregate/geosynthetic friction angle, Φ	$=45°$
The subgrade/geosynthetic friction angle, φ,	$=0°$
The angle of internal aggregate friction, ϕ,	$=45°$
Poissons ratio	$= 0.35$
Road width, B,	$= 45m$
Distance between the wheels, A,	$= 1.9m$
W	$= 0.32$
q	$= 500kPa$
S_u	$= 45kPa$
h	$= 0.4m$
γ	$= 21kN/m^3$
G	$= 35MPa$
$\sigma_v = (2 + \pi)\ S_u$	$= 231kPa$

and therefore the width of the subgrade mobilising plastic bearing capacity,

$$b = \frac{Wq}{\Delta\sigma_v} = 0.693m$$

Deflection

The deflections under the wheel load $\Delta w = (b-W)^2 \frac{q}{8Gh} \frac{\Delta\sigma_v}{q - \Delta\sigma_v} = 0.5mm$ (2.30)

Aggregate Stresses

$$\sigma_h = \frac{1}{2}(b - W)\,\Delta\sigma_v \tan\Phi + \frac{1}{2}\gamma h^2 \frac{1+\sin\phi}{1-\sin\phi} \qquad (2.32)$$

= 52.87kPa (maximum permissible horizontal aggregate force, controlled by passive failure.)

or $\sigma_{hmax} = (\sec^2\phi$ -\f(1,2)) $(\Delta\sigma_v+q)h - \sec\phi$ \r(\b{ $\Delta\sigma_v+ q\ h$}$0^2 \tan^2\phi - (\sigma_v-\gamma h)^2$ $(b-W)^2)) = 42.16$kPa (actual) (2.31)

$$\sigma_h = \frac{\nu}{(1-\nu)}\gamma h = 4.52\text{kPa}$$

Equation 2.31 suggests that the horizontal forces should decay to σ_h in Section 1. However, in this case $\Delta\sigma_v$ is large (due to the high shear strength) and thus the forces will decay to σ_h at a piont in Section 2.

$$\sigma_{hmax} - \sigma_h - x\,\Delta\sigma_v \tan\Phi = 0$$

$$x = 0.16$$

And thus the length of geosynthetic required to dissipate these forces, $\frac{1}{2}(B-A)_{new}$ is:

$$\frac{1}{2}(B-A)_{new} = \frac{W}{2} + x = 0.32\text{m}.$$

Geosynthetic Stresses

$$T_m = \sigma_{hmax} - \sigma_h + \frac{1}{2}((B-A)-b)\,(S_u + \gamma h\tan\varphi) + \frac{1}{2}(b-W)\,(S_u+\Delta\sigma_v\tan\varphi) \qquad (13)$$

But $\varphi = o$ and $\frac{1}{2}(B-A)_{new} - b = 0$ as the geosynthetic stops working in Section 2. Furthermore, as the term $\frac{1}{2}(b-W)$ relates to section 2 it should be replaced by x and so

$$T_m = \sigma_{hmax} - \sigma_h + xS_u = 44.84\text{kN/m}.$$

These geosynthetic stresses dissipate over the length, A, $= \frac{W}{2} + x$

where x is 0.16m

Strain Compatibility

By Equating 19 and 21 as shown below

$$\frac{2Gh}{E}\{(B\text{-}A\text{-}W)^2 + (A\text{-}W)^2\}\{S_u + \Delta\sigma_v(\tan\Phi + \tan\varphi)\} + \frac{1}{8}\{B\text{-}A\text{-}b)^2 + (A\text{-}b)^2\}(\Delta\sigma_v - \gamma h)(\tan\Phi + \tan\varphi)$$

$$= vh\left(\frac{B}{4}\gamma h + Wq\right) + \left[\frac{1}{8}\{(B\text{-}A\text{-}W)^2 + (A\text{-}W)^2\}\Delta\sigma_v\tan\Phi - \frac{1}{2}B\sigma_{hmax} - \frac{1}{8}\{(B\text{-}A\text{-}b)^2 + (A\text{-}b)^2\}(\Delta\sigma_v - \gamma h)\tan\Phi\right]$$

Thus E can be found to be 37kN/m and by knowing that:
$\tan\varphi = 0$ $(B\text{-}A\text{-}b) = 0$ and $A\text{-}b = 0$.

Thus, for a 40kN wheel load acting on a 0.43m thick aggregate layer, overlying a subgrade of shear strength 45kPa, a tensile force of 45kN/m is developed in the geosynthetic and the required stiffness of the geosynthetic is 37kN/m per cent strain.